Universidade de Aveiro Departamento de Engenharia Civil
2009

Nuno Filipe Ferreira Soares Borges Lopes

Comportamento ao fogo de estruturas em aço inoxidável

Behaviour of stainless steel structures in case of fire

Universidade de Aveiro Departamento de Engenharia Civil
2009

Nuno Filipe Ferreira Soares Borges Lopes

Comportamento ao fogo de estruturas em aço inoxidável

Dissertação apresentada à Universidade de Aveiro para cumprimento dos requisitos necessários à obtenção do grau de Doutor em Engenharia Civil, realizada sob a orientação científica do Doutor Paulo Jorge de Melo Matias Faria de Vila Real, Professor Catedrático da Universidade de Aveiro e co-orientação do Doutor Luís Alberto Proença Simões da Silva, Professor Catedrático da Universidade de Coimbra

Universidade de Aveiro Departamento de Engenharia Civil
2009

Nuno Filipe Ferreira Soares Borges Lopes

Behaviour of stainless steel structures in case of fire

Thesis submitted to the University of Aveiro to fulfil the necessary requirements for the degree of Doctor of Philosophy in Civil Engineering, made under the scientific supervision of Doctor Paulo Jorge de Melo Matias Faria de Vila Real, Professor at the University of Aveiro and co-supervision of Doctor Luís Alberto Proença Simões da Silva, Professor at the University of Coimbra.

Aos meus pais

To my parents

o júri

presidente

Prof. Doutor Casimiro Adrião Pio
professor catedrático da Universidade de Aveiro

Prof. Doutor Enrique Mirambell Arrizabalaga
professor catedrático da Universidade Politécnica de Catalunha

Prof. Doutor Peter Schaumann
professor catedrático da Universidade de Hanôver

Prof. Doutor Jean-Marc Franssen
professor catedrático da Universidade de Liège

Prof. Doutor Luís Alberto Proença Simões da Silva
professor catedrático da Faculdade de Ciências e Tecnologia da Universidade de Coimbra

Prof. Doutor Paulo Jorge de Melo Matias Faria de Vila Real
professor catedrático da Universidade de Aveiro

Prof. Doutor Dinar Reis Zamith Camotim
professor associado do Instituto Superior Técnico da Universidade Técnica de Lisboa

Prof. Doutor Paulo Barreto Cachim
professor associado da Universidade de Aveiro

Prof. Doutor João Paulo Correia Rodrigues
professor auxiliar da Faculdade de Ciências e Tecnologia da Universidade de Coimbra

Prof. Doutor Paulo Alexandre Gonçalves Piloto
professor coordenador do Instituto Politécnico de Bragança

the jury

chairman

Prof. Doctor Casimiro Adrião Pio
professor at the University of Aveiro

Prof. Doctor Enrique Mirambell Arrizabalaga
professor at the Polytechnic University of Catalonia

Prof. Doctor Peter Schaumann
professor at the University of Hanover

Prof. Doctor Jean-Marc Franssen
professor at the University of Liege

Prof. Doctor Luís Alberto Proença Simões da Silva
professor at the Faculty of Science and Technology of the University of Coimbra

Prof. Doctor Paulo Jorge de Melo Matias Faria de Vila Real
professor at the University of Aveiro

Prof. Doctor Dinar Reis Zamith Camotim
associate professor at the Superior Technical Institute of the Technical University of Lisbon

Prof. Doctor Paulo Barreto Cachim
associate professor at the University of Aveiro

Prof. Doctor João Paulo Correia Rodrigues
assistant professor at the Faculty of Science and Technology of the University of Coimbra

Prof. Doctor Paulo Alexandre Gonçalves Piloto
coordinator professor at the Polytechnic Institute of Braganza

agradecimentos

O desenvolvimento da presente tese não seria possível sem a excelente supervisão do Professor Paulo Vila Real, meu orientador, a quem estou muito grato por todo o conhecimento, motivação e empenho transmitidos.

Ao meu co-orientador Professor Luís Simões da Silva pelas valiosas sugestões e ajudas fornecidas durante a preparação desta tese.

Estou igualmente grato ao Professor Jean-Marc Franssen, pela calorosa recepção e supervisão proporcionadas durante um ano na Universidade de Liège, Bélgica, e pelas suas claras respostas às minhas incontáveis perguntas e dúvidas.

Ao Departamento de Engenharia Civil da Universidade de Aveiro na pessoa do Professor Claudino Cardoso, presidente do departamento, pelas facilidades proporcionadas durante a preparação desta tese.

Ao Departamento ArGEnCo da Universidade de Liège na pessoa do Professor Serge Cescotto, presidente do departamento, pelas facilidades proporcionadas durante o período que passei neste departamento.

Ao Professor Paulo Piloto pelo seu auxílio na obtenção da validação de alguns resultados numéricos. Também, ao Professor Enrique Mirambell pelas sugestões dadas a parte do trabalho.

A todos os colegas e amigos da Universidade de Aveiro e da Universidade de Liège pelas ajudas e incentivos, em particular a Carlos Coelho, José Alexandre Henriques, François Hanus, David Janssen e Barbara Rossi.

À Fundação Calouste Gulbenkian pelo apoio financeiro dado durante minha estadia na Universidade de Liège.

À Fundação para a Ciência e a Tecnologia pelo apoio financeiro dado sob a forma de bolsa de doutoramento.

Aos meus pais e irmãos pelos sempre disponíveis apoio e motivação.

Muito obrigado

acknowledgements

The development of this thesis would not be possible without the excellent guidance of Professor Paulo Vila Real, my supervisor, to whom I am very grateful for all the transmitted knowledge, encouragement and dedication.

I wish to acknowledge my co-supervisor Professor Luís Simões da Silva for the valuable suggestions and help given during the preparation of this thesis.

I am also grateful to Professor Jean-Marc Franssen, for the warm welcome and supervision provided during one year at the University of Liege, Belgium, and for his clear answers to my countless questions and doubts.

To the Department of Civil Engineering of the University of Aveiro in the person of Professor Claudino Cardoso, president of the department, for the facilities provided during the preparation of this thesis.

To the Department ArGEnCo of the University of Liege in the person of Professor Serge Cescotto, president of the department, for the facilities provided during the period that I spent in this department.

To Professor Paulo Piloto for his assistance in the achievement of the validation of some numerical results. Also, to Professor Enrique Mirambell for the consultancy provided to part of the work.

To all colleagues and friends from the University of Aveiro and from the University of Liege for the help and encouragement, in particular to Carlos Coelho, José Alexandre Henriques, François Hanus, David Janssen and Barbara Rossi.

To the Calouste Gulbenkian Foundation (Fundação Calouste Gulbenkian) for the financial support given during my stay in the University of Liege.

To the Foundation for Science and Technology (Fundação para a Ciência e a Tecnologia) for the financial support given in the form of a doctoral scholarship.

To my parents and brothers for their always available support and motivation.

Many thanks

palavras-chave

aço inoxidável, estruturas, fogo, encurvadura, elementos estruturais.

resumo

A presente tese resulta de um trabalho de investigação, cujo objectivo se centrou no aumento de conhecimento do comportamento estrutural do aço inoxidável, na construção.

O aço inoxidável tem várias características desejáveis num material estrutural. Embora inicialmente mais caras que em aço carbono convencional, estruturas em aço inoxidável podem ser competitivas em virtude de necessitarem de uma menor quantidade de material de protecção térmica, e de terem um custo de ciclo de vida mais baixo, contribuindo assim para uma construção mais sustentável.

O principal objectivo desta tese consiste em realizar uma avaliação numérica da resistência ao fogo de estruturas em aço inoxidável.

Os estudos numéricos foram efectuados através do programa de elementos finitos SAFIR com análises material e geométrica não lineares, que foi especialmente desenvolvido na Universidade de Liège para o estudo de estruturas em situação de incêndio. Estas análises numéricas enquadram-se na metodologia habitualmente designada por GMNIA - *geometrically and materially non-linear imperfect analysis*. O programa foi também objecto de modificações tendo em vista a realização desses estudos.

É demonstrado que, devido às diferenças existentes entre as leis constitutivas do aço carbono e do aço inoxidável, não é possível utilizar em ambos os materiais as mesmas fórmulas para o cálculo da estabilidade de elementos, como é proposto no Eurocódigo 3. Os resultados mostram também que, para alguns elementos estruturais, as fórmulas, preconizadas nessa norma europeia, não estão do lado da segurança, existindo assim necessidade de as melhorar.

Estes estudos foram realizados em colunas, vigas e vigas-coluna em aço inoxidável tanto à temperatura ambiente como a altas temperaturas, resultando em novas propostas de dimensionamento para esses elementos. O comportamento de vigas em aço carbono sujeitas a temperaturas elevadas foi também analisado, devido a não ser suficientemente conhecido e as propostas apresentadas nesta tese, para vigas em aço inoxidável, terem sido baseadas nesse comportamento.

Esta tese contém também um estudo em elementos de paredes finas em aço inoxidável sujeitos a incêndio, onde é avaliada a influência das tensões residuais nas suas cargas últimas.

Por fim apresenta-se uma análise do comportamento estrutural global de duas estruturas em aço inoxidável sujeitas a incêndio, comparando os resultados obtidos com o comportamento das mesmas estruturas em aço carbono.

keywords

stainless steel, structures, fire, buckling, structural elements.

abstract

This thesis is a research work aimed at increasing the knowledge of the structural behaviour of the stainless steel in construction.

The stainless steel has countless desirable characteristics for a structural material. Although initially more expensive than conventional carbon steel, stainless steel structures can be competitive because of its smaller need for thermal protection material, and lower life-cycle cost, thus contributing to a more sustainable construction.

The main objective of this thesis consists in making a numerical evaluation of the fire resistance of stainless steel structures.

The numerical studies were performed using the finite element program SAFIR, with non-linear material and geometric analysis, which was specially developed at the University of Liege, for the study of structures in case of fire. These numerical analyses fit the methodology usually designated GMNIA - geometrically and materially non-linear imperfect analysis. The program was also object of some modifications in order to enable those studies.

It is demonstrated that, due to the existing differences in the constitutive laws of carbon steel and stainless steel, it is not possible to use in both materials the same formulae for the member stability calculation, as proposed in Eurocode 3. Moreover, the results show that, the formulae, prescribed on that european norm, are not on the safe side for some structural elements, being necessary their improvement.

These studies were made in stainless steel columns, beams and beam-columns at room temperature and at high temperatures, resulting in new design proposals for those members. The behaviour of carbon steel beams at elevated temperatures was also analysed, due to not being sufficiently known and to the proposals presented in this thesis, for stainless steel beams, being based on that behaviour.

This thesis contains also a study on thin-walled stainless steel elements in case of fire, where it is evaluated the influence of the residual stresses on their ultimate loads.

Finally, an analysis on the global structural behaviour of two stainless steel structures subjected to fire is presented, followed by a comparison of their results with the behaviour of the same structures in carbon steel.

mots-clés

acier inoxydable, structures, feu, déversement, éléments structurels.

résumé

La présente thèse est un travail de recherche, avec l'objectif d'élever la connaissance du comportement structurel de l'acier inoxydable, dans la construction.

L'acier inoxydable a plusieurs caractéristiques souhaitables dans un matériau structurel. Même initialement plus chères qu'en acier au carbone traditionnel, les structures en acier inoxydable peuvent être compétitives car elles nécessitent la mise en place d'une quantité moins importante de protection thermique, et induisent un coût de cycle de vie plus faible, contribuant ainsi à une construction plus durable.

Le principal objectif de cette thèse consiste à réaliser une évaluation numérique de la résistance au feu des structures en acier inoxydable.

Les études numériques ont été réalisées avec le programme d'éléments finis SAFIR, d'analyse non linéaire matérielle et géométrique, et qui a été spécialement développé à l'Université de Liège pour l'étude des structures soumises au feu. Ces études numériques s'inscrivent dans la méthodologie habituellement désignée de GMNIA - *geometrically and materially non-linear imperfect analysis*. Le programme a été aussi l'objet de quelques modifications afin de rendre possibles ces études.

On démontre que, en raison des différences existantes dans les lois constitutives de l'acier au carbone et de l'acier inoxydable, il n'est pas possible d'employer dans les deux matériaux les mêmes formules pour le calcul de stabilité d'éléments, comme proposé dans l'Eurocode 3. Les résultats prouvent aussi que les formules préconisées dans cette norme européenne ne sont pas du côté de la sécurité pour quelques éléments structurels, ce qui suggère leur amélioration.

Ces études ont été effectuées dans des poteaux, des poutres et des poutres-poteaux d'acier inoxydable à la température ambiante et à hautes températures, les études ont résulté en nouveaux propositions de calcul pour ces éléments. Le comportement des poutres en acier au carbone soumises à des températures élevées est également étudié, car sa connaissance est insuffisante et des propositions présentées dans cette thèse, pour le calcul des poutres en acier inoxydable, êtres basés sur ce comportement.

Cette thèse contient aussi une étude des éléments à parois minces en acier inoxydable soumis au feu, où l'influence des contraintes résiduelles sur les charges ultimes est avalisée.

Finalement, une évaluation du comportement structurel global de deux structures d'acier inoxydable en cas de feu est présentée, et les résultats sont comparés à ceux obtenus dans le cas de structures similaires en acier au carbone.

Contents

Chapter 1. Introduction

Chapter 2. Materials

Chapter 3. Numerical analysis

Chapter 4. Prescribed design rules for structural elements

Chapter 5. Design proposals for stainless steel structural elements

Chapter 7. Global behaviour of stainless steel structures in case of fire

Chapter 8. Conclusions

References

List of figures

Chapter 1. Introduction

Chapter 2. Materials

Chapter 3. Numerical analysis

Chapter 4. Prescribed design rules for structural elements

Chapter 5. Design proposals for stainless steel structural elements

Chapter 6. Thin-walled stainless steel structural elements in case of fire

Chapter 7. Global behaviour of stainless steel structures in case of fire

List of tables

Chapter 2. Materials

Chapter 3. Numerical analysis

Chapter 4. Prescribed design rules for structural elements

Chapter 5. Design proposals for stainless steel structural elements

Chapter 6. Thin-walled stainless steel structural elements in case of fire

Chapter 7. Global behaviour of stainless steel structures in case of fire

Notation

Roman upper case letters

A	area
A_{eff}	effective section area
$A_d(t)$	calculation value of the action resulting from the fire exposition
C_1, C_2, C_3	coefficient for determining M_{cr}
Cr	chromium
E	modulus of elasticity, also known as Young's modulus
E_0	initial modulus of elasticity
$E_{a,\theta}$	slope of the linear elastic range at temperature θ_a
$E_{ct,\theta}$	slope at proof strength at temperature θ_a
E_{sec}	secant modulus
E_t	tangent modulus on the stress-strain relationship
G	shear modulus
G_k	characteristic value of the permanent actions;
H	value of the g in the second branch of the stainless steel constitutive law
I_i	second moment of area in axis i
I_t	torsion constant
I_ω	warping constant
K	coefficient to determining the buckling length in beam-columns theory
$K_{i,fi}$	amplification factor in axis i in case of fire
$K_{LT,fi}$	amplification factor when occurring LTB in case of fire
L	length of the element

L_{cr}	effective buckling length of the element
$M_{b,Rd}$	LTB resistance bending moment
M	bending moment
M_A	bending moment in extremity A
M_B	bending moment in extremity B
$M_{b,fi,t,Rd}$	LTB resistant bending moment in case of fire
M_{cr}	elastic critical bending moment
M_{Ed}	design acting bending moment value
$M_{fi,Rd}$	resistant bending moment in case of fire
$M_{i,Ed}$	design acting bending moment value in axis i
$M_{i,fi,Ed}$	design acting bending moment value in axis i in case of fire
$M_{i,Rk}$	characteristic moment resistance of the critical cross-section in axis i
M_{pl}	plastic resistant bending moment
M_{Rd}	resistant bending moment
M_{Safir}	ultimate bending moment obtained in the SAFIR simulations
M_u	ultimate bending moment
$M_{ult,i}^{SAFIR}$	ultimate bending moment obtained in the SAFIR simulation i
$M_{ult,i}^{Analytical}$	analytical ultimate bending moment
M^*	quotient between the design bending moment and the resistant bending moment
N	axial force
$N_{b,fi,t,Rd}$	buckling resistant axial force in case of fire
$N_{b,Rd}$	buckling resistant axial force
$N_{b,Rd,i}$	buckling resistant axial force in axis i
$N_{b,Rd,\min}$	minimum buckling resistant axial force $N_{b,Rd,i}$
N_{cr}	critical axial force
$N_{cr,i}$	critical axial force in axis i

N_{Ed} design axial force value

$N_{fi,Ed}$ design axial force value in case of fire

$N_{fi,Rd}$ resistant axial force in case of fire

N_{Rd} resistant axial force

N_{Rk} characteristic resistance to normal force of the critical cross-section

N^* quotient between the design axial force and the resistant axial force

Ni nickel

N_{pl} plastic axial force

$Q_{k,1}$ characteristic value of the main or dominant variable action;

$W_{eff,i}$ effective section modulus in axis i

$W_{el,i}$ elastic section modulus in axis i

$W_{pl,i}$ plastic section modulus in axis i

Roman lower case letters

a,b,c parameters to calculate the carbon steel stress-strain relationship at high temperatures

a,b,c,d parameters to calculate the approximation proposed to the stainless steel hardening rule

a,b,c,d,e parameters to calculate the stainless steel stress-strain relationship at high temperatures

a_i^n displacement after iteration i

a_{LT} coefficient necessary for beam-column design with LTB

b width of a cross-section

b_{eff} effective width of a cross-section

c_a steel specific heat

c_{ii} coefficient necessary for beam-column design in axis i

c_m equivalent moment factor

c_{mi} , $c_{mi,0}$	equivalent bending moment coefficients for beam-column formulae in axis i
c_{mLT}	equivalent bending moment coefficients for beam-column formulae with LTB
f	coefficient for accounting with non-uniform bending diagram in LTB
$f_{0.2p}$	stainless steel proof strength at 0.2% plastic strain
$f_{0.2p,\theta}$	stainless steel proof strength at 0.2% plastic strain at temperature θ_a
$f_{2\%,\theta}$	stress at 2% total strain at temperature θ_a
$f_{p,\theta}$	carbon steel proportional limit at temperature θ_a
f_u	ultimate tensile strength
$f_{u,\theta}$	ultimate tensile strength at temperature θ_a
f_y	yield strength
$f_{y,\theta}$	yield strength at temperature θ
g	first derivative of the approximation to the hardening rule
h	depth of a cross-section
k_c	correction factor for non-uniform bending
k	plastic strain in the definition of the hardening rule
k	amplification factor
$k_{0.2p,\theta}$	reduction factor for stainless steel proof strength at temperature θ_a
$k_{2\%,\theta}$	factor for the determination of the stainless steel yield strength at high temperatures
$k_{E,\theta}$	reduction factor for the slope of the linear elastic range at temperature θ_a
$k_{Ect,\theta}$	reduction factor for the stainless steel slope at proof strength at temperature θ_a
k_i	amplification factor in axis i
k_{LT}	amplification factor when occurring LTB
$k_{p,\theta}$	reduction factor for the carbon steel proportional limit at temperature θ_a
$k_{u,\theta}$	reduction factor for stainless steel ultimate tensile strength at temperature θ_a
k_{yy}, k_{zz}, k_{zy}	interaction factors in beam-columns design formulae
$k_{y,\theta}$	reduction factor for the yield strength at temperature θ_a

k_z effective length factor related to the end rotation on the plan

k_ω effective length factor related to the end warping

n total number of numerical simulations

s standard deviation

t thickness of a cross-section

t time

v volume

x longitudinal position

x_i quotient between $M_{ult,i}^{Analytical}$ and $M_{ult,i}^{SAFIR}$

z_g distance between the shear centre and the point of load application

z_j distance necessary for determining M_{cr}

z_s coordinate of the shear centre

Greek upper case letters

$\Delta l/l$ thermal elongation

$\Delta M_{i,Ed}$ moments due to the shift of the centroidal axis i

Greek lower case letters

α imperfection factor

α angle between a tangent to stress-strain relationship and horizontal direction

α_i imperfection factor in axis i

α_{LT} imperfection factor for the LTB

β coefficient for determining χ_i

$\beta_{M,i}$ equivalent moment factor in axis i

$\beta_{M,LT}$ equivalent moment factor when occurring LTB

γ_{GA} partial safety factor of the permanent actions in case of accident, which should take the unit value

γ_{M1}	partial safety factor at room temperature
$\gamma_{M,fi}$	partial safety factor in fire situation
ε	strain
ε	coefficient for the cross-section classification
ε_c	strain due to creep effect at elevated temperatures
$\varepsilon_{c,\theta}$	stainless steel total strain at proof strength at temperature θ_a
ε_{pl}	plastic strain
$\varepsilon_{p,\theta}$	carbon steel strain at the proportional limit at temperature θ_a
ε_{res}	strain due to residual stress
ε_{res}^{el}	strain due to residual stress not accounting with the material non-linearity
ε_{res}^{pl}	remaining strain to account the material non-linearity in the strain due to residual stress
ε_t	total strain
ε_{th}	strain due to thermal elongation
$\varepsilon_{t,\theta}$	carbon steel limiting strain for yield strength at temperature θ_a
$\varepsilon_{u,\theta}$	ultimate strain at temperature θ_a
ε_y	coefficient necessary for beam-column design with LTB
$\varepsilon_{y,\theta}$	carbon steel yield strain at temperature θ_a
ε_σ	strain due to stress
η	coefficient to determine α
θ	temperature
θ_a	steel temperature
$\overline{\lambda}$	element slenderness value
λ_a	steel thermal conductivity
$\overline{\lambda}_0$	limiting slenderness value for dispending buckling calculations
$\overline{\lambda}_i$	element slenderness value in axis i
$\overline{\lambda}_{i,\theta}$	element slenderness value in axis i at high temperatures

$\overline{\lambda}_{LT}$	element slenderness value for the LTB
$\overline{\lambda}_{LT,0}$	limiting slenderness value for dispending LTB calculations
$\overline{\lambda}_{LT,\theta}$	element slenderness value for the LTB in case of fire
$\overline{\lambda}_{\theta}$	element slenderness value at high temperatures
μ	coefficient to determining the amplification factors k
μ	average value
μ_i	coefficient to determining the amplification factors k_i
μ_i	coefficient necessary for beam-column design in axis i
$\mu_{i,\theta}$	coefficient to determining the amplification factors $K_{i,fi}$
μ_{LT}	coefficient to determining the amplification factor k_{LT}
$\mu_{LT,\theta}$	coefficient to determining the amplification factor $K_{LT,fi}$
$\mu_{Safir,\theta}$	coefficient to determining the amplification factors $K_{i,fi}$ obtained with M_{Safir}
ν	poisson's ratio
τ	stress from the hardening rule
$\tau_{xy,res}$	residual tangential stresses
σ	stress
σ_1, σ_2	principal stresses
$\sigma_{Aproximation}$	stress according to the developed approximation of the stainless steel constitutive law
$\sigma_{c,res}$	comparison stress of the residual stresses
σ_{EC3}	stress according to the stainless steel constitutive law in EC3
σ_{res}	residual stresses
$\sigma_{x,res}$	residual stresses in axis x
$\sigma_{y,res}$	residual stresses in axis y
ϕ	coefficient used in the determination of the buckling reduction factor
ϕ	angle formed by the deformed tangent of the beam and its initial position
ϕ_i	coefficient for determining the reduction factor χ_i

$\phi_{i,\theta}$	coefficient for determining the reduction factor $\chi_{i,fi}$
ϕ_{LT}	coefficient for determining the reduction factor χ_{LT}
$\phi_{LT,\theta,com}$	coefficient for determining the reduction factor $\chi_{LT,fi}$
χ_i	reduction factor for the flexural buckling in axis i
$\chi_{i,fi}$	reduction factor for the flexural buckling in axis i in case of fire
χ_{LT}	reduction factor for the LTB
$\chi_{LT,fi}$	reduction factor for the LTB in case of fire
$\chi_{LT,fi,\mathrm{mod}}$	modified reduction factor for the LTB in non-uniform bending in case of fire
$\chi_{LT,\mathrm{mod}}$	modified reduction factor for the LTB in non-uniform bending
$\chi_{\min}$	minimum of the reduction factor χ_i
$\chi_{\min,fi}$	minimum of the reduction factor $\chi_{i,fi}$
ψ	quotient between the moments in the extremities
$\psi_{1,1}$	combination coefficient associated to the main or dominant variable action;
$\psi_{2,i}$	combination coefficient associated to the remaining variable actions;
ψ_i	quotient between the moments in the extremities in axis i

Vectors

$[D]$	matrix of Hooke in linear elasticity
$\{\varepsilon_{res}\}$	matrix of residual strains $(x,\ y$ and $xy)$
$\{\sigma_{res}\}$	matrix of residual stresses $(x,\ y$ and $xy)$

Sub-script

i	axis y or z
θ	steel temperature

Abbreviations

CEN	European Committee for Standardisation (in French *Comité Européen de Normalisation*)
EC3	Eurocode 3
GMNIA	Geometrically and materially non-linear imperfect analysis
LTB	Lateral torsional buckling
SHS	Steel hollow section

Chapter 1

Introduction

Chapter 1. Introduction

1.1 General considerations

1.2 Objectives

1.3 Thesis outline

Chapter 1. Introduction

1.1 General considerations

The use of stainless steel for structural purposes has been limited to projects with high architectural value, where the innovative character of the adopted solutions is intended to add value to the structure. The high initial cost of stainless steel, coupled with: (i) limited design rules, (ii) reduced number of available sections and (iii) lack of knowledge on the additional benefits of its use as a structural material, are some of the reasons that force designers to avoid its use. However, more accurate analysis points to a good performance of stainless steel when compared against conventional carbon steel (Gardner, 2005; Estrada *et al*., 2007; Cruise, 2007).

The most important advantage of stainless steels is their corrosion resistance, however, their aesthetic appearance, ease of maintenance, durability and the low life-cycle costs are also valuable characteristics. Engineers often disregard these advantages of stainless steel due to its high initial cost, although scenarios of short-term savings leading to bigger long-term expenditure are numerous throughout the construction industry. Moreover, greater importance is being given to total life costing because of high maintenance, shut-down, demolition and parts replacement costs. Experience has shown that the benefits of a long life with low maintenance and repair requirements more than compensates for the higher purchase cost of stainless steel.

With the objective of eliminating technical obstacles to trade and harmonization of technical specifications in the Member States of the European Community, the European Commission took the initiative to establish a set of harmonized technical rules for the design of construction works. These technical rules were prepared and published by the European Committee for Standardization (CEN) that conducted to the development of the Structural Eurocodes (CEN, 2005a). The Eurocodes consist of a group of ten parts dedicated to: basis and actions required in the design of structures; particular rules and recommendations necessary for structures made of different materials (concrete, steel, timber, masonry and aluminium), geotechnical design and design for earthquake

resistance. From these set of rules one is dedicated exclusively to the design of steel structures, designated as Eurocode 3 (EC3).

Codes of practice are aimed at providing safe, competitive and, as far as possible, simple procedures for the design of structures. Drafting and implementing a consistent set of structural Eurocodes involving a large number of groups of experts is naturally a recursive task where each part must reflect the scientific advances and design options of all other related parts.

Regarding fire structural resistance, simplified design rules provided by those codes of practice, are of the utmost importance to designers that do not always have access to applications dealing with advanced calculation methods.

Axially loaded carbon steel columns in fire have been studied by Franssen *et al*. (1995; 1996; 1998) who proposed a procedure for the safety evaluation of columns subjected to high temperatures, later adopted by part 1-2 of EC3 (CEN, 2005b).

Vila Real *et al*. (2001; 2003b) analyzed the problem of lateral torsional buckling (LTB) of beams in case of fire, and equally proposed an expression adopted in part 1-2 of EC3 (CEN, 2005b). This proposal was developed for the case of simply supported beams with fork supports and uniform bending diagrams, being the most severe situation.

The safety evaluation, of steel structural elements, subjected to axial compression and bending, is made through interaction formulae that combine the compression and bending resistances. For beam-columns in case of fire, part 1-2 of the EC3, named also as EN 1993-1-2 (CEN, 2005b) adopts the format given in part 1-1 of EC3 of 1992 (CEN, 1992), replacing: i) the yield stress and the modulus of elasticity for its values at high temperatures; ii) the buckling reduction factors for flexural buckling and LTB in fire; and also, when no LTB exists, iii) the interaction curves, resulted from studies by Talamona *et al*. (1995; 1997). The final version of part 1-1 of EC3, EN 1993-1-1 (CEN, 2005a), introduced several changes in the cold design formulae for carbon steel beam-columns when compared with the previous versions of EC3 (CEN, 1992). Two new methods, which are the result of the work carried out by two working groups who followed different approaches (Boissonnade *et al*., 2006), are proposed in the EN version of EC3 (CEN, 2005a). Following these modifications, some studies (Vila Real *et al*., 2003d; Lopes *et al*., 2003; 2004; Lopes, 2003; Knobloch

et al., 2008) have been made to check if those room temperature design approaches can also be used in case of fire, concluding that additional changes, to these new methods, should be made in order to be possible to use them at high temperatures.

Numerical modelling of the LTB of carbon steel beams at elevated temperature has shown the beam design curve from EN 1993-1-2 to be over-conservative in case of non-uniform bending. Based on the newly proposed methodology for cold design from part 1-1 of EC3 of 2005, named as EN 1993-1-1 (CEN, 2005a), an improved proposal for the LTB of unrestrained carbon steel beams subjected to fire is presented in this thesis, addressing the issue of the influence of: the loading type; steel grade; pattern of the residual stresses (hot rolled or welded sections) and ratio h/b (slenderness of the cross-section) between the depth h and the width b of the cross-section on the resistance of the beam. With this methodology, better agreement is achieved with the numerical behaviour while maintaining safety. The proposal is found to be safe and accurate through an extensive comparison and a statistical study with the results of finite element method numerical simulations. This proposal was the basis of a similar proposal for the LTB in stainless steel beams.

As previously stated, stainless steel has a number of desirable characteristics as a structural material. Whilst its use in construction is increasing, there is still a need to develop a more comprehensive understanding of its behaviour as a structural material.

Part 1-4 of EC3 "Supplementary rules for stainless steels", also named as EN 1993-1-4 (CEN, 2006a) gives design rules for stainless steel structural elements at room temperature. The approach followed in part 1-4 of EC3 was to adopt the rules for carbon steel in part 1-1 of EC3, making some modifications where stainless steel tests shown to be necessary (Greiner *et al.*, 2005). Gardner (2002) developed a design method for stainless steel elements that, instead of the discrete Classes in EC3 (Class 1, 2, 3 and 4), uses a single numerical value that consists in a measure of the cross-section deformation capability.

Part 1-4 of EC3 (CEN, 2006a) only mentions the stainless steel structural elements fire resistance by referring to the fire part of the same Eurocode, EN 1993-1-2 (CEN, 2005b). Although carbon steel and stainless steel have different constitutive laws, EC3 states that the structural elements made of these two materials must be checked for its fire resistance using the same formulae. Thus, based on the formulae in part 1-4 of EC3, Uppfeldt

et al. (2008) presented a design model for stainless steel hollow columns in case of fire based in both experimental and numerical tests.

In this thesis the accuracy and safety of the currently prescribed design rules in EC3 for the evaluation of the resistance of stainless steel uniform members (columns, beams and beam-columns) at room temperature (CEN, 2006a) and at high temperatures (CEN, 2005b) is evaluated. This evaluation is carried out by performing numerical simulations on Class 1 and Class 2 (CEN, 2006a) stainless steel I-cross-sections. Comparisons between the numerical results and the buckling curves from EC3 for those different elements are presented. Based on these comparisons, safer and more accurate proposals, for the flexural buckling of columns, LTB resistance and for the interaction curves of beam-columns, are presented.

These alternative expressions for stainless steel structural elements at room temperature and in case of fire try to ensure the compatibility and coherence between part 1-1, part 1-2 and part 1-4 of EC3, as well as supply simple, competitive and safe procedures. Again, statistical evaluations were made for these design proposals in stainless steel structural elements.

In this thesis, a numerical study in stainless steel thin-walled elements, showing the influence of the residual stresses and initial imperfections on the ultimate load bearing resistance of Class 4 stainless steel structural elements in case of fire, is also presented. The use of thin-walled sections in stainless steel structural elements is common, thus is of great interest to understand their behaviour in case of fire. In fact, the knowledge of the performance of Class 4 steel elements in case of fire is still limited, justifying the necessity of this study.

Finally, the behaviour of two structures (a portal frame and a truss) subjected to a standard fire curve will be compared both in stainless steel and in carbon steel. The mechanical and thermal properties considered for both materials were the ones prescribed in the fire part of EC3 (CEN, 2005b). It will be shown that the fire resistance of stainless steel structures is significantly higher than carbon steel structures, avoiding the application of fire protection to fulfil the standard fire requirements.

This resistance allows the use of the stainless steel structures without fire protection, increasing the economic advantage of the stainless steel as a structural material. Moreover

it may provide a better aesthetic appearance to structures, which is often decisive in the choice of this kind of steel in construction.

The numerical simulations described above were made using the methodology usually designated by GMNIA (geometrically and materially non-linear imperfect analysis) through the use of the program SAFIR (Franssen, 2008; 2005a). This program is a geometrical and material non-linear finite element code, specially developed in the University of Liege for the study of structures in case of fire, and it has been adapted, in this work, according to the material properties defined in part 1-4 and part 1-2 of EC3 (CEN, 2006a; 2005b), to model the behaviour of stainless steel structures. It was also introduced the possibility of the program to take into account residual stresses in shell elements. This program, widely used by several investigators, has been validated against analytical solutions, experimental tests and numerical results from other programs, and has been used in several studies that lead to proposals for safety evaluation of structural elements, already adopted in EC3.

1.2 Objectives

The main objective of this thesis is to develop more comprehensive, safe and economic guidance on the design of stainless steel structural members, especially when exposed to fire.

The overall objective was achieved through the following specific objectives:

- to generate test results on commonly used grades of stainless steel in structures;
- to develop simple models and validate them against numerical results in order to generate new formulae for calculation of member stability;
- to develop a methodology in the form of fire resistant design rules suitable for incorporation into standards that enable stainless steel members to be designed cost effectively and safely in structures;
- to ensure that the deliverables of the thesis are in a format that is readily disseminated and used in the European Union by incorporating them into European Standards;

- and to present structural solutions where it is possible to use stainless steel structural members in buildings without fire protection.

Based on the need to increase competitiveness, guaranteeing safety and assuring the compatibility and coherence between part 1-1, part 1-2 and part 1-4 of the EC3 (CEN, 2005a; 2005b; 2006a), the specific objective of this thesis is to evaluate, through a numerical analysis, the stainless steel structural members (columns, beams and beam-columns) resistance when subjected to elevated temperatures. New formulae are developed for the safety evaluation of these elements in case of fire. The behaviour of these members at room temperature and of carbon steel beams at high temperatures, were also the aim of this study in which new proposals are made in order to promote better design rules.

In the study of beam-columns it was considered using the formulation for safety evaluation of these elements, with and without LTB, prescribed in part 1-1 of EC3 at high temperatures. This is done through the adjustment of the proposed expressions in the same norm, for carbon steel at room temperature, to handle stainless steel and high temperatures. This study was followed by the development of new interaction curves in better agreement with numerical results.

It was also the objective of this thesis to increase the knowledge on the behaviour of thin-walled stainless steel elements in case of fire by testing the influence of the initial imperfections and residual stresses in these elements.

Finally, this thesis has also the objective of studying the fire response of stainless steel structures and compare that response with the one obtained from carbon steel. This input may further increase the knowledge on which material to be applied in structures.

1.3 Thesis outline

This thesis is organised in eight chapters which contemplates the several studies made in this research work. Figure 1.1 shows a schematic representation of the thesis outline.

An introductory brief and general description of the studies made in this thesis is presented in Chapter 1. Here, the objectives and methodologies applied are described.

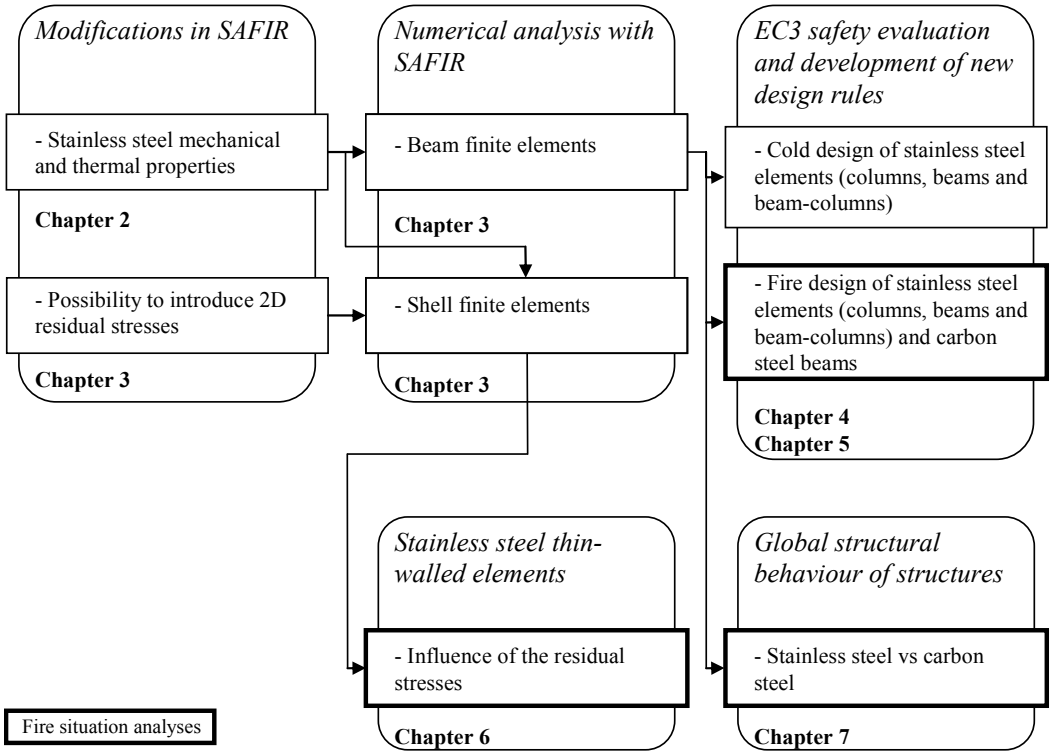

Figure 1.1 – Schematic representation of the outline of the thesis.

In Chapter 2 an explanation is made on the behaviour of stainless steel at high temperatures, presenting the different stainless steel grades and their mechanical and thermal properties in case of fire. The properties used were the ones prescribed in the EC3 (CEN, 2005b). Comparisons with the same properties of the carbon steel are also presented.

Due to the fact that the obtained results were based on the use of finite element software specifically developed for the study of structures in case of fire, in Chapter 3, a brief description of the program SAFIR (Franssen, 2005a) is made. Its results have been used to validate and propose new guidelines for the safety verifications of the different performed studies. In this chapter some modifications made to the program SAFIR are also presented. These were necessary to proceed with the study of stainless steel structural elements at room temperature and in case of fire, with or without thin-walled stainless steel sections (using shell finite elements) and with or without residual stresses. Finally, the numerical models adopted in this research project are also explained in this Chapter 3.

In Chapter 4 the prescribed design rules for stainless steel columns, beams and beam-columns with or without the possibility of occurring LTB, for both cold and fire design, according to part 1-4 and part 1-2 of EC3 (CEN, 2006a; 2005b) are presented. The different code proposals are also compared, in terms of safety and cost, with the numerical results obtained from SAFIR. In this chapter a study of the LTB of carbon steel beams in case of fire that result in a proposal for the safety evaluation of these structural elements is also shown. This study was made in hot rolled and welded section, addressing the issue of the influence of residual stresses, slenderness of the cross-section, loading type and steel grade. The obtained numerical results are compared with the prescriptions from part 1-2 of EC3 (CEN, 2005b), resulting in a new proposal for the design of carbon steel beams.

Based on the conclusions from Chapter 4, Chapter 5 presents new proposals for the design rules of stainless steel columns, beams with LTB and beam-columns with and without LTB, at room temperature and at high temperatures. For the columns and beam-columns, the possibility of buckling on the weak and strong axis of the cross-section is considered. These proposals are based on the performed numerical simulations.

In Chapter 6 a study on thin-walled stainless steel structural elements at high temperatures is shown, which addresses the influence of initial local and global imperfections, and of the residual stresses in Class 4 structural elements in case of fire. For this study it was necessary to introduce in SAFIR shell elements, the 2D stress-strain relationship of stainless steel in case of fire as well as the possibility of introducing residual stresses in these finite elements.

With the purpose of improving the knowledge of the global behaviour of stainless steel structures in case of fire, in Chapter 7 two study cases of stainless steel structures subjected to a standard fire are presented. These results are compared with the same structures made of carbon steel. The studies led to the finding of a significantly higher fire resistance of the stainless steel structures, fostering the use of no fire protection material in stainless steel structures.

The last chapter presents an overview of the main conclusions of this thesis, summarising the developed research work and identifying possible future research areas.

Chapter 2

Materials

Chapter 2. Materials

2.1 Introduction

2.2 Stainless steel

- 2.2.1 Stainless steel grades
- 2.2.2 Mechanical properties
- 2.2.3 Thermal properties

2.3 Comparison between stainless steel and carbon steel

- 2.3.1 Mechanical properties
- 2.3.2 Thermal properties

2.4 Conclusions

Chapter 2. Materials

2.1 Introduction

In this chapter the mechanical and thermal properties at high temperatures, of the stainless steel grades studied in this thesis, are described. Those properties, based on the EC3 prescriptions, are later compared to those of the carbon steel.

It is common knowledge that steel, when subject to high temperatures, suffers big changes in its mechanical properties. In fact, with the increase of temperature, reductions of the yield strength and of the elasticity modulus can be observed. Section 2.2.2 presents these variations of the stainless steel mechanical properties as a function of the temperature.

In section 2.3, a comparison is made between stainless steel and carbon steel mechanical and thermal properties at high temperatures.

2.2 Stainless steel

In this section the stainless steel mechanical and thermal properties at room and elevated temperatures are presented.

2.2.1 Stainless steel grades

There are five basic groups of stainless steel, classified according to the metallurgical structure. These are: austenitic, ferritic, martensitic, austenitic-ferritic also known as duplex, and precipitation-hardening groups (CEN, 2006b; Euro Inox and SCI, 2006; ESDEP, 2000). These types of stainless steel differ in their chemical composition as shown in Figure 2.1.

The high market value of the austenitic stainless steel is due to the price of nickel. Typically they contain 8.0 to 13.0 % of nickel (Ni) whereas ferritic stainless steel contains a lower level of nickel.

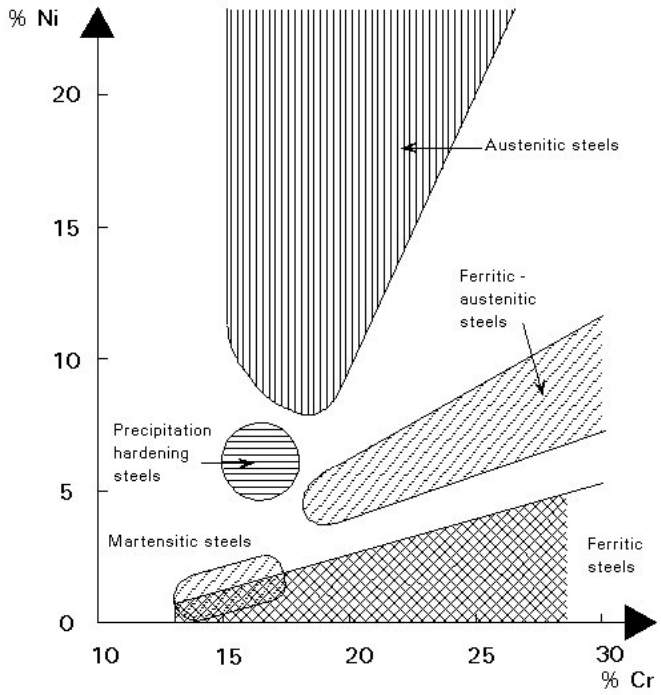

Figure 2.1 – Types of stainless steel (ESDEP, 2000).

Austenitic stainless steels provide good combination of corrosion resistance, forming and fabrication properties. Duplex stainless steels have high strength and very good resistance to corrosion. The most commonly used grades, typically referred to as standard austenitic grades, are 1.4301 (widely known as 304) and 1.4401 (widely known as 316). These austenitic stainless steels are generally the most used in structural applications.

Stainless steel alloys are characterised by their non-linear stress-strain relationship with a low proportionality stress and an extensive strain-hardening range. There is no well-defined yield stress and the yield strength is usually taken as the strength at 0.2 % proof strain.

For stainless steel, the yield strength f_y, the modulus of elasticity E and the ultimate tensile strengths f_u at room temperature, used in this thesis, and indicated in part 1-4 of EC3 (CEN, 2006a). These properties, for the stainless steel grades whose mechanical properties at high temperatures are known, are summarized in Table 2.1. Those values are characteristic values.

Table 2.1 – Nominal values for the yield strength, the ultimate tensile strength and the modulus of elasticity of structural stainless steels (CEN, 2006a).

Type	Grade	Yield strength f_y (MPa)		Ultimate tensile strength f_u (MPa)		Modulus of elasticity E (GPa)
		$t \leq 12$ mm	$t \leq 75$ mm	$t \leq 12$ mm	$t \leq 75$ mm	
Austenitic	1.4301	210		520		200
	1.4401	220		530	520	200
	1.4404	220		530	520	200
	1.4571	220		540	520	200
Ferritic	1.4003	280	250	450		220
Austenitic-ferritic	1.4462	460		660	640	200

As for carbon steel the Poisson's ratio ν is equal to 0.3, and the shear modulus is calculated with the expression

$$G = \frac{E}{2(1+\nu)} \quad \text{with} \quad \nu = 0.3 \tag{2.1}$$

EN 1993-1-4 (CEN, 2006a) only mentions the stainless steel structural element's fire resistance by referring to the fire part of the EC3, EN 1993-1-2 (CEN, 2005b). In a fire situation, because of its accidental nature, higher strains than at room temperature are acceptable, so part 1-2 of EC3 suggests the use of stress at 2 % total strain as the yield stress at elevated temperature θ_a, being $f_{y,\theta} = f_{2\%,\theta}$, for Class 1, 2 and 3 cross-sections and $f_{y,\theta} = f_{0.2p,\theta}$, for Class 4.

2.2.2 Mechanical properties

The stress-strain relationship of stainless steel at high temperatures is necessary for determining the load bearing capacity of a structure under fire conditions. Such as for room temperature, at high temperatures, the variation of the mechanical properties of steel can be determined by tensile and bending tests.

The stress-strain relationship of stainless steel proposed in part 1-2 of the EC3 (CEN, 2005b; Zhao, 2002), determined with the parameters described in Table 2.2, is presented in Figure 2.2.

Table 2.2 – Expressions to determine the stress-strain relationship of the stainless steel at high temperatures.

Strain range	Stress σ	Tangent modulus E_t
$\varepsilon \le \varepsilon_{c,\theta}$	$\dfrac{E \cdot \varepsilon}{1 + a \cdot \varepsilon^b}$	$\dfrac{E\left(1 + a \cdot \varepsilon^b - a \cdot b \cdot \varepsilon^b\right)}{\left(1 + a \cdot \varepsilon^b\right)^2}$
$\varepsilon_{c,\theta} < \varepsilon \le \varepsilon_{u,\theta}$	$f_{0.2p,\theta} - e + (d/c)\sqrt{c^2 - \left(\varepsilon_{u,\theta} - \varepsilon\right)^2}$	$\dfrac{d\left(\varepsilon_{u,\theta} - \varepsilon\right)}{c\sqrt{c^2 - \left(\varepsilon_{u,\theta} - \varepsilon\right)^2}}$
Parameters	$\varepsilon_{c,\theta} = f_{0.2p,\theta} / E_{a,\theta} + 0.002$	
	$a = \dfrac{E_{a,\theta}\,\varepsilon_{c,\theta} - f_{0.2p,\theta}}{f_{0.2p,\theta}\,\varepsilon_{c,\theta}^{\,b}}$	$b = \dfrac{(1 - \varepsilon_{c,\theta}\,E_{ct,\theta} / f_{0.2p,\theta})\,E_{a,\theta}\,\varepsilon_{c,\theta}}{(E_{a,\theta}\,\varepsilon_{c,\theta} / f_{0.2p,\theta} - 1)\,f_{0.2p,\theta}}$
Functions	$c^2 = (\varepsilon_{u,\theta} - \varepsilon_{c,\theta})\left(\varepsilon_{u,\theta} - \varepsilon_{c,\theta} + \dfrac{e}{E_{ct,\theta}}\right)$	$d^2 = e\,(\varepsilon_{u,\theta} - \varepsilon_{c,\theta})\,E_{ct,\theta} + e^2$
	$e = \dfrac{(f_{u,\theta} - f_{0.2p,\theta})^2}{(\varepsilon_{u,\theta} - \varepsilon_{c,\theta})E_{ct,\theta} - 2(f_{u,\theta} - f_{0.2p,\theta})}$	

In this stress-strain relationship two zones can be distinguished: the first is an almost linear zone until the proportional limit; the second is a curve that ends at the ultimate tensile strength.

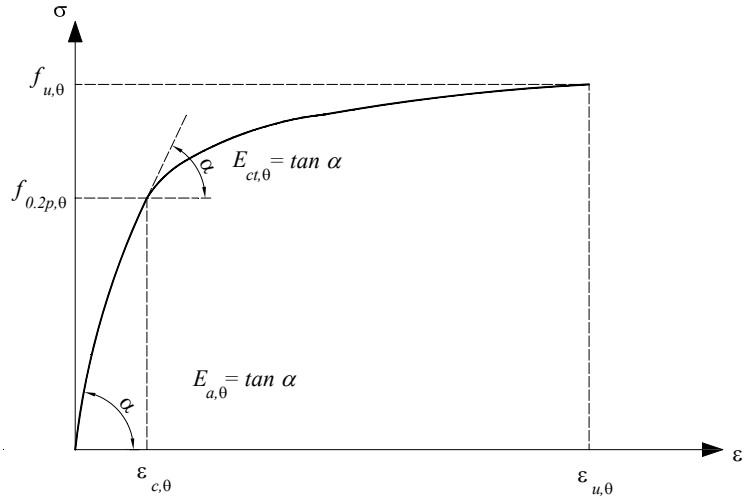

Figure 2.2 – Stress-strain relationship of the stainless steel at high temperatures (CEN, 2005b).

This stress-strain relationship, for stainless steel subject to high temperatures, can be used in the determination of the tension, compression, bending or shear resistance of stainless steel elements, in case of fire.

Like for carbon steel, the mechanical properties of stainless steel, when subjected to high temperatures, suffer significant reductions. However, for stainless steel, those reductions are different for each grade.

Table 2.3 presents the reduction factors for the stress-strain relationship of austenitic steel grades 1.4301, 1.4401, 1.4404 and 1.4571 (presented in Table 2.1) subjected to high temperatures and Table 2.4 presents the same reduction factors for the remaining steels presented in Table 2.1 (ferritic 1.4003 and austenitic-ferritic 1.4462), as proposed in (CEN, 2005b).

The reduction factors in Table 2.3 and Table 2.4 are:

- the reduction factors for the slope of the linear elastic range $k_{E,\theta} = E_{a,\theta} / E_a$;
- the reduction factor for proof strength $k_{0.2p,\theta} = f_{0.2p,\theta} / f_y$;
- the reduction factor for the ultimate tensile strength $k_{u,\theta} = f_{u,\theta} / f_u$;
- and the reduction factor for the slope at proof strength $k_{Ect,\theta} = E_{ct,\theta} / E_a$.

Table 2.3 and Table 2.4 also present:

- a factor $k_{2\%,\theta}$ for the determination of the yield strength at high temperatures to be used in equation (2.2);
- and the ultimate strain $\varepsilon_{u,\theta}$, varying with the steel temperature.

Table 2.3 – Reduction factors for the stress-strain relationship in the austenitic stainless steels 1.4301, 1.4401, 1.4404 and 1.4571 at high temperatures.

θ_a (ºC)	$k_{E,\theta}$	$k_{0.2p,\theta}$	$k_{u,\theta}$	$k_{2\%,\theta}$	$k_{Ect,\theta}$	$\varepsilon_{u,\theta}$
			Class 1.4301			
20	1.00	1.00	1.00	0.26	0.11	0.40
100	0.96	0.82	0.87	0.24	0.05	0.40
200	0.92	0.68	0.77	0.19	0.02	0.40
300	0.88	0.64	0.73	0.19	0.02	0.40
400	0.84	0.60	0.72	0.19	0.02	0.40
500	0.80	0.54	0.67	0.19	0.02	0.40
600	0.76	0.49	0.58	0.22	0.02	0.35
700	0.71	0.40	0.43	0.26	0.02	0.30
800	0.63	0.27	0.27	0.35	0.02	0.20
900	0.45	0.14	0.15	0.38	0.02	0.20
1000	0.20	0.06	0.07	0.40	0.02	0.20
1100	0.10	0.03	0.03	0.40	0.02	0.20
1200	0.00	0.00	0.00	0.40	0.02	0.20
			Class 1.4401 / 1.4404			
20	1.00	1.00	1.00	0.24	0.050	0.4
100	0.96	0.88	0.93	0.24	0.049	0.4
200	0.92	0.76	0.87	0.24	0.047	0.4
300	0.88	0.71	0.84	0.24	0.045	0.4
400	0.84	0.66	0.83	0.21	0.030	0.4
500	0.80	0.63	0.79	0.20	0.025	0.4
600	0.76	0.61	0.72	0.19	0.020	0.4
700	0.71	0.51	0.55	0.24	0.020	0.3
800	0.63	0.40	0.34	0.35	0.020	0.2
900	0.45	0.19	0.18	0.38	0.020	0.2
1000	0.20	0.10	0.09	0.40	0.020	0.2
1100	0.10	0.05	0.04	0.40	0.020	0.2
1200	0.00	0.00	0.00	0.40	0.020	0.2
			Class 1.4571			
20	1.00	1.000	1.000	0.25	0.060	0.40
100	0.96	0.890	0.880	0.25	0.060	0.40
200	0.92	0.830	0.810	0.25	0.050	0.40
300	0.88	0.770	0.800	0.24	0.040	0.40
400	0.84	0.720	0.800	0.22	0.030	0.40
500	0.80	0.690	0.770	0.21	0.025	0.40
600	0.76	0.660	0.710	0.21	0.020	0.35
700	0.71	0.590	0.570	0.25	0.020	0.30
800	0.63	0.500	0.380	0.35	0.020	0.20
900	0.45	0.280	0.220	0.38	0.020	0.20
1000	0.20	0.150	0.110	0.40	0.020	0.20
1100	0.10	0.075	0.055	0.40	0.020	0.20
1200	0.00	0.000	0.000	0.40	0.020	0.20

Table 2.4 – Reduction factors for the stress-strain relationship in the stainless steel 1.4003 and 1.4462 at high temperatures.

θ_a (ºC)	$k_{E,\theta}$	$k_{0.2p,\theta}$	$k_{u,\theta}$	$k_{2\%,\theta}$	$k_{Ect,\theta}$	$\varepsilon_{u,\theta}$
Class 1.4003						
20	1.00	1.000	1.000	0.37	0.055	0.20
100	0.96	1.000	0.940	0.37	0.030	0.20
200	0.92	1.000	0.880	0.37	0.030	0.20
300	0.88	0.980	0.860	0.37	0.030	0.20
400	0.84	0.910	0.830	0.42	0.030	0.15
500	0.80	0.800	0.810	0.40	0.030	0.15
600	0.76	0.450	0.420	0.45	0.030	0.15
700	0.71	0.190	0.210	0.46	0.030	0.15
800	0.63	0.130	0.120	0.47	0.030	0.15
900	0.45	0.100	0.110	0.47	0.030	0.15
1000	0.20	0.070	0.090	0.47	0.030	0.15
1100	0.10	0.035	0.045	0.47	0.030	0.15
1200	0.00	0.000	0.000	0.47	0.030	0.15
Class 1.4462						
20	1.00	1.000	1.00	0.35	0.100	0.20
100	0.96	0.910	0.93	0.35	0.070	0.20
200	0.92	0.800	0.85	0.32	0.037	0.20
300	0.88	0.750	0.83	0.30	0.035	0.20
400	0.84	0.720	0.82	0.28	0.033	0.20
500	0.80	0.650	0.71	0.30	0.030	0.20
600	0.76	0.560	0.57	0.33	0.030	0.20
700	0.71	0.370	0.38	0.40	0.025	0.15
800	0.63	0.260	0.29	0.41	0.025	0.15
900	0.45	0.100	0.12	0.45	0.025	0.15
1000	0.20	0.030	0.04	0.47	0.025	0.15
1100	0.10	0.015	0.02	0.47	0.025	0.15
1200	0.00	0.000	0.00	0.47	0.025	0.15

Figure 2.3 and Figure 2.4 display the stress-strain relationships of the different stainless steel grades, varying with the steel temperature. Section 2.3.1 shows a graphical illustration of the stainless steel Young's modulus varying with the steel temperature.

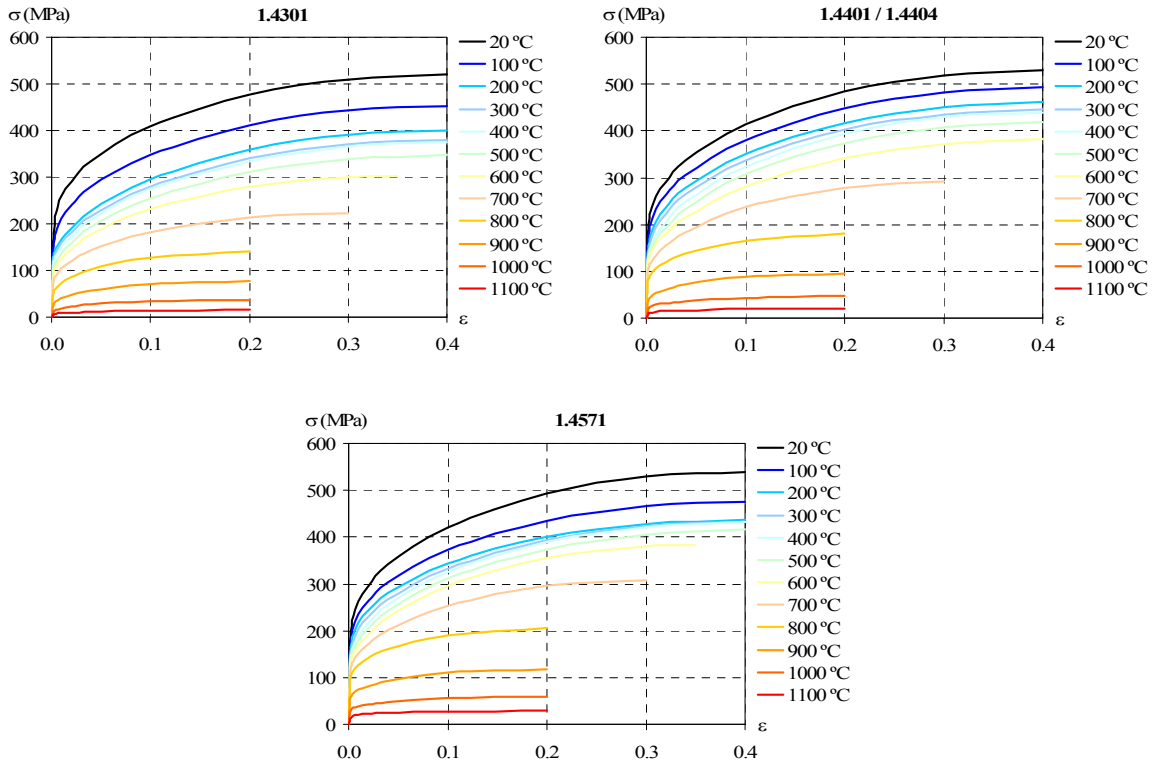

Figure 2.3 – Stress-strain relationship of the austenitic stainless steels at high temperatures.

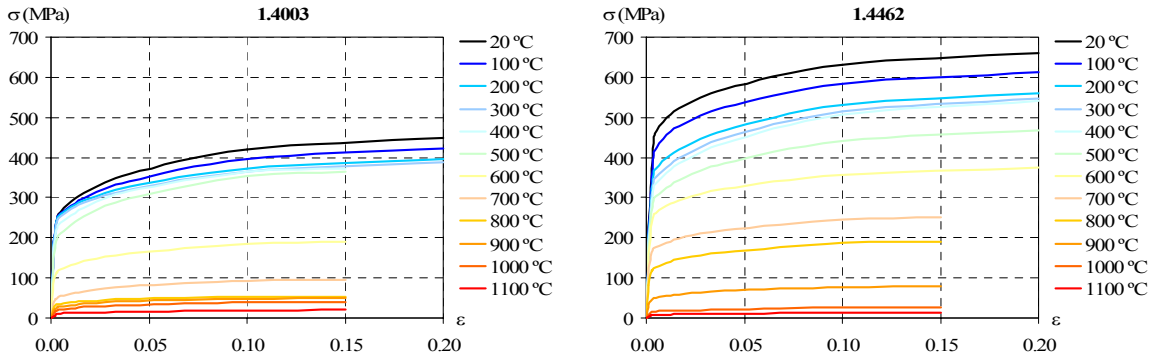

Figure 2.4 – Stress-strain relationship of the ferritic and austenitic-ferritic stainless steels at high temperatures.

From Figure 2.3 and Figure 2.4 it can be observed that the austenitic stainless steels have higher ductility than the ferritic or the austenitic-ferritic stainless steels.

Part 1-2 of EC3 gives the expression (2.2) to determine the reduction factor for the yield strength of stainless steel.

$$k_{y,\theta} = \frac{f_{0.2p,\theta} + k_{2\%,\theta}\left(f_{u,\theta} - f_{0.2p,\theta}\right)}{f_y} \tag{2.2}$$

The effective yield strength, at high temperatures, is reduced as a function of the yield strength at 20 ºC, multiplying it by $k_{y,\theta}$. A graphical illustration of the variation of this factor with the temperature is shown in section 2.3.1. This yield strength corresponds to the stress at 2 % of total strain.

The above described mechanical properties were not completely followed in this research work. The stainless steel stress-strain relationship provided by EC3, for temperatures higher than 1000 ºC, and for $\varepsilon \leq \varepsilon_{c,\theta}$ has a concave shape (see Figure 2.5). This should not happen because in these cases the Young's modulus increases with the strain, which is not possible in numerical material analysis. Therefore, in this work, for temperatures higher than 1100 ºC, a slightly different constitutive law was used, (curve designated "Used law" in Figure 2.5).

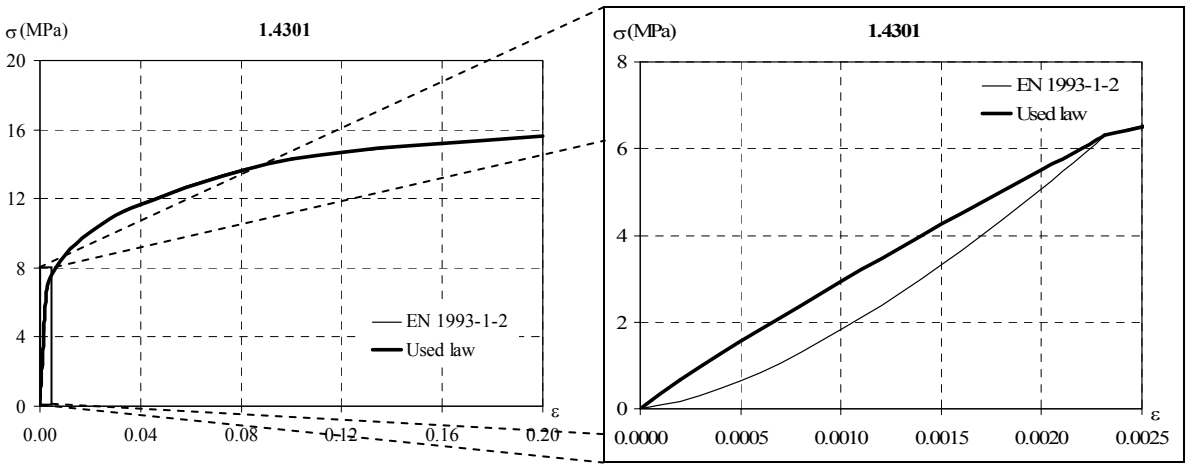

Figure 2.5 – Stress-strain relationship of the stainless steel 1.4301 at 1100 ºC.

The difficulty appears when in Table 2.2, while using the equation that provides the stresses σ, b becomes lower than 0, due to $E_{ct,\theta}$ not vary in function of the temperature from 1000 ºC to 1200 ºC. Thus, at 1200 ºC, while $E_{a,\theta}$ is equal to 0, $E_{ct,\theta}$ is greater than 0. b is negative when the expression (2.3) is negative.

$$1 - E_{ct,\theta}\left(\frac{1}{E_{a,\theta}} + \frac{0.002}{f_{0.2p,\theta}}\right) \tag{2.3}$$

The evolution of this expression with the temperature is illustrated in Figure 2.6, being here designated as "EN 1993-1-2", when using the reduction factors relative to E_a from the EC3. The used stress-strain relationship in this work differs from EC3 only in the reduction factors relative to E_a, for temperatures higher than 1100 ºC. With those new reduction factors values, expression (2.3) never becomes negative, as illustrated by the curve "Used Law" in Figure 2.6.

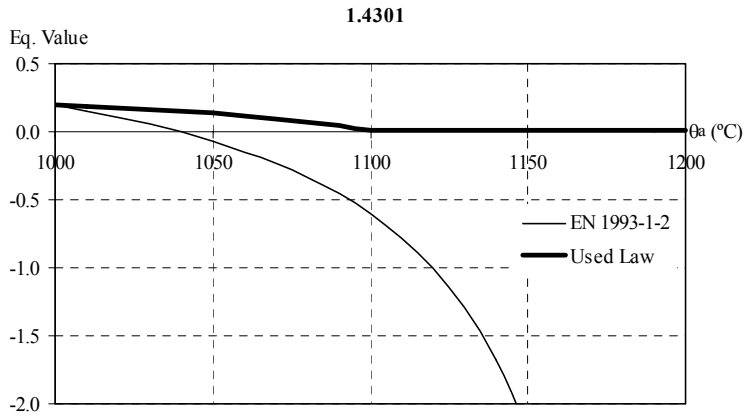

Figure 2.6 – Value of equation (2.3) for the stainless steel 1.4301.

This problem occurs in the stainless grades 1.4301, 1.4401 or 1.4404, 1.4571, 1.4003 and 1.4462, for temperatures higher than 1039 ºC, 1100 ºC, 1126 ºC, 1019 ºC and 1026 ºC respectively. In Appendix A the values of equation (2.3) for the other stainless steel grades are presented.

Lower values for the reduction factors (relative to E_a), for the slope of the linear elastic range $E_{ct,\theta}$, were tested. The values were only changed for 1100 ºC and 1200 ºC (see Table 2.3 and Table 2.4). For 1200 ºC, the value of 0 for all stainless steel grades included in this study was considered. For 1100 ºC the values of 0.0124, 0.0165 and 0.0144 were considered for the stainless grades 1.4301, 1.4003 and 1.4462 respectively. Because of these temperatures magnitude and as observed in Figure 2.5, these changes in the stress-strain relationship are small and of no significant influence in the studies presented in this work.

This study was made for the lowest yield strengths proposed in part 1-4 of EC3, with the purpose of being on the safe side for other stainless steel grades. In Figure 2.5, obtained for the stainless steel grade 1.4301, a yield strength f_y equal to 190 MPa was used.

2.2.3 Thermal properties

Part 1-2 of EC3 (CEN, 2005b) also provides rules for the thermal properties of stainless steel. The thermal elongation of austenitic stainless steel $\Delta l/l$ is determined, varying with the steel temperature, according to the equation

$$\Delta l/l = \left(16 + 4.79\times10^{-3}\theta_a - 1.243\times10^{-6}\theta_a^2\right)\times\left(\theta_a - 20\right)10^{-6} \tag{2.4}$$

Although the thermal elongation is more a mechanical property than a thermal one, in EC3 it is classified as a thermal property.

Another thermal property that also varies with temperature is the specific heat. In order to determine the specific heat of stainless steel as a function of the temperature, part 1-2 of EC3 gives the following expression

$$c_a = 450 + 0.28\theta_a + 2.91\times10^{-4}\theta_a^2 + 1.34\times10^{-7}\theta_a^3 \tag{2.5}$$

Finally, the thermal conductivity of stainless steel is determined with the expression

$$\lambda_a = 14.6 + 1.27\times10^{-2}\theta_a \tag{2.6}$$

Graphical illustrations of these expressions are presented in section 2.3.2.

2.3 Comparison between stainless steel and carbon steel

In carbon steel, the yield strength f_y and the ultimate tensile strength f_u at room temperature, indicated in the EN 10025-2 (CEN, 2004a), are summarized in Table 2.5.

Table 2.5 – Nominal values of the yield strength and the ultimate tensile strength at ambient temperatures for flat and long products of carbon steel grades (CEN, 2004a).

Steel grade	t ≤ 16 mm		16 mm ≤ t ≤ 40 mm	
	f_y (MPa)	f_u (MPa)	f_y (MPa)	f_u (MPa)
S235	235	360	225	360
S275	275	430	265	430
S355	355	510	345	510

The values in Table 2.5 are characteristic values. The presented classification is referred in part 1-1 of EC3 (CEN, 2005a). The modulus of elasticity for the carbon steel is equal to 210 GPa. The yield strength values used in this study were the ones prescribed for the thickness of steel flat and long products, lower than 16 mm.

In this section the mechanical and thermal properties of carbon steel at high temperatures are presented, comparing them with the stainless steel material properties at high temperatures.

2.3.1 Mechanical properties

For high temperatures with heating rates between 2 and 50 ºC/min, the carbon steel mechanical properties of resistance and deformability can be obtained from the recommendations included in the part 1-2 of EC3 (CEN, 2005b). The parameters in Table 2.6 are the parameters involved in the determination of the carbon steel stress-strain relationship presented in Figure 2.7.

Table 2.6 – Expressions to determine the stress-strain relationship of the carbon steel at high temperatures.

Strain range	Stress σ	Tangent modulus
$\varepsilon \le \varepsilon_{p,\theta}$	$E_{a,\theta}\varepsilon$	$E_{a,\theta}$
$\varepsilon_{p,\theta} < \varepsilon < \varepsilon_{y,\theta}$	$f_{p,\theta} - c + (b/a)\left[a^2 - (\varepsilon_{y,\theta} - \varepsilon)^2\right]^{0.5}$	$\frac{b(\varepsilon_{y,\theta} - \varepsilon)}{a\left[a^2 - (\varepsilon_{y,\theta} - \varepsilon)^2\right]^{0.5}}$
$\varepsilon_{y,\theta} \le \varepsilon \le \varepsilon_{t,\theta}$	$f_{y,\theta}$	0.00
$\varepsilon_{t,\theta} < \varepsilon < \varepsilon_{u,\theta}$	$f_{y,\theta}\left[1 - (\varepsilon - \varepsilon_{t,\theta}) \Big/ (\varepsilon_{u,\theta} - \varepsilon_{t,\theta})\right]$	-
$\varepsilon = \varepsilon_{u,\theta}$	0.00	-
Parameters	$\varepsilon_{p,\theta} = f_{p,\theta}/E_{a,\theta}$ $\varepsilon_{y,\theta} = 0.02$	$\varepsilon_{t,\theta} = 0.15$ $\varepsilon_{u,\theta} = 0.20$
Functions	$a^2 = (\varepsilon_{y,\theta} - \varepsilon_{p,\theta})(\varepsilon_{y,\theta} - \varepsilon_{p,\theta} + c/E_{a,\theta})$ $b^2 = c(\varepsilon_{y,\theta} - \varepsilon_{p,\theta})E_{a,\theta} + c^2$ $c = \frac{(f_{y,\theta} - f_{p,\theta})^2}{(\varepsilon_{y,\theta} - \varepsilon_{p,\theta})E_{a,\theta} - 2(f_{y,\theta} - f_{p,\theta})}$	

In this stress-strain relationship four zones can be distinguished:

- the first is a linear zone until the proportional limit. This relation can be described by the Hooke law with the modulus of elasticity $E_{a,\theta}$;
- the second is a transition phase that follows the equation of an ellipse (Rubert and Schaumann, 1985) and stops at the yield strength, considered as the stress at 2 % of total strain. This phase corresponds to the beginning of the yielding;
- the third represents the yield (plastic zone), characterized by values of constant stresses equal to the yield strength;
- finally, the fourth zone corresponds to a linear decreasing branch, which was introduced to represent the softening of the steel and to achieve finite numerical ductility.

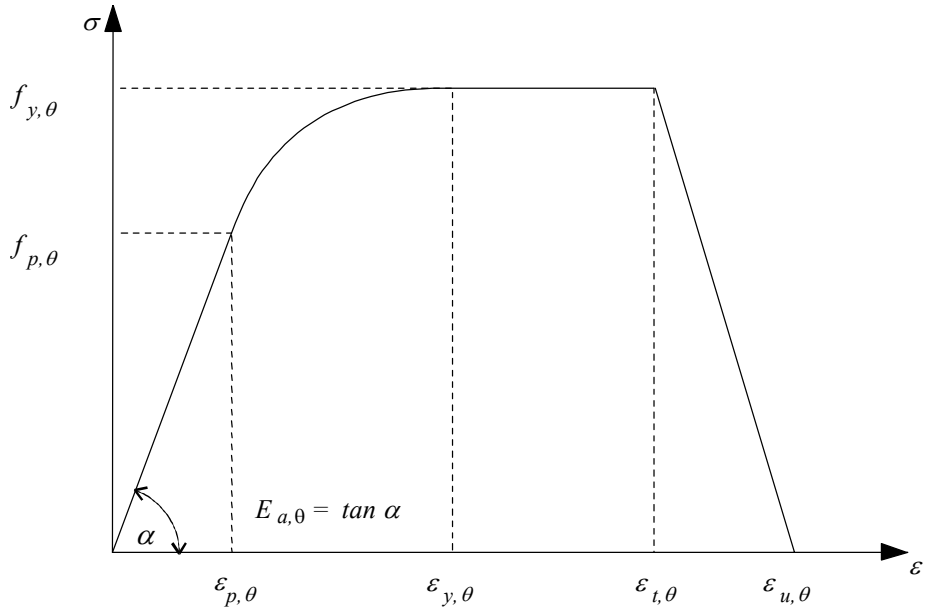

Figure 2.7 – Stress-strain relationship of the carbon steel at elevated temperatures.

As previously stated, the mechanical properties of steel, when subject to high temperatures, suffer significant reductions. Table 2.7 presents the reduction factors, of the carbon steel stress-strain relationship subject to high temperatures (proposed in CEN, 2005b).

Table 2.7 – Reduction factors of the carbon steel stress-strain relationship subject to high temperatures.

θ_a (ºC)	$k_{y,\theta}$	$k_{p,\theta}$	$k_{E,\theta}$
20	1.00	1.0000	1.0000
100	1.00	1.0000	1.0000
200	1.00	0.8070	0.9000
300	1.00	0.6130	0.8000
400	1.00	0.4200	0.7000
500	0.78	0.3600	0.6000
600	0.47	0.1800	0.3100
700	0.23	0.0750	0.1300
800	0.11	0.0500	0.0900
900	0.06	0.0375	0.0675
1000	0.04	0.0250	0.0450
1100	0.02	0.0125	0.0225
1200	0.00	0.0000	0.0000

With the referred reduction factors, the variation of the stress-strain relationship with the temperature can be obtained, as shown in Figure 2.8.

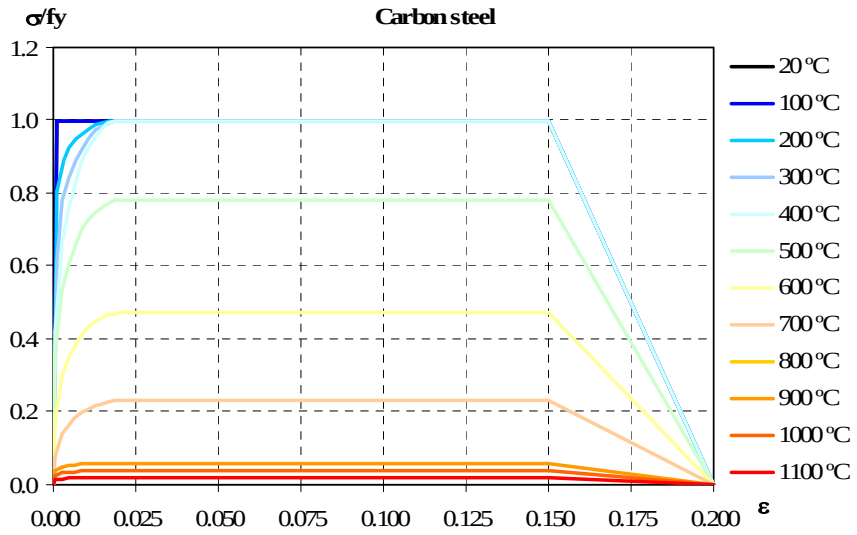

Figure 2.8 – Stress-strain relationship of the carbon steel in function of the temperature.

The effective yield strength, at high temperatures, is reduced in function of the yield strength at 20 ºC, multiplied by the factor $k_{y,\theta}$. The variation of this factor with the

temperature is presented in Figure 2.9. Analysing this figure, a big decrease of the reduction factor of the yield strength, for temperatures greater than 400 ºC, can be observed.

In Figure 2.9 it is possible to compare the yield strength reduction of carbon steel and of the different stainless steel grades at high temperatures.

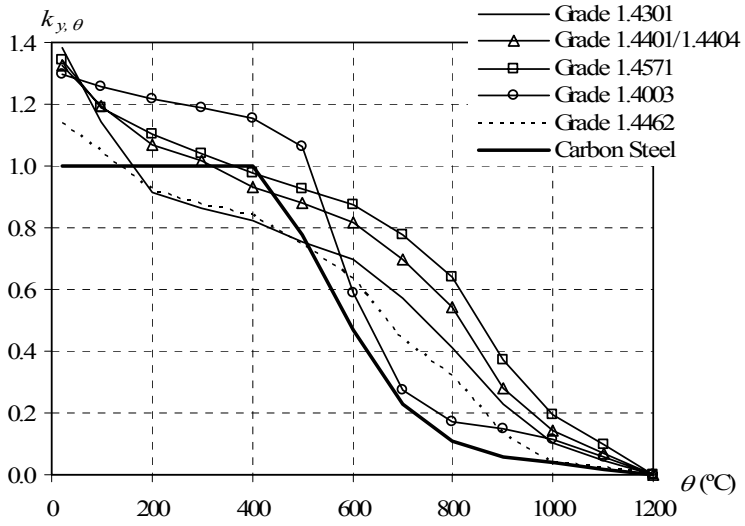

Figure 2.9 – Reduction factor of the yield strength of carbon steel and stainless steel.

The values of the yield strength reduction factor of the stainless steels can be higher than 1 (see Figure 2.9). This is due to the existing hardening in stainless steel, which is provided by the permanent non-linear pattern of its stress-strain relationship (not contemplated in the carbon steel stress-strain relationship from EC3). Figure 2.10 helps to understand this phenomenon. While, for carbon steel S235 the proportional limit stress $f_{proof,\theta}$ is equal to the stress at 2 % of total strain $f_{2\%,\theta}$ (with the value of 235 MPa), for stainless steel 1.4301 the proportional limit stress at 0.2 % $f_{0.2p,\theta}$ is equal to 210 MPa lower than the value of 291 MPa for $f_{2\%,\theta}$. This last stress is the one considered for the yield strength of stocky sections in fire situation.

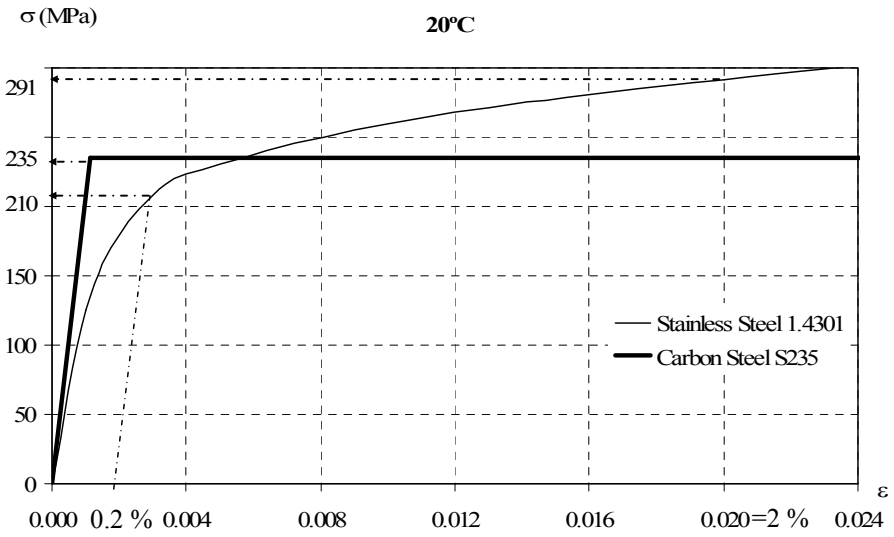

Figure 2.10 – Part of the stress-strain relationships from stainless steel 1.4301 and carbon steel S235.

As illustrated in Figure 2.11, the reduction of the stainless steel Young's modulus $E_{a,\theta}$, for temperatures up to 800 ºC is smaller than the one for carbon steel. From 800 ºC to 1200 ºC there is a bigger reduction of the stainless steel modulus of elasticity. This reduction is the same for all stainless steel grades.

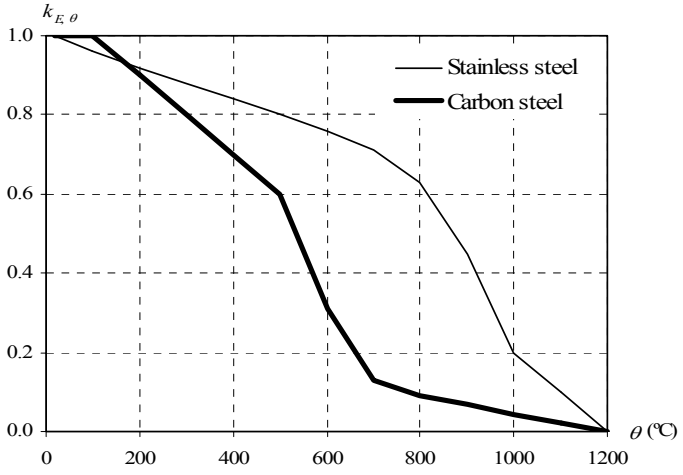

Figure 2.11 – Comparison of the modulus of elasticity reduction at high temperatures.

2.3.2 Thermal properties

For carbon steel, the thermal elongation $\Delta l/l$ is obtained by the following expressions:

- for steel temperatures between 20 ºC and 750 ºC

$$\Delta l/l = 1.2\times10^{-5}\theta_a + 0.4\times10^{-8}\theta_a^2 - 2.416\times10^{-4} \tag{2.7}$$

- for steel temperatures between 750 ºC and 860 ºC

$$\Delta l/l = 1.1\times10^{-2} \tag{2.8}$$

- and for steel temperatures between 860 ºC and 1200 ºC

$$\Delta l/l = 2\times10^{-5}\theta_a - 6.2\times10^{-3} \tag{2.9}$$

With these expressions Figure 2.12 is obtained, which compares the thermal elongation of stainless steel and carbon steel. A slightly higher thermal elongation in the stainless steel, for temperatures higher than 800 ºC, can be observed.

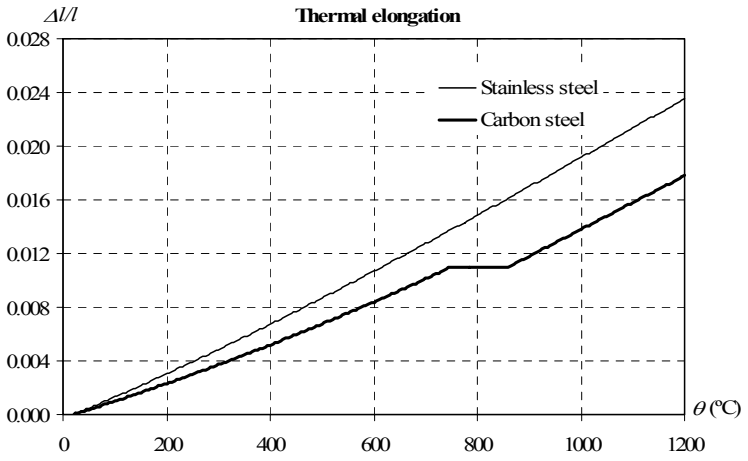

Figure 2.12 – Comparison of the thermal elongation in function of the temperature.

The specific heat in carbon steel is determined by the following expressions:

- for steel temperatures between 20 ºC and 600 ºC

$$c_a = 425 + 7.73\times10^{-1}\theta_a - 1.69\times10^{-3}\theta_a^2 + 2.22\times10^{-6}\theta_a^3 \tag{2.10}$$

- for steel temperatures between 600 ºC and 735 ºC

$$c_a = 666 + \frac{13002}{738 - \theta_a} \tag{2.11}$$

- for steel temperatures between 735 ºC and 900 ºC

$$c_a = 545 + \frac{17820}{\theta_a - 731} \tag{2.12}$$

- and for steel temperatures between 900 ºC and 1200 ºC

$$c_a = 650 \tag{2.13}$$

The main difference between the two materials is the existence of a peak of the carbon steel specific heat at temperatures of about 735 ºC. Figure 2.13 illustrates the variation of the specific heat with the steel temperature in both materials.

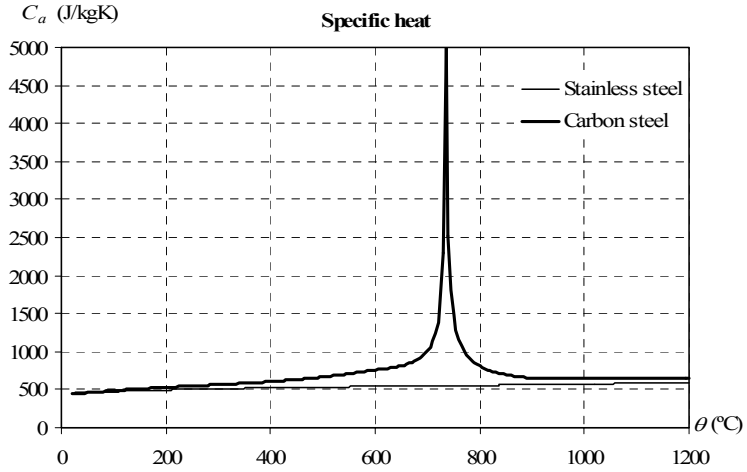

Figure 2.13 – Comparison of the specific heat in function of the temperature.

Finally, the thermal conductivity of the carbon steel also varies with the steel temperature according to the following expressions:

- for steel temperatures between 20 ºC and 800 ºC

$$\lambda_a = 54 - 3.33 \times 10^{-2} \theta_a \tag{2.14}$$

- for steel temperatures between 800 ºC and 1200 ºC

$$\lambda_a = 27.3 \tag{2.15}$$

Figure 2.14 displays the variation of the thermal conductivity with the steel temperature, where a higher thermal conductivity in the carbon steel, for temperatures lower than 800 ºC, can be observed.

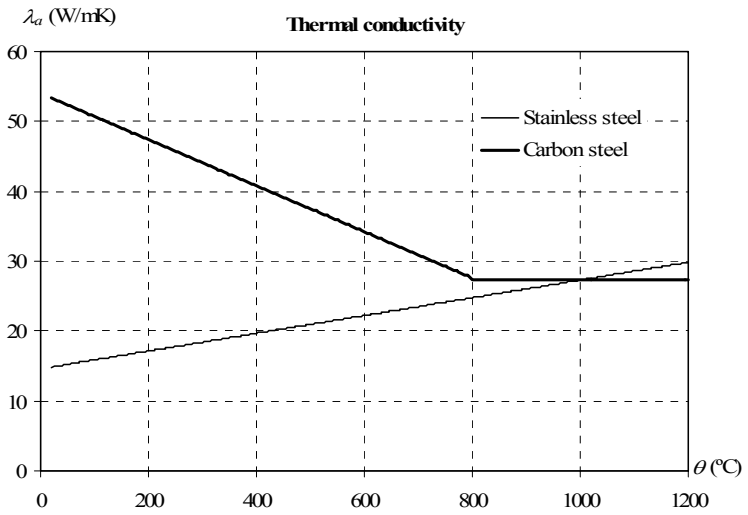

Figure 2.14 – Comparison of the thermal conductivity in function of the temperature.

Comparisons between the temperature evolution in carbon steel and stainless steel sections are shown in Chapter 7. It is shown that both materials have similar heating rates, when exposed to equal fire conditions. Only small differences appear in the range of 700 ºC to 800 ºC, due to the peak in the carbon steel specific heat (Figure 2.13).

2.4 Conclusions

This chapter presents a general overview on the characteristics of both stainless and carbon steel. It was shown that the stainless steel exhibits better thermal and mechanical properties when subjected to high temperatures. The biggest differences exist in the mechanical properties, where higher ductility and lower reductions of the yield strength and of the Young's modulus due to the temperature, for the case of the stainless steel, can be observed.

Moreover, the non-linear behaviour of the stainless steel stress-strain relationship enables considering higher yield strengths for low temperatures in case of fire when compared to the ones at cold design, because in fire situation the yield strength is the stress at 2 % of total strain instead of the proof strength at cold design.

Chapter 3

Numerical analysis

Chapter 3. Numerical analysis

Chapter 3. Numerical analysis

3.1 Introduction

The fire resistance analysis of structures can be performed using calculation programs with several complexity levels. These vary from programs based on simplified calculation methods (defined in Eurocodes), to the most complex ones, based in the finite element method, included in the advanced calculation methods (also mentioned in Eurocodes).

The existence of analysis models, based on the finite element method (Zienkiewicz and Morgan, 1983; Oñate, 1992), allows the reproduction of complex structural behaviours with material and geometric non-linearity. This powerful technique was developed for obtaining numerical solutions to complex problems in structural mechanics. In the finite element method, the structural system is modelled by a set of an appropriate discrete number of finite elements that are connected through points, called nodes. It will not be made, in this thesis, any description of this method due to the sufficient number of references on this subject (Piloto, 2000; Real, 2001; Boissonnade, 2002).

The software used in the numerical studies presented in this work is SAFIR (Franssen, 2008; 2005a). This program includes a model of finite elements, for the geometric and material non-linear analysis, especially developed in the University of Liege, Belgium, for the analysis of structures subjected to fire.

In this chapter, brief descriptions of the software SAFIR and used finite elements are presented. In the scope of this work it was necessary to introduce some modifications on SAFIR. Those modifications and their validation are also described in this chapter. Finally, a brief general description of the numerical models used throughout this thesis is presented.

3.2 The software SAFIR

In this section, a brief description, of the software SAFIR and of the necessary modifications introduced in it, is presented.

3.2.1 General description

As a finite element method program, SAFIR accommodates several types of elements, calculation procedures and material models to consider the stress-strain relationships. Truss (linear finite elements that only admit axial forces), beam (linear finite elements that admit axial forces, shear forces and bending moments), shell (plane finite elements) and solid elements are the types of finite elements included in this program. The carbon steel stress-strain relationship, contemplated in the program, is linear and elliptical, according to part 1-2 of the EC3.

The program SAFIR possesses two distinct calculation modules: one for the thermal behaviour analysis; and another one for the mechanical behaviour analysis of the structure. The non-uniform temperature evolution is calculated for each existing section type in the structure (thermal analysis). Subsequently, the mechanical module of the program reads these temperatures and determines the thermo-mechanical behaviour of the structure in an incremental analysis (structural analysis). An additional torsional analysis, prior to the mechanical analysis, is necessary for three-dimensional (3D) beam elements.

Excellent results of the several applications made with the program SAFIR have been observed. Comparisons between the numerical results achieved with the program SAFIR and experimental, numerical results from other programs (Lopes *et al.*, 2005; 2008b; Talamona, 1995) and theoretical solutions have been made.

In the work presented in this thesis only beam and shell finite elements were used, thus the following descriptions of the components of this software will focus on these two types of finite elements.

3.2.1.1 Thermal analysis

The thermal analysis is made using two-dimensional (2D) elements, to be used later on the cross-sections of beam elements or on the thickness of shell elements.

In beam elements the temperature distribution can be non-uniform in their section but with no heat transfer along their axis. Meaning, structures composed of sub-structures, with different cross-sections and/or different fire exposures, will require separate thermal analyses for each of those section types. The temperatures across the cross-section,

obtained from these analyses, are stored for subsequent structural analysis where these sections are present (Franssen, 2008).

The program considers the beam element constituted by fibres that correspond to the prolongation of the elements throughout the beam longitudinal axis. In any longitudinal integration point, all the variables (temperature, stresses and strains) are constant in each fibre, which allows the introduction of residual stresses and the possibility of introduction of pre-stressed materials in the structural elements. Those residual stresses are considered through initial strains that remain constant throughout the analysis (Franssen, 1989).

The bi-dimensional plane elements are linear and can have three (triangular element) or four nodes (quadrangular element). The cross-section used in this work was discretized using triangular and rectangular (bi-dimensional) elements, as illustrated in Figure 3.1.

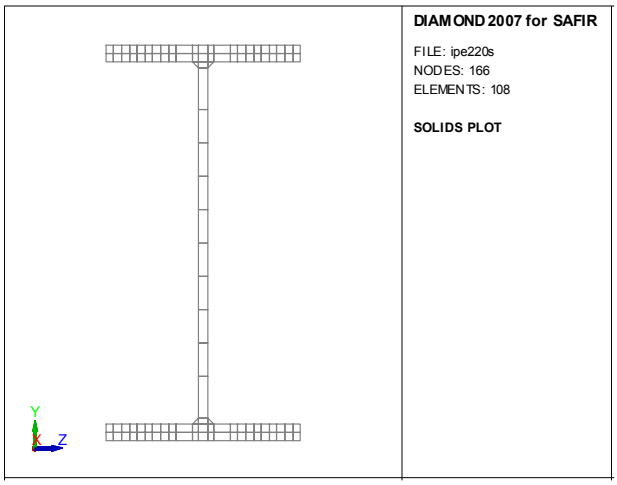

Figure 3.1 – Mesh of an I-cross-section.

In shell elements, the temperature distribution can be non-uniform across the thickness of the shell having no heat transfer in the plane of the shell. The number and the thickness of these elements are independent of the number and position of the integration points used in the structural analysis. In the structural analysis, the temperatures at the integration points are linearly interpolated from the temperatures of the nodes (Franssen, 2008).

The thermal analysis of the program SAFIR allows the use of any material, provided that its physical properties at high temperatures are known. The thermal properties already

implemented in SAFIR are the ones described in the Eurocodes. This analysis can also combine more than one material.

The temperature evolution in the profile is defined as a function of time. The format of this evolution can be defined through standard curves (for example the standard ISO 834 fire curve), proposed in the codes, or any other curve provided that it is conveniently defined by the user. The program SAFIR also allows the consideration of cooling phases.

With the purpose of making a direct comparison, between the obtained results in this work, with the program SAFIR and the simplified methods of the Eurocodes, the tests were made with uniform temperatures in the cross-section (except for the results obtained in the study of the structural global behaviour in case of fire, included in Chapter 7). Thus, the temperatures were imposed in each element of the section, such that all the section was subjected to the same temperature.

3.2.1.2 Torsional analysis

The program SAFIR is able to determine the torsional stiffness and the warping function of any cross-section, through the use of two-dimensional elements. In this program, the calculation of the torsional stiffness is made only in three-dimensional beam elements when subjected to non-uniform torsion. For these 3D beam elements, when the torsional stiffness is not available from tables or formulas it is necessary to determine it. This torsional analysis is an additional analysis that corresponds to a pre-processor to evaluate cross-sectional properties. In this analysis it is considered that the materials are in the elastic phase and at room temperature.

The obtained torsional stiffness has to be adjusted in order to account for the temperature and to reflect the decrease of the material stiffness with the increase of the temperature. Afterwards, the results are added to the ones obtained from the thermal analysis of the same cross-section for subsequent structural analysis. This torsional stiffness remains constant during the simulation of the mechanical behaviour.

In this thesis the torsional analyses were made in the study of the structural elements that were subjected to LTB.

3.2.1.3 Structural analysis

For the non-linear structural analysis, the following data are read from the input file: the temperature's time history; the torsional properties; and the section geometry (created during the previous thermal analysis, and later modified due to the section torsional analysis when necessary).

In this mechanical module truss elements (made of one single material with one uniform temperature per element), 2D and 3D beam elements, and shell elements are included. These last two elements allow the modelling of three-dimensional structures. Structures with oblique supports with any relative angle between the support and the global axis can also be analyzed. Figure 3.2 shows an example of a plane structure discretized in two-dimensional beam elements, submitted to distributed loads.

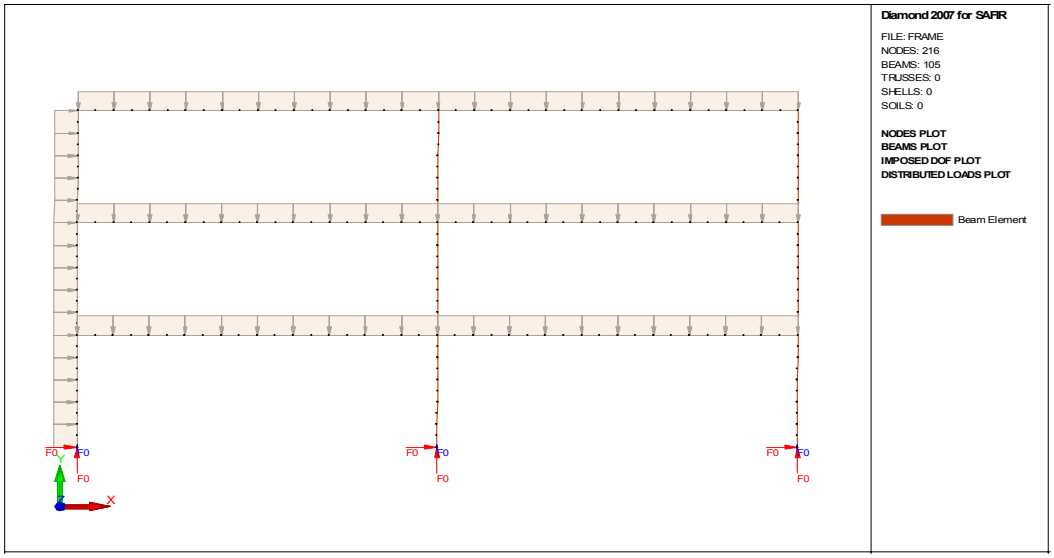

Figure 3.2 – Mesh of a structure.

The material behaviour in case of strain unloading is elastic, with equal elasticity modulus to the Young's modulus at the origin of the stress-strain relationship (Franssen, 1990).

An optimization of the stiffness matrix (in order to reduce the calculation time and the amount of information to be stored) is made by the program through a renumbering of the equations system. This renumbering can be verified by the user.

The calculation strategy is based on an incremental procedure (step by step), allowing to obtain, until failure of the structure the displacements at each node and the axial forces, shear forces, bending moments, strains, stresses and tangent modulus at the integration points of each finite element.

The non-linear stiffness matrix is evaluated, on each iteration of the convergence process, by the Newton-Raphson's method.

The truss, beam and shell finite elements allow the consideration of large displacements. In these finite elements the integration is numerically calculated through the Gauss's method. In this structural analysis it is possible to impose displacements. Also, the consideration of the effects of thermal strains can be accounted for.

In a static analysis, the failure criterion of a structure is defined as the instant when the stiffness matrix becomes not positive definite, thus becoming impossible to establish the equilibrium of the structure. However, in hyperstatic structures, failure in one element may not correspond to global failure of the structure. It is possible that, beyond local failure, part of the internal forces that can not be supported by the local element, are redistributed to other structural elements, leading to a new equilibrium position. In order to cope with this problem the program allows the use of the "arc-length" method. With this method, when an unstable situation occurs, the temperature remains constant and it is found another equilibrium point. But, it as been found that the "arc-length" method also fails in many cases (Franssen and Gens, 2004).

Thus, in SAFIR, it is possible to use a dynamic analysis (Franssen and Gens, 2004) to deal with the problem mentioned above. In this process, an acceleration term counterbalances the negative stiffness matrix, during the structural unstable states. Hence, it can handle local failure not endangering the safety of the whole structure.

In this dynamic process, the time step is automatically adapted when no convergence is obtained, by coming back to the previous converged point and trying again with a smaller time step. Finally, the structural calculation continues until the time step is smaller than the minimum time step (value defined by the user). The numerical results presented in this thesis were obtained with this dynamic analysis.

3.2.1.3.1 Beam finite elements

The beam finite element is based in the Bernoulli hypothesis, where plane sections before bending deformation remain plane after deformation and the effect of the shear deformation is not considered. On the other hand, this element does not take into account local buckling phenomena, therefore it should only be used with Class 1 and Class 2 sections profiles, as defined in EC3 (CEN, 2005a). The forming of plastic hinges is only considered in the longitudinal direction of the member, meaning as mentioned before, that uni-axial constitutive models are used.

The existing axial deformations are considered small, meaning that

$$\frac{\partial u}{\partial x} << 1 \tag{3.1}$$

where u is the longitudinal displacement and x the longitudinal position.

It is also assumed that the rotations are small, except the one that is verified around beam axis, which means that the approximations in expression (3.2) can be used where ϕ represents the angle formed by the deformed tangent of the beam and its initial position.

$$sen\phi \cong \phi \quad \text{and} \quad \cos\phi \cong 1 \tag{3.2}$$

The geometry of a cross-section is described with a fibre model. These small fibres can be triangles or quadrilaterals. The material behaviour of each fibre is calculated at the centre of the fibre, being constant for the whole fibre. Each fibre may have its own material, making possible the use of composite sections made of different materials.

In this fibre model in each fibre the temperature, the stress, the strain and other material properties are considered constant. The beam element with the fibre model allows the consideration of residual stresses, which are considered through the introduction of initial strains (Franssen, 1989).

The program SAFIR contemplates two different beam finite element types, one two-dimensional and another three-dimensional.

The two-dimensional beam finite element has its deformed shape described by the displacements of the three nodes illustrated in Figure 3.3. Two of these nodes have in the element extremities three degrees of freedom each, two displacements and one rotation.

The third node is placed in the centre of the element and has only one degree of freedom, which represents the non-linear part of the longitudinal displacement (Boreave, 1991).

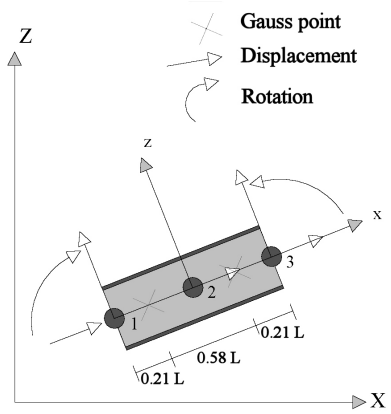

Figure 3.3 – 2D beam finite element.

The three-dimensional beam finite element possess two nodes in his extremities with seven degrees of freedom each, three displacements, three rotations and one warping amplitude, allowing to consider non-uniform torsion. The third node is in the centre of the element length and has only one degree of freedom representing the non-linear part of the longitudinal displacement. The three-dimensional beam element is illustrated in Figure 3.4. One fourth node is considered to define the position of the z local axis. This axis is perpendicular to the x axis, and is situated in a plan defined by x axis and the fourth node.

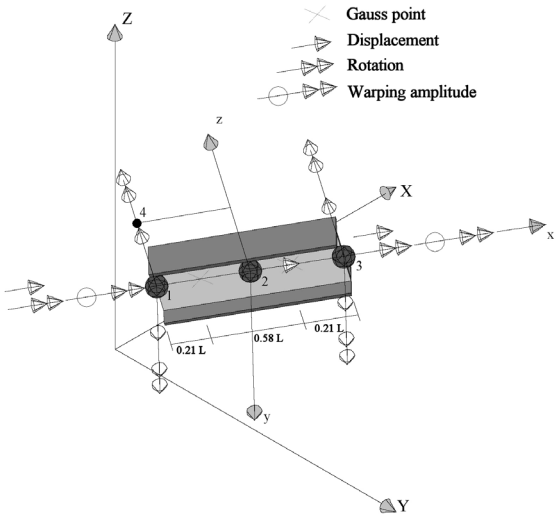

Figure 3.4 – 3D beam finite element.

The hypotheses and formulations previously presented apply for the bi-dimensional beam element and for the three-dimensional element. The main difference between these elements is the number of degrees of freedom in its nodes.

In this thesis three-dimensional beam elements were used to model beams with LTB, which can buckle in the perpendicular direction of the beam plane $x0z$. With these three-dimensional elements the flexural buckling could happen in the two possible directions (around the beam weak axis or/and around the beam strong axis). On the other hand, the choice of the bi-dimensional beam element instead of the three-dimensional one, is based on considering only flexural buckling in relation to one of the element axis and also because the considered loading and corresponded deformed shape belong to the beam plane.

3.2.1.3.2 Shell finite element

The use of finite shell elements is the most precise method when studying the behaviour of thin-walled structural elements. To model thin-walled members SAFIR has a shell element based in the Kirchhoff bending theory.

Shell elements are characterized by their capacity to combine a state of bending resistance with an axial force state resistance in the middle of the surface (designated as membrane state). In these shell elements plane constitutive models are used.

The shell element in SAFIR has four integration points on the surface of the element (see Figure 3.5). In each direction, the integration is made by the gauss method. The number of layers, with integration points, on the thickness can be from a minimum of two until a maximum of nine. It has four nodes with six degrees of freedom each: three displacements and three rotations.

The shell element from SAFIR is programmed to be used in large displacements in the plane stress state. This finite element was first introduced for elastic materials and then for two elastic-plastic material laws: one for carbon steel, and the other for concrete (Doneux and Franssen, 2003). In this work the possibility of dealing with stainless steel was introduced.

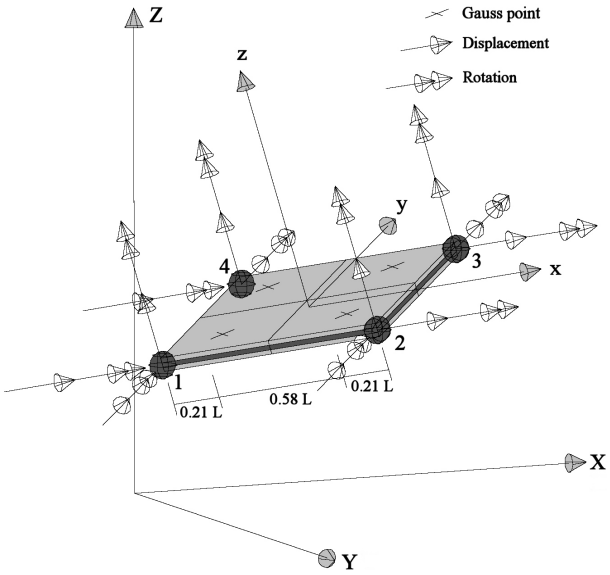

Figure 3.5 – Shell finite element.

3.2.1.3.3Global structural analysis in case of fire

In fire safety engineering it is possible to use global structural analysis by applying advanced calculation models. This allows a better understanding of the behaviour of the global structure in case of fire.

In structural analysis of steel structures, the strain of any element exposed to fire is composed of several components, given by

$$\varepsilon_t = \varepsilon_{th} + \left(\varepsilon_\sigma + \varepsilon_c\right) + \varepsilon_{res} \tag{3.3}$$

where ε_t is the total strain, ε_{th} is the strain due to thermal elongation, ε_σ is the strain due to stress, ε_c is the strain due to creep effect at elevated temperatures and ε_{res} is the strain due to residual stress. In steel the creep effect is already implicitly taken into account in its constitutive law.

In a structure subjected to fire, the material properties are constantly changing due to the temperature field, of the structural elements, variation with time. This material behaviour is taken into account in kinematical material models.

In the steel kinematical model (Figure 3.6), the value of the plastic strain remains constant in the shift of the stress-strain curve caused by the temperature evolution. This happens both in compression or tension.

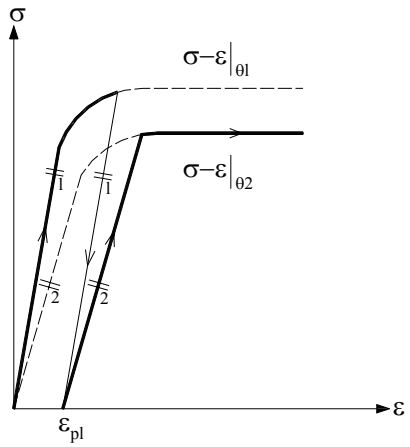

Figure 3.6 – Steel kinematical material model to account the temperature evolution.

The fire analysis is non-linear elastic-plastic having non-linear behaviour of the strength and stiffness, due to the existence of large displacements that occur with the material softening and thermal expansion. To get the equilibrium state of the structure under different temperature fields a step by step analysis is required in which, for each time step, an iterative solution procedure is needed to obtain the equilibrium state.

3.2.2 Software development

In order to make the studies presented in this thesis (with stainless steel structural elements) it was necessary to introduce some modifications in the program SAFIR. The changes were: the introduction of the stainless steel thermal and mechanical properties varying with the temperature according to EC3 (2005b) and described in Chapter 2; and the implementation of a module allowing the program SAFIR to account for residual stresses in shell elements both in elastic materials and stainless steel.

The stainless steel thermal properties (varying with the temperature) introduced in SAFIR were: the thermal elongation; the specific heat and the thermal conductivity.

The stainless steel mechanical properties were introduced in a one-dimensional constitutive model (used on the truss and beam finite elements) and a two-dimensional constitutive model (used on the shell finite elements).

3.2.2.1 Introduction of one-dimensional mechanical properties of stainless steel

As described in the Chapter 2, EC3 (CEN, 2005b) provides the stainless steel mechanical properties in function of the temperature. Those stress-strain relationships in case of fire are different for each stainless steel grade (1.4301, 1.4401 or 1.4404, 1.4571, 1.4462 and 1.4003). In SAFIR, they are designated as SLS1.4301, SLS1.4401, SLS1.4404, SLS1.4571, SLS1.4462 and SLS1.4003, as a function of the corresponding grade.

To take into consideration unloading effects, the rule of Masing (Masing, 1926) was implemented, similarly to the way it was introduced for the carbon steel model in SAFIR (Franssen, 1990). The difference lies in the stainless steel not having an initial linear phase (see Figure 3.7).

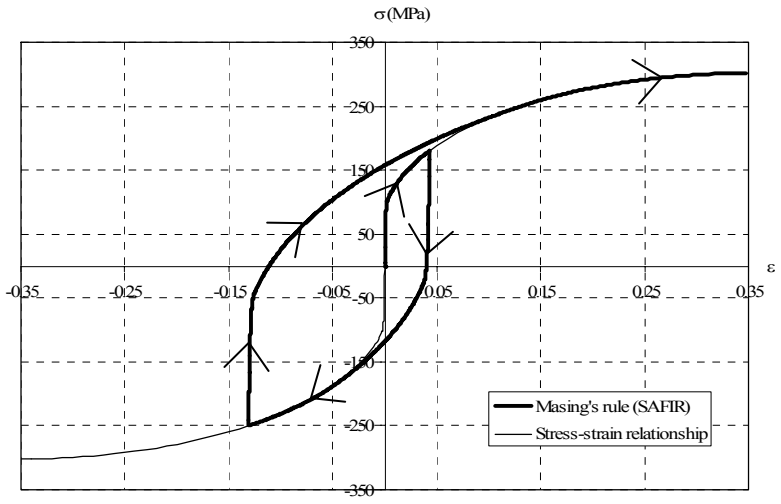

Figure 3.7 – Masing's rule in stainless steel grade 1.4301 at 600 ºC.

As for carbon steel, in cyclic loading with decreasing stress levels, the implemented algorithm does not cope with the rule of Masing. However, this case is not common on buildings structures submitted to heating.

In SAFIR, as mentioned in the section 3.2.1.3.3, the consideration of the residual stresses is made through the introduction of residual strains (Franssen, 1993). Due to the always non-linear behaviour of the stainless steel constitutive law it was necessary to implement a simple procedure, using the Newton Rapshon's method, for the determination of the strains corresponding to the residual stresses to be introduced.

3.2.2.2 Introduction of two-dimensional mechanical properties of stainless steel

The changes made on SAFIR, in order to deal with stainless steel two-dimensional material law in the elasto-plastic plane stress state, were performed with the purpose of using shell elements in the numerical simulations of thin-walled stainless steel structural elements.

The modelling of the material stainless steel was made by a non-elastic plane stress state based on the von Mises surface and on isotropic hardening. The constitutive law of the stainless steel has a permanent non-linear behaviour.

A material model developed following the classical plasticity theory is characterized by three basic functions: the initial yield surface, the hardening rule and the flow rule. The initial yield surface defines the stress level from which plastic deformations exist. The hardening rule governs the evolution of the loading surfaces during the plastic deformation. The flow rule defines the amplitude of the plastic deformation increment and its direction (Doneux and Franssen, 2003).

For the stainless steel, the same formulation as in the carbon steel (Doneux and Franssen, 2003; Talamona and Franssen, 2000) was used. However, due to the different stress-strain relationship, it was necessary to achieve a different hardening rule for the stainless steel. The stainless steel stress-strain relationship at high temperatures used in this work was based on the one prescribed in part 1-2 of EC3 (CEN, 2005b), as mentioned in the previous section, given by the function $\sigma = f(\varepsilon)$.

As described in Chapter 2, in the stainless steel stress-strain relationship two non-linear zones can be distinguished. Firstly, until the proportional limit $\varepsilon < \varepsilon_{c,\theta}$ and secondly, until the ultimate tensile strength $\varepsilon_{c,\theta} < \varepsilon < \varepsilon_{u,\theta}$.

The hardening rule $\tau = g(k)$ can be obtained using $\varepsilon = k + \sigma/E$ and making $\tau = \sigma$ (see Figure 3.8).

For the second branch ($\varepsilon_{c,\theta} < \varepsilon < \varepsilon_{u,\theta}$) it was possible to use this process to achieve the hardening rule, but for $\varepsilon < \varepsilon_{c,\theta}$ the equation $\sigma = E\varepsilon/(1 + a\varepsilon^b)$ did not allow this conversion. Therefore equation (3.4), which approximates the hardening function for the first branch of the stainless steel constitutive law, was developed.

$$\tau = bk^2 + ck + d + a\sqrt{k} \tag{3.4}$$

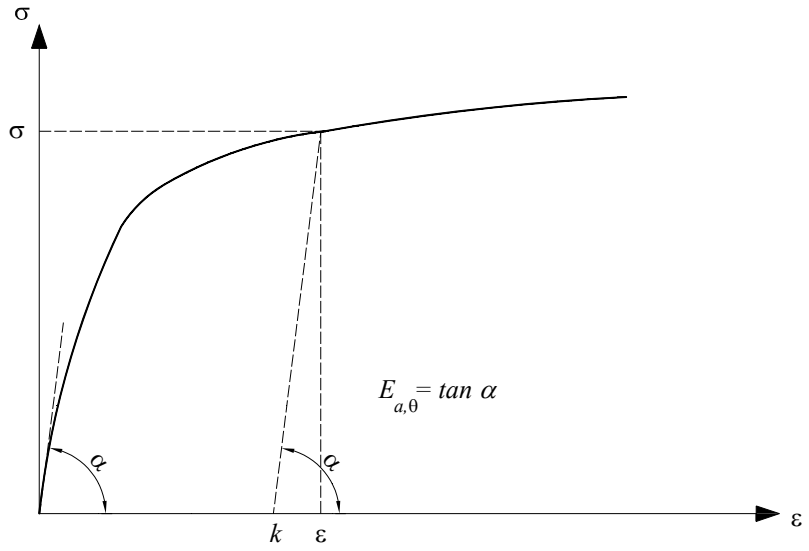

Figure 3.8 – Determination of the hardening rule.

In order to evaluate the parameters a, b, c and d in equation (3.4) the following boundary conditions were used

$$\begin{cases} \tau(0) = 0.001 f_{0.2p,\theta} \\ \tau(0.002) = f_{0.2p,\theta} \\ \dfrac{\partial \tau}{\partial k}(0.002) = H \\ \dfrac{\partial g}{\partial k}(M) = 0 \end{cases} \tag{3.5}$$

where

$$g = \frac{\partial \tau}{\partial k} = c + \frac{a}{2\sqrt{k}} + 2bk \tag{3.6}$$

and H is the value of $\partial\tau/\partial k\,(0.002)$ in the second branch that is known, guarantying the continuity of the derivative of the hardening function.

Finally, the $\partial g/\partial k\,(M) = 0$ with $M = 0.0023$ was used with the purpose of having a minimum value of g with this approximated function outside the interval $k < 0.002$. This means that the slope of this function will always be descending. Other values of M were tested, being 0.0023 the one that presented the best approximation to the stress-strain relationship in EC3.

The parameters a, b, c and d were thus obtained imposing that the equation (3.4) should satisfy the "real" hardening rule boundary conditions, resulting in

$$\begin{cases} a = 56.0362 f_{0.2p,\theta} - 0.112H \\ b = 63501.9 f_{0.2p,\theta} - 127.1H \\ c = -880.512 f_{0.2p,\theta} + 2.763H \\ d = 0.001 f_{0.2p,\theta} \end{cases} \tag{3.7}$$

Figure 3.9 shows a comparison between the stress-strain relationship obtained with EC3 and with the approximation given by equation (3.4), for stainless steel grade 1.4301 at 600 ºC.

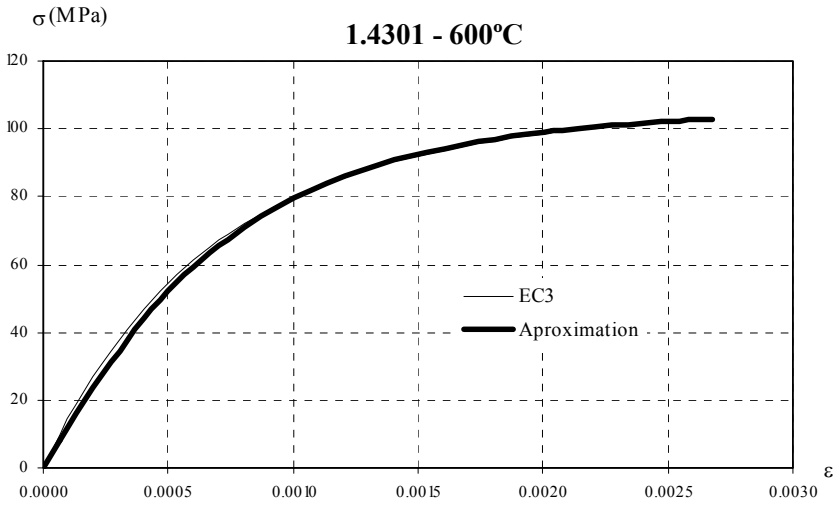

Figure 3.9 – Stainless steel constitutive law: comparison between the approximation used for 2D analysis and the EC3 at 600 ºC, for the stainless steel grade 1.4301.

Figure 3.10 shows, for the stainless steel 1.4301, the average difference (error) in percentage, obtained between the EC3 and the approximation proposed here, for a wide set of comparisons equally divided within the interval, using the expression

$$\frac{\sigma_{EC3} - \sigma_{Aproximation}}{\sigma_{Aproximation}} \tag{3.8}$$

Figure 3.9 and Figure 3.10 show the results for the stainless steel grade 1.4301. Results for other stainless steel grades can be found in Appendix B. Similar results were achieved for the other stainless steel grades. From these analyses, it is concluded that the differences are

small, being of bigger value in small stresses levels. Therefore, this approximation was introduced in SAFIR and used in this thesis.

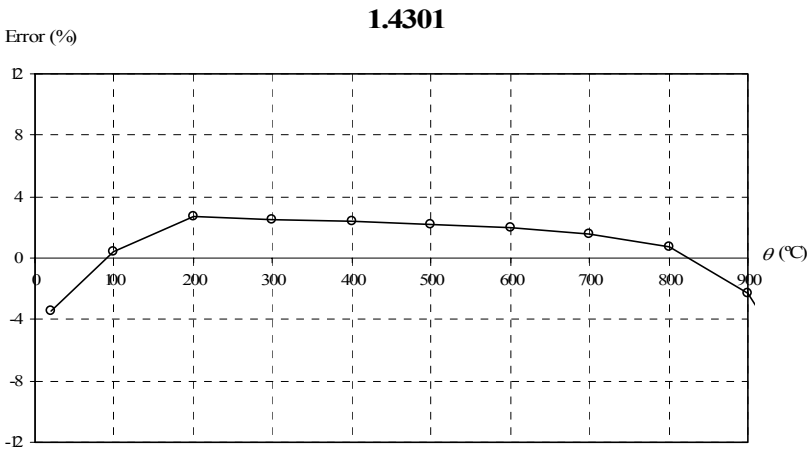

Figure 3.10 – Average error between the approximation used for 2D analysis and the EC3, for the stainless steel grade 1.4301.

Finally, the introduced grades were the same presented for uni-dimensional state in the previous section, which are designated in SAFIR as SS1.43012D, SS1.44012D, SS1.44042D, SS1.45712D, SS1.44622D and SS1.40032D, in function of the corresponding grade.

3.2.2.3 Consideration of residual stresses in shell elements

In order to enable the possibility of SAFIR accounting for residual stresses it is first necessary to transform them into residual strains and then add them to the other initial strains.

Due to this procedure the methodology to be adopted for the consideration of the residual stresses depends on the linearity or non-linearity of the material stress-strain relationship. Therefore, the introduction of this consideration was made for all the materials that have a first elastic phase in its material behaviour and provided that the residual stresses are always in that elastic phase, which is not the case for stainless steel.

As the stainless steel has a non-linear stress-strain relationship, another procedure was used. For inelastic materials, as it is the case of stainless steel, plastic strains, corresponding to the residual stresses (as shown in Figure 3.11) must be evaluated according to:

$$\varepsilon_{res} = \varepsilon_{res}^{el} + \varepsilon_{res}^{pl} = \frac{\sigma_{res}}{E_0} + \varepsilon_{res}^{pl} \tag{3.9}$$

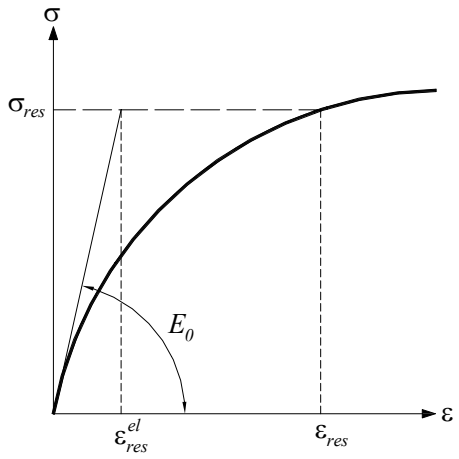

Figure 3.11 – Consideration of residual strains in non-linear constitutive laws.

This procedure begins with the determination of a von Mises "comparison stress" (3.10) of the residual stresses introduced.

$$\sigma_{c,res} = \sqrt{\sigma_{x,res}^2 - \sigma_{x,res}\sigma_{y,res} + \sigma_{y,res}^2 + 3\tau_{xy,res}} \tag{3.10}$$

With this "comparison stress" and with the constitutive law it is possible, using the Newton-Raphson's method, to achieve a residual "comparison strain". Moreover, due to the fact that it was used in SAFIR an approximation to the hardening law of the stainless steel (as explained in the previous section of this thesis), this approximation of the hardening law was also used to determine the residual "comparison strain".

With the comparison residual strain and with the comparison residual stress it is possible to determine a secant modulus $E_{\sec} = \sigma_{c,res} / \varepsilon_{c,res}$. This modulus is then used in the elasticity matrix $[D]$ necessary to evaluate the residual strains

$$\{\varepsilon_{res}\} = [D]^{-1} \cdot \{\sigma_{res}\} \tag{3.11}$$

In a similar way, in the software ABAQUS (Hibbitt, Karlsson & Sorensen, Inc., 2004) in non-linear stress-strain relationships, the residual stresses should be introduced by means of subroutines which consider the resulted plastic strains (Jandera *et al.*, 2008).

With the implemented procedure in SAFIR, the obtained residual stresses are similar to the ones introduced by the user. Figure 3.12 compares introduced and obtained principal stresses, for comparison stresses of 50 MPa and 210 MPa.

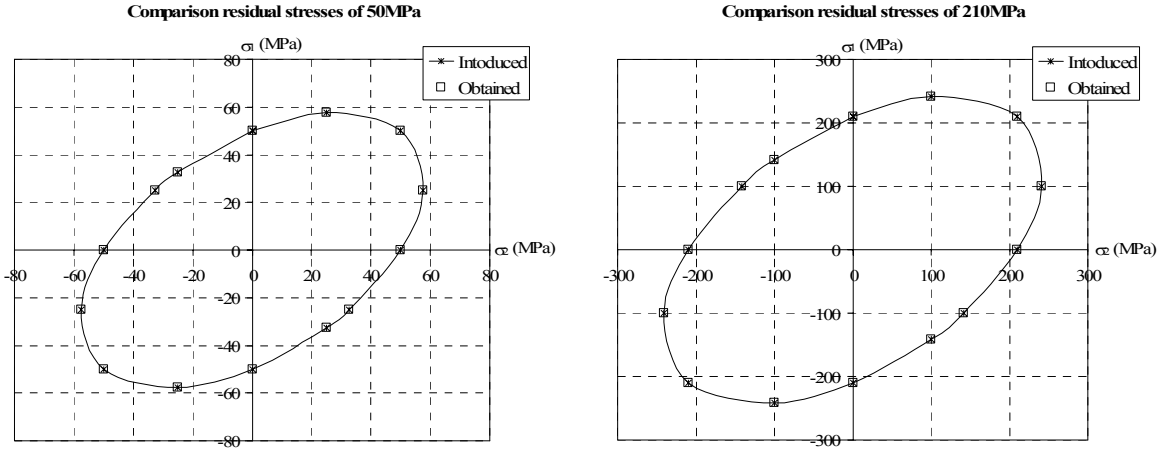

Figure 3.12 – Comparison between introduced residual stresses and obtained ones with the implemented procedure.

As mentioned before, in SAFIR each shell element can have from two to nine layers and in each layer there are four integration Gauss points. Therefore, the three residual stresses $\sigma_{x,res}$, $\sigma_{y,res}$ and $\tau_{xy,res}$ are introduced four times the number of layers for each shell element. In order to provide a faster introduction of the residual stresses, a methodology in which repeated residual stresses do not need to be written again was developed. Instructions to the introduction of these residual stresses in SAFIR are given in Appendix C.

3.3 Numerical models

In this section an explanation of the numerical models used in this thesis and the validation of the modifications introduced in SAFIR are presented.

3.3.1 General description

Several numerical models were used in this thesis. Here, those models are briefly presented in function of the study. Further information and more precise descriptions, related to the numerical models, are given in the corresponding study description.

Some of the assumptions taken into consideration in the choice of the numerical models were: the symmetry conditions applied in order to reduce the size of the domain; the element mesh was refined in order to have acceptable accuracy (for higher accuracy, smaller elements were used over the parts of higher stress gradient); and appropriate support constraints were imposed.

Here, the study cases used in isolated stocky (Class 1 and 2) cross-section elements are presented. Table 3.1 summarises the studied different stocky elements in this thesis, presenting the corresponded sections, where they are used to evaluate the EC3 design prescriptions or to develop new design proposals.

Table 3.1 – Position of the studied different stocky elements in this thesis.

Case studies			Room temperature		High temperatures	
			EC3 evaluation	Proposal development	EC3 evaluation	Proposal development
Stainless steel	Columns		4.2.1	5.2.1	4.3.1	5.3.1
	Beams		4.2.2	5.2.2	4.3.2	5.3.2
	Beam-columns	Without LTB	4.2.3.1	5.2.3.1	4.3.3.1	5.3.3.1
		With LTB	4.2.3.2	5.2.3.2	4.3.3.2	5.3.3.2
Carbon steel	Beams		4.3.4.2.1	-	4.3.4.2.2	4.3.4.3

The numerical models used in the study of thin-walled stainless steel structural elements in case of fire and of the global behaviour of stainless steel structures in case of fire can be found in the Chapter 6 and 7 respectively.

In the numerical simulations, a lateral geometric imperfection given by the following expression was considered (CEN, 2005c):

$$y(x) = \frac{L}{1000}\sin\left(\frac{\pi x}{L}\right) \tag{3.12}$$

where L is the length of the structural element. This global imperfection was imposed in function of the study case in the plane x0y or in the plane x0z.

The lengths used in this work were chosen in order to have slenderness values up to two (0.5, 1, 2, 3, 4, 5, 6, 7, 8, 10, 12, 14 and 20 m).

It was necessary to adopt different mesh sizes within the same structural element having small finite elements in the maximum bending moment values positions. This was made with the purpose of having the integration Gauss's points catching those moments, and thus the obtained results could correspond the closest possible to the failure moments of the structural element. Therefore, these different mesh sizes resulted from parametric studies that depended on the loading type introduced in the structural element.

The supports were simulated with restrictions in the extremities nodes. In the cases where the three-dimensional finite beam element was used an extremity simulated a simple support (displacements restrictions in the axis y and z, and rotation restriction around the axis x), and in the other extremity a fixed support was simulated (displacements restrictions in the axis x, y and z, and rotation restriction around the axis x). These supports are typically named fork supports.

In the cases where the two-dimensional finite beam element was used, it was constrained the displacements in the axis z and x for the fixed support, and only the axis z in the simple support, when studying only the flexural buckling around the section strong axis. When studying only the flexural buckling around the section weak axis the restriction in the axis z moved to the axis y.

For the tests at high temperatures a uniform temperature distribution in the cross-section was used, so that comparison between the numerical results and the Eurocode simple design equations could be possible. In this thesis, the temperatures chosen for columns and beams were 400, 500, 600 and 700 ºC, deemed to cover the majority of practical situations. For beam-columns, temperatures of 600 ºC were used.

In the numerical models, used to study the LTB in carbon steel elements at high temperatures, the hot rolled and equivalent welded cross-sections HEA500, IPE220 and IPE500 (ArcelorMittal, 2008), of the carbon steel grades S235, S355 and S460 were used. The rounding, between the flanges and the web, in the hot rolled sections was considered in SAFIR using the nominal cross-sections from tables, making the rounding area equal to the area of an equivalent triangle.

For hot rolled sections, a triangular distribution for the residual stresses with a maximum value of $0.3 \times 235\,\text{MPa}$ (ECCS, 1984) was chosen (see Figure 3.13). For the welded sections, the distribution used has the maximum value of the yield strength (Chen and Lui, 1991), as shown in Figure 3.14.

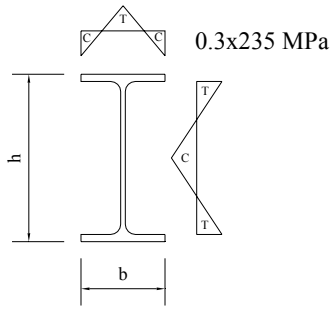

Figure 3.13 – Residual stresses in I-hot rolled sections (C – compression; T – tension).

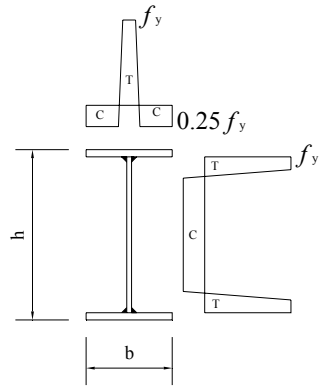

Figure 3.14 – Residual stresses in I-welded sections (C – compression; T – tension).

These adopted residual stresses were considered constant across the thickness of the web and flanges.

In the numerical models, used to study stainless steel structural elements at both ambient temperature and high temperatures, the equivalent welded cross-sections HEA200, HEA500, HEB200, HEB280, IPE220 and IPE500 (Millstock Stainless, 2008), of the stainless steel grades 1.4301, 1.4401 or 1.4004, 1.4571, 1.4003 and 1.4462 were used.

For the stainless steel sections, the used residual stresses distribution, having the maximum value of the yield strength, is similar to the one used for the welded carbon steel

sections (Chen and Lui, 1991; Gardner and Nethercot, 2004; Greiner *et al.*, 2005), as shown in Figure 3.14.

In the cases with out-of-plane buckling, an initial rotation around the x axis with a maximum value of $L/1000$ radians at mid span (Figure 3.15) was considered. For evaluating the influence of this imperfection, Table 3.2 shows the results for an IPE500 of a 10 m length simply supported beam, with uniform bending moment, of the stainless steel grade 1.4301 at 20 ºC and 600 ºC. The global lateral geometric imperfection is given by expression (3.12) and the residual stresses presented in Figure 3.14.

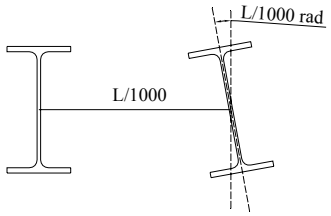

Figure 3.15 – An initial rotation around the longitudinal axis at mid span.

As it can be seen in Table 3.2 the failure bending moments are rather similar. In this table -L/1000 corresponds to a rotation in the opposite sense to the one considered in the numerical studies and presented in Figure 3.15.

Table 3.2 – Results with and without the initial rotation.

Rotation	20 ºC	600 ºC
-L/1000	127.3 kNm	84.2 kNm
0	128.9 kNm	85.6 kNm
L/1000	130.3 kNm	86.3 kNm

3.3.2Validation of the software development

In this section the developments made in SAFIR, presented in section 3.2.2 of this thesis are analysed. Here are shown some comparisons made between some results obtained with SAFIR and with ANSYS (Ansys, Inc., 2006). Also some experimental results are used in this study.

3.3.2.1 Introduction of one-dimensional mechanical properties of the stainless steels

In this section different results for a steel hollow section (SHS) are compared. The same Class 1 hollow section SHS40x40x4 used by Ala-Outinen and Oksanen (1997) to make experimental tests on stainless steel columns in case of fire, has been used. The round corners were not considered in the finite element mesh used to discretize the cross-section.

In the numerical simulations, a lateral geometric imperfection given by expression (3.12) was considered, and no residual stresses were introduced in these first simulations.

According to EC3, the yield strength and the ultimate strength considered were 210 MPa and 520 MPa respectively. The increasing of the yield strength in the corner regions wasn't considered. The comparisons were made with uniform temperature in the cross-section.

Figure 3.16 shows the results obtained for different temperatures using the beam finite elements from SAFIR and from ANSYS. These results are compared with the EC3, denoted "EN 1993-1-2" (as described in Chapter 4).

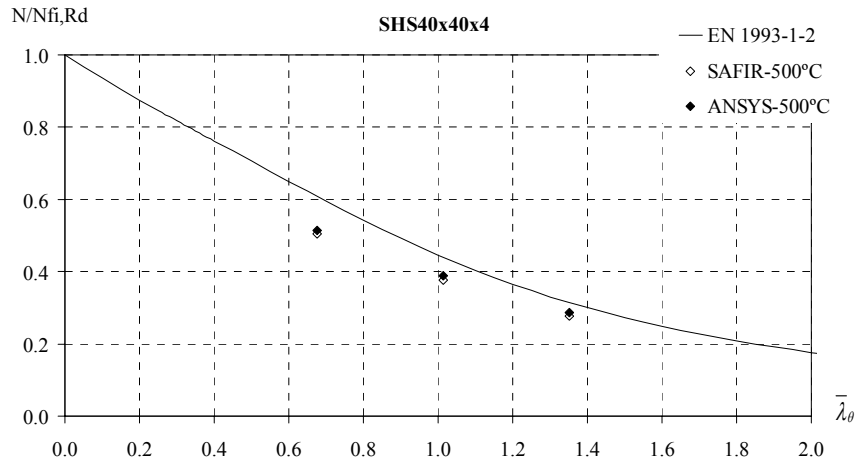

Figure 3.16 – SHS40x40x4 numerical results using beam finite elements.

From the figure, it can be observed that the uni-axial stress-strain relationship was well established in SAFIR.

3.3.2.2 Introduction of two-dimensional mechanical properties of the stainless steels

In this section the results obtained with the shell finite elements of SAFIR are compared with results using the 3D beam finite element of SAFIR and with some experimental tests made by (Ala-Outinen and Oksanen, 1997).

Here, the approximation to the stainless steel hardening law described in section 3.2.2.2 is tested. These comparisons are made for elements with Class 1 sections.

The yield strength and the ultimate strength measured in the experimental tests in (Ala-Outinen and Oksanen, 1997) have the value of 595 MPa and 736 MPa respectively, therefore these were the values considered in the results presented in Figure 3.17. The load level, the length and the support conditions of the simulations with SAFIR are the same used in the experimental tests. In the Figure 3.17 “Outinen tests” correspond to the experimental tests, “Outinen tests SAFIR B” are the simulations of the experimental tests with the beam elements from SAFIR and “Outinen tests SAFIR S” are the simulations of the experimental test with the shell elements from SAFIR (see Figure 3.18).

In the numerical simulations, a lateral geometric imperfection given by expression (3.12) was considered, and no residual stresses were introduced in these simulations.

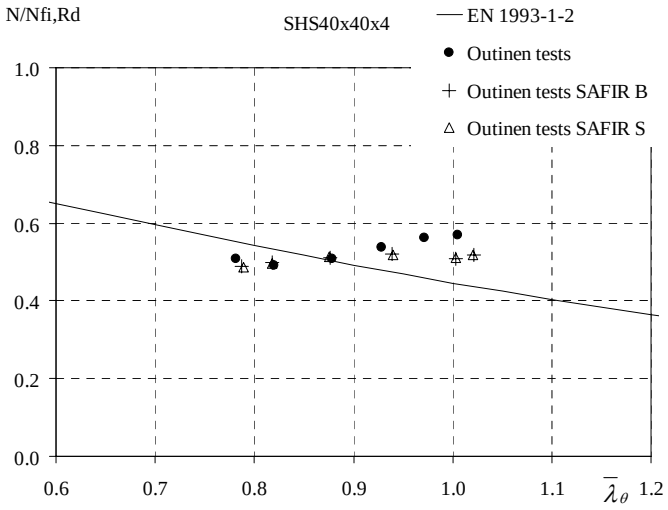

Figure 3.17 – SHS40x40x4 numerical results with SAFIR using beam and shell finite elements compared with the experimental tests.

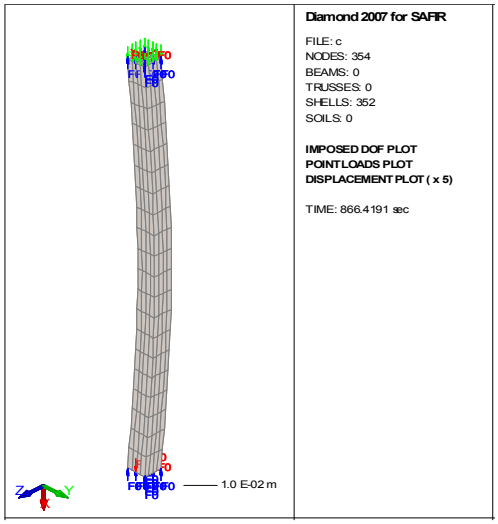

Figure 3.18 – SHS40x40x4 column simulated with shell elements.

From Figure 3.17 it can be concluded that the results obtained with the shell element from SAFIR, using an approximation to the hardening rule, are in good agreement with the experimental tests and with the results using the beam finite elements. More results showing the same conclusions will be shown in the following section.

3.3.2.3 Consideration of residual stresses in shell elements

In this section, the approximation to the stainless steel hardening law described in section 3.2.2.2 and the introduction of the consideration of the residual stresses in shell elements described in section 3.2.2.3 are tested. These comparisons are made for elements with Class 1 sections. The flexural buckling of a square hollow section and the LTB of an I-cross-section are analysed with shell and beam finite elements, being the results compared between them. The results obtained with the shell finite elements of the program SAFIR are compared with the results obtained using the 3D beam finite element of SAFIR.

The comparisons were made with uniform temperature of 600 ºC in the cross-section. The yield strength and the ultimate strength considered were (according to the EC3) 210 MPa and 520 MPa respectively. In the numerical simulations, a lateral geometric imperfection given by the expression (3.12) was considered.

A study with the SHS40x40x4 columns (with and without residual stresses) is first presented.

The adopted residual stresses are considered as constant across the thickness of the internal section members. For the square hollow section the distribution shown in Figure 3.19, which has the maximum value of half of f_y (ECCS, 1984), was used. Adopting the same methodology used by (Jandera *et al.*, 2008), prior to the applications of external loading, a preliminary load step, to allow equilibration of the residual stresses, was performed.

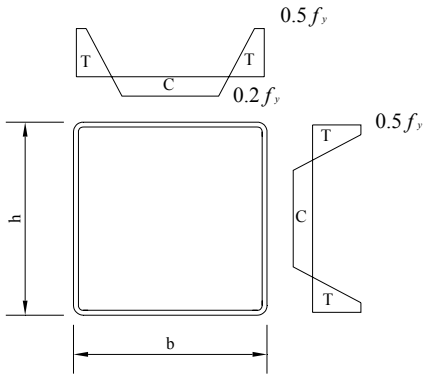

Figure 3.19 – Residual stresses in hollow sections (C – compression; T – tension).

In Table 3.3 the obtained results in this study are presented. It can be concluded that the introduction of the residual stresses in shell elements gives results that are in good agreement with the results obtained with the 3D beam elements. Here, it is also shown that the EC3 is not in the safe side.

Table 3.3 – Results for the hollow section.

		Without residual stresses	With residual stresses	EC3
L = 2 m	3D beam	23.1 kN	22.8 kN	26.9 kN
	shell	22.9 kN	22.7 kN	
L = 3 m	3D beam	13.4 kN	12.6 kN	14.8 kN
	shell	13.1 kN	12.7 kN	

It was also chosen to test simply supported beams subjected to uniform bending with fork supports with Class 1 welded IPE220 cross-section (Figure 3.20).

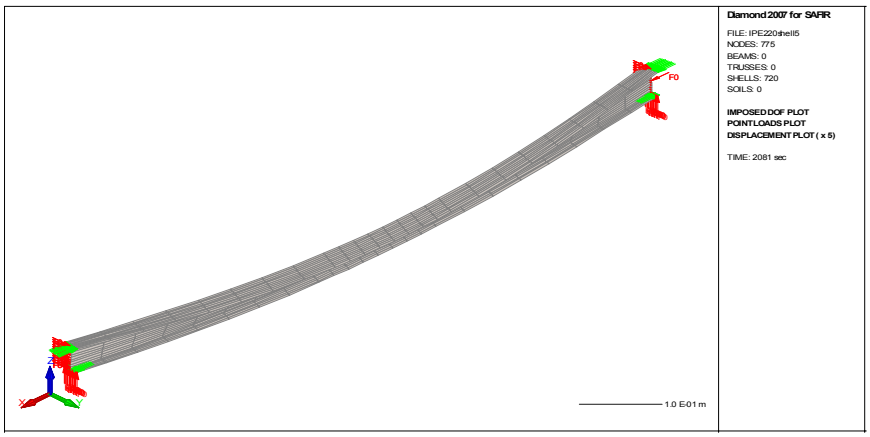

Figure 3.20 – Simply supported stainless steel beam subjected to uniform bending.

In these tests the lateral imperfection given by the expression (3.12) and the residual stresses pattern presented in Figure 3.14 were used.

From Table 3.4 it can be confirmed that the introduction of the residual stresses in shell elements gives results that are in good agreement with the results obtained with the 3D beam finite elements. Again, it can be noticed that EC3 is not in the safe side.

Table 3.4 – Results for the I-section.

		Without residual stresses	With residual stresses	EC3
L = 3 m	3D beam	20.6 kNm	19.9 kNm	20.3 kNm
	shell	19.3 kNm	19.2 kNm	
L = 5 m	3D beam	15.7 kNm	15.0 kNm	14.1 kNm
	shell	14.3 kNm	14.0 kNm	

From the tables it can also be concluded that the approximation used for the stainless steel hardening rule introduced in SAFIR gives a good approximation when compared with the results from the uni-axial stainless steel constitutive law.

3.4 Conclusions

In this chapter, a brief description of the programme SAFIR and its finite elements used on this thesis was made.

With the purpose of following the objectives within this thesis, some modifications had to be introduced on SAFIR. Those modifications and corresponding validations were described in this chapter.

Also, a general description of the main considerations made in the numerical models used in this thesis was presented.

Chapter 4

Prescribed design rules for structural elements

Chapter 4. Prescribed design rules for structural elements

Chapter 4. Prescribed design rules for structural elements

4.1 Introduction

In this chapter the prescribed expressions defined in EC3 for the design of the stainless steel structural elements: columns, beams and beam-column, at ambient temperature and at high temperatures, are presented.

As mentioned before, the part of EC3 dedicated to the cold design prescriptions of stainless steel structural elements is part 1-4 (CEN, 2006a). However, for the fire situation, this part of EC3 dedicated to the stainless steel makes reference to the part 1-2 of the same Eurocode (CEN, 2005b), meaning that the design rules are those developed for carbon steel elements. Both these design methodologies are based on the same rules for carbon steel elements included in the European Pre-standard (ENV) version of part 1-1 of EC3 (CEN, 1992).

Stainless steels are known for their non-linear stress-strain relationships with a low proportional stress and an extensive hardening phase (Rasmussen, 2003; Real and Mirambell, 2003). There is no well defined yield strength, being usually considered for design at room temperature the 0.2 % proof strength, $f_y = f_{0.2p}$. In a fire situation higher strains than at room temperature are acceptable, and part 1-2 of EC3 (CEN, 2005b) suggests the use of the stress at 2 % total strain as the yield stress at elevated temperature θ (Gardner and Baddoo, 2006), $f_{y,\theta} = f_{2,\theta}$, for Class 1, 2 and 3 cross-sections. However for Class 4 cross-sections the 0.2 % proof strength must be used, $f_{y,\theta} = f_{0.2p,\theta}$.

The results obtained with the expressions recommended on the different versions of EC3, are here compared with the obtained numerical results with the program SAFIR.

No review of the buckling stability theory is presented, since this consists of a well consolidated subject that can be found in innumerable structural stability bibliography (Allen and Bulson, 1980; Reis and Camotim, 2000; Chen and Lui, 1991; Trahair, 1993), and to avoid prolonging this thesis unnecessarily.

This chapter also deals with the simple design methods for the verification against LTB of carbon steel beams under fire conditions (Vila Real *et al.*, 2004; 2007). Unrestrained simply supported beams, with rotation along the longitudinal axis of the beam prevented at the supports (fork supports), are considered here. This study is directly connected to the LTB in stainless steel elements in case of fire, due to the fact that, as mentioned before, the design in stainless steel elements is made using the same prescriptions developed for carbon steel elements. Thus, the proposal here presented will serve as basis for the development of stainless steel design rules at high temperatures.

4.2 Design rules at room temperature

In this section the design prescriptions in part 1-4 of EC3 (CEN, 2006a) for stainless steel columns, beams with LTB and beam-columns with and without LTB, at room temperature, are presented.

Part 1-4 of EC3 recommends the use of 1.1 as the partial safety factor γ_{M1}. However, in this study, a value of 1.0 for the partial safety coefficient, as it is already prescribed for the design of carbon steel structures and of steel structures in case of fire was used.

The classification of steel cross-sections, according to the EC3, is made using a factor ε as a function of the yield strength and the Young's modulus.

$$\varepsilon = \left(\frac{235}{f_y} \frac{E}{210000} \right)^{0.5} \tag{4.1}$$

At 20 ºC the Young's modulus of the carbon steel is equal to 210 GPa (CEN, 2005a), being different for the stainless steel (CEN, 2006a). This led to the use of different factor ε for these two materials, as presented in Table 4.1.

Table 4.1 – Factor used for the cross-section classification.

In part 1-1 of EC3 for carbon steel sections	$\varepsilon = \left(\frac{235}{f_y} \right)^{0.5}$
In part 1-4 of EC3 for stainless steel sections	$\varepsilon = \left(\frac{235}{f_y} \frac{E}{210000} \right)^{0.5}$

4.2.1 Compression

In this section, the design procedure recommendations in EC3 for the evaluation of the flexural buckling of stainless steel columns, at ambient temperature (Figure 4.1) are presented.

Figure 4.1 – Element subjected to axial compression (column).

4.2.1.1 Eurocode recommendations

Using the procedure prescribed in part 1-4 of EC3, for the design of elements subjected to axial compression with class sections of 1, 2 and 3 (classification according to this part 1-4), the buckling resistance value of a compressed element is calculated with

$$N_{b,Rd} = \chi_{\min} A f_y / \gamma_{M1} \tag{4.2}$$

The factor $\chi_{\min}$ is the minimum between the reduction factors χ_i about the y axis (strong) and the z axis (weak) (Maquoi and Rondal, 1978), given by expression

$$\chi_i = \frac{1}{\phi_i + \sqrt{\phi_i^2 - \overline{\lambda}_i^2}} \quad \text{with} \quad \chi_i \leq 1 \tag{4.3}$$

and

$$\phi_i = \frac{1}{2}\left[1 + \alpha_i\left(\overline{\lambda}_i - \overline{\lambda}_0\right) + \overline{\lambda}_i^2\right] \tag{4.4}$$

where the imperfection factor α_i and the limiting slenderness $\overline{\lambda}_0$ are obtained in accordance with Table 4.2.

Table 4.2 – Imperfection factor and limiting slenderness.

Buckling mode	Type of member	α	$\overline{\lambda}_0$
Flexural	Cold formed open sections	0.49	0.40
	Hollow sections (welded and seamless)	0.49	0.40
	Welded open sections (major axis)	0.49	0.20
	Welded open sections (minor axis)	0.76	0.20
Torsional and torsional-flexural	All members	0.34	0.20

To determine coefficients ϕ_i of expression (4.4), the non-dimensional slenderness $\overline{\lambda}_i$ is obtained through expression

$$\overline{\lambda}_i = \sqrt{\frac{Af_y}{N_{cr,i}}} \tag{4.5}$$

The elastic critical force $N_{cr,i}$ for flexural buckling about axis i is determined based on the gross cross-sectional properties by

$$N_{cr,i} = \frac{\pi^2 EI_i}{L_{cr}^2} \tag{4.6}$$

where L_{cr} is the buckling length in the considered buckling plane.

EC3 states that the buckling effects may be ignored for

$$\overline{\lambda} \le \overline{\lambda}_0 \text{ or } \frac{N_{Ed}}{N_{cr}} \le \overline{\lambda}_0^2 \tag{4.7}$$

The flexural buckling safety evaluation, for profiles of Class 4 cross-section, follows the same procedure described in this section, considering the effective area A_{eff} instead of the gross cross-section A.

4.2.1.2 Comparison against numerical results

The graphics from Figure 4.2 were obtained for columns with a welded cross-section equivalent to a HEA200 of stainless steel grade 1.4301, using the numerical results

from SAFIR and the buckling curves obtained with the previous presented formulae, for both the strong and weak axis. In Figure 4.2 $N_{pl} = Af_y$.

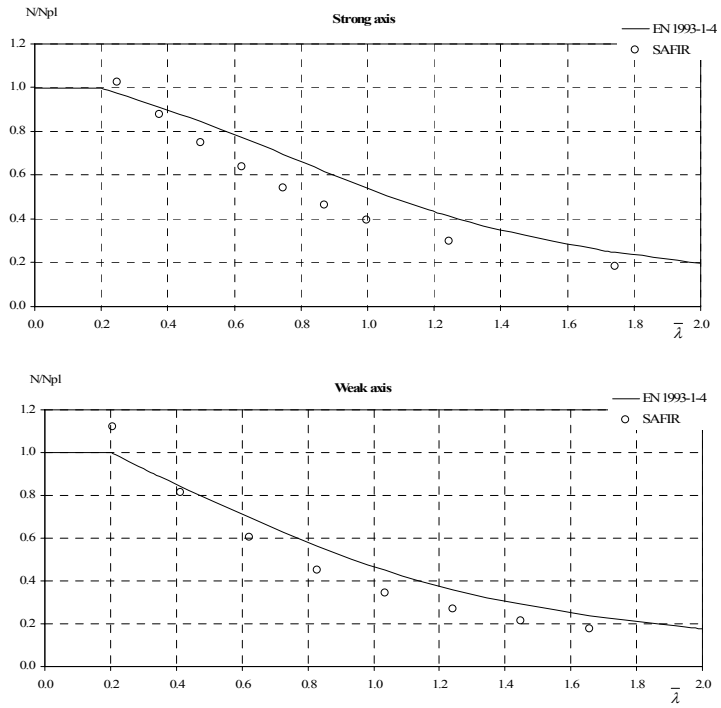

Figure 4.2 – Comparison between the curve from EC3 and the numerical results: buckling about the strong axis and the weak axis.

It can be observed in Figure 4.2 that for values of slenderness higher than 0.4, EC3 gives values for the reduction factor for flexural buckling higher than the results obtained with the program SAFIR. Assuming these numerical values as true values, it can be stated that the expressions from the Eurocode are not safe. This conclusion suggests the use of another curve, as proposed in Chapter 5 of this thesis.

4.2.2 Bending

LTB is an instability phenomenon that in I-sections is induced by the compressed flange of unrestrained beams subjected to bending around the major axis as shown in Figure 4.3.

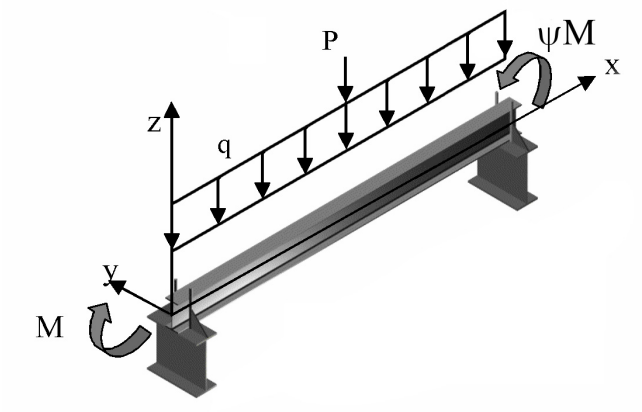

Figure 4.3 – Element subjected to bending (beam).

Figure 4.4 illustrates the deformed shape of a steel I-beam subjected to LTB.

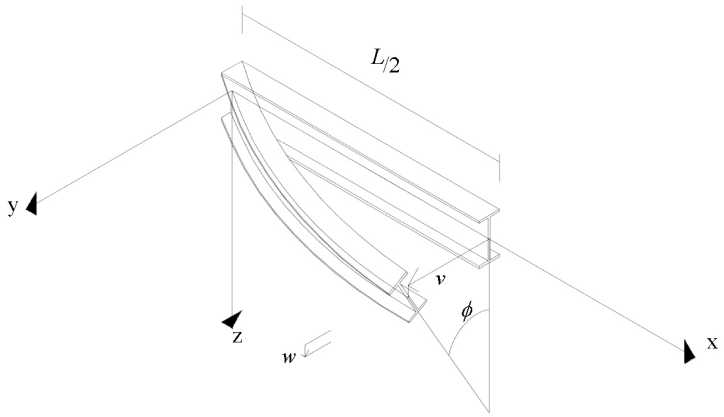

Figure 4.4 – Deformed shape of a steel I-beam due to LTB.

4.2.2.1 Eurocode recommendations

The design LTB resistance moment of laterally unrestrained stainless steel beams with Class 1 or Class 2 cross-section is determined, according to part 1-4 of EC3 (CEN, 2006a), by the following expression

$$M_{b,Rd} = \chi_{LT} W_{pl,y} f_y \frac{1}{\gamma_{M1}} \tag{4.8}$$

where χ_{LT} is given by

$$\chi_{LT} = \frac{1}{\phi_{LT} + \sqrt{\phi_{LT}^2 - \overline{\lambda}_{LT}^2}} \quad \text{but} \quad \chi_{LT} \leq 1 \tag{4.9}$$

with

$$\phi_{LT} = \frac{1}{2}\left[1 + \alpha_{LT}\left(\bar{\lambda}_{LT} - 0.4\right) + \bar{\lambda}_{LT}^{2}\right] \tag{4.10}$$

In part 1-4 of EC3, the imperfection factor α_{LT} is 0.34 for cold formed sections and hollow sections, whereas for welded open sections or other sections where tests results are not available, should be 0.76.

The non-dimensional slenderness for LTB is given by the expression

$$\bar{\lambda}_{LT} = \sqrt{\frac{W_{pl,y} f_y}{M_{cr}}} \tag{4.11}$$

where $W_{pl,y}$ is the plastic bending modulus. If $\bar{\lambda}_{LT}$ is lower or equal than 0.4, or M_{Ed}/M_{cr} is lower or equal to 0.16, no LTB check is required.

M_{cr} denotes the elastic critical moment for LTB, calculated on the basis of the gross cross-sectional properties and taking into account the loading conditions, the real moment distribution and the lateral restraints.

The elastic critical moment M_{cr} is not given in EC3, being found in the literature (Boissonnade *et al.*, 2006; Reis and Camotim, 2000). Here its application is explained for symmetrical sections about the minor axis.

$$M_{cr} = C_1 \frac{\pi^2 EI_z}{(k_z L)^2}\left[\sqrt{\left(\frac{k_z}{k_\omega}\right)^2 \frac{I_\omega}{I_z} + \frac{(k_z L)^2 GI_t}{\pi^2 EI_z} + \left(C_2 z_g - C_3 z_j\right)^2} - C_2 z_g + C_3 z_j\right] \tag{4.12}$$

The effective length factors k_z and k_ω vary from 0.5 for full restraint to 1.0 for no restraint and 0.7 for one end fixed and one end free. The k_z relates to the end rotation in the plane, and it can be determined in the same way as in the buckling length of compressed members. k_ω relates to the end warping, and unless there is some special provision to the warping restraint, the value 1.0 should be used. I_t is the torsional constant and I_ω the warping constant that for the case of commercial profiles is supplied by the manufacturers (for example: ArcelorMittal, 2008). The coefficients C_1, C_2 and C_3 depend on the loading and on the end restraint conditions. For values of k_z equal to 1.0 and for the different studied loading types, C_1 is given in Table 4.3 (Boissonnade *et al.*, 2006).

Table 4.3 – Coefficients for determining the elastic critical moment.

Bending diagrams	C_1
ψ = 1 	1.00
ψ = 1/2 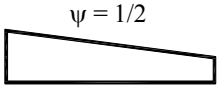	1.31
ψ = 0 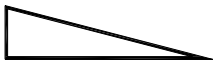	1.77
ψ = -1/2 	2.35
ψ = -1 	2.60
Concentrated load 	1.35
Distributed load 	1.12

In expression (4.12), z_g is the distance between the shear centre and the point of load application, and is obtained through expression (4.13). In the cases studied in this thesis, z_g was always assumed as equal to zero, due to the fact that the loads considered were applied in the shear centre.

$$z_g = z_a - z_s \tag{4.13}$$

z_a being the coordinate of the point of load position and z_s the coordinate of the shear centre. z_j can be determined with the following expression

$$z_j = z_s - 0.5\int_A (y^2 + z^2)\frac{z}{I_y}dA \tag{4.14}$$

The LTB safety evaluation, for profiles with cross-sections of Classes 3 and 4, follows the same procedure considering the elastic section modulus $W_{el,y}$ and the effective section modulus $W_{eff,y}$ respectively, instead of the plastic section modulus $W_{pl,y}$.

4.2.2.2 Comparison against numerical results

The graphics from Figure 4.5 were obtained for a simply supported beam with fork supports with a welded cross-section equivalent to an IPE220 of stainless steel grade 1.4301. Regarding the bending moment variation along the member length, in this figure it is shown the results obtained for values (-1, 0, 1) of the ψ ratio as well as a mid span concentrated load and a uniformly distributed load. In the graphics it is used $M_{pl} = W_{pl,y} f_y$.

From Figure 4.5 it can be observed that EC3 is always safe, but too conservative for non-uniform bending.

Recently, it was introduced in EN 1993-1-1 (CEN, 2005a) significant changes in the evaluation of the LTB resistance of unrestrained beams in carbon steel at room temperature, compared to the conservative approach of ENV 1993-1-1 (CEN, 1992) in the case of non-uniform bending. The LTB curves proposed in the ENV version only took into consideration the loading type in the determination of the elastic critical moment, not accounting for the additional beneficial effect resulting from the reduction of the plastic zones. These are directly related to the fact that the bending diagrams are variable along the beam, leading to over-conservative results in beams not subjected to uniform bending diagrams. As for other international regulations (Trahair *et al.*, 1998; 2001) that already considered this effect, a correction factor that considers the loading type was introduced in the EN 1993-1-1 (CEN, 2005a) for carbon steel elements. However, as shown in the figures, part 1-4 of EC3 (CEN, 2006a) does not consider that effect as it should be expected.

It should be noticed that this evaluation was only performed for loading in the shear centre. The same conclusions can not be assured for loading not applied in the shear centre.

In this thesis a new proposal for the LTB of stainless steel beams using the approach already adopted in EC3 for carbon steel, considering the influence of the loading type will be presented in Chapter 5.

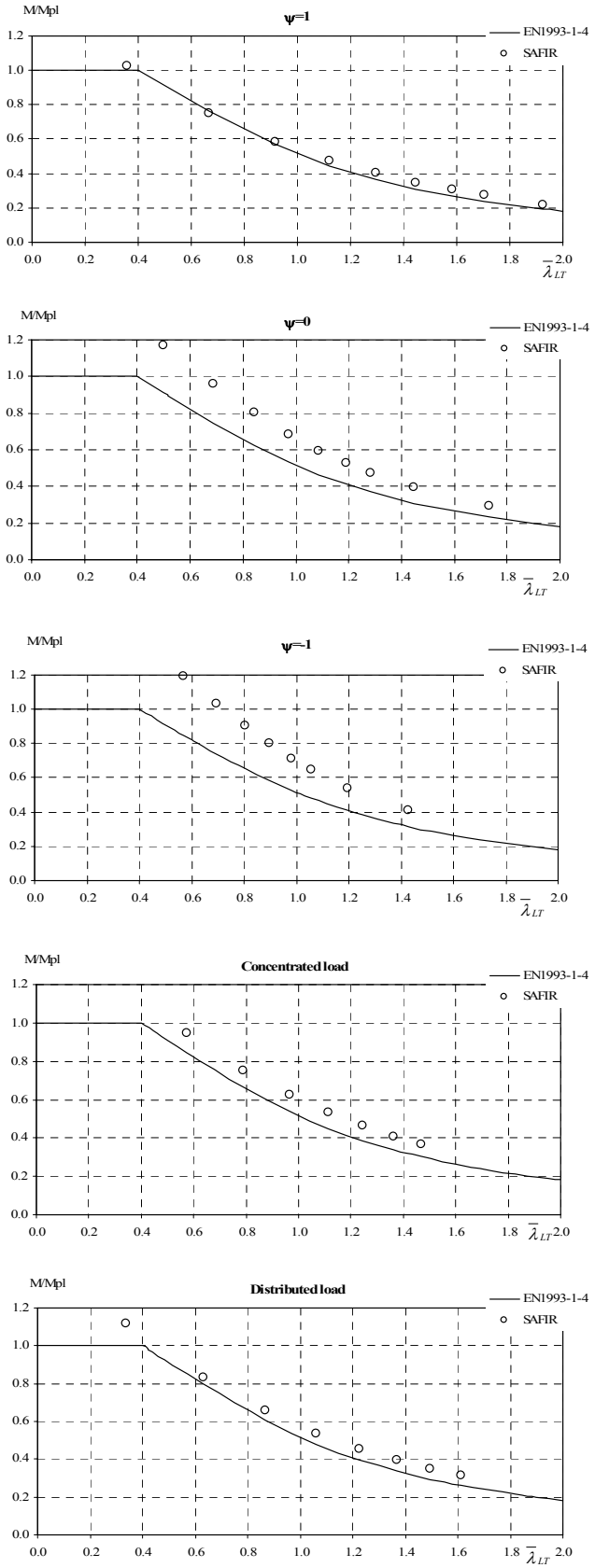

Figure 4.5 – Comparison between the numerical results and the EC3 for welded IPE220 beams of the stainless steel grade 1.4301.

4.2.3 Bending and axial compression

Beam-columns, structural elements simultaneously subjected to axial compression and bending moments (see Figure 4.6), are the most common structural elements used in construction.

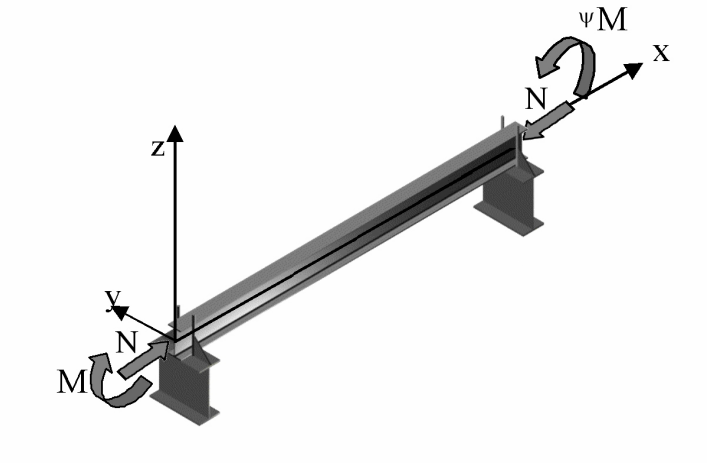

Figure 4.6 – Element subjected to axial compression and bending (beam-column).

The safety evaluation of steel beam-columns is made through interaction formulae that combine the compression and bending resistances.

In this section the prescribed formulae in EC3 (CEN, 2006a) for the design of stainless steel beam-columns, at ambient temperature, are presented.

Regarding combined bending and axial compression of stainless steel members, part 1-4 of EC3 (CEN, 2006a) has two notes stating that the national annexes may give other interaction formulae and other interaction factors. This suggests that the beam-columns formulae and the interaction factors were not well established for stainless steel members, at the time of the conversion from ENV to EN.

4.2.3.1 Without lateral torsional buckling

In the study presented here, it was only considered axial compression: with bending in the strong axis, assuming that the element is restrained about the z axis; and with bending in the weak axis, assuming that the element is restrained about the y axis.

4.2.3.1.1 Eurocode recommendations

Part 1-4 of EC3, gives the following expressions for the design of Class 1 and 2 stainless steel beam-columns subjected to axial compression and bending without LTB.

$$\frac{N_{Ed}}{N_{b,Rd,\min}} + k_y \frac{M_{y,Ed}}{W_{pl,y}\dfrac{f_y}{\gamma_{M1}}} + k_z \frac{M_{z,Ed}}{W_{pl,z}\dfrac{f_y}{\gamma_{M1}}} \le 1 \tag{4.15}$$

where

$$k_y = 1.0 + 2\left(\overline{\lambda}_y - 0.5\right)\frac{N_{Ed}}{N_{b,Rd,y}} \quad \text{but} \quad 1.2 \le k_y \le 1.2 + 2\frac{N_{Ed}}{N_{b,Rd,y}} \tag{4.16}$$

and

$$k_z = 1.0 + 2\left(\overline{\lambda}_z - 0.5\right)\frac{N_{Ed}}{N_{b,Rd,\min}} \quad \text{but} \quad 1.2 \le k_z \le 1.2 + 2\frac{N_{Ed}}{N_{b,Rd,\min}} \tag{4.17}$$

It should be noticed that, with the minimum limit value of 1.2, the actual plastic resistant bending moment M_{pl} is never reached by the design acting bending moment M_{Ed}, even if there is no axial force. This limitation is conservative and not coherent with the EC3 stainless steel prescriptions for beams at room temperature.

4.2.3.1.2 Comparison against numerical results

The graphics from Figure 4.7 and Figure 4.8 were obtained for beam-columns with welded cross-sections equivalent to a HEA200 of stainless steel grade 1.4301, for the buckling modes about the y and z axes, with uni-axial bending in the strong and weak axes respectively. Regarding the bending moment variation along the member length, in these figures the results obtained for values (-1, 0, 1) of the ψ ratio are shown. Here, the length of 3 m corresponds to non-dimensional slenderness values of $\overline{\lambda}_y = 0.37$ and $\overline{\lambda}_z = 0.62$, while the length of 7 m corresponds to $\overline{\lambda}_y = 0.87$ and $\overline{\lambda}_z = 1.45$.

The unsafe character, observed in section 4.2.1.2 for the flexural buckling, is also found in these beam-columns graphics (see the vertical axis with $M = 0$). Also, from these results it is concluded that EC3 is, most of the times, too conservative for non-uniform bending, leading to believe that the interaction factors (4.16) and (4.17) should depend on the bending diagram, as prescribed for the carbon steel beam-columns.

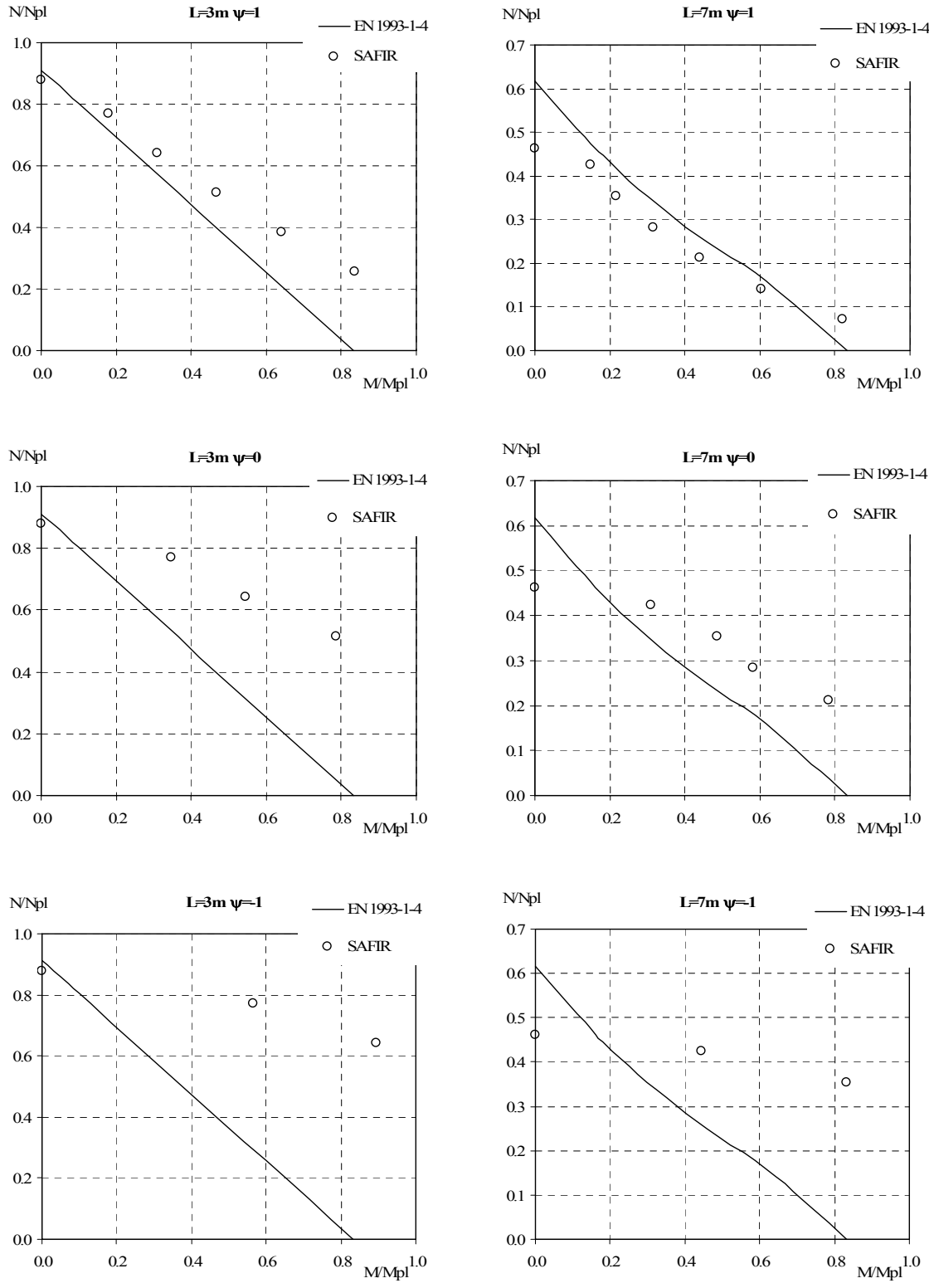

Figure 4.7 – Comparison between the numerical results and the EC3 for welded HEA200 beam-columns of the stainless steel grade 1.4301, regarding the buckling mode and uni-axial bending about the strong axis.

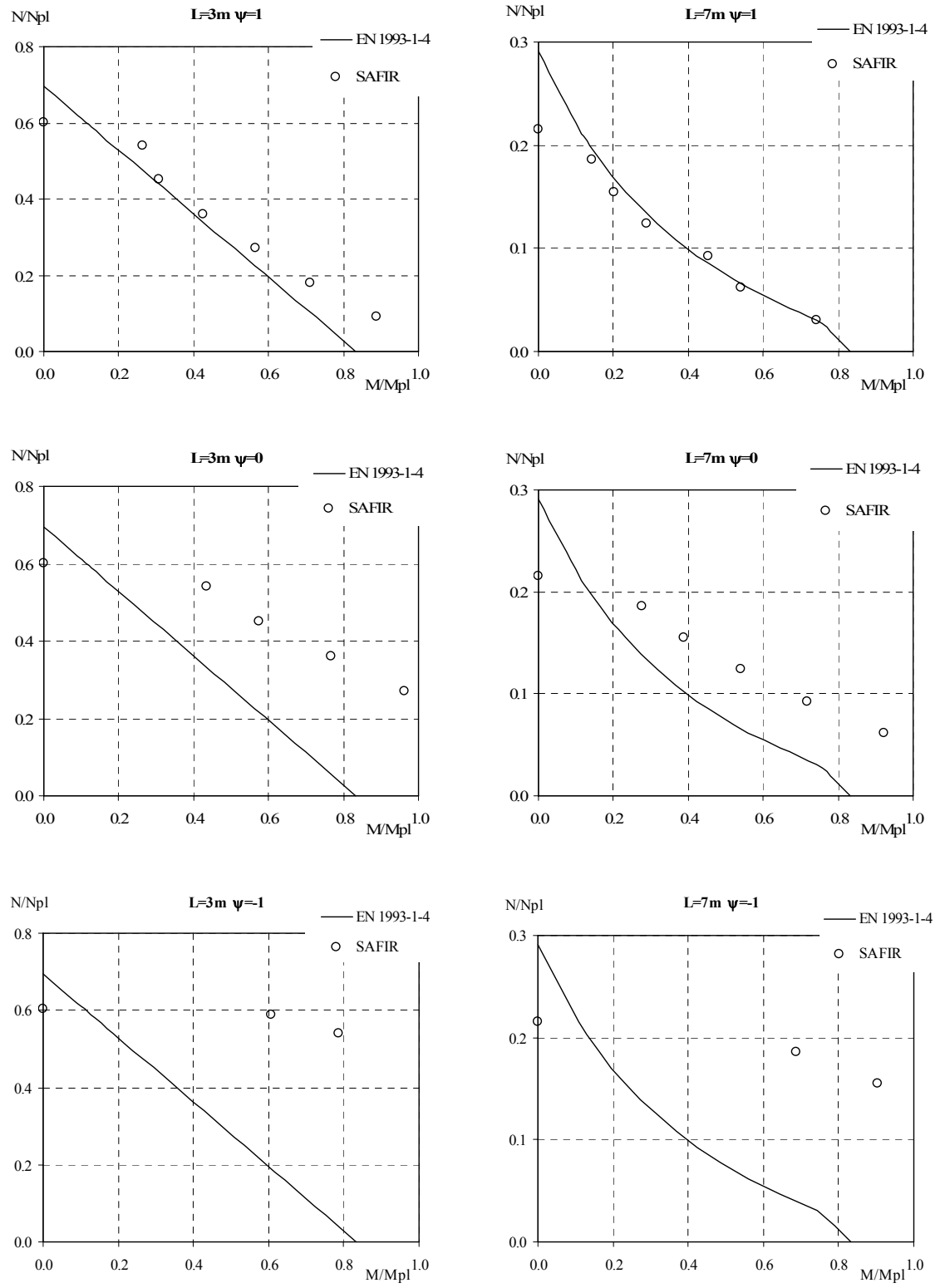

Figure 4.8 – Comparison between the numerical results and the EC3 for welded HEA200 beam-columns of the stainless steel grade 1.4301, regarding the buckling mode and uni-axial bending about the weak axis.

4.2.3.2 With lateral torsional buckling

In the study presented in this section, were only considered axial compression and bending about the strong axis.

4.2.3.2.1 Eurocode recommendations

Part 1-4 of EC3, gives the following expressions for the design of Class 1 and 2 stainless steel beam-columns subjected to axial compression and bending and having the possibility to occur LTB.

$$\frac{N_{Ed}}{\left(N_{b,Rd}\right)_{\min}} + k_{LT}\frac{M_{y,Ed}}{M_{b,Rd}} + k_z\frac{M_{z,Ed}}{W_{pl,z}\dfrac{f_y}{\gamma_{M1}}} \le 1 \tag{4.18}$$

where

$$k_{LT} = 1.0 \tag{4.19}$$

and k_z is given by expression (4.17).

4.2.3.2.2 Comparison against numerical results

The graphics from Figure 4.9 were obtained for beam-columns with welded cross-sections equivalent to a HEA200 of the stainless steel grade 1.4301, with the possibility of occurring LTB, with bending in the strong axis. Regarding the bending moment variation along the member length, in these figures the results obtained for values of (-1, 0, 1) of the ψ ratio are shown. Here, the length of 3 m corresponds to non-dimensional slenderness values of $\overline{\lambda}_z = 0.62$, while the length of 7 m corresponds to $\overline{\lambda}_z = 1.45$. The non-dimensional slenderness values for LTB are given in Table 4.4.

Table 4.4 – Non-dimensional slenderness values for LTB of the cases presented.

Moment diagram	$\overline{\lambda}_{LT}$ for $L = 3$ m	$\overline{\lambda}_{LT}$ for $L = 7$ m
$\psi = 1$	0.51	0.93
$\psi = 0$	0.39	0.69
$\psi = -1$	0.32	0.57

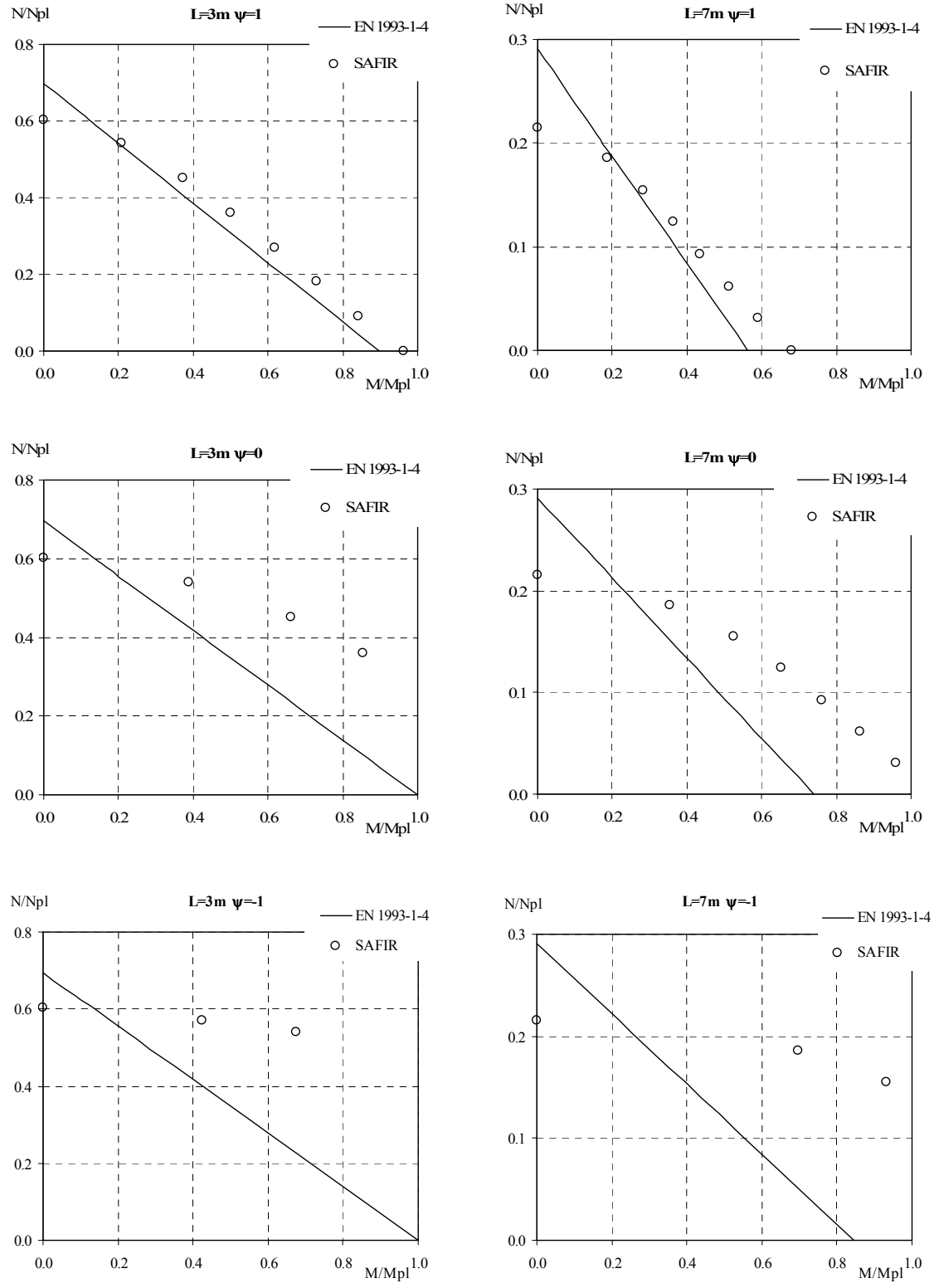

Figure 4.9 – Comparison between the numerical results and the EC3 for welded HEA200 beam-columns of the stainless steel grade 1.4301, with LTB and uni-axial bending about the strong axis.

Again, it is concluded that EC3 interaction factor k_{LT} should vary with the bending diagram, as it is prescribed for carbon steel beam columns (CEN, 2005a, 2005b).

As concluded in section 4.2.1.2, unsafe results appeared in low bending, due to also unsafe flexural buckling curve for the weak axis.

Moreover, the too conservative values for elements with low axial compression are the consequences of not considering the bending moment diagram in the LTB curve, as concluded in section 4.2.2.2.

4.3 Design rules at high temperatures

Despite the fact that stainless steel exhibits different mechanical behaviour in case of fire when compared to carbon steel (as shown in Chapter 2) part 1-4 of EC3 (CEN, 2006a) states that stainless steel structural elements (columns, beams with LTB and beam-columns with and without LTB) subjected to fire shall be designed with the same formulae developed and used for carbon steel, included in part 1-2 of EC3 (CEN, 2005b). In this section those formulae are described and evaluated based on numerical results.

Part 1-2 of EC3 recommends the use of the value 1.0 for the partial safety factor in fire situation $\gamma_{M,fi}$.

The factor ε, for the cross-section classification, determined using equation (4.1), varies with the temperature, due to the fact that the yield strength and the modulus of elasticity have different reduction factors (as presented in Chapter 2).

As can be seen in Figure 4.10 the factor ε, for carbon steel, reduces for high temperatures. Meaning that, the classification made at 20 ºC is unsafe for high temperatures. Due to this, part 1-2 of EC3 (CEN, 2005b) recommends the use of a reduced factor ε for the fire design, given by

$$\varepsilon = 0.85\left(\frac{235}{f_y}\right)^{0.5} \tag{4.20}$$

As shown in Figure 4.10, stainless steel exhibits a different behaviour from carbon steel, but with a factor ε value always bigger than the one given by equation (4.20). Therefore it

can be concluded that it is safe to use this equation to determine the classification of stainless steel cross-section in case of fire.

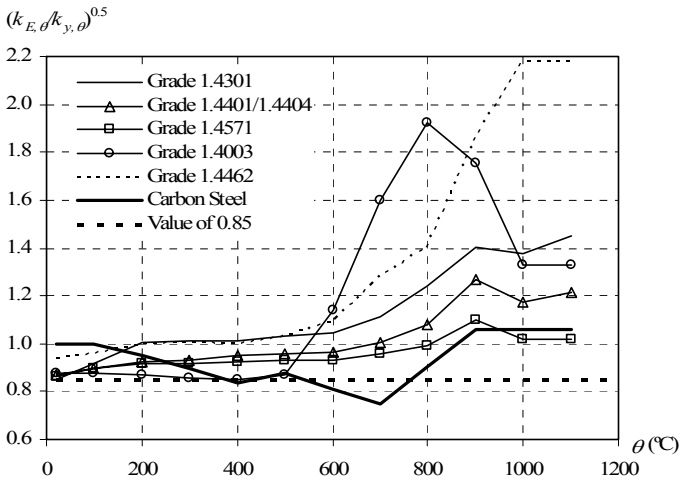

Figure 4.10 – Reduction of the factor to determine the cross-section classes, at high temperatures.

4.3.1 Compression

The calculation of the compression resistance of Class 1 and 2 sections, subjected to high temperatures (Figure 4.11) recommended by part 1-2 of EC3 (CEN, 2005b) was proposed by Franssen *et al*. (1998) and was mainly based in experimental tests on carbon steel columns.

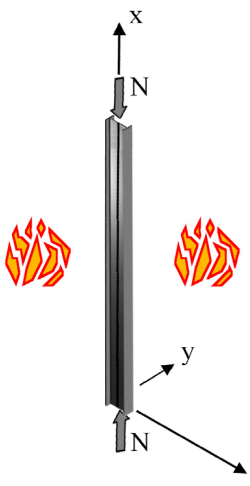

Figure 4.11 – Element subjected to axial compression in case of fire.

4.3.1.1 Eurocode recommendations

For stainless steel structural elements subjected to high temperatures, the part 1-2 of EC3 (CEN, 2005b) states that the flexural buckling resistance, for Class 1, 2 and 3 sections, is given by

$$N_{b,fi,t,Rd} = \chi_{\min,fi} A k_{y,\theta} \, f_y \Big/ \gamma_{M,fi} \tag{4.21}$$

where the reduction factor $\chi_{\min,fi}$ is the minimum of the values $\chi_{y,fi}$ and $\chi_{z,fi}$, which are determined with the expression

$$\chi_{i,fi} = \frac{1}{\phi_{i,\theta} + \sqrt{\phi_{i,\theta}^2 - \overline{\lambda}_{i,\theta}^2}} \quad \text{with} \quad \chi_{i,fi} \le 1 \tag{4.22}$$

with

$$\phi_{i,\theta} = \frac{1}{2}\left(1 + \alpha \overline{\lambda}_{i,\theta} + \overline{\lambda}_{i,\theta}^2\right) \tag{4.23}$$

In this expression, the imperfection factor α depends on the steel grade and is determined by

$$\alpha = 0.65\varepsilon \tag{4.24}$$

where ε is given in part 1-1 of EC3 (CEN, 2005a) as

$$\varepsilon = \sqrt{235 / f_y} \tag{4.25}$$

The imperfection factor is then given by

$$\alpha = 0.65\sqrt{235 / f_y} \tag{4.26}$$

The normalized slenderness for buckling at high temperatures is given by

$$\overline{\lambda}_\theta = \overline{\lambda} \left[\frac{k_{y,\theta}}{k_{E,\theta}}\right]^{0.5} \tag{4.27}$$

The flexural buckling safety evaluation, for profiles with cross-section Class 4, follows the same procedure, considering the effective section area A_{eff} instead of the gross cross-section A and assuming $f_{y,\theta} = f_{0.2p,\theta}$.

4.3.1.2 Comparison against numerical results

As Figure 4.12 shows, the curve resulting from the EC3 (denoted "EN 1993-1-2") is not on the safe side when the buckling curves for the strong and for the weak axis are compared with the numerical values of a HEA200 profile of stainless steel grade 1.4301 at 400, 500, 600 and 700 ºC. In the graphics $N_{fi,Rd} = Ak_{y,\theta} f_y / \gamma_{M,fi}$.

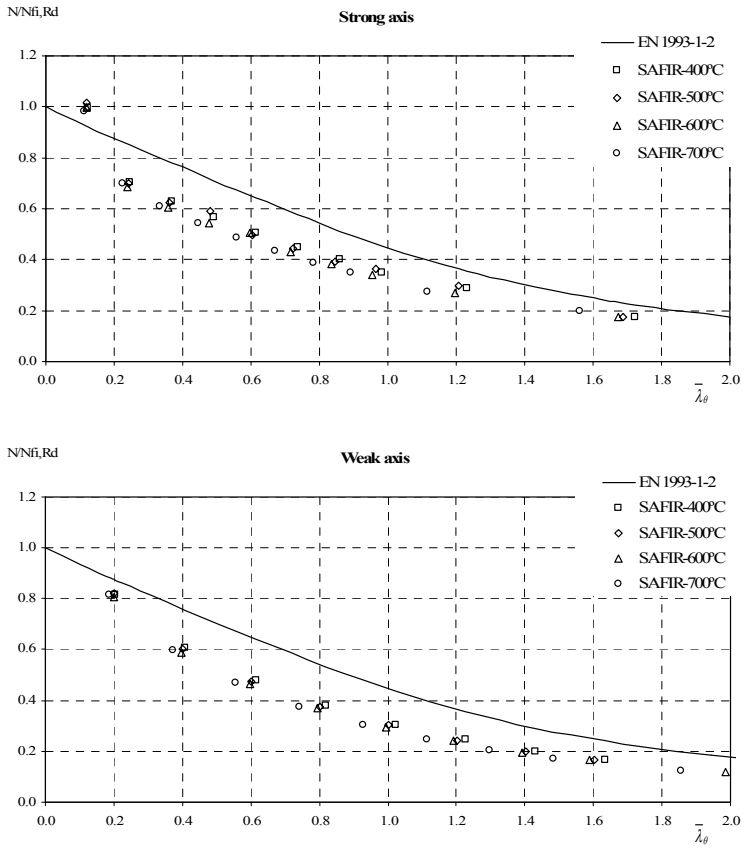

Figure 4.12 – Comparison between the curve from EC3 and the numerical results: buckling about the strong axis and the weak axis, at high temperatures.

4.3.2 Bending

As mentioned before, the procedure adopted by part 1-2 of EC3 (CEN, 2005b) for the safety evaluation of stainless steel beams is the same used for carbon steel beams.

For carbon steel beams under fire conditions, the design equation from ENV version of EC3 (CEN, 1995) proved to yield unsafe results, as shown mainly by numerical research works (Vila Real and Franssen, 1999; 2001) and partially confirmed by experimental

evidence (Vila Real *et al.*, 2003b). A new design equation was thus introduced in the EN version of EC3 (CEN, 2005b) providing a significant improvement, although all research performed at that time had considered only the case of a uniform bending distribution along the members.

From the results observed in section 4.2.2 for LTB at room temperature, it is expected that the influence of non-uniform bending moment distributions, in carbon steel and stainless steel beams in case of fire (see Figure 4.13), will be significant. In this section the stainless steel beams EC3 design prescriptions, at elevated temperatures, are evaluated. Section 4.3.4 presents a study performed in the scope of this thesis on carbon steel beams, which resulted in an improved proposal that is also used in Chapter 5 for LTB on stainless steel beams in case of fire.

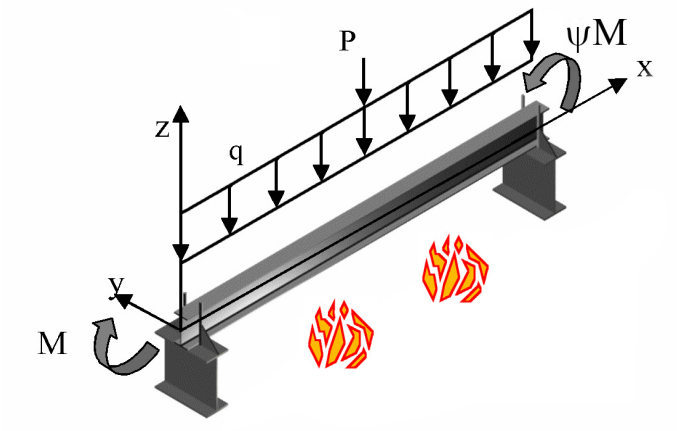

Figure 4.13 – Element subjected to bending in case of fire.

4.3.2.1 Eurocode recommendations

According to EN 1993-1-2 (CEN, 2005b), the LTB resistant moment for Class 1 and Class 2 cross-sections at high temperatures is given by

$$M_{b,fi,t,Rd} = \chi_{LT,fi} W_{pl,y} k_{y,\theta} \, f_y / \gamma_{M,fi} \tag{4.28}$$

where $\chi_{LT,fi}$ is given by

$$\chi_{LT,fi} = \frac{1}{\phi_{LT,\theta,com} + \sqrt{\phi^2_{LT,\theta,com} - \overline{\lambda}^2_{LT,\theta,com}}} \quad \text{with} \quad \chi_{LT,fi} \leq 1 \tag{4.29}$$

with

$$\phi_{LT,\theta,com} = \frac{1}{2}\left(1 + \alpha\bar{\lambda}_{LT,\theta,com} + \bar{\lambda}^{2}_{LT,\theta,com}\right) \tag{4.30}$$

In this expression, the imperfection factor α depends on the steel grade and is determined by expression (4.24).

The non-dimensional slenderness LTB at high temperatures $\bar{\lambda}_{LT,\theta,com}$ (or $\bar{\lambda}_{LT,\theta}$, if the temperature field in the cross-section is uniform) is given by

$$\bar{\lambda}_{LT,\theta,com} = \bar{\lambda}_{LT,\theta} = \bar{\lambda}_{LT}\left[\frac{k_{y,\theta}}{k_{E,\theta}}\right]^{0.5} \tag{4.31}$$

The LTB safety evaluation, for profiles with sections of the Classes 3 and 4, follows the same procedure, considering the elastic section modulus $W_{el,y}$ and the effective section modulus $W_{eff,y}$ respectively, instead of the plastic section modulus $W_{pl,y}$. For Class 4 sections it is also necessary to make $f_{y,\theta} = f_{0.2p,\theta}$.

4.3.2.2 Comparison against numerical results

The graphics from Figure 4.14 were obtained for a simply supported beam with fork supports with a welded cross-section equivalent to an IPE220 of stainless steel grade 1.4301, at 400, 500, 600 and 700 ºC. Regarding the bending moment variation along the member length, in this figure it is shown the results obtained for values (-1, 0, 1) of the ψ ratio as well as a mid span concentrated load and a uniformly distributed load. In the graphics $M_{fi,Rd} = W_{pl}k_{y,\theta}f_y/\gamma_{M,fi}$.

It can be observed that EC3 is too conservative for non-uniform bending and unsafe for uniform bending in a slenderness range between 0.3 and 0.7.

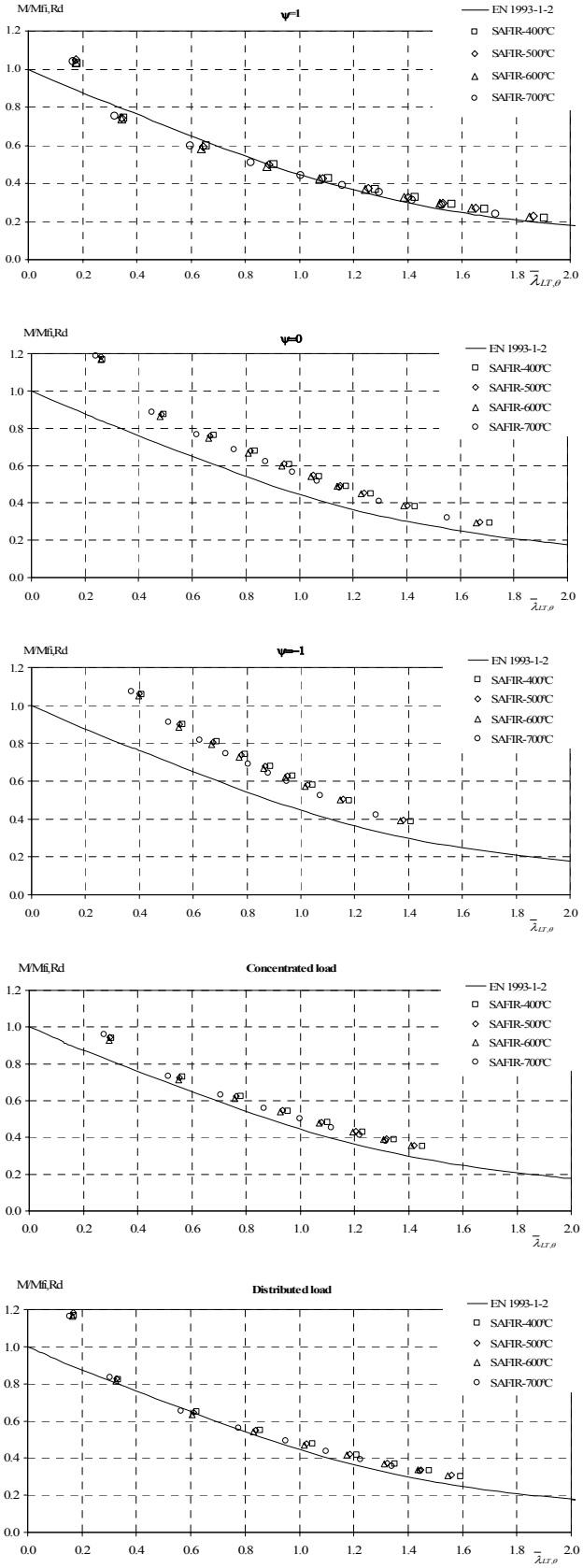

Figure 4.14 – Comparison between the numerical results and the EC3 for welded IPE220 beams of the stainless steel grade 1.4301, at high temperatures.

4.3.3 Bending and axial compression

Again, for stainless steel beam-columns design in case of fire (Figure 4.15), it is necessary to use the formulae developed for carbon steel elements.

The two new methods in EC3 (CEN, 2005a), for the carbon steel beam-columns cold design formulae, are designated by "Method 1" and "Method 2", and present a significant different format from the EC3 design formulae for elevated temperatures.

The procedure for the determination of the interaction factors for "Method 1" is reported in Annex A of part 1-1 of EC3 and was developed by a French-Belgian team (Boissonnade *et al.*, 2006; Villette *et al.*, 2000) by combining theoretical rules and numerical calibration to account for all the differences between the real model and the theoretical one. "Method 2" is described in Annex B of part 1-1 of Eurocode 3 and results from an Austrian-German proposal (Greiner, 2001) that attempted to simplify the verification of the stability of beam-columns. All interaction factors were obtained by means of numerical calibration.

In order to study the possibility of having, in part 1-1 and part 1-2 of the Eurocode 3, the same approach, numerical researches were made (Vila Real *et al.*, 2003d; Lopes *et al.*, 2003; 2004; Lopes, 2003; Knobloch *et al.*, 2008), concluding that additional changes, to these new methods, should be made in order to be possible to use them at high temperatures.

In this section it will only be evaluated on stainless steel beam-columns, the interaction formulae presented in EC3 (CEN, 2005b), while the two methods from part 1-1 of EC3 (CEN, 2005a) will be used on the parametric study presented on Chapter 5.

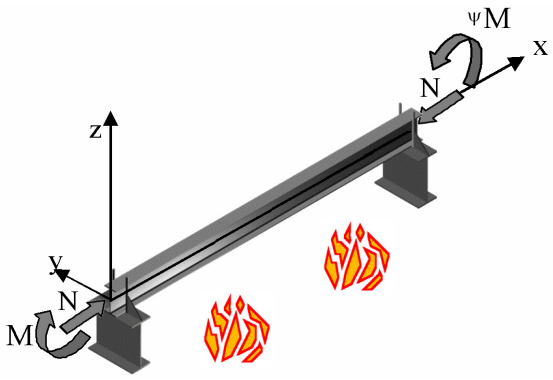

Figure 4.15 – Element subjected to axial compression and bending in case of fire.

4.3.3.1 Without lateral torsional buckling

In this section, the origin of the interaction curves for carbon steel beam-columns without the LTB, used in this thesis, will be explained. The use of these formulae will be evaluated in stainless steel elements with bending and axial compression.

In 1995, a procedure for the calculation of steel beam-columns interaction curves in case of fire was proposed (Talamona, 1995; Talamona *et al.*, 1997; Franssen *et al.*, 1998). This proposal was accepted to become part of the fire part of the EC3 (CEN, 2005b).

The equations that ended up in the official version of EN 1993-1-2 (CEN, 2005b) differ somehow from the equations presented in the original works of Talamona (1995).

Here, the differences will be pointed out and the consequences of these differences will be examined.

4.3.3.1.1 Original proposal for carbon steel elements

According to the original proposal, elements with cross-sections Classes 1 and 2 submitted to bending and axial compression, in case of fire, must satisfy the following condition:

$$\frac{N_{fi,Ed}}{\chi_{\min,fi} A \frac{k_{y,\theta} f_y}{\gamma_{M,fi}}} + K_{y,fi} \frac{M_{y,fi,Ed}}{W_{pl,y} \frac{k_{y,\theta} f_y}{\gamma_{M,fi}}} + K_{z,fi} \frac{M_{z,fi,Ed}}{W_{pl,z} \frac{k_{y,\theta} f_y}{\gamma_{M,fi}}} \leq 1 \tag{4.32}$$

The interaction factors $K_{y,fi}$ and $K_{z,fi}$ should be determined by:

$$K_{y,fi} = 1 - \frac{\mu_{y,\theta} N_{fi,Ed}}{\chi_{y,fi} A k_{y,\theta} \frac{f_y}{\gamma_{M,fi}}} \quad \text{with} \quad K_{y,fi} \leq 3 \tag{4.33}$$

$$K_{z,fi} = 1 - \frac{\mu_{z,\theta} N_{fi,Ed}}{\chi_{z,fi} A k_{y,\theta} \frac{f_y}{\gamma_{M,fi}}} \quad \text{with} \quad K_{z,fi} \leq 3 \tag{4.34}$$

To determine the values of $\mu_{y,\theta}$ and $\mu_{z,\theta}$ the following equations should be used.

$$\mu_{y,\theta} = (2\beta_{M,y} - 5)\overline{\lambda}_{y,\theta} + 0.44\beta_{M,y} + 0.29 \leq 0.8 \text{ with } \overline{\lambda}_{y,20°C} \leq 1.1 \tag{4.35}$$

and

$$\mu_{z,\theta} = (1.2\beta_{M,z} - 3)\overline{\lambda}_{z,\theta} + 0.71\beta_{M,z} - 0.29 \leq 0.8 \tag{4.36}$$

Finally, the equivalent uniform moment factor $\beta_{M,y}$ and $\beta_{M,z}$ can be determined in function of the bending diagram shape, according to the expression

$$\beta_{M,i} = 1.8 - 0.7\psi_i \tag{4.37}$$

The differences with the original equations lay in the equations used to determine the values of $\mu_{y,\theta}$ and $\mu_{z,\theta}$. In EC3 they are given by equations (4.38) and (4.39) hereafter, to be compared with equations (4.35) and (4.36) of the original proposal.

$$\mu_{y,\theta} = \left(1.2\beta_{M,y} - 3\right)\overline{\lambda}_{y,\theta} + 0.44\beta_{M,y} - 0.29 \le 0.8 \tag{4.38}$$

and

$$\mu_{z,\theta} = \left(2\beta_{M,z} - 5\right)\overline{\lambda}_{z,\theta} + 0.44\beta_{M,z} - 0.29 \le 0.8 \text{ with } \overline{\lambda}_{z,\theta} \le 1.1 \tag{4.39}$$

4.3.3.1.2 Interaction curves

The interaction curve given by equations (4.32) and (4.33) or (4.34) can be written in the following schematic way if bending is only around one axis (weak or strong).

$$N^* + M^* - \mu N^* M^* = 1 \tag{4.40}$$

Figure 4.16 shows the shape of the interaction curves for different values of the coefficient μ. It is concave for positive values of μ (meaning higher resistance is available) and turns convex with negative values of μ (meaning lower resistance is available). The short linear branch near the N^* axis comes from the limitation of $K_{y,fi} = 1 - \mu N^*$ to the value of 3 in expression (4.33).

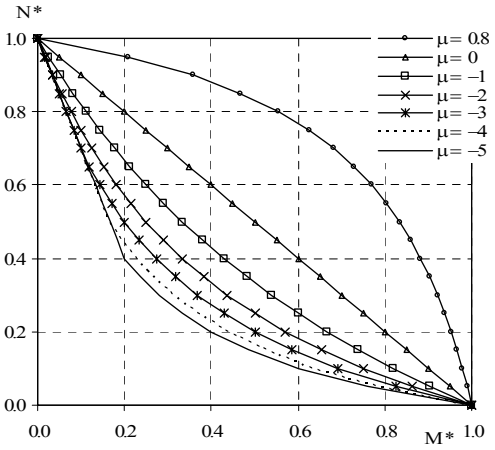

Figure 4.16 – Interaction curves.

4.3.3.1.3 Parametric study in carbon steel elements

New numerical simulations in carbon steel beam-columns were made with the program SAFIR. No significant differences were observed between these recently obtained numerical results and the numerical results presented by Talamona.

The partial study presented here is based on numerical simulations made on steel beam-columns without lateral-torsional buckling at 400 ºC, with non-uniform bending, in the strong or in the weak axis (Talamona, 1995).

According to the procedure adopted by Talamona, the following expression has been used in order to extract from each numerical simulation the value of $\mu_{y,\theta}$ or $\mu_{z,\theta}$ that fulfils equation (4.32).

$$\mu_{Safir,\theta} = \frac{M_{Safir} \cdot N_{b,Rd} - M_{Rd} \cdot N_{b,Rd} + M_{Rd} \cdot N_{Ed}}{M_{Safir} \cdot N_{Ed}} \tag{4.41}$$

The results were then presented in graphics showing the evolution of μ_θ as a function of the slenderness $\overline{\lambda}_\theta$. Six different figures are presented, Figure 4.17 for the strong axis and Figure 4.18 for the weak axis (3 different shapes of the bending diagram in each case).

In each of these figures,

- all the individual points that line up vertically correspond to the individual numerical results obtained by Talamona in 1995;
- the curve noted “Average from Talamona” is the average of the individual points obtained under a) and presented by Talamona in his thesis;
- the full line noted “Talamona proposal” is a simplification of the curve calculated under b) presented by Talamona in his thesis. This can be considered as the original proposal;
- the doted line noted “EN 1993-1-2” is the proposal that is currently in the Eurocode.

The comparison between the curves “Talamona proposal” and “EN 1993-1-2” gives an idea of the introduced differences, the consequence of which can be estimated from Figure 4.16. When lower values of μ have been introduced, the load bearing capacity has been reduced and this modification went in the safe direction, and in the opposite direction when higher values of μ were introduced.

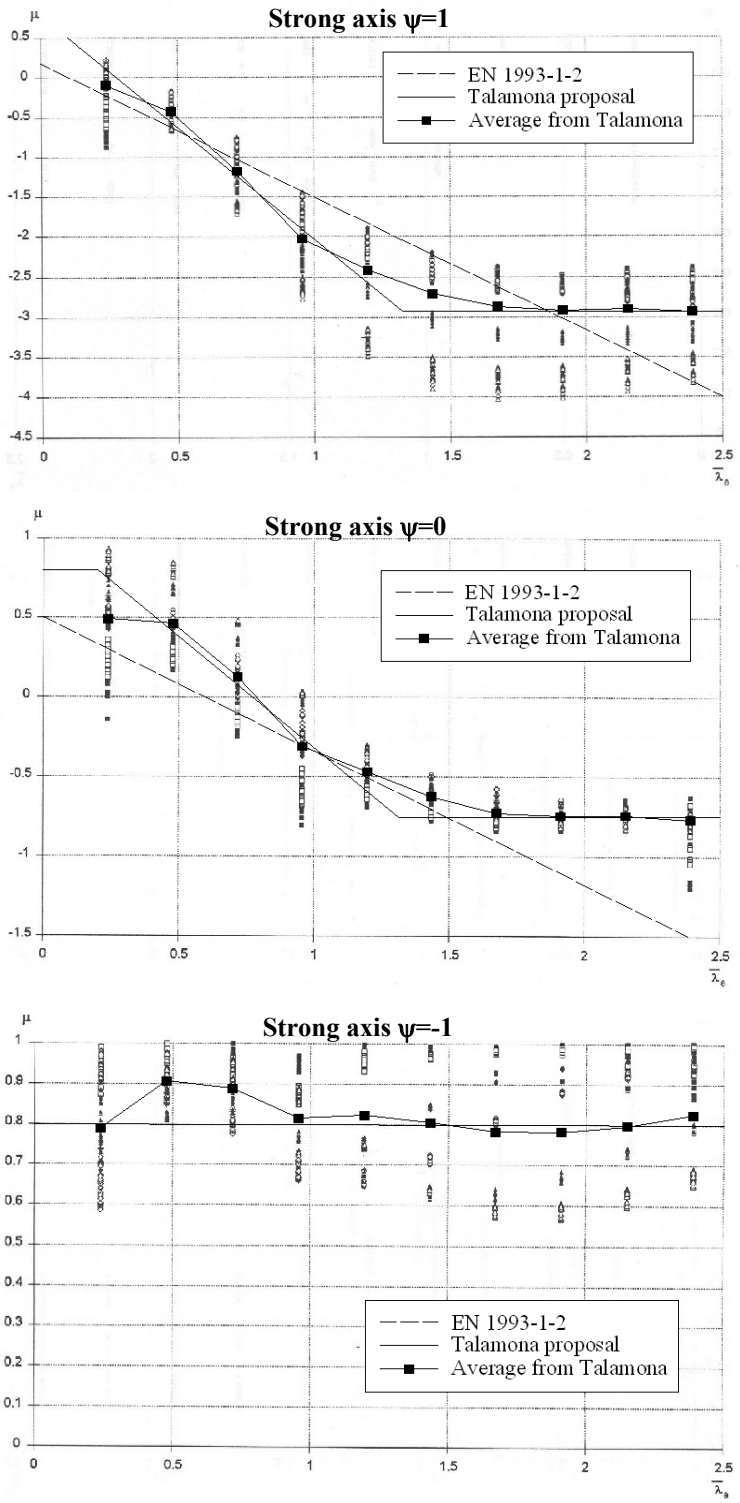

Figure 4.17 – Comparison between the different formulae with bending on the strong axis.

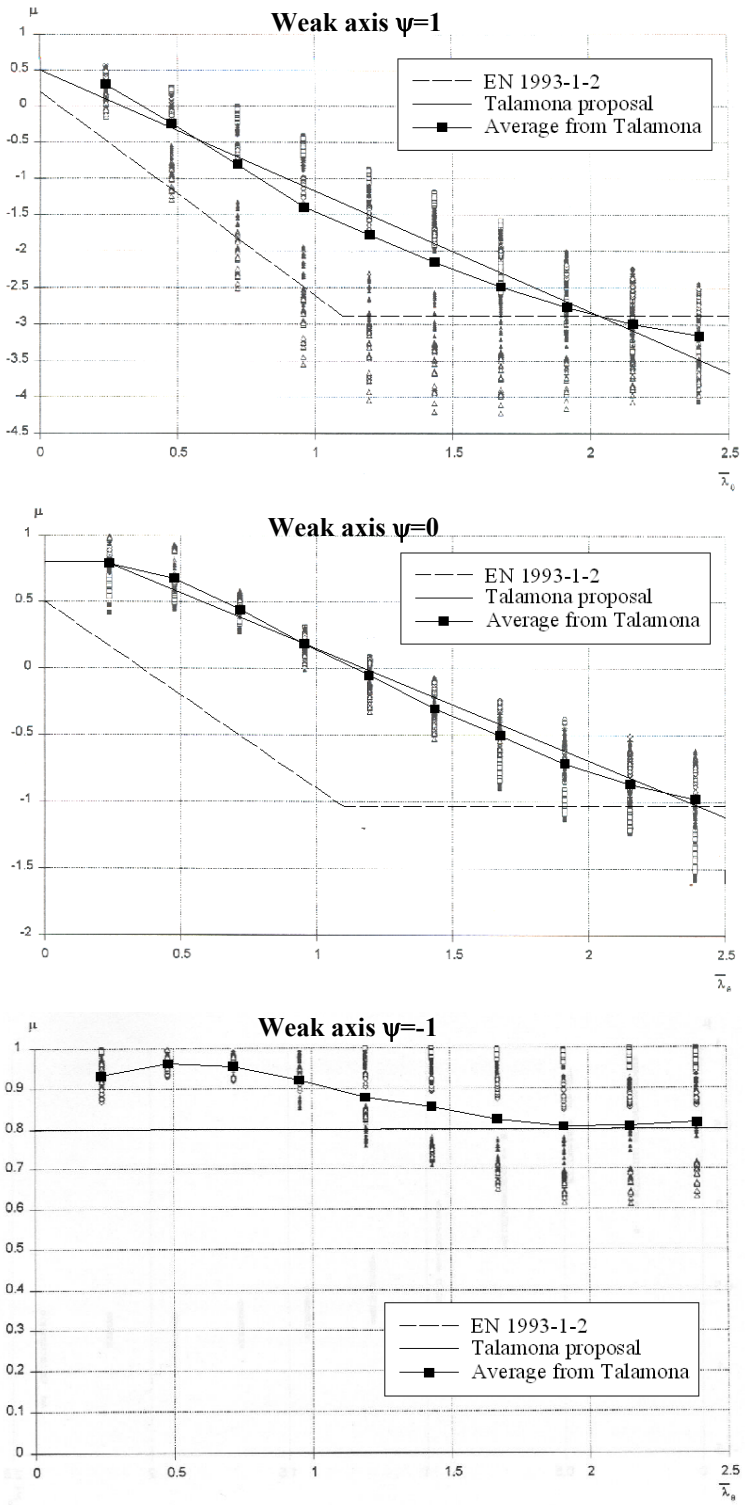

Figure 4.18 – Comparison between the different formulae with bending on the weak axis.

There is no difference at all for bi-triangular moment distributions ($\psi = -1$) because of the limit of 0.8 imposed in the ψ ratios.

For the strong axis with triangular and constant moment distribution (Figure 4.17), the differences are rather small and are mostly on the safe side. The fact that the Eurocode proposal is higher for the intermediate range of slenderness and uniform moments has to be analysed from Figure 4.16; it can be seen that a variation of μ from -3 to -2 has small implications on the shape of the interaction curve.

Higher differences are observed for the weak axis (Figure 4.18). For triangular moment diagram, the Eurocode proposal is significantly different, but on the safe side. For constant moment distribution, the Eurocode proposal is also significantly different, also on the safe side but it seems to represent in a better way the individual numerical results than the curve proposed by Talamona.

In order to highlight the later observation, the graphic with the uniform bending diagram results in Figure 4.18 was redrawn as Figure 4.19. It shows, for each slenderness, the median of the maximum and minimum individual result (the average could not be calculated because there is no access to all the individual values). It appears that the new Eurocode curve covers in a better and safer way the individual results than the proposal of Talamona.

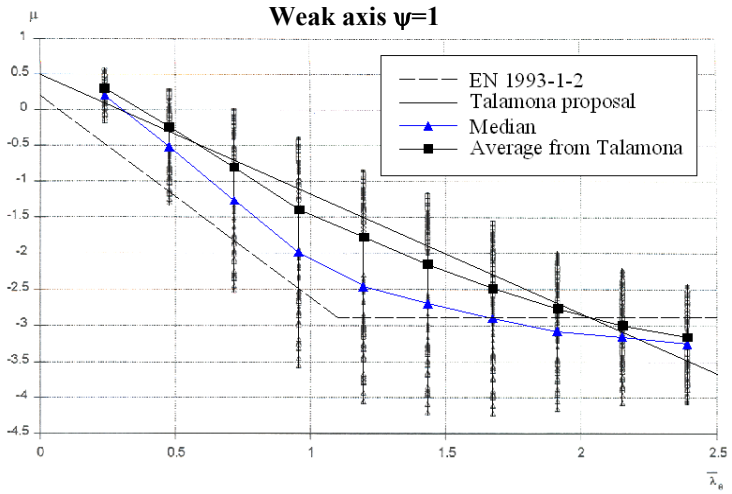

Figure 4.19 – Median with uniform bending diagram on the weak axis.

It can be concluded that the proposal made by Talamona is in good agreement with the individual numerical results for all cases but one (namely the uniform bending diagram

around the weak axis). In that case, the average determined by Talamona does not seem to fit the numerical results.

The Eurocode proposal is: either exactly the same (Figure 4.17 and Figure 4.18 for $\psi = -1$), rather similar (Figure 4.17 for $\psi = 1$ and $\psi = 0$) or, when significantly different, on the safe side compared with the original proposal (Figure 4.18 for $\psi = 1$ and $\psi = 0$).

The Eurocode proposal may lead to uneconomical design in the case of triangular moment distribution around the weak axis, and may have introduced an improvement in the case of uniform bending moments around the weak axis.

4.3.3.1.4 Comparison against stainless steel numerical results

In this section a comparison between the original proposal for carbon steel elements presented in section 4.3.3.1.1 (expected to be included in a corrigenda of the EC3 and therefore the considered proposal in this thesis) and the stainless steel numerical results, is made. Thus the name of the curve plotted in the graphics, obtained with the original proposal from Talamona (1995), will be "EN 1993-1-2".

Figure 4.20 and Figure 4.21 were obtained for beam-columns at 600 ºC with welded cross-sections equivalent to a HEA200 of the stainless steel grade 1.4301, for buckling about the y and z axis, with uni-axial bending in the strong and weak axis respectively. Regarding the bending moment variation along the member length, in these figures it is shown the results obtained for values (-1, 0, 1) of the ψ ratio. Here, the length of 3 m corresponds to non-dimensional slenderness values of $\overline{\lambda}_{y,\theta} = 0.36$ and $\overline{\lambda}_{z,\theta} = 0.60$, while the length of 7 m corresponds to $\overline{\lambda}_{y,\theta} = 0.84$ and $\overline{\lambda}_{z,\theta} = 1.39$.

This study concluded that these interaction curves don't provide a good approximation to the numerical results obtained with SAFIR, being always on the unsafe side. This unsafe character can be justified by the also unsafe results obtained for stainless steel columns (see section 4.3.1.2), reinforcing the need to improve the flexural buckling in case of fire included in EC3.

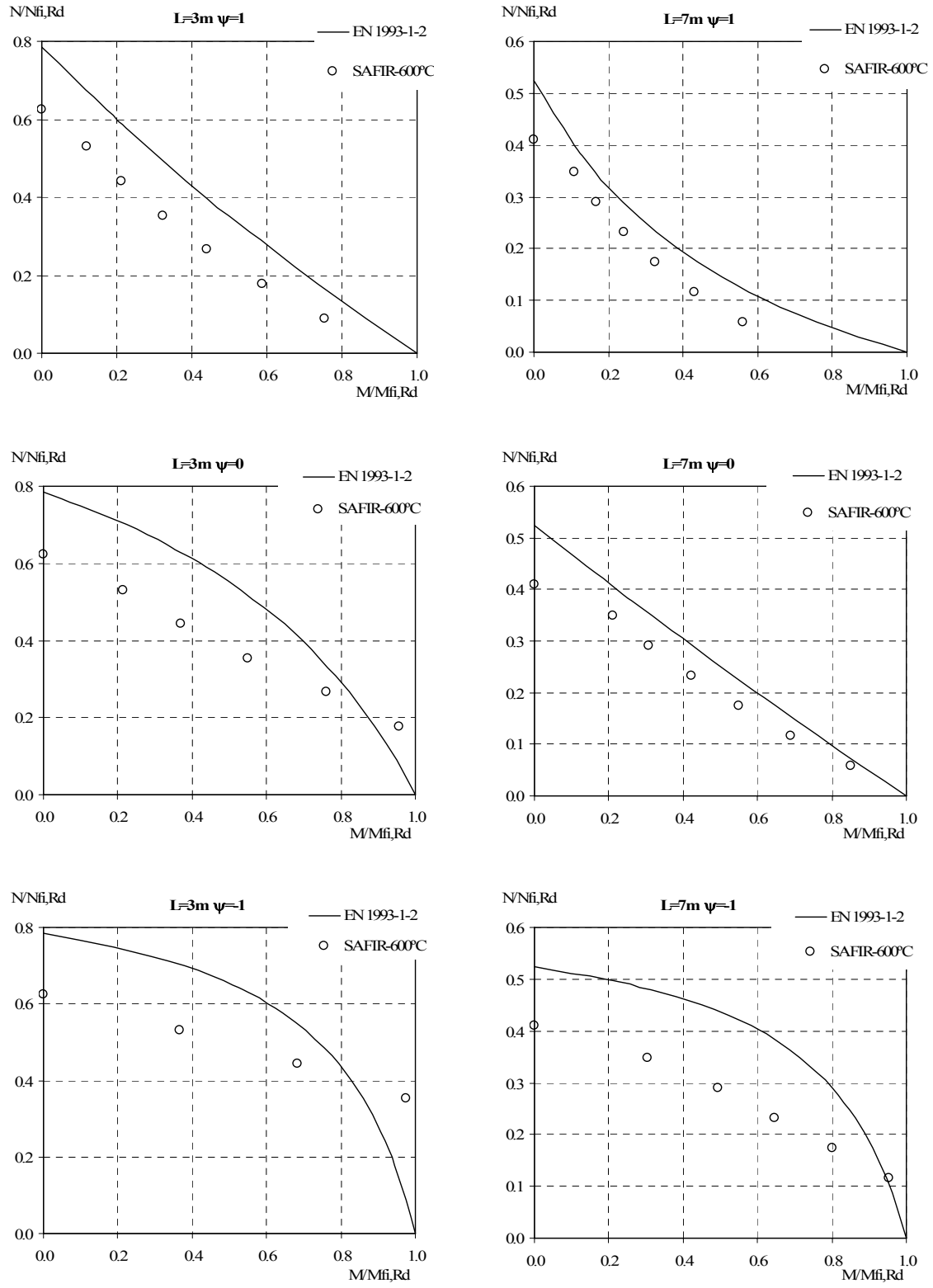

Figure 4.20 – Comparison between the numerical results and the EC3 for welded HEA200 beam-columns, at 600 ºC, of the stainless steel grade 1.4301, regarding the buckling mode and uni-axial bending about the strong axis.

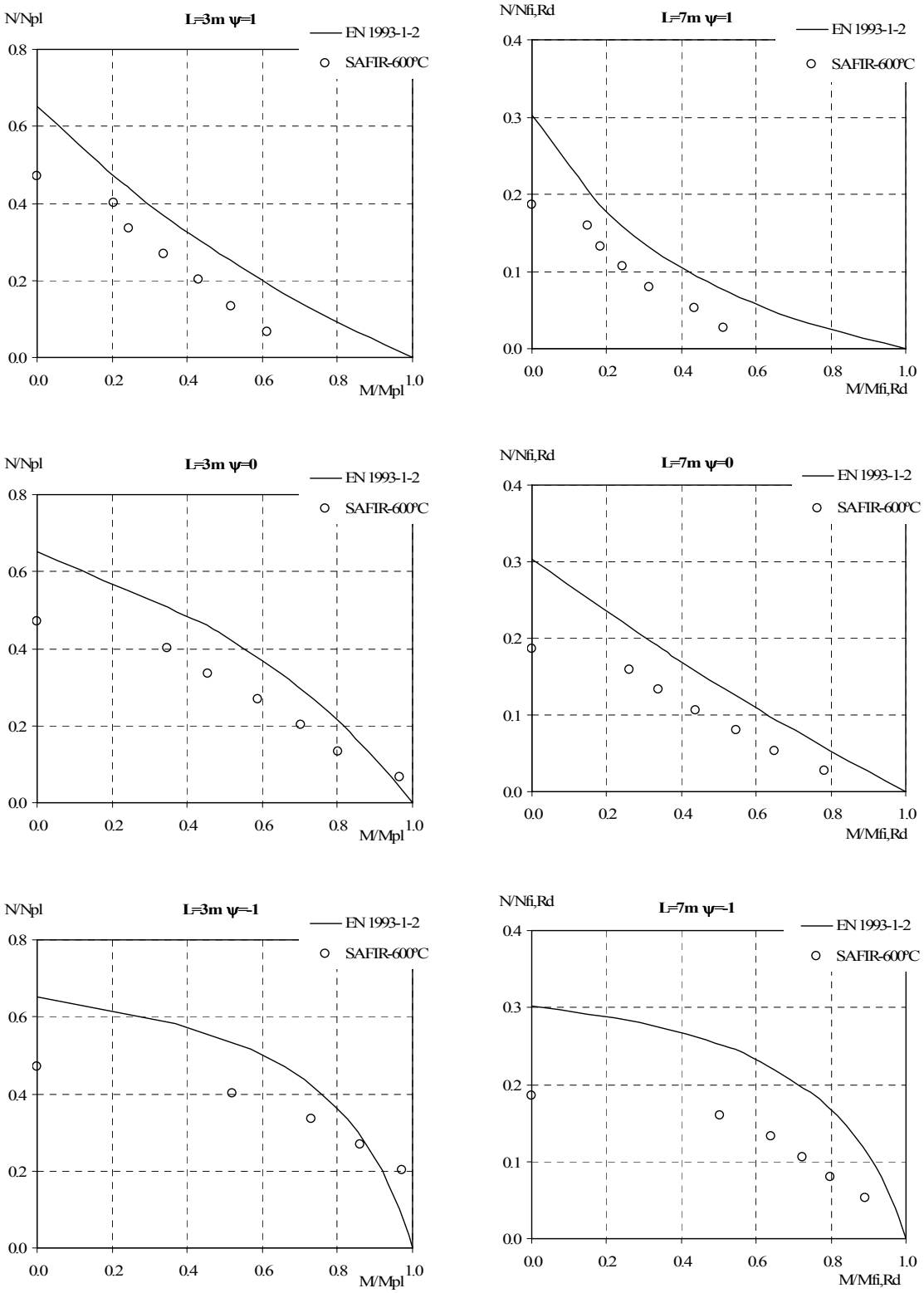

Figure 4.21 – Comparison between the numerical results and the EC3 for welded HEA200 beam-columns, at 600 ºC, of the stainless steel grade 1.4301, regarding the buckling mode and uni-axial bending about the weak axis.

4.3.3.2 With lateral torsional buckling

In this section it is studied the performance of the EC3 safety evaluation prescriptions for stainless steel beam-columns with LTB, at elevated temperatures.

4.3.3.2.1 Eurocode recommendations

Part 1-2 of EC3, gives the following expressions for the design of Class 1 and 2 stainless steel beam-columns at high temperatures subjected to axial compression and bending and having the possibility to occur LTB phenomena.

$$\frac{N_{fi,Ed}}{\chi_{z,fi} A \frac{k_{y,\theta} f_y}{\gamma_{M,fi}}} + K_{LT,fi} \frac{M_{y,fi,Ed}}{\chi_{LT} W_{pl,y} \frac{k_{y,\theta} f_y}{\gamma_{M,fi}}} + K_{z,fi} \frac{M_{z,fi,Ed}}{W_{pl,z} \frac{k_{y,\theta} f_y}{\gamma_{M,fi}}} \leq 1 \qquad (4.42)$$

The interactions factor $K_{z,fi}$ should be obtained according to expression (4.34) and $K_{LT,fi}$ determined by:

$$K_{LT,fi} = 1 - \frac{\mu_{LT,\theta} N_{fi,Ed}}{\chi_{z,fi} A k_{y,\theta} \frac{f_y}{\gamma_{M,fi}}} \quad \text{with} \quad K_{LT,fi} \leq 1 \qquad (4.43)$$

These design formulae are based in the ENV version of the part 1-1 of EC3 (CEN, 1992), for carbon steel elements at ambient temperature, and according to it part 1-2 states that $\mu_{LT,\theta}$ is calculated using

$$\mu_{LT,\theta} = 0.15 \overline{\lambda}_{z,\theta} \beta_{M,LT} - 0.15 \leq 0.9 \qquad (4.44)$$

Finally, the equivalent uniform moment factor $\beta_{M,LT}$ can be determined in function of the bending diagram shape in the strong axis, according to the expression

$$\beta_{M,LT} = 1.8 - 0.7 \psi_y \qquad (4.45)$$

where ψ_y is the quotient between the moments in the extremities in the strong axis.

4.3.3.2.2 Comparison against numerical results

The graphics from Figure 4.22 were obtained for beam-columns at 600 ºC, with welded cross-sections equivalent to a HEA200 of the stainless steel grade 1.4301, with the possibility of occurring LTB, with uni-axial bending in the strong axis. Regarding the bending moment variation along the member length, in these figures the results obtained for values (-1, 0, 1) of the ψ ratio are shown. Here, the length of 3 m corresponds to non-dimensional slenderness values of $\overline{\lambda}_{z,\theta} = 0.60$, while the length of 7 m corresponds to $\overline{\lambda}_{z,\theta} = 1.39$. The non-dimensional slenderness values for the LTB phenomena are given in Table 4.5.

Table 4.5 – Non-dimensional slenderness values for LTB of the cases presented at 600 ºC.

Moment diagram	$\overline{\lambda}_{LT,\theta}$ for $L = 3\,\text{m}$	$\overline{\lambda}_{LT,\theta}$ for $L = 7\,\text{m}$
$\psi = 1$	0.49	0.89
$\psi = 0$	0.37	0.67
$\psi = -1$	0.31	0.55

It can be concluded that the interaction curve should vary with the bending moment diagram.

The observed unsafe results can be justified by the also unsafe flexural buckling curve in the minor axis, as shown in section 4.3.1.2.

Also, the over conservative values for elements with low axial compression are the consequences of not considering the bending moment diagram in the LTB curve (see section 4.3.2.2).

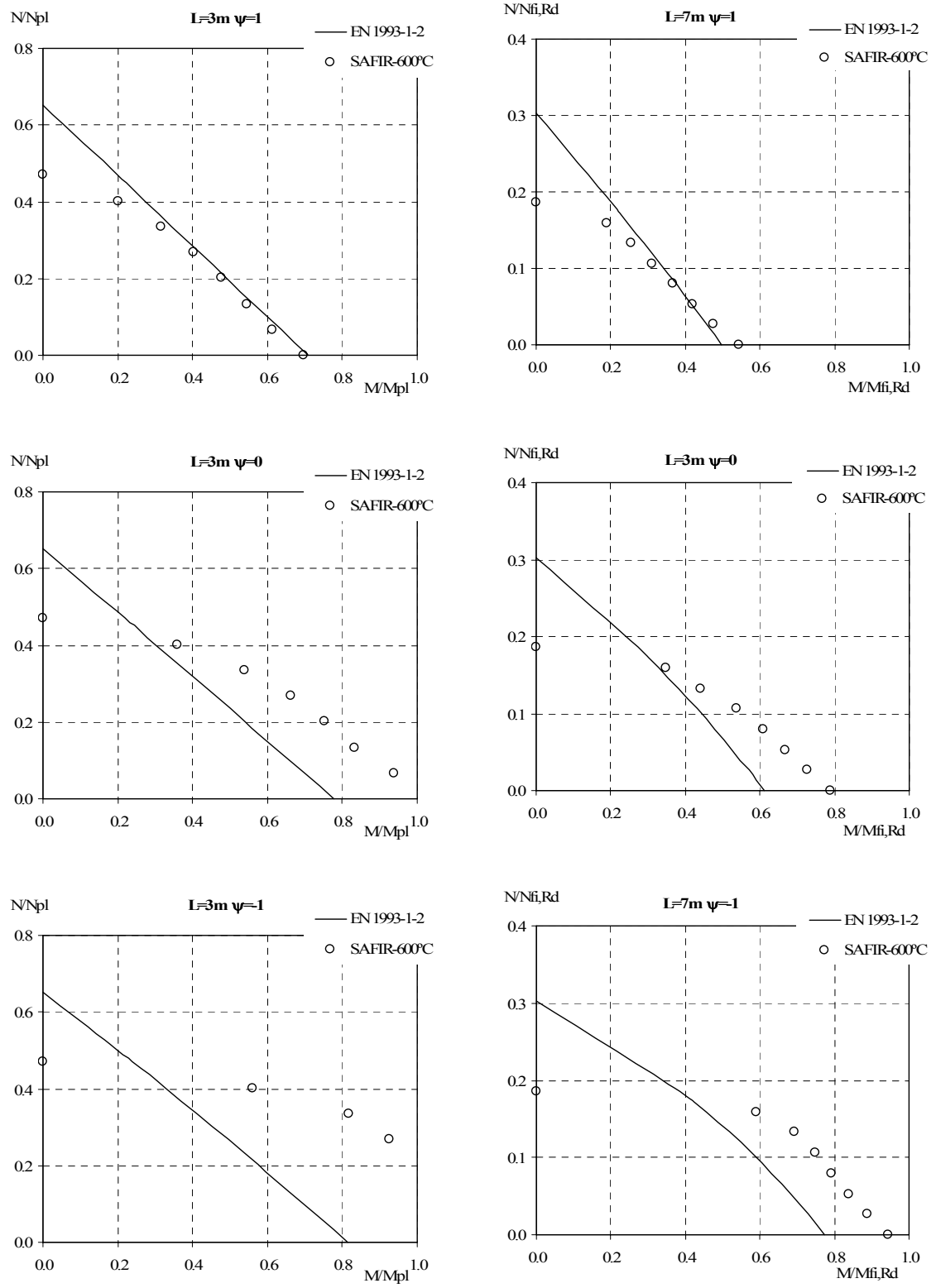

Figure 4.22 – Comparison between the numerical results and the EC3 for welded HEA200 beam-columns, at 600 ºC, of the stainless steel grade 1.4301, with LTB and uni-axial bending about the strong axis.

4.3.4 Lateral torsional buckling design proposal in carbon steel members

As mentioned in section 4.2.2, for carbon steel beams at room temperature, significant changes were introduced from the ENV version (CEN, 1992) to the EN version (CEN, 2005a) of EC3. The main differences lye in the EN version consider the: non-uniform bending moment distributions; and cross-section shape. These factors and the residual stress patterns (welded and hot rolled profiles), considered at room temperature, are totally ignored at elevated temperatures.

The influence of non-uniform bending moment distributions in fire condition has been analyzed by (Vila Real *et al.*, 2003c; Lopes, 2003) who showed that the beneficial effect resulting from reduced plastic zones connected with variable bending along the beam (Boissonnade *et al.*, 2006) should also be considered at elevated temperature. If not, the design is too conservative for the case of non-uniform bending diagrams.

In this work the influence of the carbon steel grade (S235 to S460), the influence of the cross-sectional shape and the influence of the pattern of residual stresses (rolled and welded sections) on the LTB of carbon steel I-beams under fire conditions will be also evaluated. The objective is to see whether it could also be worth taking these parameters into account when designing a carbon steel beam at elevated temperature. For the sake of clarity in the discussions, Table 4.6 shows the effects that are considered or not in EN 1993-1-1, EN 1993-1-2, Vila Real *et al.* (2003c), and the proposal presented in this work.

Table 4.6 – Comparison between the several LTB proposals.

	20°C	Elevated temperatures		
	EN 1993-1-1	EN 1993-1-2	Vila Real *et al.* (2003c)	New proposal
Steel grade	NO	YES*	YES*	YES**
Load type	YES	NO	YES	YES
Cross-section (through the relation h/b)	YES	NO	NO	YES
Residual stresses	YES	NO	NO	YES

* All the carbon steel grades are treated in the same way; ** The grade S460 is treated in a different way.

4.3.4.1 Case study

A simply supported beam with fork supports was chosen to explore the influence of the various parameters mentioned in the previous section.

Regarding the bending moment variation along the member length, five values (-1, - 1/2, 0, 1/2 and 1) of the ψ ratio (see Figure 4.23) have been investigated as well as a uniformly distributed load and a mid span concentrated load. The influence of the h/b ratio, for both hot rolled and welded sections, has also been investigated.

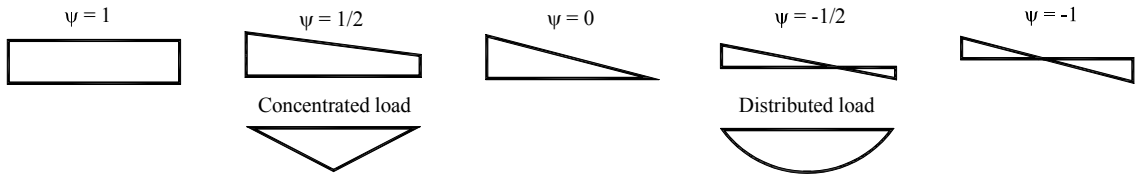

Figure 4.23 – Studied bending diagrams in carbon steel beams.

The following rolled and welded cross-sections were used: IPE220 section (representative of $h/b = 2$), HEA500 section (representative of $h/b < 2$) and IPE500 section (representative of $h/b > 2$). Three types of carbon steel grade were used: S235, S355 and S460 for each cross-section.

Table 4.7 shows all the cases that have been studied. More than 5000 finite element simulations were performed corresponding to an average of 10 beam lengths analysed for each case.

Table 4.7 – Cases studied for the LTB of carbon steel beams.

	High temperatures (400, 500, 600 and 700 ºC)													
	Hot rolled beams subjected to LTB							Welded beams subjected to LTB						
	ψ					Point Load	Distrib. Load	ψ					Point Load	Distrib. Load
	1	1/2	0	-1/2	-1			1	1/2	0	-1/2	-1		
HEA500														
S 235	✓	✓	✓	✓	✓	✓	✓	✓	✓	✓	✓	✓	✓	✓
S 355	✓	✓	✓	✓	✓	✓	✓	✓	✓	✓	✓	✓	✓	✓
S 460	✓	✓	✓	✓	✓	✓	✓	✓	✓	✓	✓	✓	✓	✓
IPE220														
S 235	✓	✓	✓	✓	✓	✓	✓	✓	✓	✓	✓	✓	✓	✓
S 355	✓	✓	✓	✓	✓	✓	✓	✓	✓	✓	✓	✓	✓	✓
S 460	✓	✓	✓	✓	✓	✓	✓	✓	✓	✓	✓	✓	✓	✓
IPE500														
S 235	✓	✓	✓	✓	✓	✓	✓	✓	✓	✓	✓	✓	✓	✓
S 355	✓	✓	✓	✓	✓	✓	✓	✓	✓	✓	✓	✓	✓	✓
S 460	✓	✓	✓	✓	✓	✓	✓	✓	✓	✓	✓	✓	✓	✓

4.3.4.2 The lateral torsional buckling code provisions of Eurocode 3

In order to provide a basis for the subsequent parametric study, comparisons of the code provisions for the LTB of beams at room and high temperatures against numerical results are described below.

4.3.4.2.1 Eurocode formulae at room temperature

At room temperature, as for stainless steel prescriptions, carbon steel beams cross-sectional Classes 1 and 2 subjected to major-axis bending must generically satisfy the following relation:

$$M_{b,Rd} = \chi_{LT} W_{pl,y} \frac{f_y}{\gamma_{M1}} \tag{4.46}$$

where χ_{LT} represents the reduction factor for LTB and depends on the so-called non-dimensional slenderness, $\overline{\lambda}_{LT}$, given by

$$\overline{\lambda}_{LT} = \sqrt{\frac{W_{pl,y} f_y}{M_{cr}}} \tag{4.47}$$

The calculation of M_{cr} is given in section 4.2.2.1.

In both the ENV and EN versions of part 1-1 of EC3, the reduction factor χ_{LT} is formally based on the Rondal-Maquoi formula, detailed derivations being found in Maquoi and Rondal (1978). In contrast to the ENV implementation that presented a single option for the evaluation of the LTB reduction factor χ_{LT}, summarized in Table 4.8, the EN version allows two alternatives, also summarized in Table 4.8 and explained below, where α_{LT} denotes the imperfection factors for LTB curves given by Table 4.10, Table 4.11 and Table 4.12.

The first method described in the EN 1993-1-1, denoted “General Case” in Figure 4.24, basically reproduces the ENV proposal with a modified level of imperfection factors α_{LT}, and more strict conditions to neglect the LTB check (see Table 4.8).

A careful examination of the general procedure discussed above reveals that the influence of the bending moment diagram on the LTB resistance of the beam only appears indirectly through the value of the elastic critical moment. This assumption is over-conservative, as

can easily be seen by comparing with, for example, the Australian code of practice, or the theoretical results of Trahair and Bradford (1998).

The second method, denoted "Special case" in Figure 4.24, applicable for the particular case of rolled sections or equivalent welded sections, yields greater LTB resistance. The detailed procedure for this method is also shown in Table 4.8. It is noted that two modifying parameters $\bar{\lambda}_{LT,0}$ and β are introduced, which should be taken as: $\lambda_{LT,0} = 0.4$ (maximum value) and $\beta = 0.75$ (minimum value). The dispensing conditions for LTB check are relaxed as shown in Table 4.8.

Additionally, for the second method, and to address the issue of the influence of the bending moment diagram, the use of a modified reduction factor $\chi_{LT,\mathrm{mod}}$ (see Table 4.8), is allowed, which depends on the moment distribution diagram.

Table 4.8 – Comparison between ENV 1993-1-1 and EN 1993-1-1 formulae.

	ENV 1993-1-1	EN 1993-1-1	
	(5.5.3)	General Case (6.3.2.2)	Special Case (6.3.2.3)
$\chi_{LT} = \min$ of	$\dfrac{1}{\phi_{LT} + \sqrt{\phi_{LT}^2 - \bar{\lambda}_{LT}^2}}, 1$		$\dfrac{1}{\phi_{LT} + \sqrt{\phi_{LT}^2 - \beta\bar{\lambda}_{LT}^2}}, 1, \dfrac{1}{\bar{\lambda}_{LT}^2}$
$\chi_{LT,\mathrm{mod}} =$			$\dfrac{\chi_{LT}}{f}$
$f = \min$ of			$1 - \dfrac{1}{2}(1-k_c)\left[1 - 2(\bar{\lambda}_{LT} - 0.8)^2\right], 1$
$\phi_{LT} =$	$\dfrac{1}{2}\left[1 + \alpha_{LT}(\bar{\lambda}_{LT} - 0.2) + \bar{\lambda}_{LT}^2\right]$		$\dfrac{1}{2}\left[1 + \alpha_{LT}(\bar{\lambda}_{LT} - \bar{\lambda}_{LT,0}) + \beta\bar{\lambda}_{LT}^2\right]$
		Dispensing Conditions	
$\bar{\lambda}_{LT}$	0.4	0.2	0.4
M_{Ed}/M_{cr}	-	0.04	0.16

To determine factor f, Table 4.9 gives the correction factor k_c in function of the loading type.

The imperfection factor α_{LT} depends on the buckling curve that is selected according to the relation h/b, as illustrated in Table 4.10 and Table 4.11 for the two different cases ("General case" and "Special case").

Table 4.9 – Correction factors for LTB of carbon steel elements at room temperature.

Moment distribution	Class 1, 2, 3 sections k_c
$-1 \le \psi \le 1$ 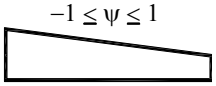	$\frac{1}{1.33 - 0.33\psi}$
Concentrated load 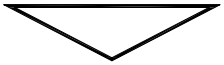	0.86
Distributed load 	0.94

Table 4.10 – Selection of LTB curve for the general case.

Cross-section	Limits	Buckling curve
Rolled I-sections	$h/b \le 2$	a
	$h/b > 2$	b
Welded I-sections	$h/b \le 2$	c
	$h/b > 2$	d
Other cross-sections	-	d

Table 4.11 – Selection of LTB curve for the special case.

Cross-section	Limits	Buckling curve
Rolled I-sections	$h/b \le 2$	b
	$h/b > 2$	c
Welded I-sections	$h/b \le 2$	c
	$h/b > 2$	d
Other cross-sections	-	d

The imperfection factors for the LTB are given in Table 4.12.

Table 4.12 – Imperfection factors for LTB curves.

Buckling curve	a	b	c	d
Imperfection factor α_{LT}	0.21	0.34	0.49	0.76

Figure 4.24 shows the beam design curve for LTB using the two methods presented at the EN 1993-1-1 (CEN, 2005a). The case of an IPE220 of the carbon steel grade S235, for the three values of the ψ ratio, -1, 0 and 1 shown in Figure 4.23, is presented here. The beam design curves from EC3 are compared with the numerical results from SAFIR. This parametric study was also made for the cases presented in Table 4.7, but at ambient temperature. This study (that can be found in Appendix D) shows that the method General case with the factor f, according to the loading type, also provides safe and accurate results (Vila Real *et al.*, 2006).

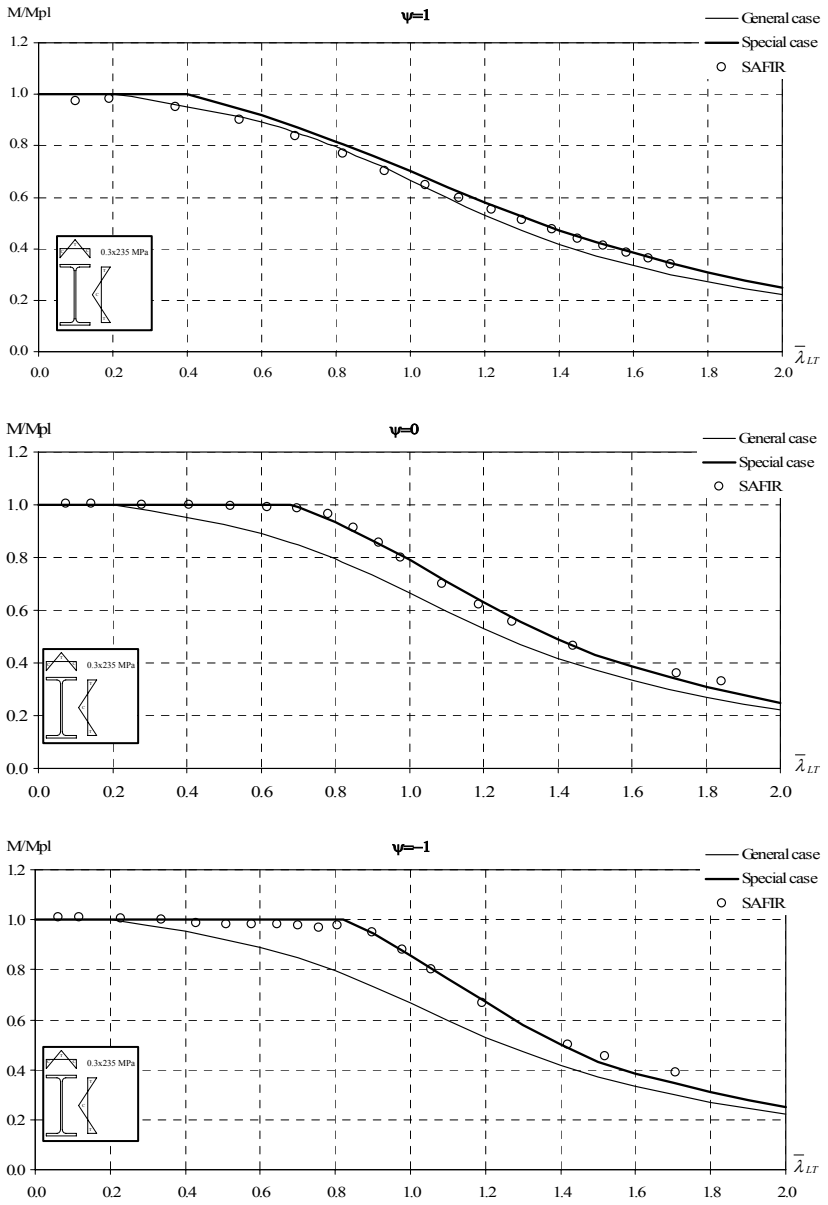

Figure 4.24 – Numerical results for an IPE220 of carbon steel grade S235 at room temperature.

4.3.4.2.2 Lateral torsional buckling at high temperatures

The EC3 design formulae for the LTB, of steel elements at high temperatures, are presented in section 4.3.2.1. This proposal was based on researches (Vila Real and Franssen, 1999, 2001) on the behaviour of the European hot rolled profile IPE220, in carbon steel grades S235 and S355 submitted to uniform bending.

In this section, the influence of the carbon steel grade, the type of the cross-section, the pattern of the residual stresses (hot rolled or welded section) and finally the influence of the shape of the bending diagrams will be examined and the results compared to the formulae from EN 1993-1-2.

The influence of the steel grade

To show here the influence of the carbon steel grade, an IPE220 profile has been considered submitted to a uniform bending moment diagram ($\psi = 1$). Figure 4.25 shows that the EC3 proposal is in good agreement with the numerical results for the carbon steel grades S235 and S355 (see Figure 4.25a and Figure 4.25b).

However, for the carbon steel grade S460 the beam design curve should go down slightly (in the intermediate range of the non-dimensional slenderness) to ensure a similar level of accuracy as for the other two carbon steel grades (see Figure 4.25c).

The influence of the cross-section

To study the influence of the type of the cross-section, an IPE220 section (representative of $h/b = 2$), a HEA500 section (representative of $h/b < 2$) and a IPE500 section (representative of $h/b > 2$) were chosen.

Figure 4.26 compares the EC3 proposal with the numerical results for the three cross-sections for the case of uniform bending ($\psi = 1$) and for the carbon steel grade S235. This figure shows that as the h/b ratio of the cross-section increases, the beam design curve should go down to ensure a similar level of accuracy.

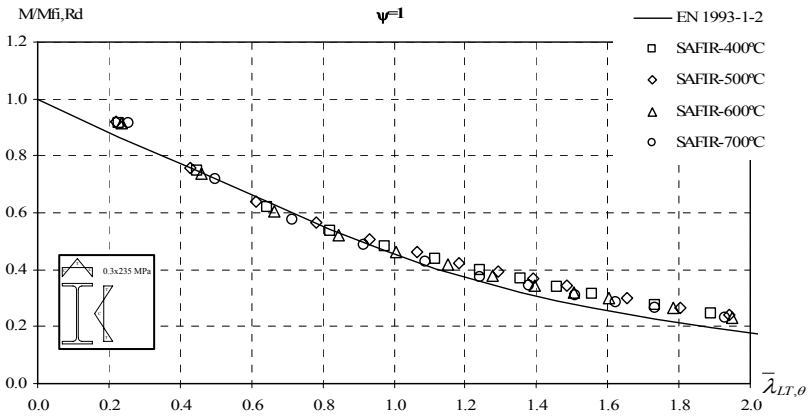

a) S235

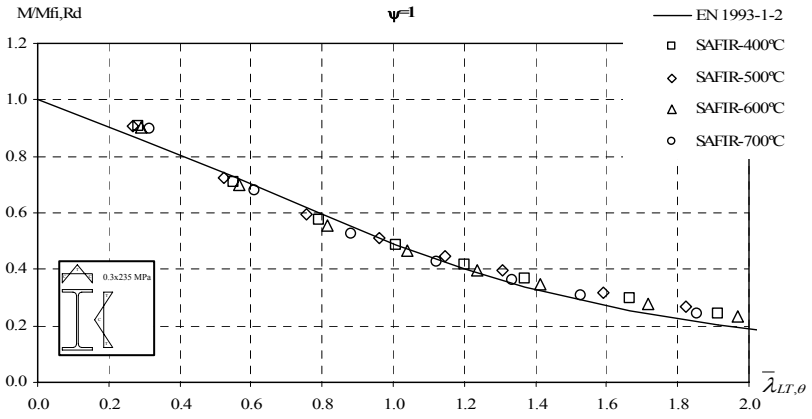

b) S355

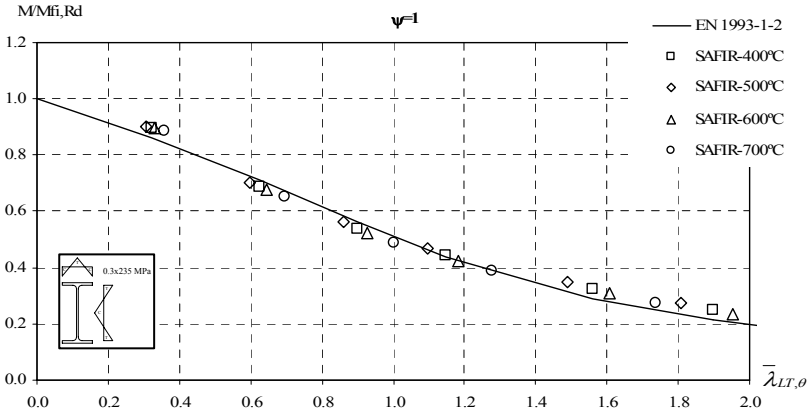

c) S460

Figure 4.25 – Beam design curve from EN 1993-1-2: comparison with numerical results for an IPE220.

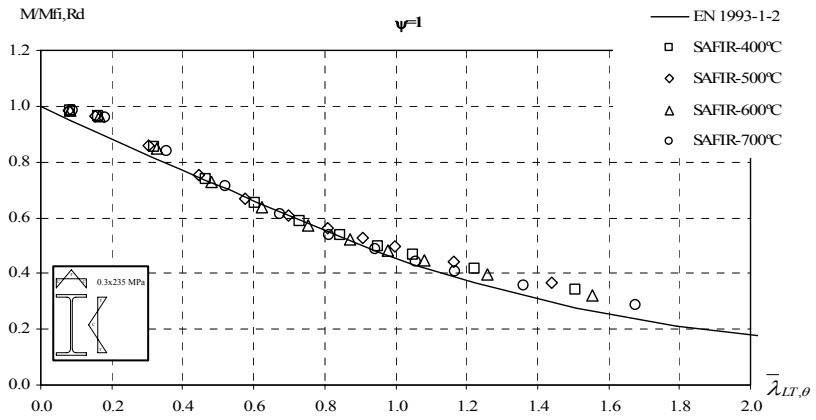

a) HEA500

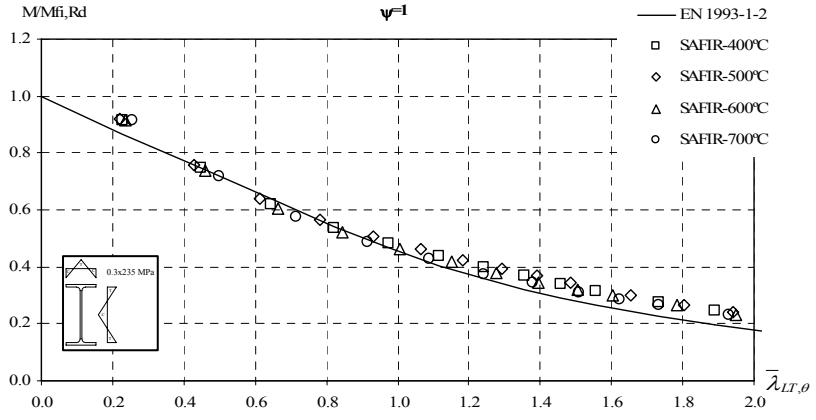

b) IPE220

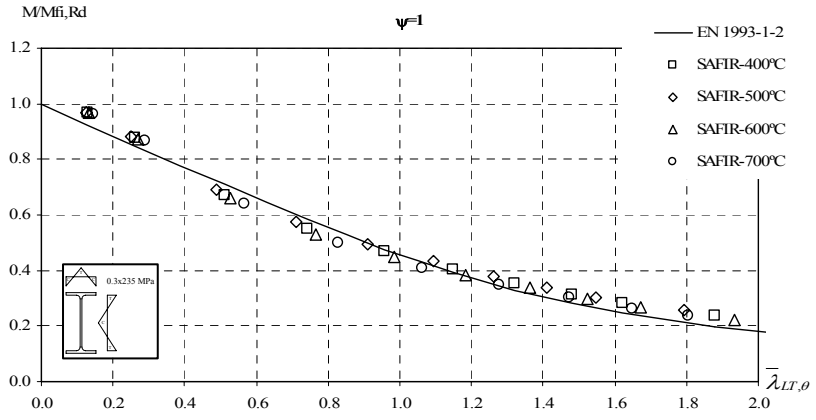

c) IPE500

Figure 4.26 – Influence of the cross-section on the LTB curve: comparison with EN 1993-1-2.

The influence of the residual stresses (hot rolled or welded sections)

To analyse the influence of the residual stresses, the proposal of the EC3 was compared with the numerical results obtained for a hot rolled and a welded section which exhibit different patterns of residual stresses (as shown in section 3.3.1).

Figure 4.27 compares the EC3 proposal with the numerical results for a hot rolled and a welded HEA500 profile in carbon steel grade S355 submitted to uniform bending diagrams ($\psi = 1$). This figure shows that for the welded section, the beam design curve of the EC3 proposal should go down slightly, to ensure the same degree of accuracy as for the hot rolled section.

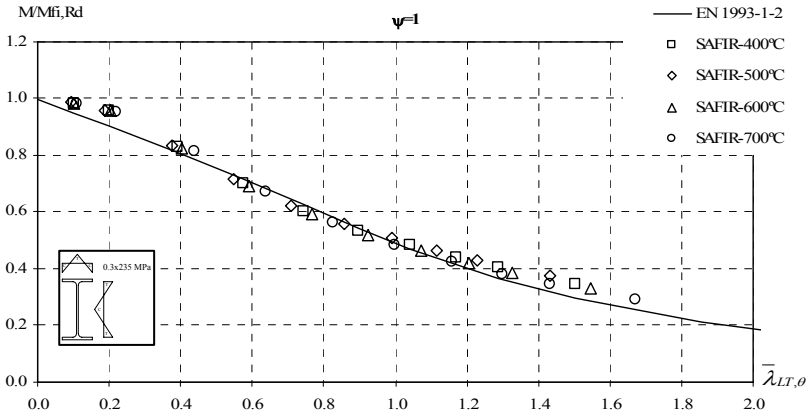

a) HEA500 (Hot rolled)

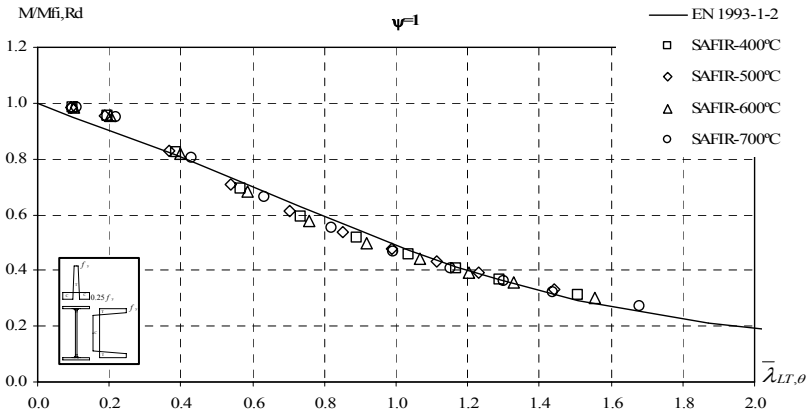

b) HEA500 (Welded)

Figure 4.27 – Influence of the residual stresses on the LTB curve for the HEA500: comparison with EN 1993-1-2.

The influence of the applied loads

As shown in Figure 4.26, for the case of non-uniform bending, i. e. for values of the ψ ratio equal to -1 and 0, the equations prescribed in EC3 (see section 4.3.2.1) lead to over-conservative results (Vila Real *et al.*, 2003c) when compared to the numerical results (illustrated for a IPE220 of carbon steel grade S235 in Figure 4.28). This is due to the fact that the LTB curves from EC3 were based on bending moment distributions that are constant along the beam (Vila Real and Franssen, 2001). As can be seen in Figure 4.28, non-uniform moment diagrams yield significantly higher buckling resistance moments. This figure clearly highlights the fact that there is room for improvement in the evaluation of the LTB resistance of carbon steel beams under fire conditions.

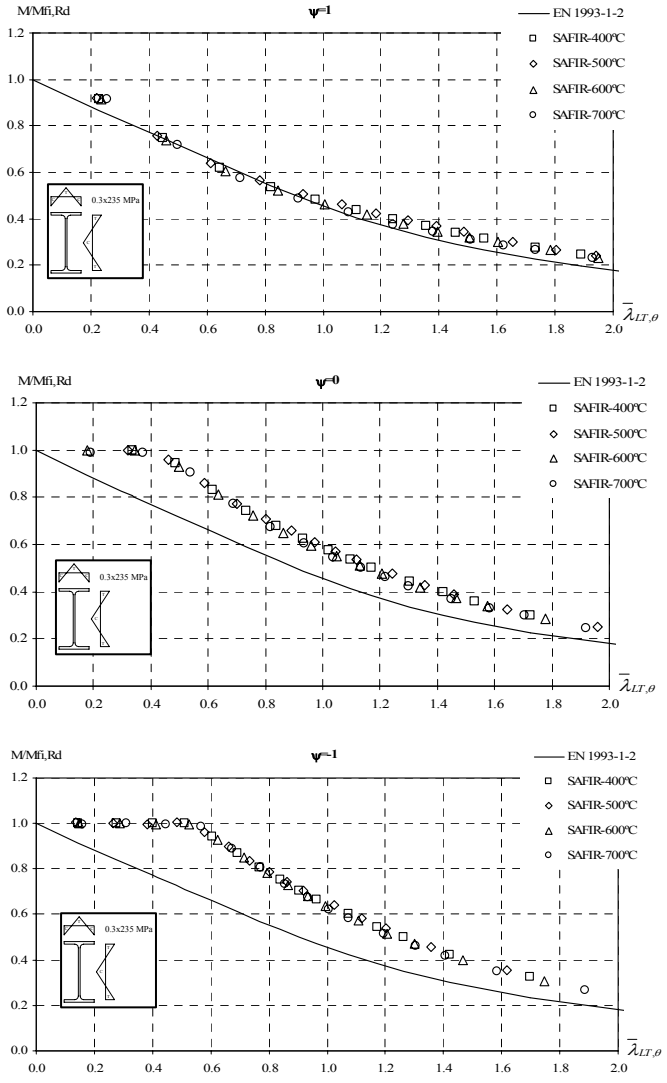

Figure 4.28 – Influence of the applied load on the LTB: comparison with EN 1993-1-2.

4.3.4.3 Improvement of Eurocode 3 formulae at high temperatures: a new proposal

The influence of the carbon steel grade, the type of the cross-section and the effect of the residual stresses is not too big when considered separately as shown in figures Figure 4.25 to Figure 4.27. However, when these three effects play simultaneously, the present design equation is more markedly on the unsafe side, as shown in Figure 4.29, justifying the adoption of a new proposal.

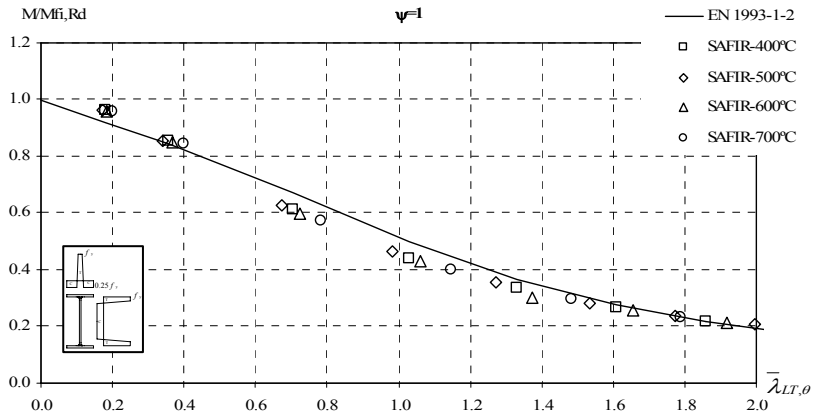

Figure 4.29 – Numerical results for a welded IPE500 in carbon steel grade S460: comparison with EN 1993-1-2.

The equation (4.26), which defines the imperfection factor at high temperatures α, is rewritten in function of a severity factor η

$$\alpha = \eta\sqrt{235/f_y} \tag{4.48}$$

The severity factor η is given in Table 4.13. The results suggest that, for values of the relation h/b smaller than 2, other imperfections factors should be adopted. However, due to the fact that these smaller relations are more common in columns, and being the study of steel columns in case of fire based on experimental results (Franssen *et al.*, 1996), the new proposal presented here will focus mainly on typical beams I-steel sections, providing, at the same time, safety to those sections with smaller h/b relation.

To take into account the moment distribution between the lateral restrains of members the reduction factor $\chi_{LT,fi}$ must be modified as follows:

$$\chi_{LT,fi,\mathrm{mod}} = \frac{\chi_{LT,fi}}{f} \quad \text{but} \quad \chi_{LT,fi,\mathrm{mod}} \leq 1 \tag{4.49}$$

where f depends on the loading type.

Table 4.13 – Severity factor for the LTB of carbon steel elements in case of fire.

Cross-section	limits	η	
		S235, S275, S355, S420	S460
Rolled I-section	$h/b \leq 2$	0.65	0.70
	$h/b > 2$	0.75	0.80
Welded I-section	$h/b \leq 2$	0.70	0.75
	$h/b > 2$	0.80	0.85
Other cross-sections	-	0.80	0.85

Initially, the adequacy of part 1-1 proposals for f and k_c (see Table 4.8 and Table 4.9) were tested. The results, denoted as "EN 1993-1-2 / f" in Figure 4.31, are better and closer to the numerical values but still remain conservative. Consequently, in order to have a better approximation, taking into account the moment distribution between the lateral restraints of members, new coefficients for f and k_c were adjusted (Lopes, 2003), given by the following equation

$$f = 1 - 0.5(1 - k_c) \tag{4.50}$$

and k_c is a correction factor according to Table 4.14, established by numerical adjustment to match as closely as possible a representative sample of finite element numerical results.

Table 4.14 – Correction factors for the LTB of carbon steel elements in case of fire.

Moment distribution	Class 1, 2, 3 sections k_c
$-1 \leq \psi \leq 1$ 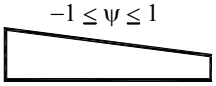	$0.6 + 0.3\psi + 0.15\psi^2$ but $k_c \leq 1$
Concentrated load 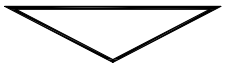	0. 79
Distributed load 	0.91

Note: for others bending diagrams $k_c = 1$.

Figure 4.30 shows the beam design curves of the new proposal for different bending diagrams.

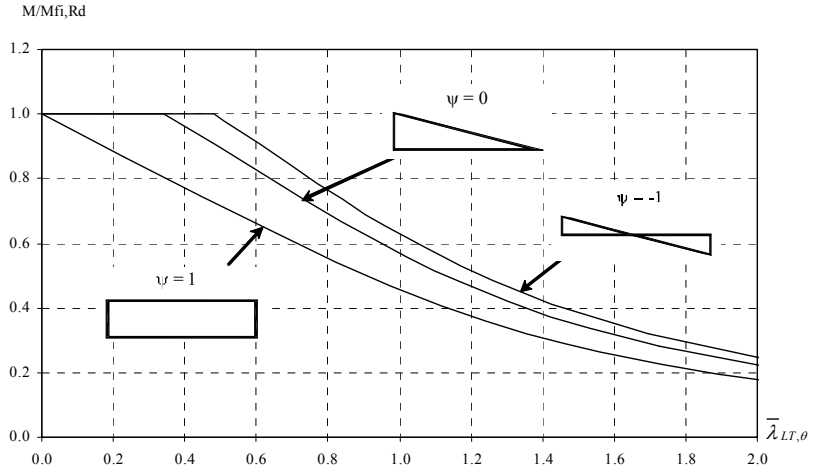

Figure 4.30 – New proposal for different bending diagrams.

The Figure 4.31 compares the performance of the utilization of the factor f from the part 1-1 (see Table 4.8 and Table 4.9) with the utilization of the factor f proposed in equation (4.50) in the formulae from the fire part of EC3. The numerical results were obtained for a hot rolled IPE220 of the carbon steel grade S235.

Using this design proposal for non-uniform bending, it is possible to state a maximum slenderness value for dispending the LTB (Lopes *et al.*, 2008a).

The maximum slenderness value for dispending the LTB in beams is the value corresponding to the plateau length in the buckling curves for loading types different from moments applied in the extremities (see Figure 4.30).

In the next section the new proposal is validated for different cross-sections, different load cases, different carbon steel grades and different residual stresses (hot rolled sections and welded sections).

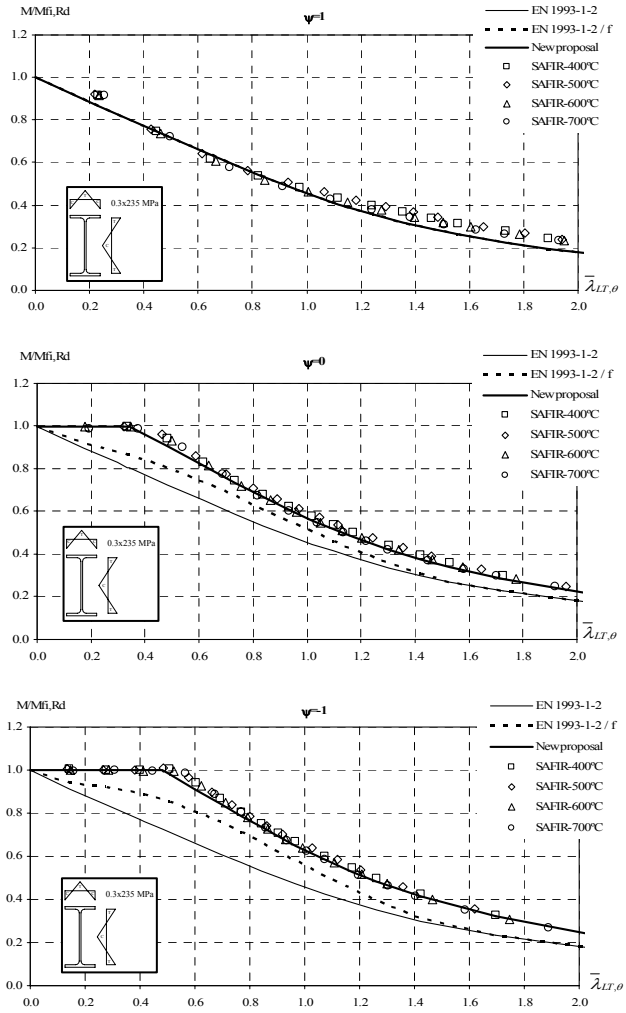

Figure 4.31 – Comparison between the EN 1993-1-2 / f, the new proposal and the numerical results.

4.3.4.4 Accuracy of the proposal

In this section, it is shown the validation of this new proposal for different cross-sections, different load cases, different carbon steel grades and different residual stresses.

Numerical validation

The beam design curve from part 1-2 of the EC3 is denoted here as "EN 1993-1-2", and the curve obtained adopting the new factor f and the severity factor as defined in Table 4.8 is denoted as "New proposal". The welded section equivalent to the IPE500, representative of $h/b > 2$ in the grade S460 for all the studied load cases, is shown in Figure 4.32. Other comparisons as presented in Table 4.7 can be seen in Appendix E.

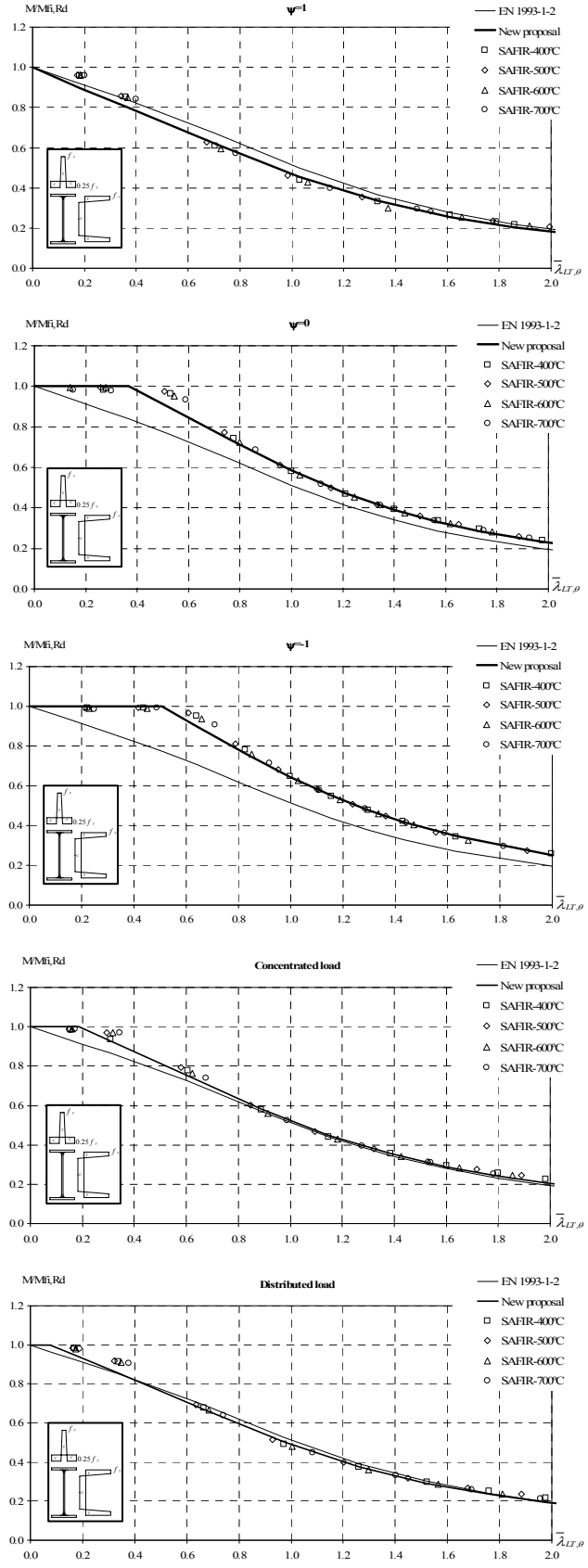

Figure 4.32 – Numerical results for a welded IPE500 of carbon steel grade S460 at high temperatures for all load cases studied.

Statistical evaluation

The values of the severity factor η defined in the Table 4.8 were chosen so that the new proposal has the same degree of accuracy as the formulae of the EN 1993-1-2 for a hot rolled IPE220 submitted to uniform bending (Vila Real and Franssen, 1999; 2001).

This statistical study was only performed for uniform bending due to the improvement, provided by the new proposal for other loading types, being clear in the numerical validation (see Figure 4.32).

For each chosen severity factor, it is possible to evaluate the ratio between the analytical value of the ultimate design LTB resistance moment $M_{ult,i}^{Analytical}$ and the corresponding SAFIR moment. This ratio is also the ratio between the analytical and the SAFIR LTB coefficient as follows:

$$x_i = \frac{M_{ult,i}^{Analytical}}{M_{ult,i}^{SAFIR}} = \frac{\chi_{LT,i}^{Analytical}}{\chi_{LT,i}^{SAFIR}} \tag{4.51}$$

Figure 4.33 presents a comparison between the results obtained with SAFIR and the design proposals, where the continuous line represents values of x_i equal to 1 and the dashed lines values of x_i equal to 0.9 and 1.1. The proposal is safe if it leads to values of x_i lower than 1, and unsafe for values higher than 1.

The average value μ, and the standard deviation s, were calculated as:

$$\mu = \frac{\sum_{i=1}^{n} x_i}{n} \tag{4.52}$$

$$s = \sqrt{\frac{\sum_{i=1}^{n} (x_i - \mu)^2}{n-1}} \tag{4.53}$$

where n is the total number of numerical simulations.

The 632 results obtained with EN 1993-1-2 for uniform bending on both hot rolled and welded IPE220 section (representative of $h/b = 2$), HEA500 section (representative of $h/b < 2$) and IPE500 section (representative of $h/b > 2$), in carbon steel grades, S235, S355 and S460 are shown in Figure 4.33. The average value and the standard deviation are, respectively, $\mu = 0.969$ and $s = 0.075$ (see Table 4.15).

Table 4.15 – Statistical results of carbon steel beams at elevated temperatures.

	EN 1993-1-2	New proposal
Average value	0.969	0.943
Standard deviation	0.075	0.066

If the new proposal is used with hot rolled and welded IPE220, HEA500 and IPE500, in carbon steel grades S235, S355 and S460 the average value and the standard deviation take the values $\mu = 0.943$ and $s = 0.066$, respectively. This shows that the new proposal is safer than the EC3 with a smaller value of the standard deviation.

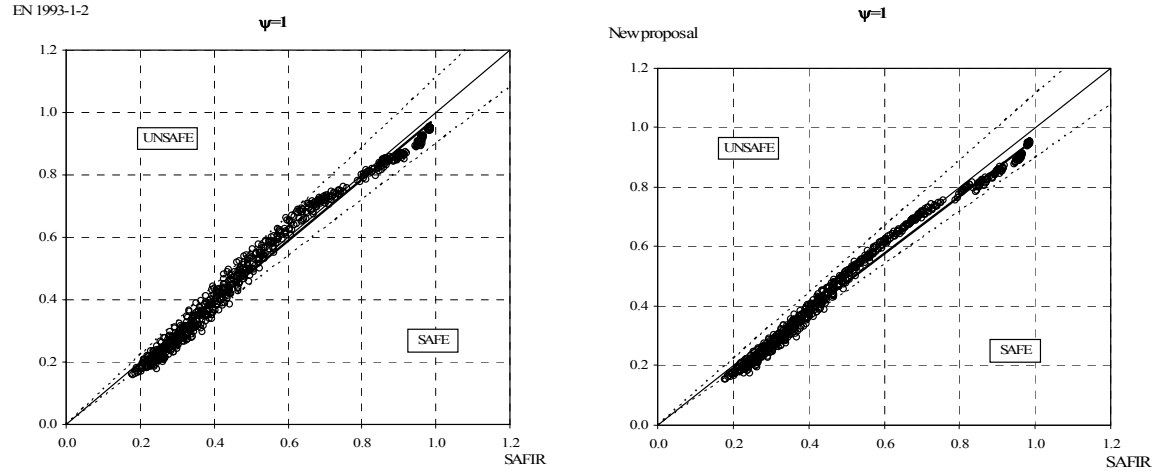

Figure 4.33 – Comparison between EN 1993-1-2, the new proposal and numerical results for the hot rolled and welded HEA500, IPE220 and IPE500 in carbon steel grade S235, S355 and S460.

Figure 4.34 shows the ratio x_i when EN 1993-1-2 is used with the hot rolled IPE220 in carbon steel grade S235 and S355 submitted to uniform bending moment. The maximum unsafe error is 5.3 % and the average unsafe error is 2.5 %. If EN 1993-1-2 is used with hot rolled and welded IPE220, HEA500 and IPE500, in the carbon steel grades S235, S355 and S460 (see Figure 4.35) these values increase to 12.8 % and 4.6 %, respectively.

The severity factor of Table 4.8 was derived so that the accuracy of the new proposal was similar to the accuracy of the EN 1993-1-2 proposal for the considered case from (Vila Real and Franssen, 1999; 2001), i.e., for the case of the hot rolled IPE220 in carbon steel grade S235 and S355. The new proposal gives the results shown in Figure 4.36, with the same unsafe error of 5.3 % as the EN 1993-1-2 and an unsafe average error of 1.8 %.

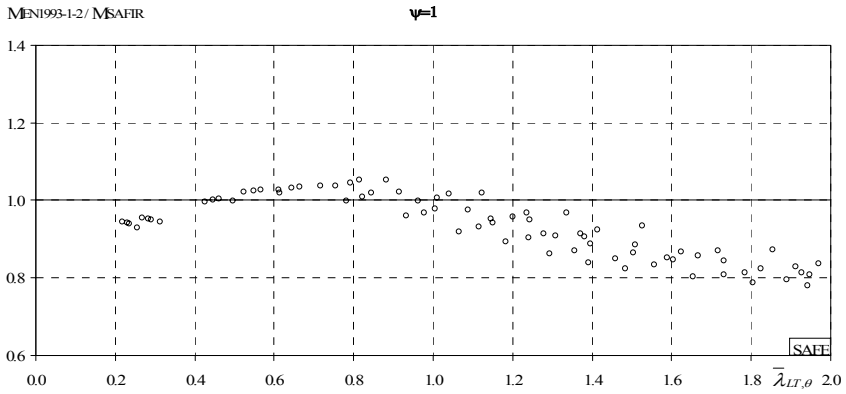

Figure 4.34 – Ratio between analytical and SAFIR, for EN 1993-1-2 with hot rolled IPE220 in carbon steel grade S235 and S355.

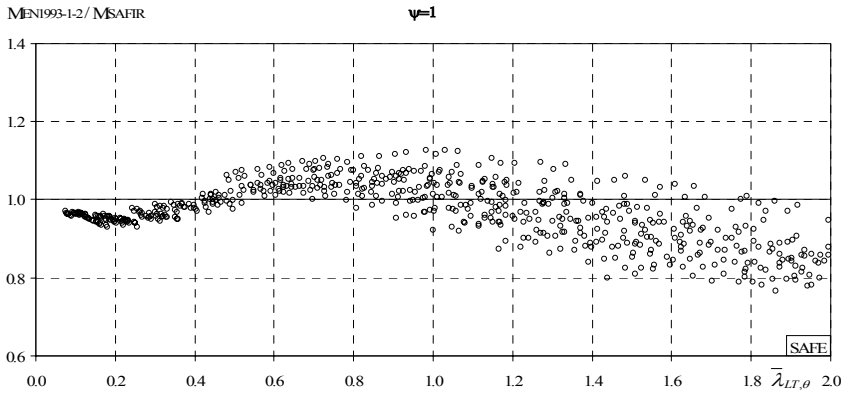

Figure 4.35 – Ratio between analytical and SAFIR, for EN 1993-1-2 with the hot rolled and welded HEA500, IPE220 and IPE500 in carbon steel grade S235, S355 and S460.

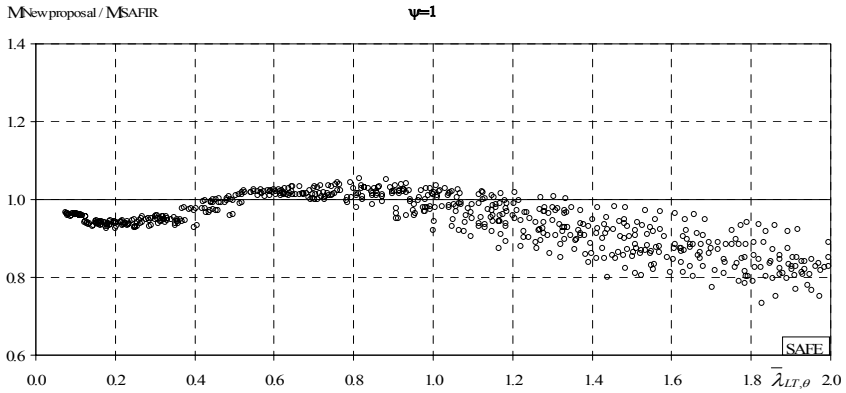

Figure 4.36 – Ratio between analytical and SAFIR, for the new proposal with the hot rolled and welded HEA500, IPE220 and IPE500 in carbon steel grade S235, S355 and S460.

4.3.4.5 Interaction formulae for beam-columns

In this section the improvement obtained with new proposal for lateral torsional buckling is evaluated in the interaction formulae for beam-columns according to EC3.

A simply supported beam-column with span L and fork supports was chosen to test the validity of the beam-column safety verifications, loaded with end-moments in the major axis and axial compression. Regarding the bending moment variation along the member length, two values (0 and -1) of the ψ ratio (see Figure 4.37) have been investigated. The uniform bending diagram, corresponding to $\psi = 1$, was not considered because in this situation the new proposal for LTB coincides with the actual version of the EC3. A hot rolled IPE220 carbon steel section of grade S235 was used, with a uniform temperature distribution in the cross-section of 600 ºC. A triangular distribution for the residual stresses (as shown in section 3.3.1) was adopted.

Figure 4.37 – Studied bending diagrams in carbon steel beam-columns.

The interaction formulae prescribed in EC3 for the design of steel structural elements with axial compression and bending with the possibility of occurring LTB are given in section 4.3.3.2.1.

Figure 4.38 and Figure 4.39 show a parametric study comparing the interaction formulae from EN 1993-1-2 with and without the new proposal for the LTB (factor f) for bending ratios $\psi = 0$ and $\psi = -1$. The beam-columns tested had 1, 2, 3 and 4m, corresponding to the non-dimensional slenderness values $\bar{\lambda}_{z,\theta} = 0.53$, $\bar{\lambda}_{z,\theta} = 1.06$, $\bar{\lambda}_{z,\theta} = 1.59$ and $\bar{\lambda}_{z,\theta} = 2.12$ respectively. The LTB non-dimensional slenderness values are given in Table 4.5.

Table 4.16 – Non-dimensional slenderness values for LTB of the cases presented at 600 ºC.

Moment diagram	$L = 1\,\text{m}$	$L = 2\,\text{m}$	$L = 3\,\text{m}$	$L = 4\,\text{m}$
$\psi = 0$	0.34	0.62	0.84	1.02
$\psi = -1$	0.28	0.51	0.69	0.84

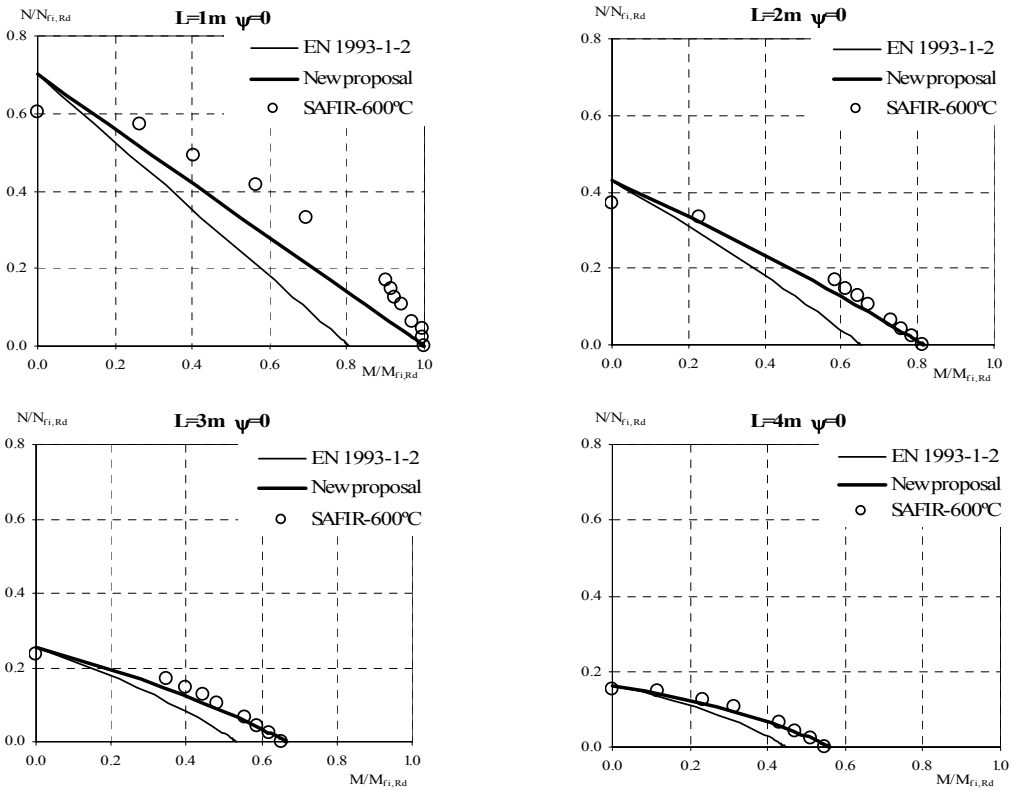

Figure 4.38 – Interaction diagrams of EN 1993-1-2, for triangular bending moment diagrams.

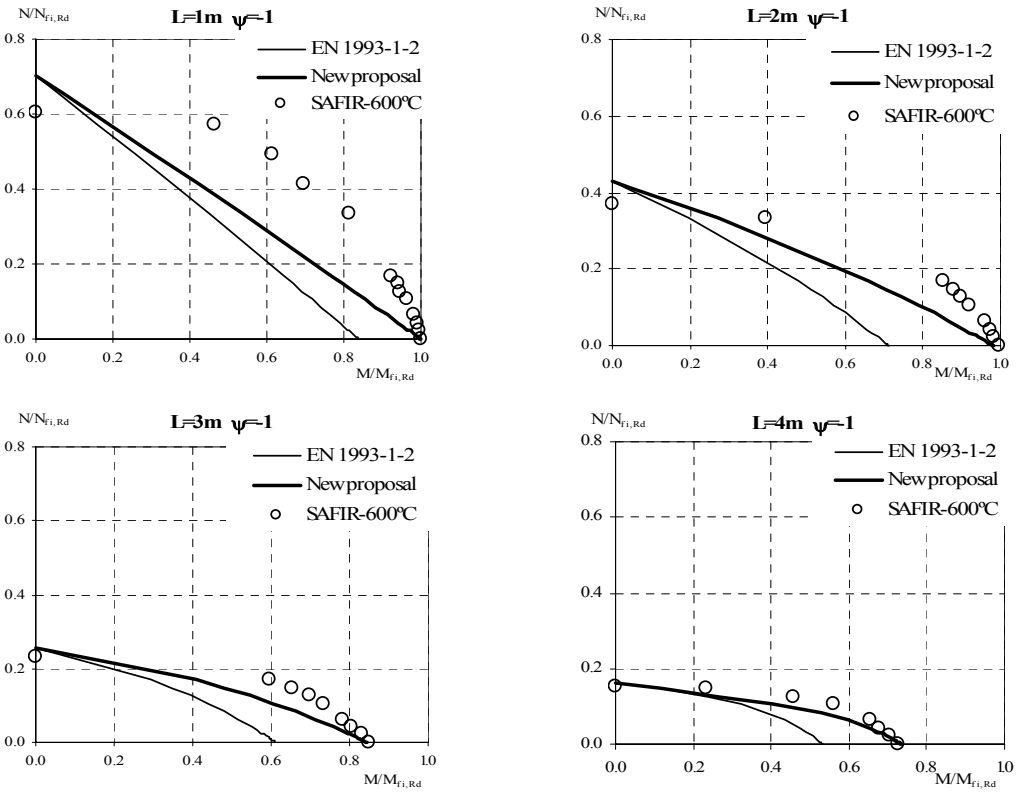

Figure 4.39 – Interaction diagrams of EN 1993-1-2, for bi-triangular bending moment diagrams.

It can be seen, comparing the analytical values with the numerical ones, that a significant improvement was introduced when the new proposal for LTB is used.

4.4 Conclusions

In this chapter the prescribed methodologies, in accordance with EC3, for the design of the stainless steel structural elements: columns, beams and beam-column, at ambient temperature and at high temperatures were presented.

It can be concluded that for welded I-stainless steel sections, the design formulae included in part 1-4 of EC3 (CEN, 2006a):

- are unsafe for the flexural buckling in the strong and in the weak axis;
- are too conservative for the LTB in the case of non-uniform bending;
- are, most of the times, over conservative for bending and axial compression without LTB, this is due to the fact that the interaction curves do not vary with the bending diagram, as it should be expected;
- and finally, the interaction curves, for axial compression with bending and with the possibility of occurring LTB, do not provide a good approximation to the numerical results.

The design formulae for welded I-stainless steel profiles at high temperatures, originally developed for carbon steel elements, and included in part 1-2 of EC3 (CEN, 2005b):

- are unsafe for the flexural buckling in the strong and in the weak axis;
- are too conservative for the LTB in the case of non-uniform bending, and present some unsafe results for an intermediate range of slenderness;
- are unsafe for bending and axial compression without LTB, when considering the original proposal for carbon steel beam-columns (Talamona, 1995). This fact can be partially justified by the unsafe nature of the flexural buckling curves;
- and finally, the interaction curves, for axial compression with bending and with the possibility of occurring LTB, are too conservative for high moment ratios in the case

of non-uniform bending and again unsafe for low axial compression ratios, not providing a good approximation to the numerical results.

Finally, the numerical research on carbon steel elements reported in this chapter has confirmed that the influence of the bending moment distribution along the member has to be taken into account when evaluating the resistance to LTB of carbon steel members subjected to fire. Otherwise, basing the design on a constant moment distribution can lead to a very uneconomical design.

Other factors that influence the LTB of carbon steel beams under fire situation have been investigated, namely, the carbon steel grade, the pattern of the residual stresses (hot rolled or welded sections) and the ratio h/b. Their influence when considered separately is rather limited; nevertheless the combination of these three factors provides a more significant effect. It has been shown that the consideration of these three factors: i) can be done easily by a slight modification of the existing design equations; ii) slightly improves the safety level; iii) allows restoring consistency between the equations used at room temperature and at elevated temperatures.

The numerical results reported here have been compared to the simple design equation of the EC3. The influence of the different investigated factors is nevertheless independent of the code used for a simple design. The influence of these factors could thus be taken into account in any simple design equation. Also, this proposal for carbon steel elements, will also serve as base for the development of stainless steel design rules at high temperatures.

Based on these conclusions, in Chapter 5 new proposals for the design procedures for stainless steel structural elements, at ambient temperature and in case of fire, will be presented and validated.

Chapter 5

Design proposals for stainless steel structural elements

Chapter 5. Design proposals for stainless steel structural elements

Chapter 5. Design proposals for stainless steel structural elements

5.1 Introduction

In Chapter 4 it was shown that the design formulae, for stainless steel structural elements (columns, beams, beam-columns), proposed in EC3 (CEN, 2006a; CEN, 2005b) did not provide good approximations to their real behaviour. EC3 revealed to be some times uneconomical, and more importantly and critical, other times unsafe. Based on numerical results achieved with SAFIR, in this chapter new design proposals will be presented, for those structural elements.

The study presented here was made in I-welded open sections, at ambient temperature and in case of fire.

The studies on the flexural buckling, of stainless steel columns, resulted in the proposal of safer buckling curves. Also, it is shown that these flexural buckling curves at high temperatures (CEN, 2005b) should vary with the buckling axis, as it is already prescribed at room temperature, according to part 1-4 of EC3 (CEN, 2006a).

In stainless steel beams the beneficial influence, of non-uniform bending moment distributions, resulting from the reduced plastic zones connected with variable bending along the beam, is not taken into account. This fact provides an over conservative design for the case of non-uniform bending diagrams. In a similar way to the proposed design approach for carbon steel elements at room temperature (CEN, 2005a), proposals for the cold and fire design of stainless steel elements with LTB are here presented.

The study made on stainless beam-columns started by evaluating the possibility of introducing coherence between the different parts of EC3 (carbon steel, stainless steel and fire parts). Thus, the recently proposed formulae for carbon steel beam-columns at room temperature, already introduced in EC3 (CEN, 2005a; Boissonnade *et al.*, 2006), are tested with the obtained results, after the necessary adaptation to stainless steel and to fire design. Additionally, new interaction curves, for the design of stainless steel beam-columns with and without LTB, at both room temperature and elevated temperatures, are presented.

Although, proposals from the literature, for the evaluation of stainless steel members in case of fire, adopt the proportional limit strain of 0.2 % (Ng and Gardner, 2007; Uppfeldt *et al.*, 2008), the use of higher deformations in fire design (2 % total strain) is recommended from EC3. Thus in the proposals presented in this chapter this assumption is considered, preserving the philosophy of the Eurocode.

5.2 At room temperature

As mentioned in Chapter 4, the safety factor γ_{M1} in stainless steel structures at room temperature takes the value of 1.1. In order to compare the actual buckling curves, in the studies presented here this factor was considered with the value of 1.0, as already adopted in carbon steel design (CEN, 2005a).

5.2.1 Compression

Based on the comparison between the numerical results obtained with SAFIR and the buckling curves given by the expressions from part 1-4 of EC3 for stainless steel structural elements subjected to axial compression, presented in section 4.2.1, a proposal for the flexural buckling resistance of columns at room temperature is made. This new proposal is shown to be safer than the formulae from the EC3.

5.2.1.1 Case study

A simply supported column, subjected to axial compression with flexural buckling about the strong axis or about the weak axis, was chosen for the parametric study. Initial imperfections and residual stresses were considered as described in section 3.3.1.

The following welded cross-sections were used: HEA200, HEB280 and HEB200 stainless steel section. The types of stainless steel grade used were: 1.4301, 1.4401 or 1.4404, 1.4571, 1.4003 and 1.4462. Table 5.1 shows all the cases that have been studied. An average of 10 lengths were analysed for each case.

Table 5.1 – Cases studied for the flexural buckling at room temperature.

	Room temperature	
	Strong axis	Weak axis
HEA200		
1.4301	✓	✓
1.4401	✓	✓
1.4404		
1.4571	✓	✓
HEB280		
1.4301	✓	✓
1.4401	✓	✓
1.4404		
1.4571	✓	✓
1.4003	✓	✓
HEB200		
1.4003	✓	✓
1.4462	✓	✓

5.2.1.2 Improvement of the Eurocode 3 formulae: a new proposal

With the purpose of achieving a better approximation to the numerical results, in compressed columns with high slenderness, a proposal to improve the EC3 formulae for the buckling of stainless steel elements is made in this section.

As in part 1-4 of EC3, in this new proposal for the design of stainless steel elements subjected to axial compression, the buckling resistance value of a compressed element is obtained with

$$N_{b,Rd} = \chi_{\min} A f_y / \gamma_{M1} \tag{5.1}$$

where the factor $\chi_{\min}$ is the minor of the reduction factors χ_i about the strong and the weak axis.

This proposal was developed in order to minimize the changes in EC3. Thus, as in part 1-1 of EC3 for the design of beams in carbon steel with LTB (CEN, 2005a; Boissonnade *et al.*, 2006), the introduction of a factor β with the value 1.5, in the equations used to determining the reduction factor χ_i and the coefficient ϕ, is suggested according to the following formulae

$$\chi_i = \frac{1}{\phi_i + \sqrt{\phi_i^2 - \beta\overline{\lambda}_i^2}} \quad \text{with} \quad \chi_i < 1 \tag{5.2}$$

$$\phi_i = \frac{1}{2}\left[1 + \alpha_i\left(\overline{\lambda}_i - \overline{\lambda}_0\right) + \beta\overline{\lambda}_i^2\right] \tag{5.3}$$

where the imperfection factor α_i and the limiting slenderness value $\overline{\lambda}_0$ are given in Table 5.2 and Table 5.3, respectively.

Table 5.2 – Imperfection factor.

Buckling mode	Type of member	α_i	
		1.4301, 1.4401, 1.4404, 1.4571, 1.4301	1.4462
Flexural	Welded open sections (major axis)	0.76	0.49
	Welded open sections (minor axis)	1.00	0.76

In this case it was observed that the behaviour of the 1.4462 stainless steel columns were rather conservative when compared to the other stainless steel grades columns, which led to the proposal of lower imperfection factors. It should be noticed that EC3 recommendations (CEN, 2005a) also acknowledge, for the flexural buckling of carbon steel elements at room temperature, the necessity of different imperfection factors for the S460 grade. This grade has, as the stainless steel 1.4462, higher yield strength than the other grades of the same material.

Table 5.3 – Limiting slenderness value.

Buckling mode	Type of member	$\overline{\lambda}_0$
Flexural	Welded open sections (major axis)	0.20
	Welded open sections (minor axis)	0.20

It will be shown in the following sections that this proposal results in an improvement on the behaviour of the buckling curves.

5.2.1.3 Accuracy of the proposal

In this section the accuracy of this new proposal is evaluated by direct comparison with the numerical results and by a statistical study.

Numerical validation

In Figure 5.1 and Figure 5.2 the results for stainless steel columns subjected to flexural buckling, about the strong axis and the weak axis, are shown. Here only the results for HEA200 and HEB200 of the stainless steel grades 1.4301 and 1.4462 are presented.

A comparison is made between the curve obtained through the formulae from part 1-4 of EC3, described on the section 4.2.1 of this thesis ("EN 1993-1-4" in the graphics), the curve based on the proposal made here (named "New proposal"), and the numerical results determined with SAFIR.

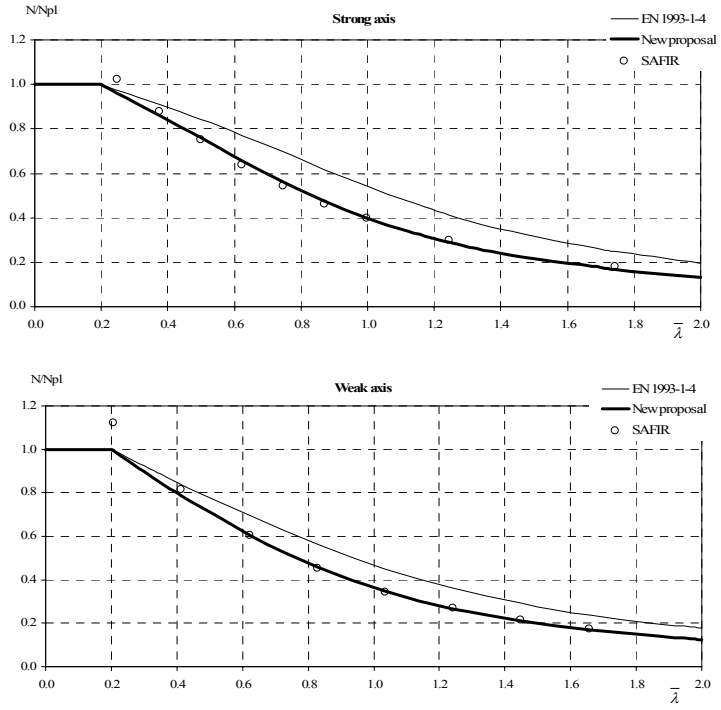

Figure 5.1 – Column with cross-section HEA200 in stainless steel grade 1.4301.

Stainless steels do not have a linear perfectly plastic zone in their stress-strain relationships, as the carbon steels. This fact justifies the occurrence of higher than 1.0 numerical results, when divided by the resistant force using the proportional limit stress corresponding to 0.2 % strain as stated in EC3 (CEN, 2005a).

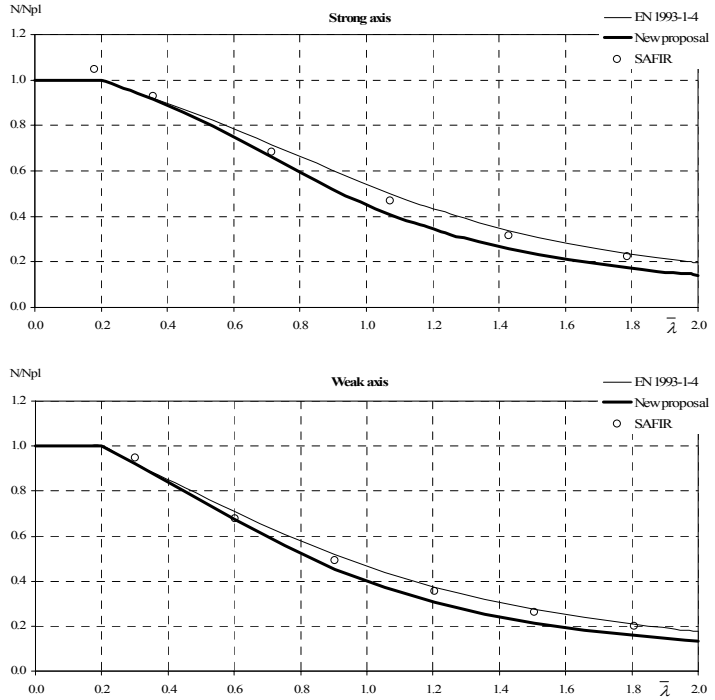

Figure 5.2 – Column with cross-section HEB200 in stainless steel grade 1.4462.

The figures show that the new proposal improves the behaviour of the buckling curves obtained with the formulae prescribed in the part 1-4 of EC3. The same behaviour was observed for other stainless steel grades and other cross-sections (see Appendix F).

Statistical evaluation

As presented in section 4.3.4, for each buckling axis, it is possible to evaluate the ratio between the analytical value of the ultimate design axial force $N_{ult,i}^{Analytical}$ and the corresponding SAFIR axial force. This ratio is also the ratio between the analytical and the SAFIR buckling coefficient as follows:

$$x_i = \frac{N_{ult,i}^{Analytical}}{N_{ult,i}^{SAFIR}} = \frac{\chi_i^{Analytical}}{\chi_i^{SAFIR}} \tag{5.4}$$

The results obtained with EN 1993-1-4 for welded HEA200, HEB280 and HEB200 sections, in stainless steel grades, 1.4301, 1.4401, 1.4571, 1.4003 and 1.4462, in a total of 73 and 69 numerical simulations for the strong and weak axis respectively, are shown in Figure 5.3 and Figure 5.4. The average value and the standard deviation are: $\mu = 1.202$

and $s = 0.116$ for the strong axis, and $\mu = 1.180$ and $s = 0.114$ for the weak axis (see Table 5.4). If the new proposal is used in those numerical results the average value and the standard deviation take the values $\mu = 0.952$ and $s = 0.069$ for the strong axis, and $\mu = 0.948$ and $s = 0.058$ for the weak axis, showing that the new proposal is safer than the EC3 with a smaller value of the standard deviation.

Table 5.4 – Statistical results of columns at room temperature.

		EN 1993-1-4	New proposal
Strong axis	Average value	1.202	0.952
	Standard deviation	0.116	0.069
Weak axis	Average value	1.180	0.948
	Standard deviation	0.114	0.058

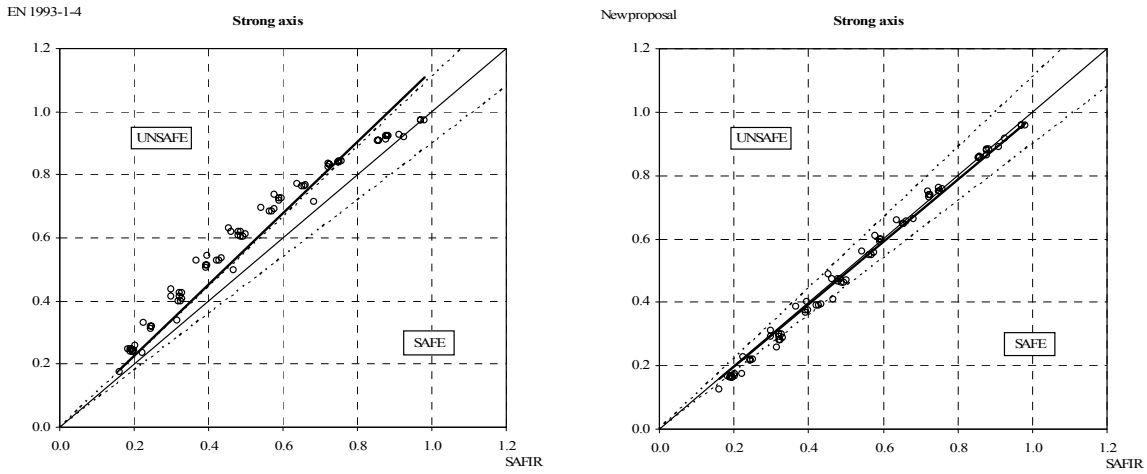

Figure 5.3 – Comparison between EN 1993-1-4, the new proposal and numerical results for the strong axis.

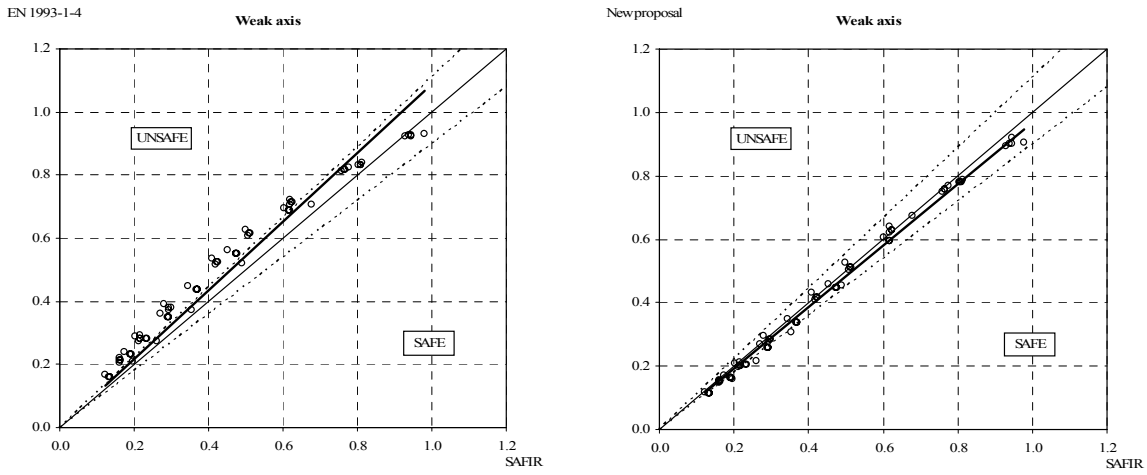

Figure 5.4 – Comparison between EN 1993-1-4, the new proposal and numerical results for the weak axis.

Figure 5.5 and Figure 5.7 show the ratio x_i, see equation (5.4), when EN 1993-1-4 is used with all the numerical results for the strong and weak axis. The maximum unsafe error is 46.6 % and 43.0 % for the strong and for the weak axis, respectively. The average unsafe error is 21.1 % and 19.6 % for the strong and for the weak axis, respectively.

The new proposal gives the results shown in Figure 5.6 and Figure 5.8, with the maximum unsafe error of 7.0 % and 5.3 % for the strong and weak axis, respectively, and an average unsafe error of 2.5 % and 2.3 % for the strong and weak axis, respectively.

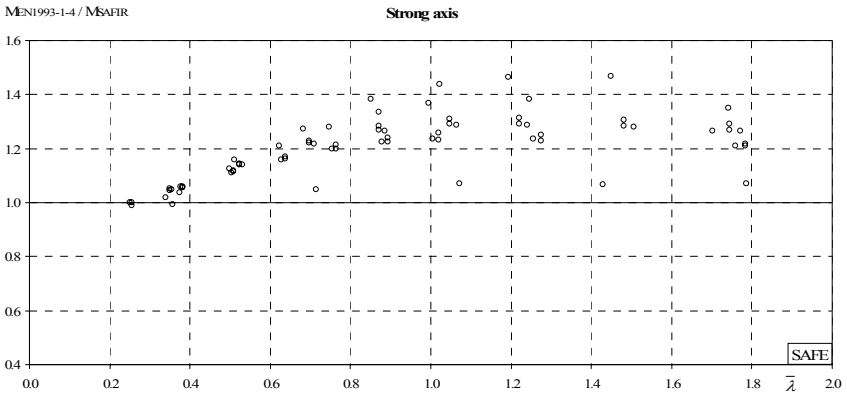

Figure 5.5 – Ratio between analytical and SAFIR results, for EN 1993-1-4 in the strong axis.

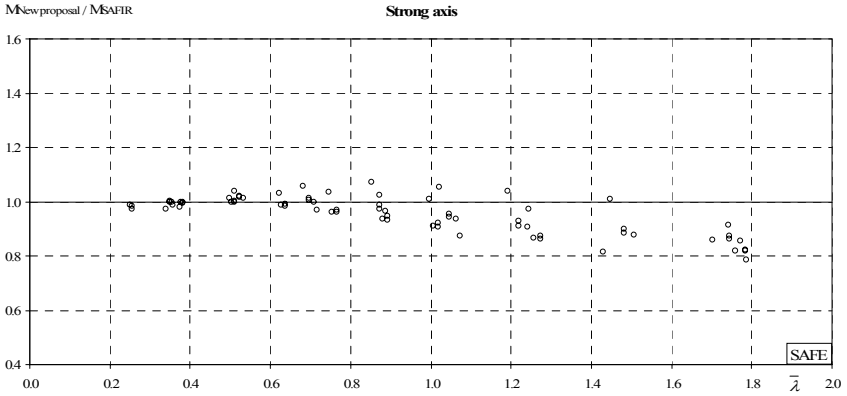

Figure 5.6 – Ratio between analytical and SAFIR results, for the new proposal in the strong axis.

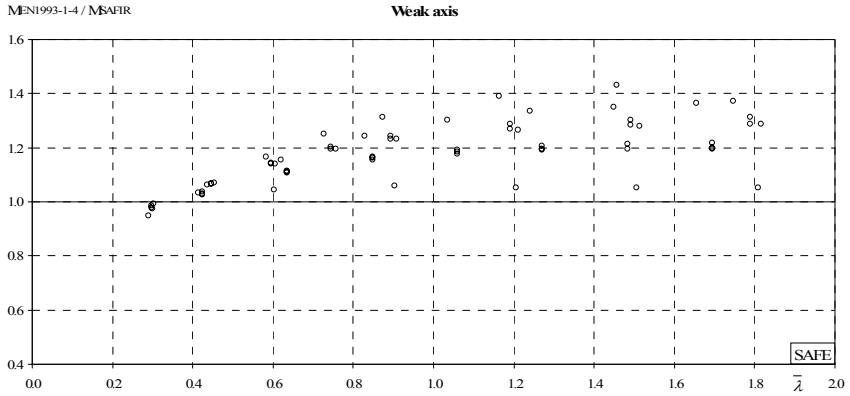

Figure 5.7 – Ratio between analytical and SAFIR results, for EN 1993-1-4 in the weak axis.

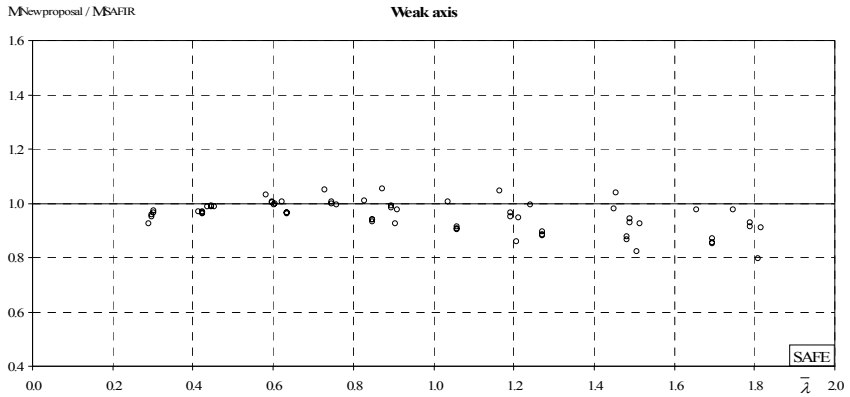

Figure 5.8 – Ratio between analytical and SAFIR results, for the new proposal in the weak axis.

The average unsafe errors, determined for the buckling curves from part 1-4 of EC3 (21.1 % and 19.6 %), suggest that this design formulae is not safe.

As illustrated, the new proposal presented here, with a safety factor of 1.0, gives a much safer approximation to the numerical results than the part 1-4 of EC3.

5.2.2 Bending

Section 4.2.2 of this thesis showed that LTB formulae included in part 1-4 of EC3 should be improved in order to give better results for non-uniform bending. Therefore, in this section a new proposal for the LTB safety evaluation of stainless steel structural elements at room temperature will be presented.

5.2.2.1 Case study

Simply supported beams with fork supports were chosen to explore the validity of the beam safety verifications. Regarding the bending moment variation along the member length, five values (-1, -1/2, 0, 1/2 and 1) of the ψ ratio have been investigated as well as a mid span concentrated load and a uniformly distributed load.

The following welded cross-sections were used: IPE220, HEA500, IPE500, HEA200, HEB280 and HEB200 section. The stainless steel grades 1.4301, 1.4401, 1.4571, 1.4003 and 1.4462 for each cross-section were studied. Table 5.5 and Table 5.6 show all the cases that have been studied with an average of 10 lengths for each case.

Table 5.5 – Cases studied with uniform bending at room temperature.

Room temperature	
	$\psi = 1$
HEA500	
1.4301	✓
1.4401 1.4404	✓
1.4571	✓
1.4003	✓
1.4462	✓
IPE220	
1.4301	✓
1.4401 1.4404	✓
1.4571	✓
1.4003	✓
1.4462	✓
IPE500	
1.4301	✓
1.4401 1.4404	✓
1.4571	✓
1.4003	✓
HEA200	
1.4301	✓
HEB280	
1.4301	✓
1.4003	✓
HEB200	
1.4462	✓

Table 5.6 – Cases studied with non-uniform bending at room temperature.

	Room temperature					
	ψ					
	1/2	0	-1/2	-1	Point Load	Distributed Load
HEA500						
1.4301	✓	✓	✓	✓	✓	✓
IPE220						
1.4301	✓	✓	✓	✓	✓	✓
1.4462	✓	✓	✓	✓	✓	✓
IPE500						
1.4301	✓	✓	✓	✓	✓	✓

Initial imperfections and residual stresses were considered as described in section 3.3.1.

5.2.2.2 Improvement of the Eurocode 3 formulae: a new proposal

Based on the part 1-1 of EC3 (CEN, 2005a), it is proposed that the design LTB resistance moment, of a laterally unrestrained stainless steel beam with Class 1 or Class 2, be determined with the expression

$$M_{b,Rd} = \chi_{LT,\mathrm{mod}} W_{pl,y} \frac{f_y}{\gamma_{M1}} \tag{5.5}$$

where the modified reduction factor is determined as for the carbon steel (see section 4.3.4), with the equations

$$\chi_{LT,\mathrm{mod}} = \frac{\chi_{LT}}{f} \quad \text{with} \quad \chi_{LT,\mathrm{mod}} \le 1 \tag{5.6}$$

where

$$\chi_{LT} = \frac{1}{\phi_{LT} + \sqrt{\phi_{LT}^{\ 2} - \beta \overline{\lambda}_{LT}^{\ 2}}} \tag{5.7}$$

and

$$\phi_{LT} = \frac{1}{2}\left[1 + \alpha_{LT}(\overline{\lambda}_{LT} - \overline{\lambda}_{LT,0}) + \beta \overline{\lambda}_{LT}^{\ 2}\right] \tag{5.8}$$

To consider the loading type, factor f is determined with

$$f = 1 - \frac{1}{2}(1 - k_c)\left[1 - 2\left(\overline{\lambda}_{LT} - 0.8\right)^2\right] \quad \text{with} \quad f \le 1 \tag{6.9}$$

where the correction factor k_c is given in Table 5.7.

Table 5.7 – Correction factors for LTB of stainless steel elements at room temperature.

Moment distribution	Class 1, 2 sections k_c
$-1 \le \psi \le 1$ 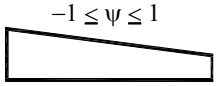	$\frac{1}{1.33 - 0.33\psi}$
Concentrated load 	0.86
Distributed load 	0.94

It is noted that the two parameters, $\overline{\lambda}_{LT,0}$ and β, should be taken as $\overline{\lambda}_{LT,0} = 0.4$ and $\beta = 0.75$.

This design procedure is similar to the adopted in part 1-1 of EC3 (CEN, 2005a) for hot rolled and equivalent welded carbon steel sections. However, in this proposal the imperfection factor is defined as a linear function of the ratio h/b.

$$\alpha_{LT} = 0.4\left(\frac{h}{b}\right) + 0.1 \tag{5.10}$$

This imperfection factor improves the conservative nature of LTB for H-sections, which have small values of h/b. The influence of the stainless steel grade did not need to be considered. Figure 5.9 shows the imperfection factor as a function of the ratio h/b.

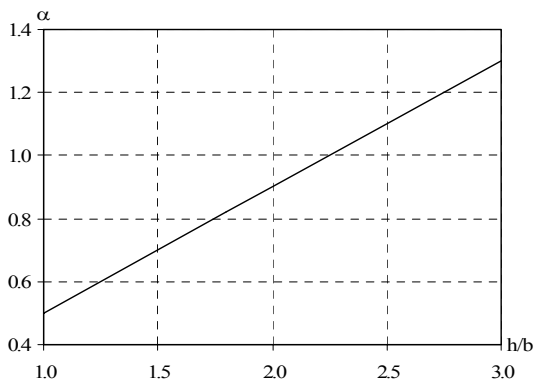

Figure 5.9 – Imperfection factor for the LTB in function of the cross-section slenderness.

Using this design proposal for non-uniform bending, it is possible to state higher maximum slenderness values for dispending the LTB evaluation as a function of the loading type (Lopes *et al.*, 2008a), when compared to the prescribed value in EC3 (CEN, 2006a).

5.2.2.3 Accuracy of the proposal

Again, a direct comparison with the numerical results and a statistical study are used to validate this new proposal.

Numerical validation

In Figure 5.10, the results for stainless steel beams subjected to LTB are shown. Here only the results for an IPE220 of stainless steel grade 1.4301 (see Appendix G for the other results) are presented.

Results for stainless steel beams subjected to LTB are shown in Figure 5.10 for all the load cases studied. The graphics compare the curves obtained using part 1-4 of EC3 (described in section 4.2.2 and denoted "EN 1993-1-4" in the graphics), the curve obtained with the new proposal (denoted "New proposal" in the graphics), and the numerical results obtained with the program SAFIR.

Figure 5.11 shows the performance of the proposal for a HEA200 ($h/b = 0.95$). From this figure the better agreement provided by the new proposal for sections with small values of h/b, when compared against EC3 can be seen.

The figures show that the use of a modified reduction factor, for the LTB on stainless steel beams equal to the one that has been adopted in EC3 for carbon steel, improves the beam design curve when compared with numerical simulations.

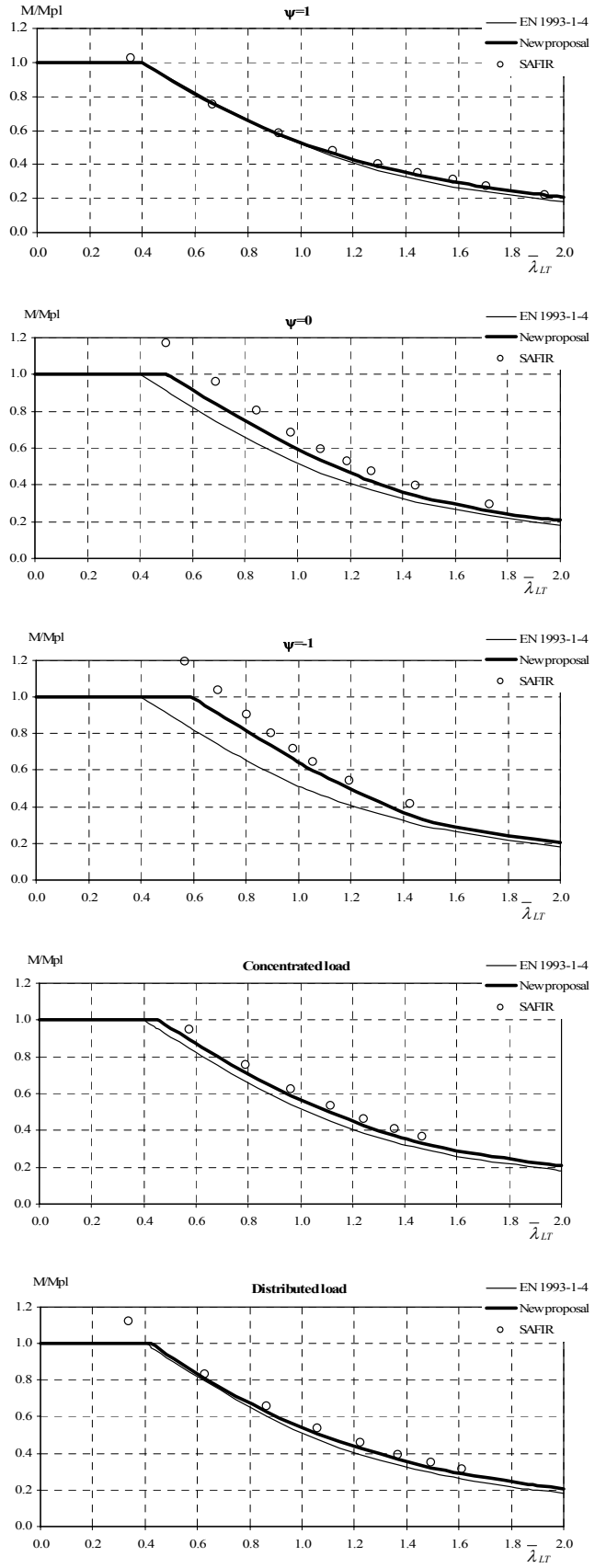

Figure 5.10 – Numerical results for a welded IPE220 of stainless steel grade 1.4301.

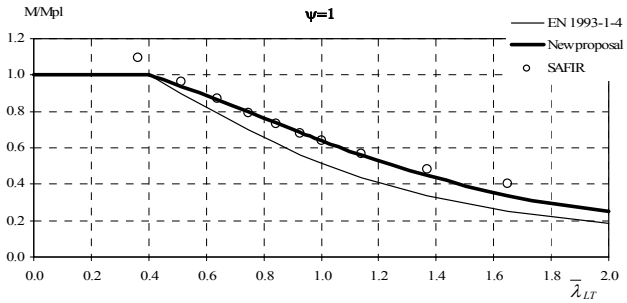

Figure 5.11 – Numerical results for a welded HEA200 of stainless steel grade 1.4301.

Statistical evaluation

As presented in section 4.3.4, the ratio between the analytical value of the ultimate design moment and the corresponding SAFIR moment was evaluated. The statistical evaluation presented here was made only for uniform bending diagrams due to the improvement, provided by the new proposal for other loading types, being clear in the numerical validation (Figure 5.10 and Figure 5.11).

The 147 results obtained with EN 1993-1-4 for welded HEA200, HEB280, HEB200, HEA500, IPE220 and IPE500 sections, in stainless steel grades, 1.4301, 1.4401, 1.4571, 1.4003 and 1.4462 are shown in Figure 5.12. The average value and the standard deviation are, respectively, $\mu = 0.924$ and $s = 0.107$.

Table 5.8 – Statistical results of beams at room temperature.

	EN 1993-1-4	New proposal
Average value	0.924	0.975
Standard deviation	0.107	0.052

If the new proposal is used in those numerical results, the average value and the standard deviation take the values $\mu = 0.975$ and $s = 0.052$, showing that the new proposal provides a better approximation to the numerical results, maintaining safety, with a smaller value for the standard deviation (see Table 5.8).

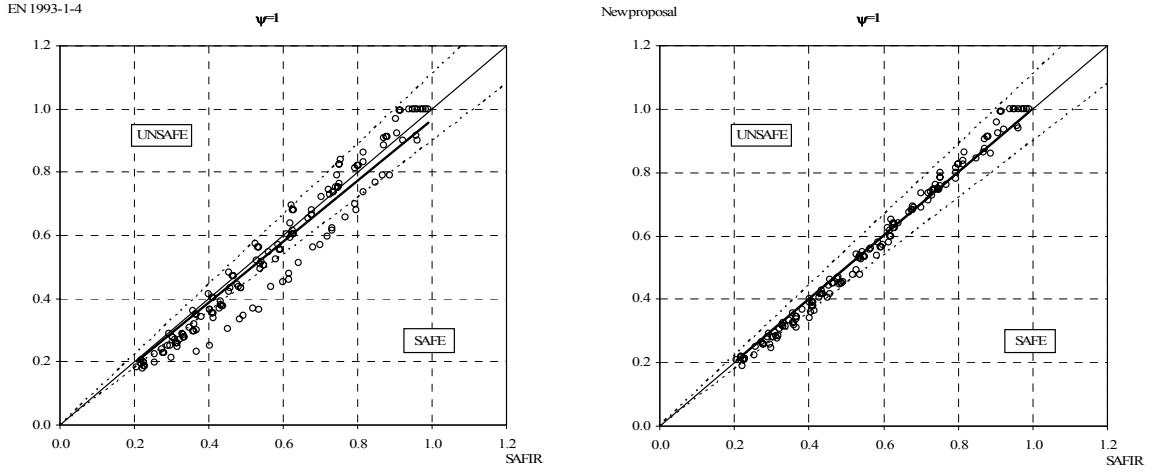

Figure 5.12 – Comparison between EN 1993-1-4 and numerical results with LTB.

Figure 5.13 shows the ratio x_i when EN 1993-1-4 is used with all the numerical results for the strong and weak axis. The maximum unsafe error is 11.4 % and the average unsafe error is 4.1 %. The new proposal gives the results shown in Figure 5.14, with the maximum unsafe error of 8.6 % and average unsafe error of 2.6 %.

Maintaining the coherence within the EC3 (CEN, 2005a) the new proposal presented here provides better approximation to the numerical results, when compared with part 1-4 of EC3.

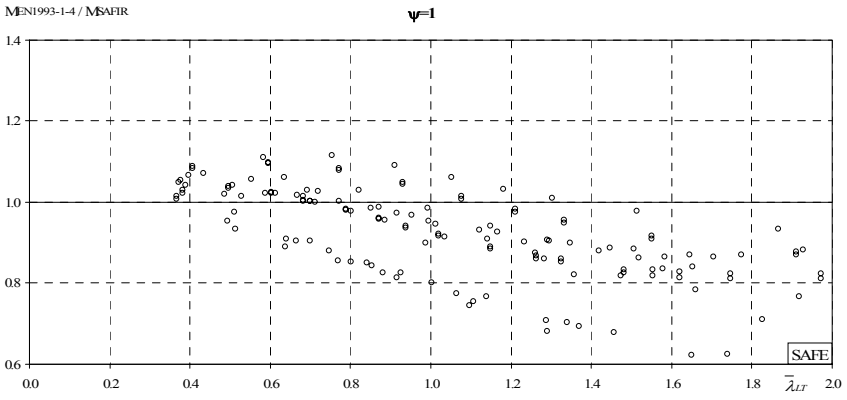

Figure 5.13 – Ratio between analytical and SAFIR results, for EN 1993-1-4.

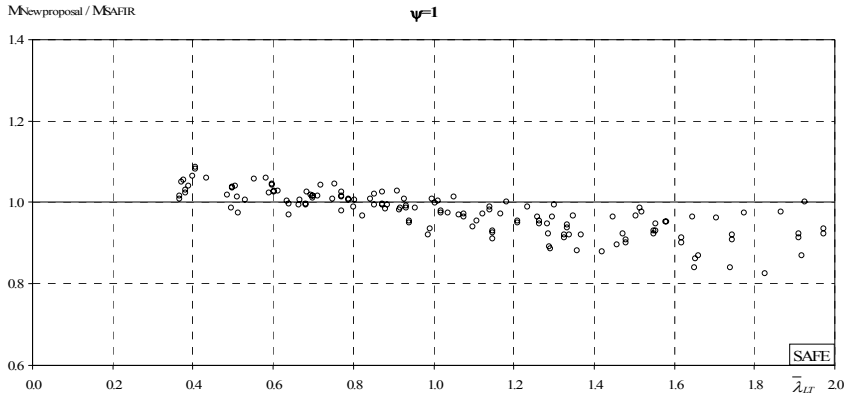

Figure 5.14 – Ratio between analytical and SAFIR results, for the new proposal.

5.2.3 Bending and axial compression

The results presented in section 4.2.3 acknowledged the necessity of the development of new improved interaction formulae for the safety evaluation of stainless steel beam-columns.

Two new methods for the design of carbon steel beam-columns at room temperature are in part 1-1 of EC3 (CEN, 2005a; Boissonnade *et al.*, 2006). In order to study the possibility of having in parts 1-1 and 1-4 of the EN versions of EC3 the same approach for beam-column safety evaluation, a numerical investigation was carried out and is here presented. This numerical investigation addressed the possibility of occurring or not LTB.

Following this study, alternative expressions for the stainless steel interaction curves were developed and are proposed.

Previously in this chapter, new proposals for the evaluation of flexural buckling and LTB in stainless steel members were presented. As these new proposals necessarily affect the behaviour of the interaction formulae for beam-columns, its influence will be here considered.

5.2.3.1 Without lateral torsional buckling

Beam-columns without LTB were first studied.

5.2.3.1.1 Case study

A simply supported column, subjected to axial compression plus bending and flexural buckling in the strong axis or bending and flexural buckling in the weak axis, was chosen for the parametric study. Initial imperfections and residual stresses were considered as described in section 3.3.1.

The following welded cross-sections were used: HEA200, HEB280 and HEB200 stainless steel section. The types of stainless steel grade used were: 1.4301, 1.4003 and 1.4462. Table 5.9 shows all the cases that have been studied. An average of 5 lengths and 8 axial load ratios were analysed for each case.

Table 5.9 – Cases studied for beam-columns without LTB at room temperature.

	Room temperature					
	$\psi = 1$		$\psi = 0$		$\psi = -1$	
	Strong axis	Weak axis	Strong axis	Weak axis	Strong axis	Weak axis
HEA200						
1.4301	✓	✓	✓	✓	✓	✓
HEB280						
1.4301	✓	✓	✓	✓	✓	✓
1.4003	✓	✓	✓	✓	✓	✓
HEB200						
1.4462	✓	✓	✓	✓	✓	✓

5.2.3.1.2 Adaptation of the carbon steel interaction curves

Methods 1 and 2 of part 1-1 of EC3 were here adapted to take into account the reduction factor for flexural buckling of stainless steel columns (see section 5.2.1).

General format

According to EN 1993-1-1 (CEN, 2005a), the stability of beam-columns (of Classes 1 and 2), in the case of bending around the strong or the weak axis, is checked in accordance with the following interaction formulae:

$$\frac{N_{Ed}}{\chi_y \frac{N_{Rk}}{\gamma_{M1}}} + k_{yy} \frac{M_{y,Ed}}{\frac{M_{y,Rk}}{\gamma_{M1}}} \leq 1 \tag{5.11}$$

and

$$\frac{N_{Ed}}{\chi_z \frac{N_{Rk}}{\gamma_{M1}}} + k_{zz} \frac{M_{z,Ed}}{\frac{M_{z,Rk}}{\gamma_{M1}}} \leq 1 \tag{5.12}$$

where

$$N_{Rk} = Af_y, \quad M_{z,Rk} = W_{pl,z} f_y \quad \text{and} \quad M_{y,Rk} = W_{pl,y} f_y \tag{5.13}$$

k_{yy} and k_{zz} are the interaction factors.

Determination of the interaction factors using Method 1

The procedure for the determination of the interaction factors for "Method 1" is reported in Annex A of part 1-1 of EC3. Without attempting to explain the background (Boissonnade *et al.*, 2006) of this proposal, the interaction factors are expressed through the following relations:

$$k_{yy} = c_{my} \frac{\mu_y}{1 - \frac{N_{Ed}}{N_{cr,y}}} \frac{1}{c_{yy}} \tag{5.14}$$

$$k_{zz} = c_{mz} \frac{\mu_z}{1 - \frac{N_{Ed}}{N_{cr,z}}} \frac{1}{c_{zz}} \tag{5.15}$$

where

$$c_{my} = c_{my,0} \quad \text{and} \quad c_{mz} = c_{mz,0} \tag{5.16}$$

and

$$c_{my,0} = 0.79 + 0.21\psi + 0.36(\psi - 0.33)\frac{N_{Ed}}{N_{cr,y}} \tag{5.17}$$

$$c_{mz,0} = 0.79 + 0.21\psi_z + 0.36(\psi_z - 0.33)\frac{N_{Ed}}{N_{cr,z}} \tag{5.18}$$

The other coefficients not described here can be obtained in Annex A of part 1-1 of EC3

Determination of the interaction factors using Method 2

"Method 2" is described in Annex B of part 1-1 of EC3. According to this approach, the interaction factors are expressed through the following relations

$$k_{yy} = c_{my}\left(1+\left(\overline{\lambda}_y - 0.2\right)\frac{N_{Ed}}{\chi_y \frac{N_{Rk}}{\gamma_{M1}}}\right) \quad \text{but} \quad k_{yy} \le c_{my}\left(1+0.8\frac{N_{Ed}}{\chi_y \frac{N_{Rk}}{\gamma_{M1}}}\right) \tag{5.19}$$

and

$$k_{zz} = c_{mz}\left(1+\left(2\overline{\lambda}_z - 0.6\right)\frac{N_{Ed}}{\chi_z \frac{N_{Rk}}{\gamma_{M1}}}\right) \quad \text{but} \quad k_{zz} \le c_{mz}\left(1+1.4\frac{N_{Ed}}{\chi_z \frac{N_{Rk}}{\gamma_{M1}}}\right) \tag{5.20}$$

with

$$c_{mi} = 0.6 + 0.4\psi_i \ge 0.4 \tag{5.21}$$

5.2.3.1.3 Formulation of a new proposal

Part 1-4 of EC3 (CEN, 2006a) states that the safety evaluation of elements subjected to bending and axial compression should satisfy:

$$\frac{N_{Ed}}{\chi_{\min} A \frac{f_y}{\gamma_{M1}}} + k_y \frac{M_{y,Ed}}{W_{pl,y}\frac{f_y}{\gamma_{M1}}} + k_z \frac{M_{z,Ed}}{W_{pl,z}\frac{f_y}{\gamma_{M1}}} \le 1 \tag{5.22}$$

Based on the procedure adopted by Talamona (1995) for the determination of the carbon steel interaction curves at high temperatures (see section 4.3.3), new formulae, for the stainless steel beam-columns safety evaluation, were developed and are here presented.

These formulae follow the approaches recommended in part 1-2 of EC3 (CEN, 2005b) and the ENV version of part 1-1 of the same EC3 (CEN, 1992).

In comparison against EC3 (CEN, 2006a) the main changes appear in the determination of the interactions factors k_y and k_z.

$$k_y = 1 - \frac{\mu_y N_{Ed}}{\chi_y A \frac{f_y}{\gamma_{M1}}} \quad \text{with} \quad k_y \leq 1.5 \tag{5.23}$$

and

$$k_z = 1 - \frac{\mu_z N_{Ed}}{\chi_z A \frac{f_y}{\gamma_{M1}}} \quad \text{with} \quad k_z \leq 1.5 \tag{5.24}$$

To determine the values of μ_y and μ_z the following equations should be used.

$$\mu_y = \left(0.97\beta_{M,y} - 2.11\right)\overline{\lambda}_y + 0.44\beta_{M,y} + 0.09 \leq 0.9 \tag{5.25}$$

and

$$\mu_z = \left(1.09\beta_{M,z} - 2.32\right)\overline{\lambda}_z + 0.29\beta_{M,z} + 0.48 \leq 0.9 \tag{5.26}$$

Finally the equivalent uniform moment factor $\beta_{M,y}$ and $\beta_{M,z}$ can be determined in function of the bending diagram shape, according to the expression

$$\beta_{M,i} = 1.8 - 0.7\psi_i \tag{5.27}$$

The evolution of μ as a function of the slenderness $\overline{\lambda}$ for the strong and weak axis, is shown in Figure 5.15 and Figure 5.16 respectively.

In these figures, “Linear (SAFIR)” are the linear trend lines of the numerical results obtained with SAFIR.

Equations (5.25) and (5.26) were developed to be a good approximation of those trend lines and provide safety at the same time, meaning that those chosen functions were developed to have mainly μ values lower than the trend lines.

Having μ values lower than the trend lines was achieved by not accounting with the numerical results with higher values of μ for the several slenderness values (see Figure 5.15 and Figure 5.16).

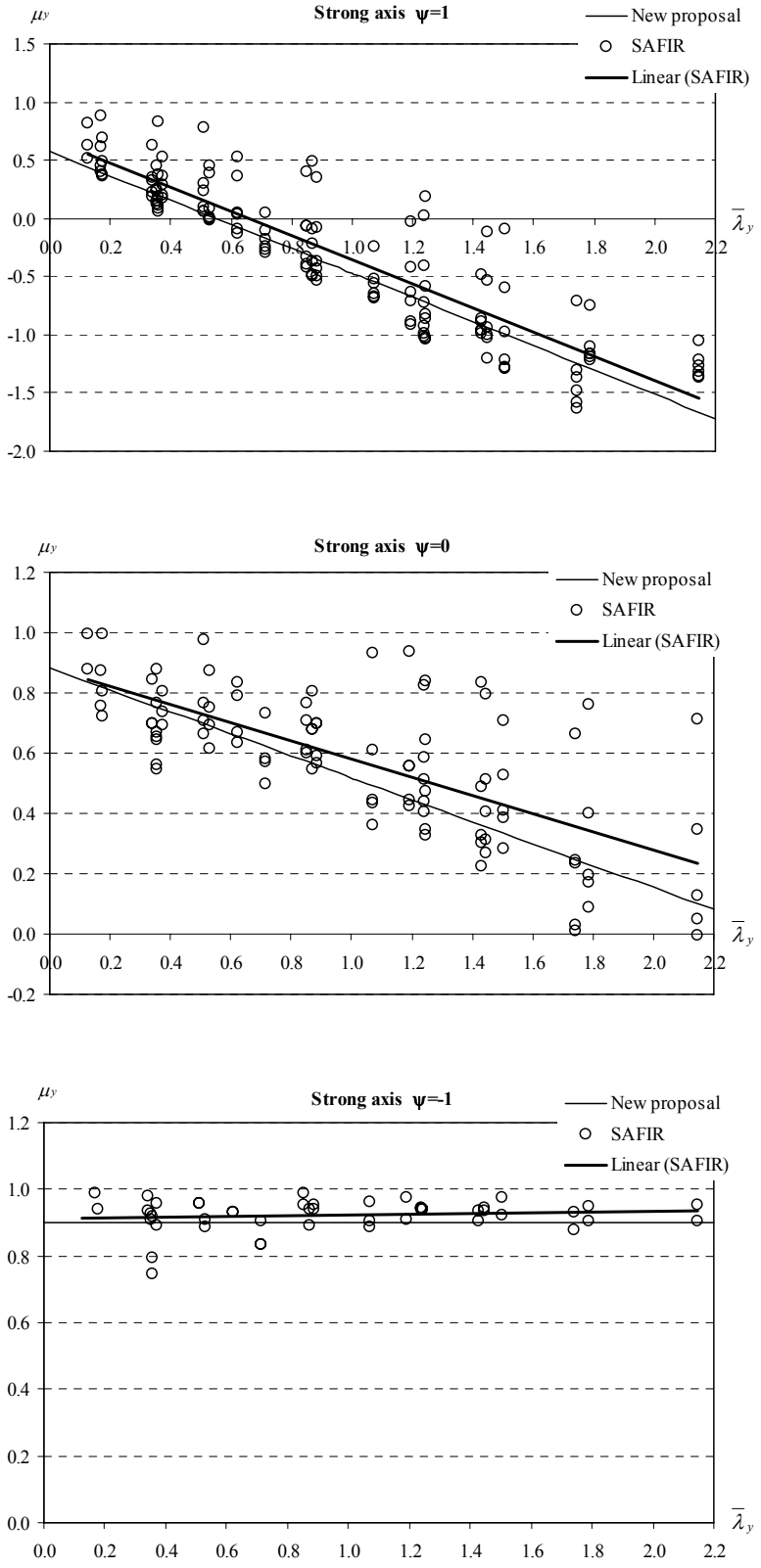

Figure 5.15 – Formulation of new interaction curves for the strong axis.

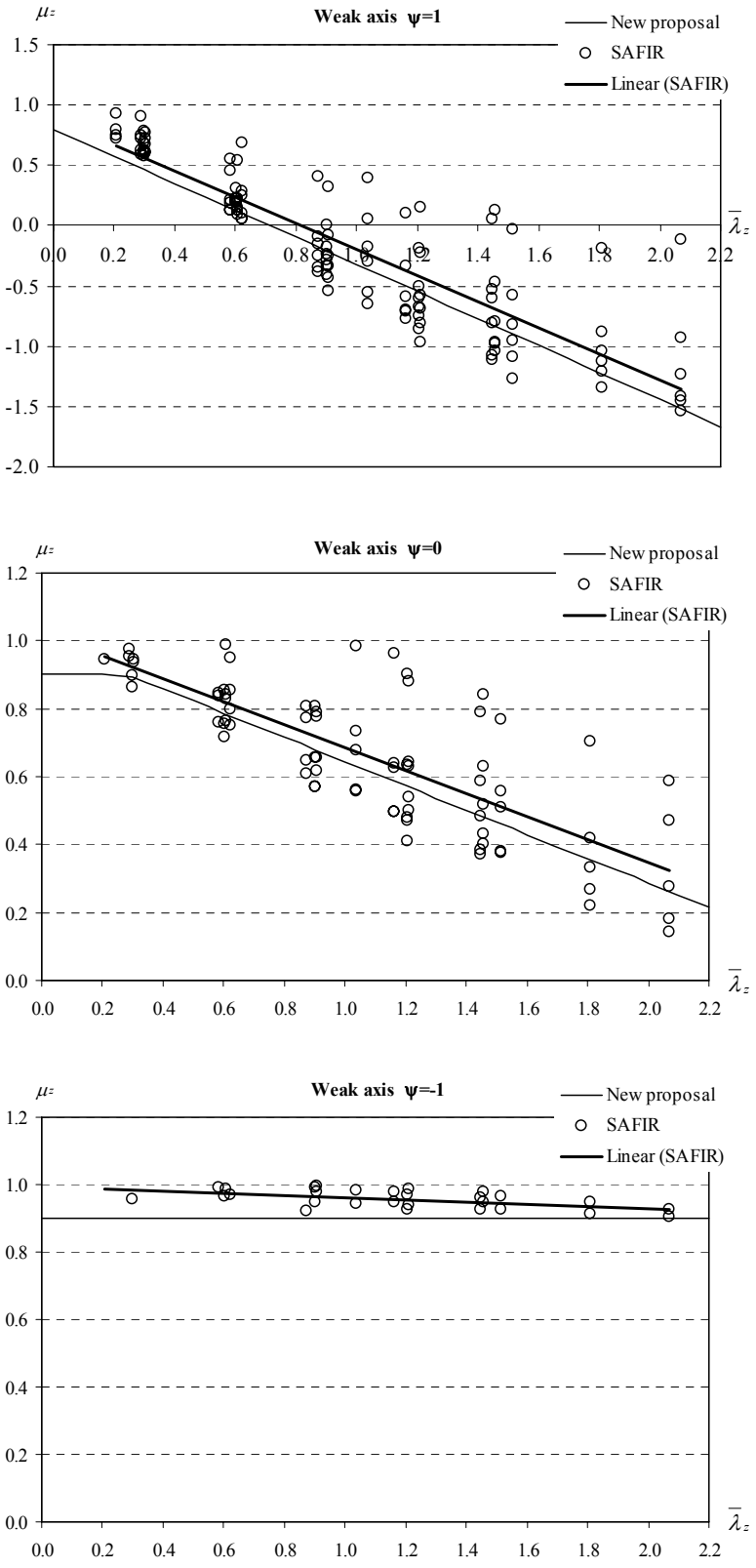

Figure 5.16 – Formulation of new interaction curves for the weak axis.

5.2.3.1.4 Accuracy of the proposals

In this section the new proposals are evaluated by means of a direct comparison with the numerical results and a statistical study.

Numerical validation

The graphics from Figure 5.17 and Figure 5.18 were obtained for beam-columns with welded cross-sections equivalent to a HEA200 of the stainless steel grade 1.4301, for the buckling modes about the y and z axis, with uni-axial bending in the strong and weak axis respectively. Here, the length of 3 m corresponds to non-dimensional slenderness values of $\overline{\lambda}_y = 0.37$ and $\overline{\lambda}_z = 0.62$, while the length of 7 m corresponds to $\overline{\lambda}_y = 0.87$ and $\overline{\lambda}_z = 1.45$. The other cross-section and length studied are included in Appendix H.

The interaction curves in the graphics from Figure 5.17 and Figure 5.18 are obtained from:

- part 1-4 of EC3 "EN 1993-1-4";
- part 1-4 of EC3 with the new proposal for columns presented in section 5.2.1 "EN 1993-1-4 mod";
- part 1-1 of EC3 for carbon steel beam-columns with the new proposal for columns presented in section 5.2.1 "Method 1"and "Method 2";
- and the formulated interaction curves presented in the previous section "New proposal".

The numerical results obtained with M/M_{Rd} higher than 1.0, were not considered. These values are due to the strain hardening of the stainless steel.

The method which better approximates the numerical results from SAFIR is the "New proposal", corresponding to the formulated interaction curves.

"Method 1" and "Method 2" adapted from the formulae from part 1-1 of EC3 for carbon steel and the new proposal for stainless steel columns also present good approximations. From these two methods, the one that has a better behaviour is "Method 1", but still not as good as the one from "New proposal". It can also be observed that the new proposal for columns presented in section 5.2.1 of this thesis introduces a significant improvement in the interaction curves approximations to the numerical results.

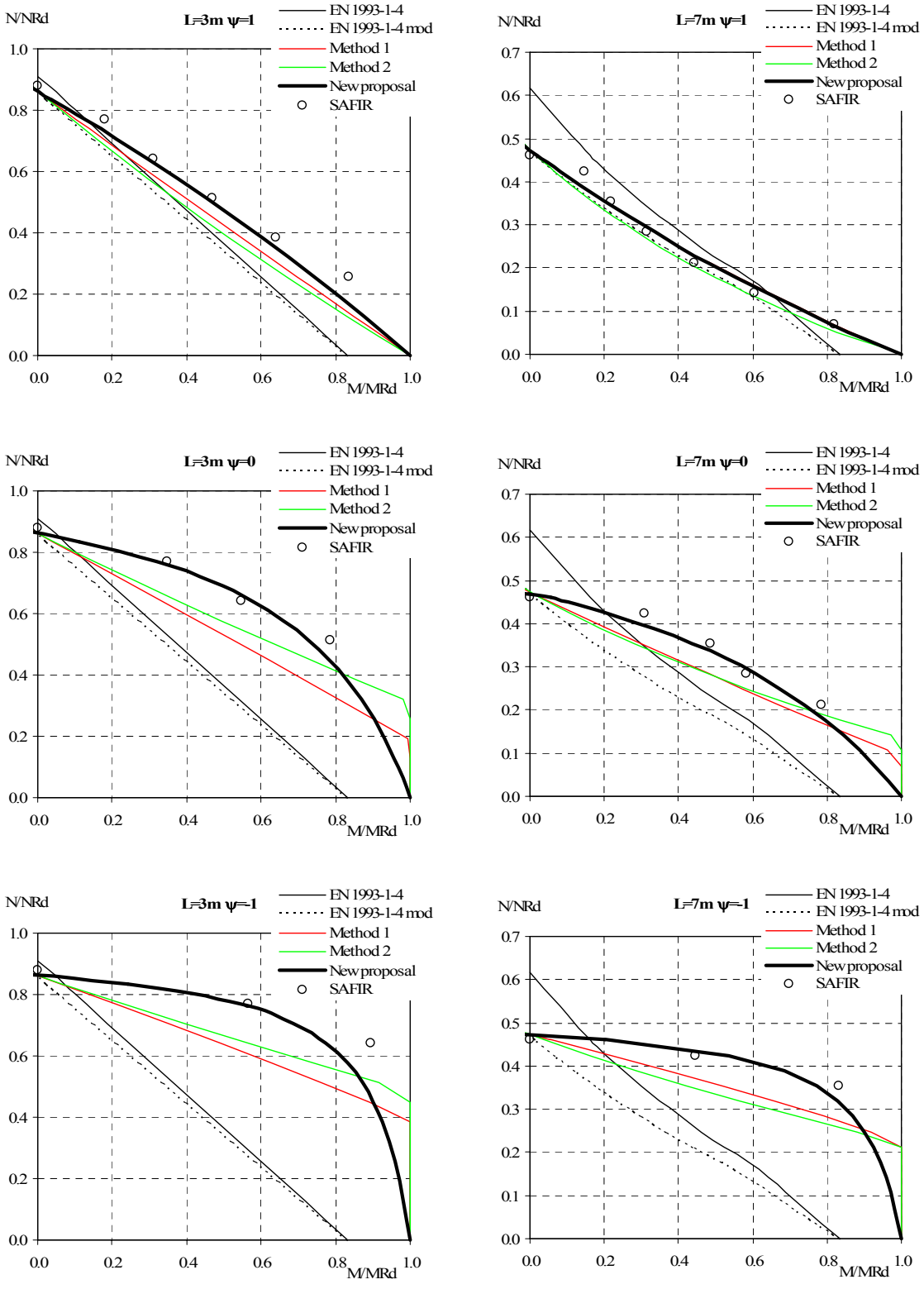

Figure 5.17 – Comparison between different interaction curves for welded HEA200 beam-columns of the stainless steel grade 1.4301, regarding the buckling mode and uni-axial bending about the strong axis.

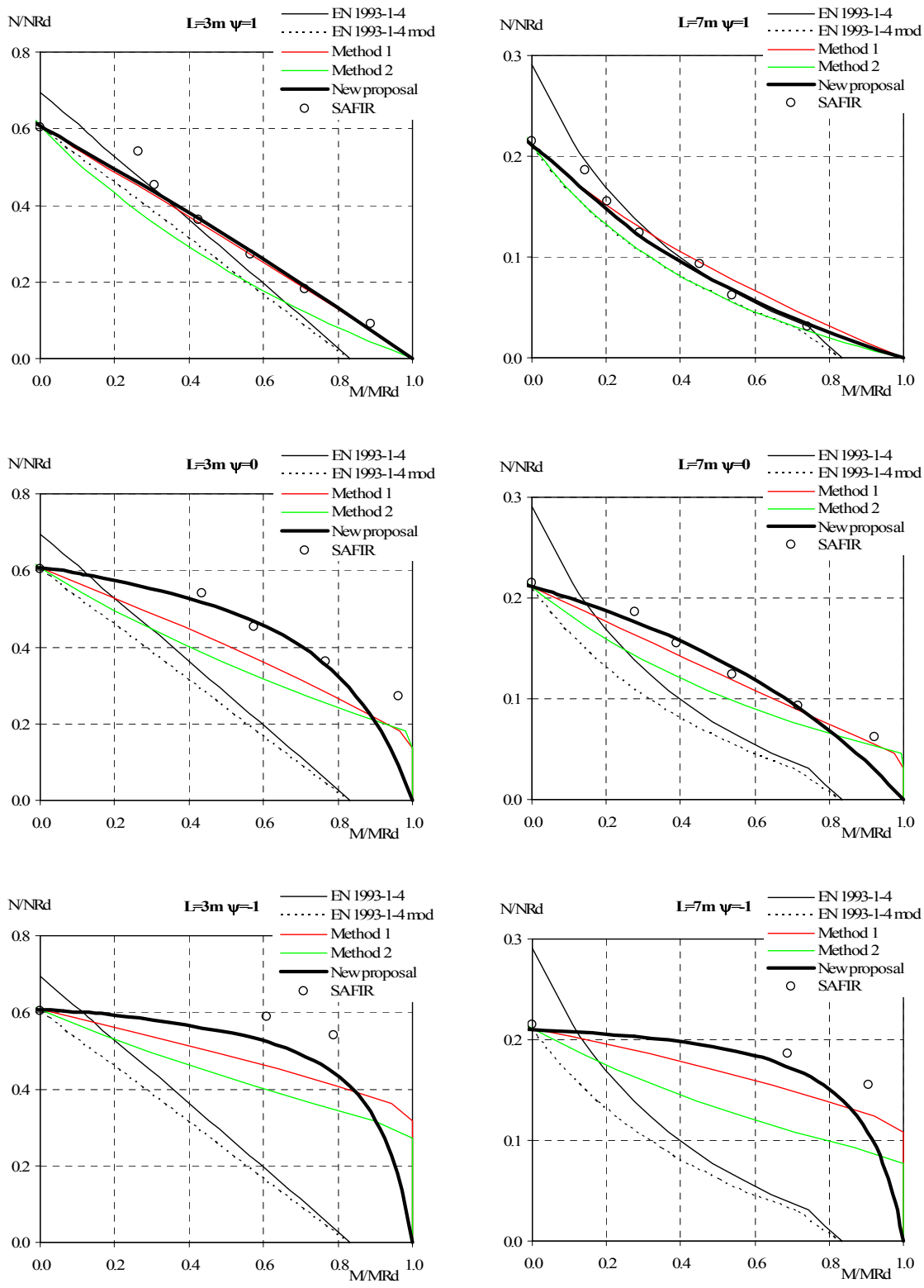

Figure 5.18 – Comparison between different interaction curves for welded HEA200 beam-columns of the stainless steel grade 1.4301, regarding the buckling mode and uni-axial bending about the weak axis.

Statistical evaluation

The 269 and 219 results for respectively the strong and weak axis, obtained with the several proposals for the interaction curves (EC3, "Method 1", "Method 2" and "New proposal") for welded HEA200, HEB280 and HEB200 sections, in stainless steel grades, 1.4301, 1.4003 and 1.4462, are shown in Figure 5.19 and Figure 5.20. These comparisons were made with the new proposal for stainless steel columns.

As determined in 4.3.4 in the statistical evaluation, Table 5.10 presents the average and standard deviation obtained with the different methods for determining the stainless steel beam columns interaction curves.

It can be observed that, although having some few unsafe results, the new proposal presents the best agreement with the numerical results.

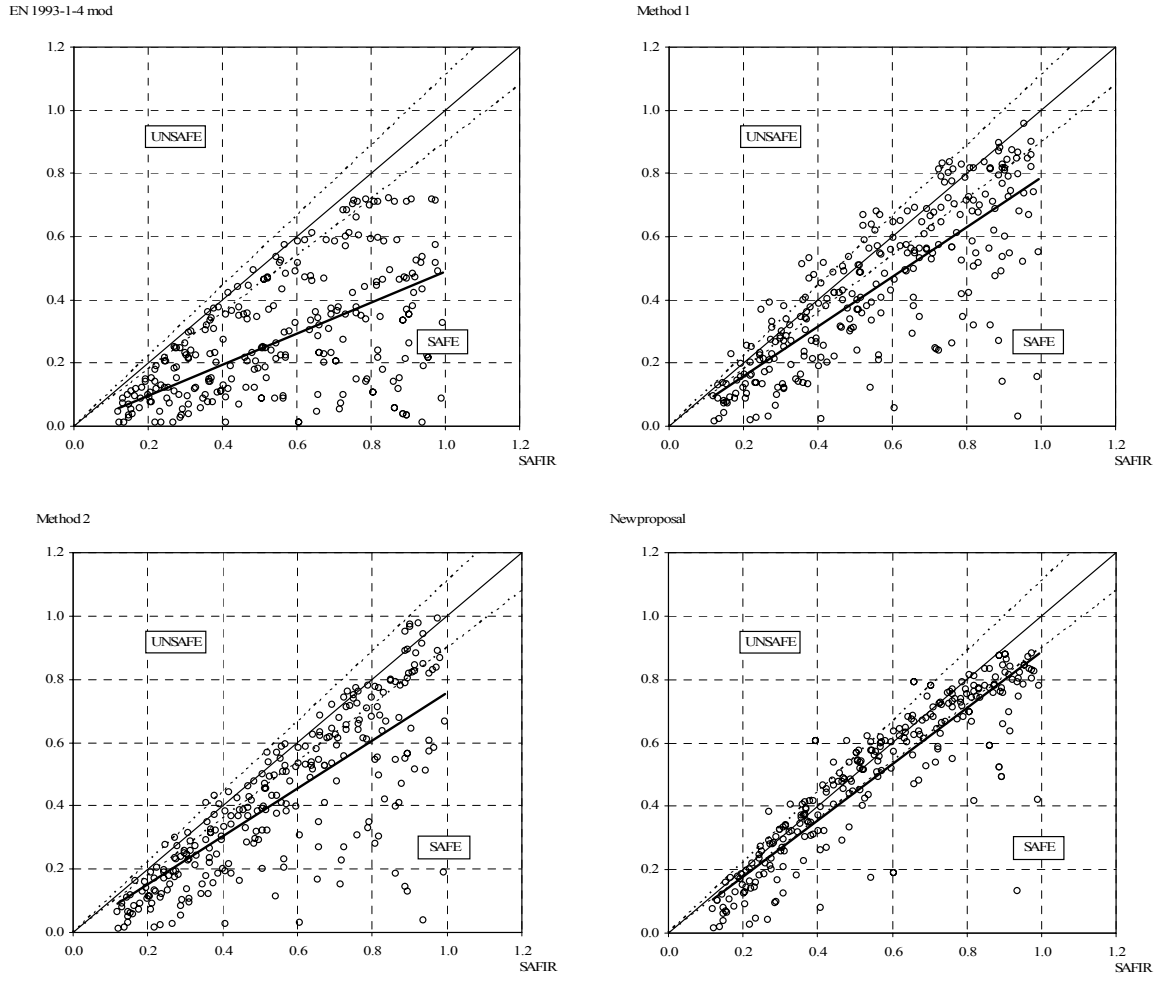

Figure 5.19 – Comparison between the proposals and the numerical results for the strong axis.

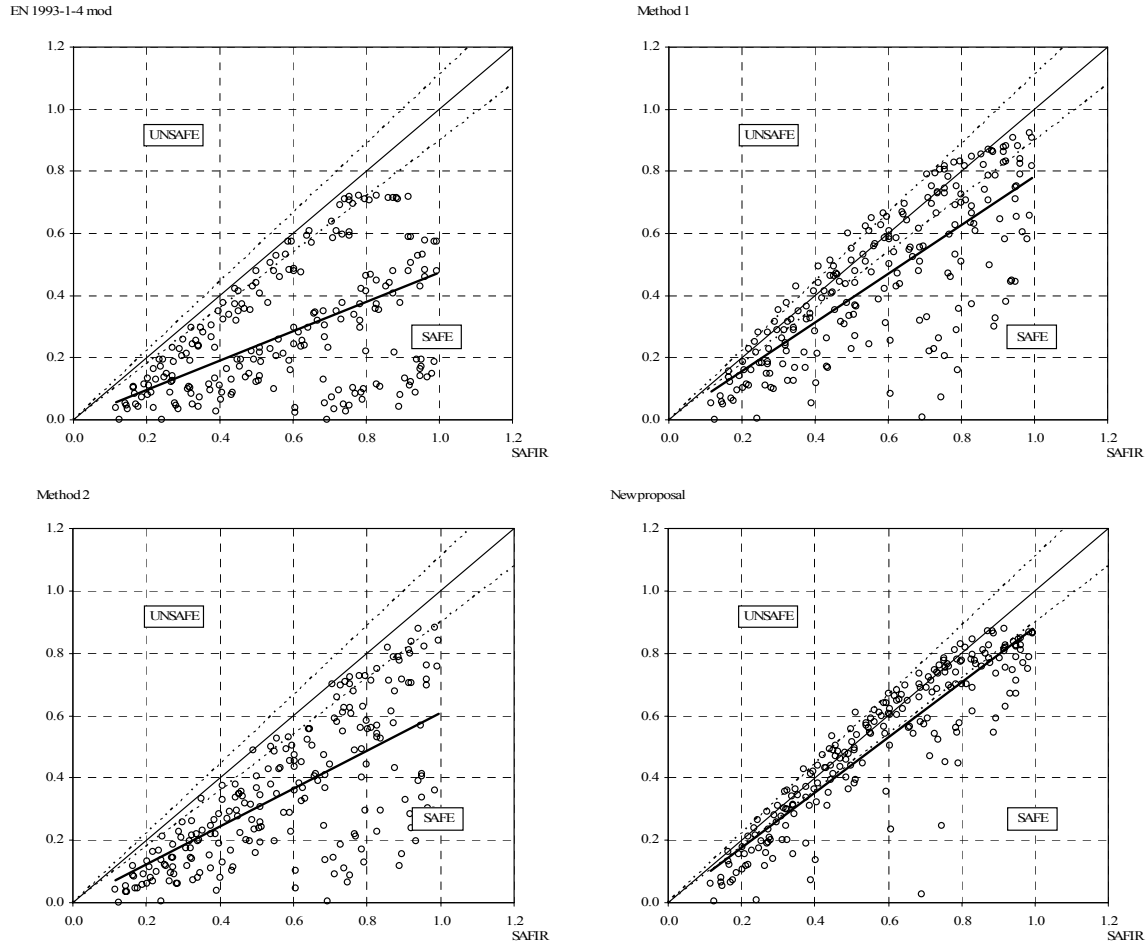

Figure 5.20 – Comparison between the proposals and the numerical results for the weak axis.

Table 5.10 – Statistical results of beam-columns without LTB at room temperature.

		EN 1993-1-4 mod	Method 1	Method 2	New proposal
Strong axis	Average value	0.515	0.783	0.723	0.877
	Standard deviation	0.276	0.273	0.251	0.227
Weak axis	Average value	0.497	0.775	0.577	0.865
	Standard deviation	0.276	0.264	0.246	0.207

5.2.3.2 With lateral torsional buckling

In this section it is presented the study made on stainless steel beam-columns with LTB.

5.2.3.2.1 Case study

A simply supported column, subjected to axial compression plus bending in the strong axis with the possibility of occurring buckling in both strong and weak axis, was chosen.

Initial imperfections and residual stresses were considered as described in section 3.3.1. The following welded cross-sections were used: HEA200, HEB280 and HEB200. The stainless steel grades used were: 1.4301, 1.4003 and 1.4462. Table 5.11 shows all the studied cases. An average of 5 lengths and 8 axial load ratios were analysed for each case.

Table 5.11 – Cases studied for beam-columns with LTB at room temperature.

	Room temperature		
	$\psi = 1$	$\psi = 0$	$\psi = -1$
HEA200			
1.4301	✓	✓	✓
HEB280			
1.4301	✓	✓	✓
1.4003	✓	✓	✓
HEB200			
1.4462	✓	✓	✓

5.2.3.2.2 Adaptation of the carbon steel interaction curves

As for structural elements subjected to axial compression and bending without LTB, the possibility of using the interaction curves recommended in part 1-1 of EC3 (CEN, 2005a), adapted to the stainless steel material properties in beam-columns with LTB was studied. These two methods were changed in order to account for the proposed reduction factors for flexural buckling and LTB of stainless steel members (sections 5.2.1 and 5.2.2).

General format

According to EN 1993-1-1 (CEN, 2005a), the stability of beam-columns with LTB (of Classes 1 and 2), in the case of bending about the strong axis, is checked in accordance with the following interaction formulae:

$$\frac{N_{Ed}}{\chi_y \frac{N_{Rk}}{\gamma_{M1}}} + k_{yy} \frac{M_{y,Ed} + \Delta M_{y,Ed}}{\chi_{LT} \frac{M_{y,Rk}}{\gamma_{M1}}} \leq 1 \tag{5.28}$$

$$\frac{N_{Ed}}{\chi_z \frac{N_{Rk}}{\gamma_{M1}}} + k_{zy} \frac{M_{y,Ed} + \Delta M_{y,Ed}}{\chi_{LT} \frac{M_{y,Rk}}{\gamma_{M1}}} \leq 1 \tag{5.29}$$

The interaction factors k_{yy} and k_{zy} are different from the ones prescribed for beam-columns without LTB.

Determination of the interaction factors using Method 1

The procedure for the determination of the interaction factors for the "Method 1" is reported in Annex A of part 1-1 of EC3, and consists on the following relations. The coefficients not described here can be obtained in that Annex A of EC3.

$$k_{yy} = c_{my} c_{mLT} \frac{\mu_y}{1 - \frac{N_{Ed}}{N_{cr,y}}} \frac{1}{c_{yy}} \tag{5.30}$$

$$k_{zy} = c_{my} c_{mLT} \frac{\mu_z}{1 - \frac{N_{Ed}}{N_{cr,y}}} \frac{1}{c_{zy}} 0.6 \sqrt{\frac{w_y}{w_z}} \tag{5.31}$$

where

$$c_{my} = c_{my,0} + \left(1 - c_{my,0}\right) \frac{\sqrt{\varepsilon_y} a_{LT}}{1 + \sqrt{\varepsilon_y} a_{LT}} \tag{5.32}$$

$$c_{mLT} = c_{my}^2 \frac{a_{LT}}{\sqrt{\left(1 - \frac{N_{Ed}}{N_{cr,z}}\right)\left(1 - \frac{N_{Ed}}{N_{cr,T}}\right)}} \geq 1 \tag{5.33}$$

being

$$\varepsilon_y = \frac{M_{y,Ed}}{N_{Ed}} \frac{A}{W_{el,y}} \tag{5.34}$$

Determination of the interaction factors using Method 2

"Method 2" is described in Annex B of part 1-1 of EC3. According to this method, the interaction factors are expressed by

$$k_{yy} = c_{my} \left(1 + \left(\overline{\lambda}_y - 0.2\right) \frac{N_{Ed}}{\chi_y \frac{N_{Rk}}{\gamma_{M1}}} \right) \quad \text{but} \quad k_{yy} \leq c_{my} \left(1 + 0.8 \frac{N_{Ed}}{\chi_y \frac{N_{Rk}}{\gamma_{M1}}} \right) \tag{5.35}$$

$$k_{zy} = \left(1 - \frac{0.1\overline{\lambda}_z}{(c_{mLT} - 0.25)} \cdot \frac{N_{Ed}}{\chi_z \frac{N_{Rk}}{\gamma_{M1}}}\right) \quad \text{but} \quad k_{zy} \geq \left(1 - \frac{0.1}{(c_{mLT} - 0.25)} \cdot \frac{N_{Ed}}{\chi_z \frac{N_{Rk}}{\gamma_{M1}}}\right) \tag{5.36}$$

for $\overline{\lambda}_z < 0.4$:

$$k_{zy} = 0.6 + \overline{\lambda}_z \quad \text{with} \quad k_{zy} \leq \left(1 - \frac{0.1\overline{\lambda}_z}{(c_{mLT} - 0.25)} \cdot \frac{N_{Ed}}{\chi_z \frac{N_{Rk}}{\gamma_{M1}}}\right) \tag{5.37}$$

with

$$c_{my} = c_{mLT} = 0.6 + 0.4\psi_y \geq 0.4 \tag{5.38}$$

5.2.3.2.3 Formulation of a new proposal

It is proposed that the safety evaluation of elements subjected to bending and axial compression with LTB should satisfy:

$$\frac{N_{Ed}}{\chi_z A \frac{f_y}{\gamma_{M1}}} + k_{LT} \frac{M_{y,Ed}}{\chi_{LT} W_{pl,y} \frac{f_y}{\gamma_{M1}}} + k_z \frac{M_{z,Ed}}{W_{pl,z} \frac{f_y}{\gamma_{M1}}} \leq 1 \tag{5.39}$$

Similar to the study in section 5.2.3.1.3 for beam-columns without LTB, the formulation of new interaction curves is presented. In these proposed interaction curves the interaction factor k_{LT} should be determined with

$$k_{LT} = 1 - \frac{\mu_{LT} N_{Ed}}{\chi_z A \frac{f_y}{\gamma_{M1}}} \quad \text{with} \quad k_{LT} \leq 1 \tag{5.40}$$

where

$$\mu_{LT} = (-0.07\beta_{M,LT} - 0.07)\overline{\lambda}_z + 0.60\beta_{M,LT} - 0.10 \leq 0.9 \tag{5.41}$$

And finally the equivalent uniform moment factor $\beta_{M,LT}$ can be determined in function of the bending diagram shape in the strong axis, according to the expression

$$\beta_{M,LT} = 1.8 - 0.7\psi_y \tag{5.42}$$

The evolution of μ_{LT}, as a function of the slenderness $\overline{\lambda}_z$, is shown in Figure 5.21.

The equation (5.41) was developed to be a good approximation to the trend line named "Linear (SAFIR)" in the graphics of Figure 5.21.

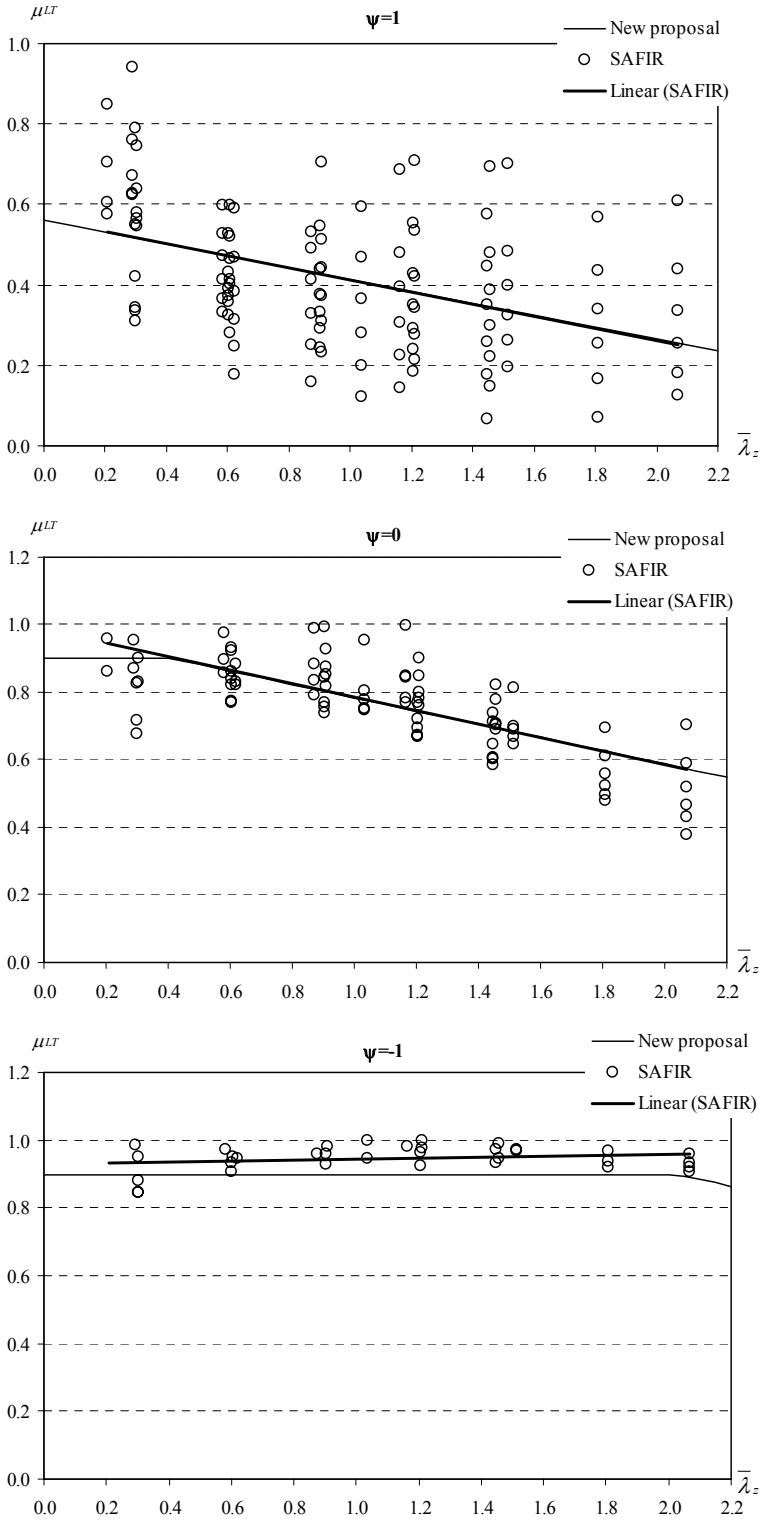

Figure 5.21 – Formulation of new interaction curves for beam-columns with LTB.

5.2.3.2.4 Accuracy of the proposals

Again, a direct comparison with the numerical results and a statistical study are used to validate these new proposals.

Numerical validation

The graphics from Figure 5.22 were obtained for beam-columns with welded cross-sections equivalent to a HEA200 of the stainless steel grade 1.4301, with the possibility of occurring LTB, with bending in the strong axis. Regarding the bending moment variation along the member length, in these figures the results obtained for values (-1, 0 and 1) of the ψ ratio are shown. Here, the length of 3 m corresponds to non-dimensional slenderness values of $\overline{\lambda}_z = 0.62$, while the length of 7 m corresponds to $\overline{\lambda}_z = 1.45$. The non-dimensional slenderness values for the LTB phenomena are given in Table 5.12. The other cross-sections and lengths studied are included in Appendix I.

Table 5.12 – Non-dimensional slenderness values for LTB of the cases presented.

Moment diagram	$\overline{\lambda}_{LT}$ for $L = 3$ m	$\overline{\lambda}_{LT}$ for $L = 7$ m
$\psi = 1$	0.51	0.93
$\psi = 0$	0.39	0.69
$\psi = -1$	0.32	0.57

The interaction curves named “EN 1993-1-4 mod” in the graphics from Figure 5.22 are obtained from part 1-4 of EC3 with the new proposal for columns presented in section 5.2.1 and with the new proposal for LTB presented in section 5.2.2.

Again, the method providing a better approximation to the numerical results is the method “New proposal”.

“Method 1” and “Method 2” also present safe approximations. From these two methods, the one that has a closer behaviour to the numerical results is “Method 1”.

It can also be observed that the new proposals, for columns presented in section 5.2.1 and for LTB of beams included in section 5.2.2 of this thesis, introduce significant improvements in the interaction curves approximations to the numerical results.

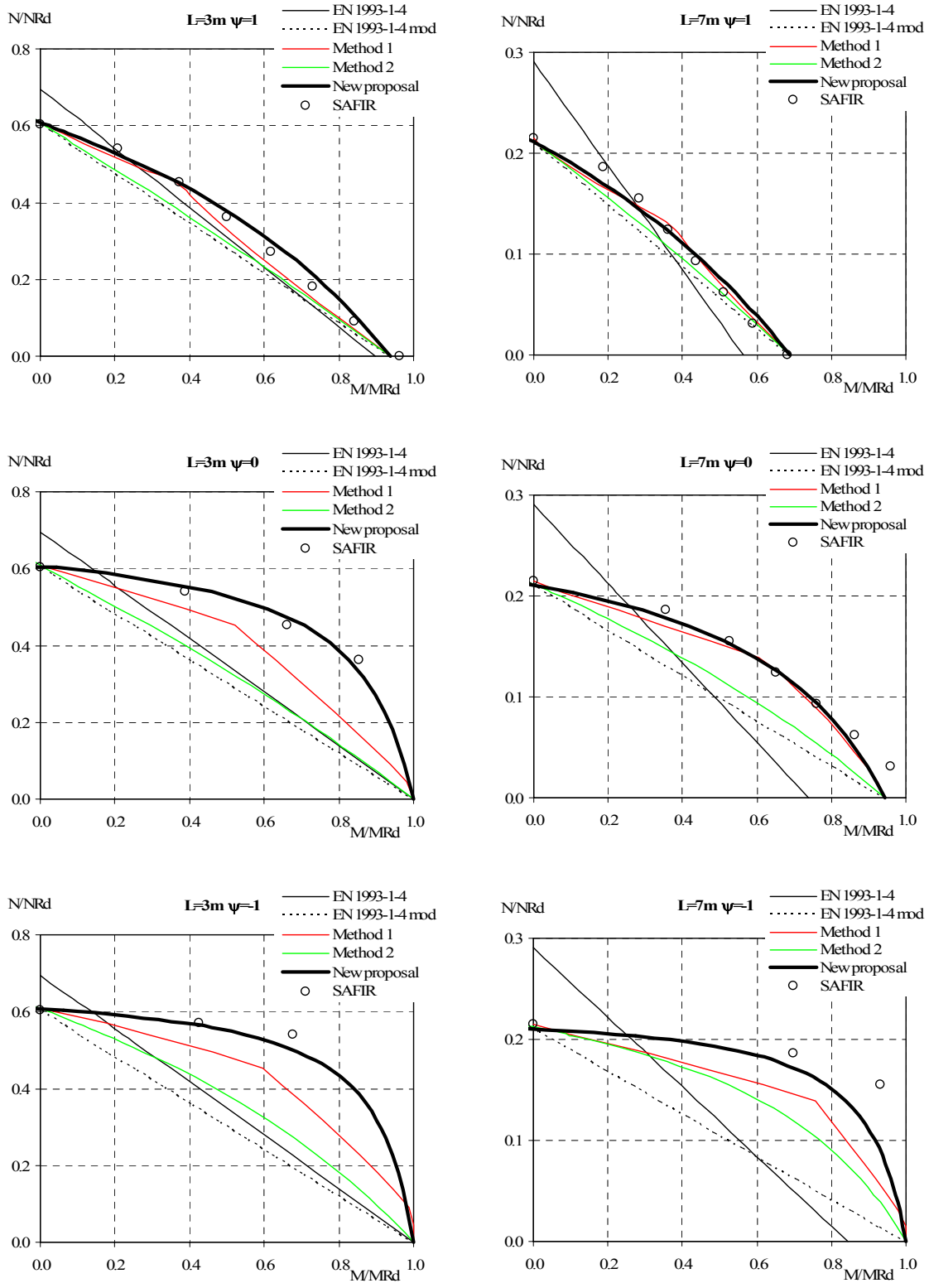

Figure 5.22 – Comparison between different interaction curves for welded HEA200 beam-columns of the stainless steel grade 1.4301, with LTB.

Statistical evaluation

The 249 results, obtained with the several proposals for the interaction curves (EC3, "Method 1", "Method 2" and "New proposal") for welded HEA200, HEB280 and HEB200 sections, in stainless steel grades, 1.4301, 1.4003 and 1.4462, are shown in Figure 5.23. In these comparisons, the new proposals for stainless steel columns and for stainless steel beams were used.

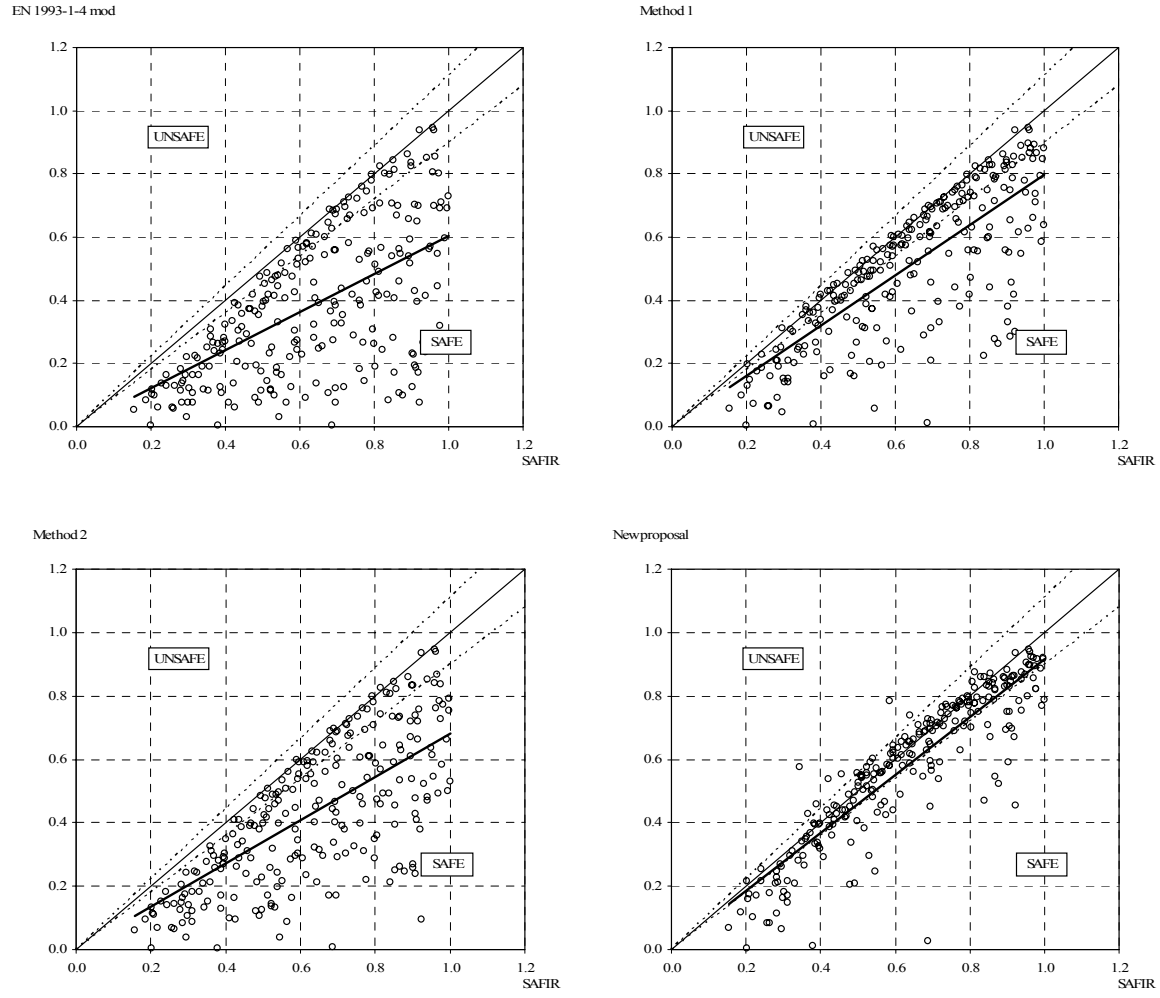

Figure 5.23 – Comparison between the proposals and the numerical results with LTB.

Table 5.13 presents the average and standard deviation obtained, with the different methods for determining the stainless steel beam columns interaction curves with LTB.

Table 5.13 – Statistical results of beam-columns with LTB at room temperature.

	EN 1993-1-4 mod	Method 1	Method 2	New proposal
Average value	0.589	0.783	0.658	0.900
Standard deviation	0.273	0.230	0.248	0.197

It can be observed that, although having some few unsafe results, the new proposal presents the best agreement with the numerical results.

5.3 At high temperatures

As shown in Chapter 2, the stainless steel mechanical properties at high temperatures vary significantly from grade to grade. This fact could lead to the use of different design formulae for each grade. In the proposals presented in this section, those different behaviours were taken into account, but with the minimum introduction of complexity. Meaning that, in most cases, only one set of design formulae was developed for all the stainless steel grades.

5.3.1 Compression

Based on the comparison between the numerical results and the design formulae given in part 1-2 of EC3 (CEN, 2005b), for stainless steel columns in case of fire (presented in section 4.3.1), an improvement proposal is made. It will be shown that this new proposal is safer than the formulae from EC3.

5.3.1.1 Case study

A simply supported column, subjected to axial compression with flexural buckling about the strong axis or about the weak axis, was chosen for the parametric study. Initial imperfections and residual stresses were considered as described in section 3.3.1.

The following welded cross-sections were used: HEA200, HEB280 and HEB200 stainless steel section. The types of stainless steel grade used were: 1.4301, 1.4401 or 1.4404, 1.4571, 1.4003 and 1.4462. Table 5.1 shows all the cases that have been studied. An

average of 10 lengths were analysed for each case. The temperatures of 400, 500, 600 and 700 ºC were used.

Table 5.14 – Cases studied for the flexural buckling at high temperatures.

	High temperatures	
	Strong axis	Weak axis
HEA200		
1.4301	✓	✓
1.4401	✓	✓
1.4404		
1.4571	✓	✓
HEB280		
1.4301	✓	✓
1.4401	✓	✓
1.4404		
1.4571	✓	✓
1.4003	✓	✓
HEB200		
1.4003	✓	✓
1.4462	✓	✓

5.3.1.2 Improvement of the Eurocode 3 formulae: a new proposal

As shown in Chapter 2, each stainless steel grade has a different structural behaviour when subjected to high temperatures (CEN, 2005b). Their yield strength and Young's modulus reductions at high temperatures are rather different from each other. And, as it can be seen in equation (5.43), the normalized slenderness at room temperature is multiplied by the relation $\left(k_{y,\theta}/k_{E,\theta}\right)^{0.5}$ in order to obtain the slenderness in case of fire.

Figure 5.24 presents the variation of this relation in function of the temperature. This graphic shows that different buckling curves should be provided for each different stainless steel grade.

$$\overline{\lambda}_{\theta} = \overline{\lambda} \left[\frac{k_{y,\theta}}{k_{E,\theta}}\right]^{0.5} \tag{5.43}$$

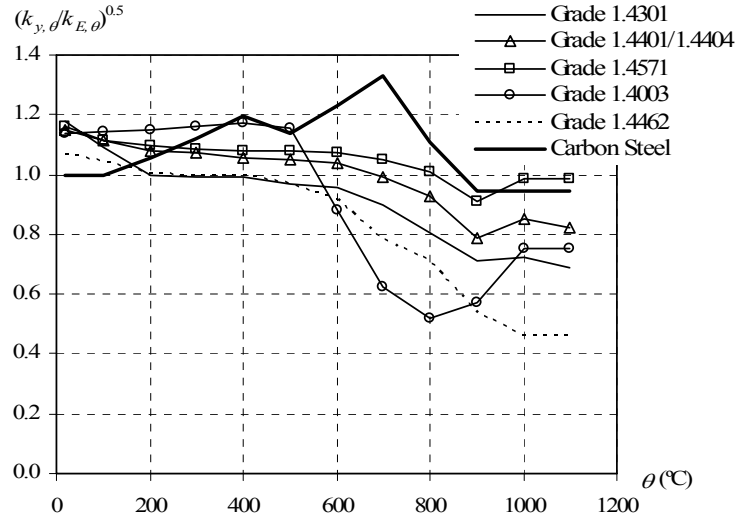

Figure 5.24 – Slenderness variation at high temperatures.

From Figure 5.24 it can be observed that from 500 ºC to 700 ºC there is a great decrease of the relation $\left(k_{y,\theta}/k_{E,\theta}\right)^{0.5}$ for the 1.4003 stainless steel, which does not occur with the other stainless steel grades.

In the proposal presented here, the necessity of different buckling curves, for different stainless steel grades, will be taken into consideration but with only one set of design formulae. This proposed design procedure only differentiates the stainless steel grade 1.4462.

As in part 1-2 of EC3 (CEN, 2005b), in this new proposal for the design of stainless steel elements subjected to axial compression in case of fire, the buckling resistance value of a compressed element is calculated with

$$N_{b,fi,t,Rd} = \chi_{\min,fi} A k_{y,\theta} \, f_y / \gamma_{M,fi} \tag{5.44}$$

where the reduction factor $\chi_{\min,fi}$ is the minimum of the values $\chi_{y,fi}$ and $\chi_{z,fi}$.

A new reduction factor χ_{fi}, similar to the proposal for room temperature in section 5.2.1, is proposed according to

$$\chi_{fi} = \frac{1}{\phi_\theta + \sqrt{\phi_\theta^{\,2} - \beta \overline{\lambda}_\theta^{\,2}}} \tag{5.45}$$

with

$$\phi_\theta = \frac{1}{2}\left[1 + \alpha\bar{\lambda}_\theta + \beta\bar{\lambda}_\theta^{\,2}\right] \tag{5.46}$$

where the factor β should vary, as at room temperature, in function of the buckling axis as presented in Table 5.15.

Table 5.15 – Coefficient for determining the reduction factor.

	β
Strong axis	1.0
Weak axis	1.5

A new imperfection factor α as function of a severity factor η is used, based on the equation proposed in EC3 (CEN, 2005b) for this factor and explained in section 4.3.1.

$$\alpha = \eta\varepsilon \tag{5.47}$$

and using ε given in part 1-4 of the EC3 (CEN, 2006a)

$$\varepsilon = \sqrt{\frac{235}{f_y}\frac{E}{210000}} \tag{5.48}$$

In order to consider the different behaviour at high temperatures provided by the different stainless steel grades shown in Figure 5.24, the imperfection factor can be written in function of the temperature as

$$\alpha = \eta\sqrt{\frac{235}{f_y}\frac{E}{210000}}\sqrt{\frac{k_{E,\theta}}{k_{y,\theta}}} \tag{5.49}$$

The proposal for the values of the factor η, to be used with this equation, are given in Table 5.16.

Table 5.16 – Severity factor for the flexural buckling of stainless steel elements in case of fire.

	1.4301, 1.4401, 1.4404, 1.4571, 1.4301	1.4462
η	1.3	0.9

5.3.1.3 Accuracy of the proposal

In this section, the validation of this new proposal for the fire design of stainless steel columns at elevated temperatures is presented.

Numerical validation

In Figure 5.25, the results for stainless steel columns subjected to flexural buckling in the strong axis and around the weak axis are shown. Here only the results for a HEA200 of the stainless steel grade 1.4301 are presented.

A comparison is made between the curve obtained through the formulae from part 1-2 of EC3, described in the section 4.3.1 of this thesis ("EN 1993-1-2" in the graphics), the curve based on the proposal made here (noted "New proposal"), and the numerical results determined with SAFIR.

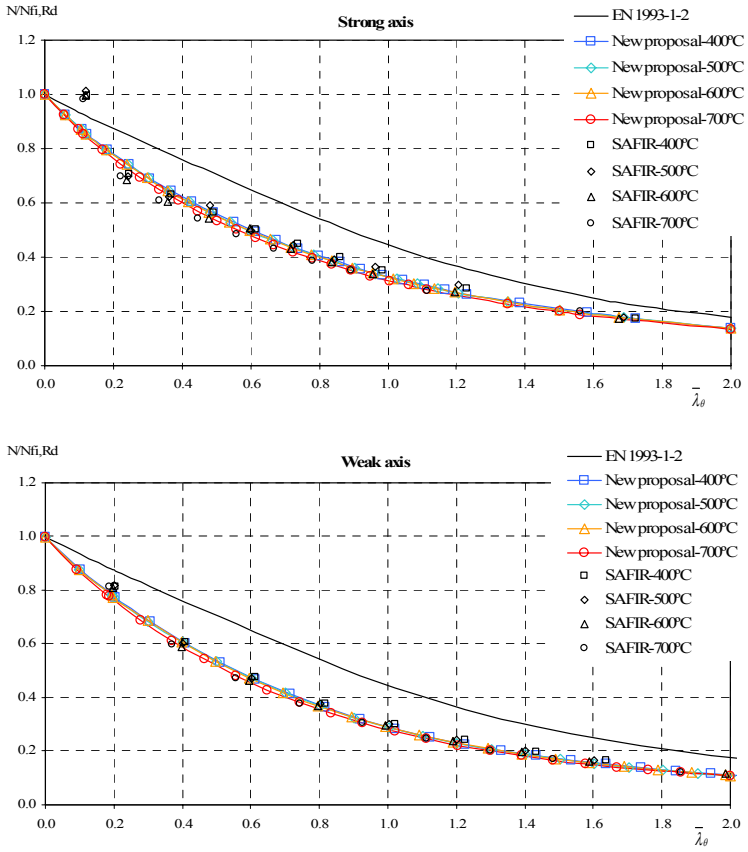

Figure 5.25 – Column with cross-section HEA200 in stainless steel grade 1.4301, at high temperatures.

Figure 5.25 shows that the new proposal improves the behaviour of the buckling curves obtained with the formulae prescribed in part 1-2 of EC3.

Although the graphics may suggest that the buckling curve does not depend on the temperature, with this dependence, it is possible to use the same equations for the other

stainless steel grades without having to change the imperfection factor or other coefficient (as shown in Appendix J).

More significant, the observed relation $\left(k_{y,\theta}/k_{E,\theta}\right)^{0.5}$ for the ferritic stainless steel grade 1.4003 introduces, in the temperature range of 500 ºC to 700 ºC, a high variation of the normalised slenderness at high temperatures, which lead to the results shown in Figure 5.26. As it can be observed, the slenderness values for 700 ºC and 600 ºC are quite different from the corresponding values for 400 ºC and 500 ºC. With the proposal presented here this behaviour can be more accurately predicted.

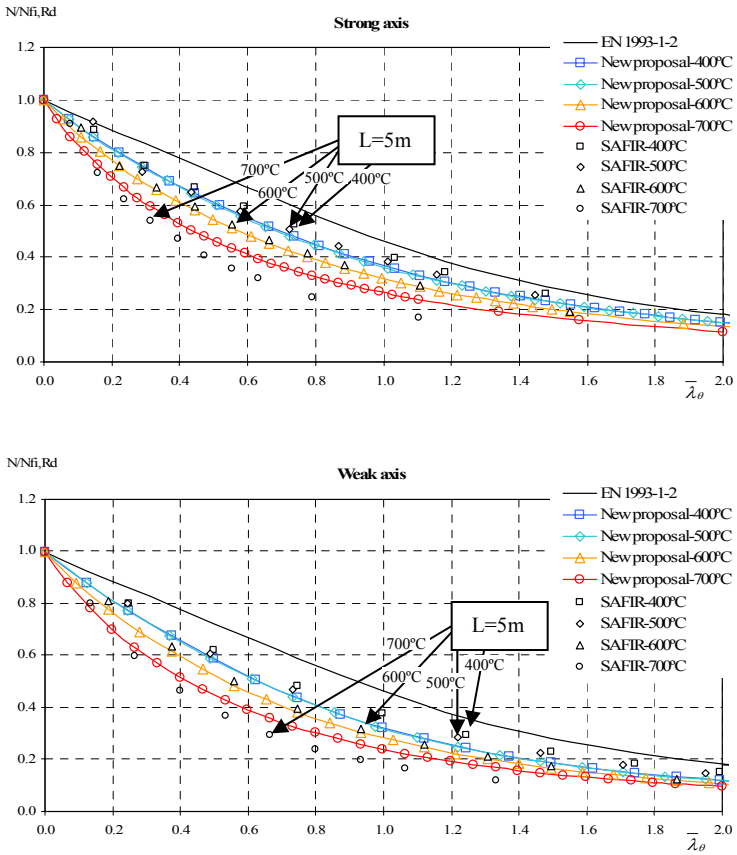

Figure 5.26 – Column with cross-section HEB200 in stainless steel grade 1.4003, at high temperatures.

It can be observed that the results obtained with the new proposal for stainless steel grade 1.4003 columns at 700 ºC are not safe. Due to the fact that this temperature starts to get outside of the common steel critical temperatures, it was not given great importance to these unsafe results, accepting these differences.

Statistical evaluation

Similarly to section 5.2.1, here the ratio between the analytical value of the ultimate design axial force and the corresponding SAFIR axial force is evaluated.

The 308 and 294 results, for respectively the strong and weak axis, obtained with EN 1993-1-2 for welded HEA200, HEB280 and HEB200 sections in stainless steel grades 1.4301, 1.4401, 1.4571, 1.4003 and 1.4462 are shown in Figure 5.27 and Figure 5.28. The average value and the standard deviation are, respectively, $\mu = 1.169$ and $s = 0.250$ for the strong axis, and $\mu = 1.345$ and $s = 0.194$ for the weak axis (see Table 5.17).

Table 5.17 – Statistical results of columns at elevated temperatures.

		EN 1993-1-2	New proposal
Strong axis	Average value	1.169	0.978
	Standard deviation	0.250	0.049
Weak axis	Average value	1.345	0.956
	Standard deviation	0.194	0.076

If the new proposal is used in those numerical results, the average value and the standard deviation take the values $\mu = 0.978$ and $s = 0.049$ for the strong axis, and $\mu = 0.956$ and $s = 0.076$ for the weak axis, showing that the new proposal is safer than the EC3 with a smaller value of the standard deviation.

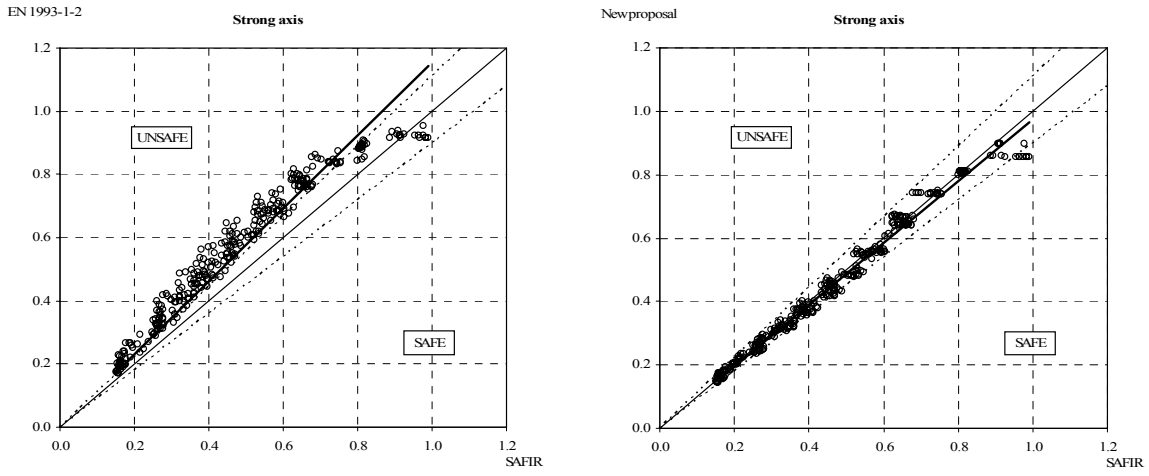

Figure 5.27 – Comparison between EN 1993-1-2, the new proposal and numerical results for the strong axis, at high temperatures.

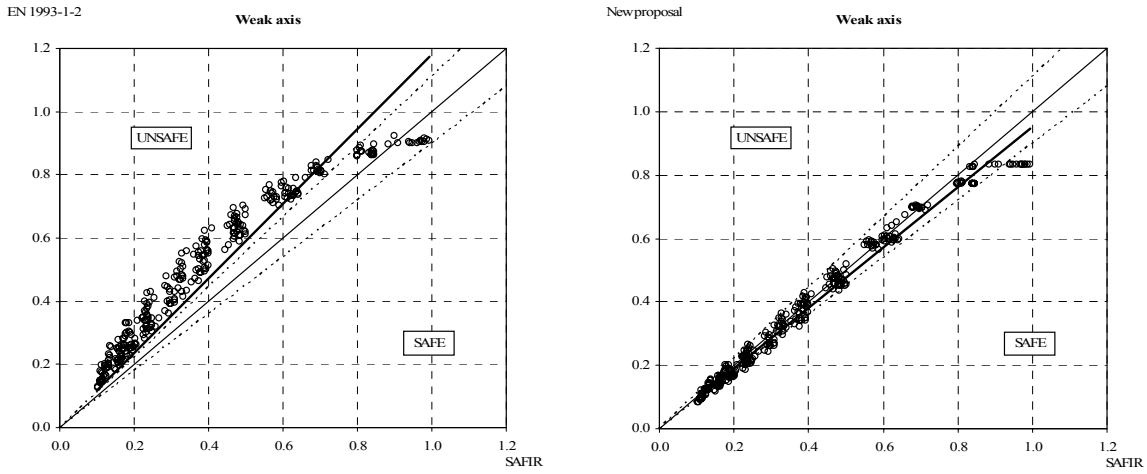

Figure 5.28 – Comparison between EN 1993-1-2, the new proposal and numerical results for the weak axis, at high temperatures.

Figure 5.29 and Figure 5.31 show the ratio x_i when EN 1993-1-2 is used with all the numerical results for the strong and weak axis. The maximum unsafe error is 51.4 % and 87.6 % for the strong and for the weak axis, respectively. The average unsafe error is 22.0 % and 36.2 % for the strong and for the weak axis, respectively.

The new proposal gives the results shown in Figure 5.30 and Figure 5.32, with the maximum unsafe error of 11.2 % and 13.4 % for the strong and weak axis, respectively, and an average unsafe error of 3.2 % and 3.9 % for the strong and weak axis, respectively. These last values are small suggesting that the proposal is satisfactorily safe.

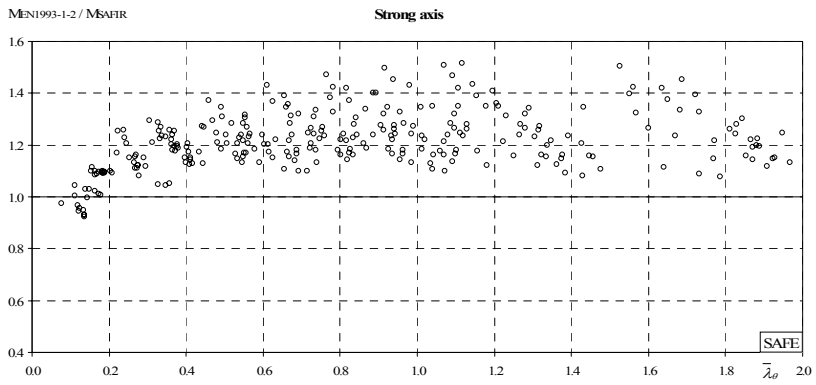

Figure 5.29 – Ratio between analytical and SAFIR results, for EN 1993-1-2 in the strong axis, at high temperatures.

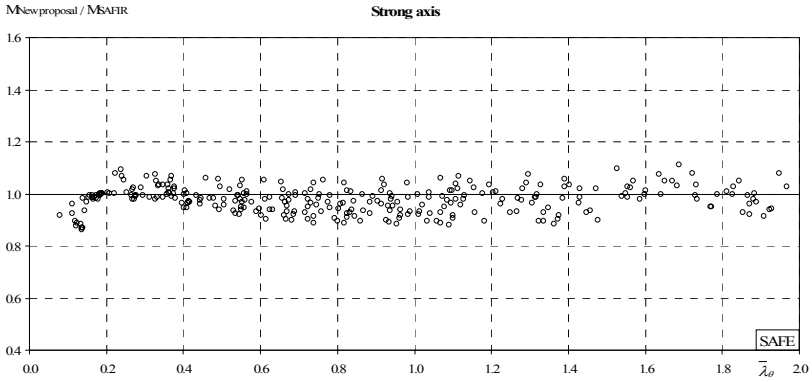

Figure 5.30 – Ratio between analytical and SAFIR results, for the new proposal in the strong axis, at high temperatures.

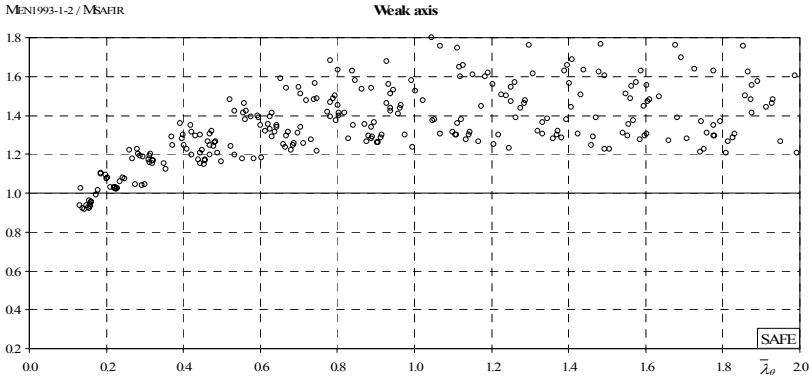

Figure 5.31 – Ratio between analytical and SAFIR results, for EN 1993-1-2 in the weak axis, at high temperatures.

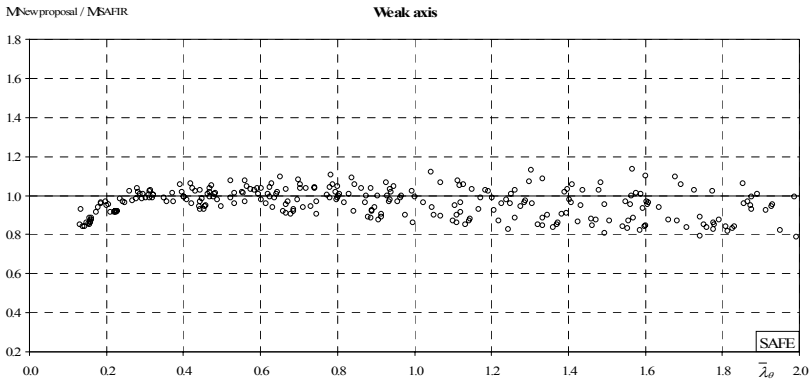

Figure 5.32 – Ratio between analytical and SAFIR results, for the new proposal in the weak axis, at high temperatures.

From these graphics it can be concluded that the new proposal gives a much safer approximation to the numerical results than the part 1-2 of EC3.

5.3.2 Bending

Section 4.3.2 of this thesis shows that LTB formulae included in part 1-2 of EC3 should be improved in order to give better results for non-uniform bending. Therefore, in this section a new proposal for the LTB safety evaluation of stainless steel structural elements at high temperatures will be presented.

5.3.2.1 Case study

A simply supported beam with fork supports was chosen to explore the validity of the beam safety verifications. Table 5.18 and Table 5.19 summarizes all the studied cases

Table 5.18 – Cases studied with uniform bending at high temperatures.

	High temperatures
	$\psi = 1$
HEA500	
1.4301	✓
1.4401 1.4404	✓
1.4571	✓
1.4003	✓
1.4462	✓
IPE220	
1.4301	✓
1.4401 1.4404	✓
1.4571	✓
1.4003	✓
1.4462	✓
IPE500	
1.4301	✓
1.4401 1.4404	✓
1.4571	✓
1.4003	✓
HEA200	
1.4301	✓
HEB280	
1.4301	✓
1.4003	✓
HEB200	
1.4462	✓

As shown in Table 5.18, the following welded cross-sections were used: IPE220, HEA500, IPE500, HEA200, HEB280 and HEB200 section. The stainless steel grade 1.4301, 1.4401, 1.4571, 1.4003 and 1.4462 for each cross-section were studied. An average of 10 lengths for each case presented in Table 5.18 and Table 5.19 were studied. Temperatures of 400, 500, 600 and 700 ºC were used.

Regarding the bending moment variation along the member length, five values (-1, -1/2, 0, 1/2 and 1) of the ψ ratio have been investigated as well as a mid span concentrated load and an uniformly distributed load (see Table 5.19).

Table 5.19 – Cases studied with non-uniform bending at high temperatures.

	High temperatures					
	ψ					
	1/2	0	-1/2	-1	Point Load	Distributed Load
HEA500						
1.4301	✓	✓	✓	✓	✓	✓
IPE220						
1.4301	✓	✓	✓	✓	✓	✓
1.4462	✓	✓	✓	✓	✓	✓
IPE500						
1.4301	✓	✓	✓	✓	✓	✓

Initial imperfections and residual stresses were considered as described in section 3.3.1.

5.3.2.2 Improvement of the Eurocode 3 formulae: a new proposal

Similarly to the proposal made for the flexural buckling of stainless steel in case of fire (see section 5.3.1), in this section a proposal for the evaluation of the LTB of stainless steel elements in case of fire (Vila Real *et al.*, 2008), which takes into account the different behaviour at high temperatures of the different stainless steel grades is presented.

Based on part 1-1 of EC3 (CEN, 2005a), it is proposed that the design LTB resistance moment of a laterally unrestrained stainless steel beam with Class 1 or Class 2 in case of fire, be determined with the expression

$$M_{b,fi,t,Rd} = \chi_{LT,fi,\mathrm{mod}} W_{pl,y} k_{y,\theta} \left. f_y \middle/ \gamma_{M,fi} \right. \tag{5.50}$$

where the modified reduction factor is determined as for the carbon steel (see section 4.3.4), with the equations

$$\chi_{LT,fi,\text{mod}} = \frac{\chi_{LT,fi}}{f} \quad \text{but} \quad \chi_{LT,fi,\text{mod}} \leq 1 \tag{5.51}$$

where $\chi_{LT,fi}$ is given by

$$\chi_{LT,fi} = \frac{1}{\phi_{LT,\theta,com} + \sqrt{\phi^2_{LT,\theta,com} - \overline{\lambda}^2_{LT,\theta,com}}} \quad \text{with} \quad \chi_{LT,fi} \leq 1 \tag{5.52}$$

with

$$\phi_{LT,\theta,com} = \frac{1}{2}\left(1 + \alpha\overline{\lambda}_{LT,\theta,com} + \overline{\lambda}^2_{LT,\theta,com}\right) \tag{5.53}$$

As proposed for stainless steel columns (see section 5.3.1), in order to consider the different behaviour at high temperatures provided by the different stainless steel grades shown in Figure 5.24, the imperfection factor can be written in function of the temperature as

$$\alpha = \eta\sqrt{\frac{235}{f_y}}\sqrt{\frac{E}{210000}}\sqrt{\frac{k_{E,\theta}}{k_{y,\theta}}} \tag{5.54}$$

The proposal for the values of factor η to be used with this equation, are given in Table 5.20 in a linear function of the ratio h/b, as it was also proposed in the approach for the LTB at room temperature (see section 5.2.2).

Table 5.20 – Severity factor for the LTB of stainless steel elements in case of fire.

	1.4301; 1.4401; 1.4404; 1.4571	1.4462 and 1.4003
η	$0.22\left(\frac{h}{b}\right) + 0.38$	$0.16\left(\frac{h}{b}\right) + 0.34$

Again, as in previous proposals, the stainless steel grade 1.4462 had to be differentiated. Moreover, it was observed that the LTB curves for the ferritic grade 1.4003 did not need to be as severe as for the austenitic stainless steels, being the curves developed for the 1.4462 grade suitable. Figure 5.33 shows the severity factor in function of the ratio h/b.

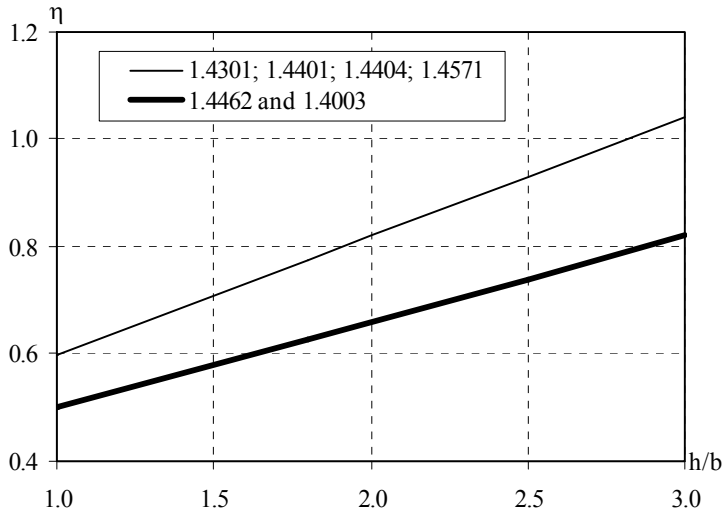

Figure 5.33 – Severity factor for the LTB at high temperatures in function of the cross-section slenderness.

To consider the loading type, the factor f is determined with

$$f = 1 - 0.5(1 - k_c) \tag{5.55}$$

where the correction factor k_c given in Table 5.21 is similar to the one proposed for carbon steel elements in case of fire (section 4.3.4).

Table 5.21 – Correction factors for LTB of stainless steel elements at high temperatures.

Moment distribution	Class 1, 2 sections k_c
$-1 \leq \psi \leq 1$	$0.6 + 0.3\psi + 0.15\psi^2$ but $k_c \leq 1$
Concentrated load	0.79
Distributed load	0.91

Using this design proposal for non-uniform bending, it is possible to state maximum slenderness values for dispending the LTB evaluation as a function of the loading type (Lopes *et al.*, 2008a).

5.3.2.3 Accuracy of the proposal

Again, to evaluate this new proposal for the LTB of stainless steel elements, a direct comparison with the numerical results and a statistical study are used.

Numerical validation

In this section, the results for stainless steel beams subjected to LTB are shown.

In Figure 5.34 only the results for an IPE220 of the stainless steel grade 1.4301 are presented (see Appendix K for remaining results).

The results for stainless steel beams subjected to LTB, shown in Figure 5.34, are presented for all the load cases studied.

The graphics compare the curves obtained through part 1-4 of EC3, described in section 4.2.2 of this thesis (denoted "EN 1993-1-4" in the graphics), against the curve obtained with the new proposal presented in the last section (denoted "New proposal" in the graphics), and the numerical results obtained with the program SAFIR.

The figures show that the use of a modified reduction factor for the LTB improves the beam design curve when compared with the numerical simulations.

Figure 5.35 shows the performance of the proposal for a HEA200, which has $h/b = 0.95$. From this figure a better agreement provided by the new proposal for sections with small values of h/b, when compared against EC3, is noticed.

As for the proposal for stainless steel columns at high temperatures presented in section 5.3.1, with the buckling curves varying with the temperature, it is possible to have a better prediction of the behaviour of the LTB in beams of the stainless steel grade 1.4003 (see Figure 5.36).

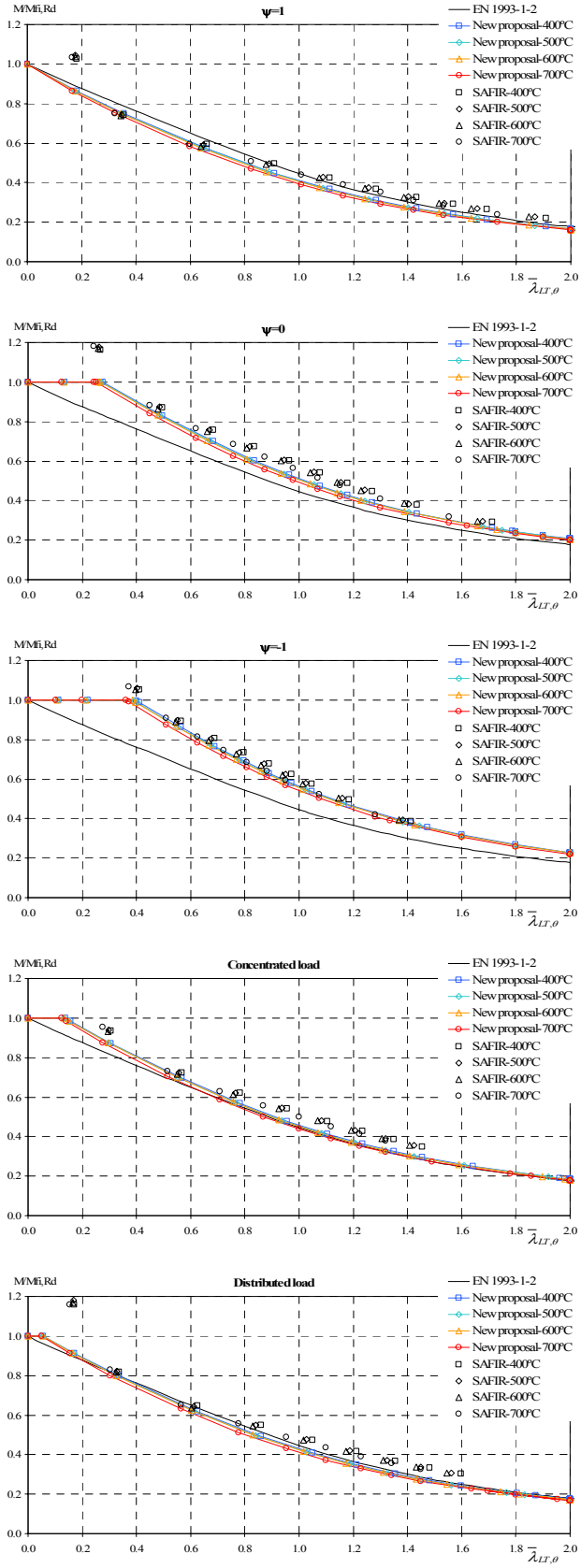

Figure 5.34 – Numerical results for a welded IPE220 of stainless steel grade 1.4301, at high temperatures.

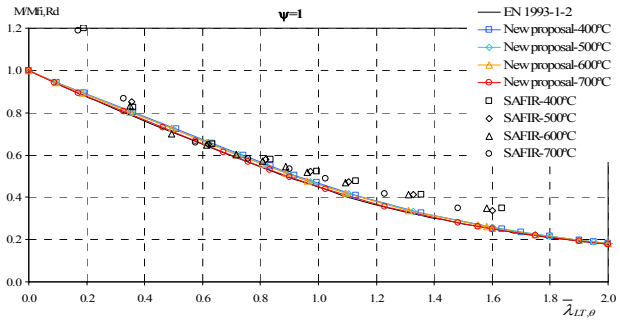

Figure 5.35 – Numerical results for a welded HEA200 of stainless steel grade 1.4301, at high temperature.

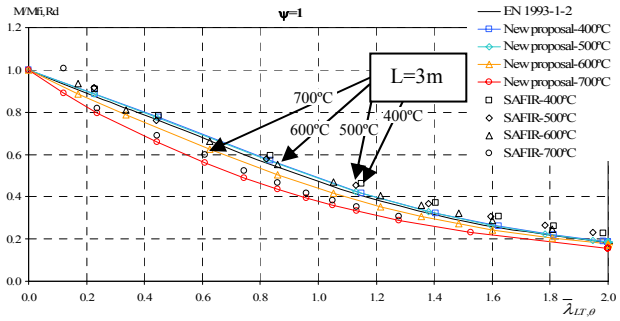

Figure 5.36 – Numerical results for a welded IPE220 in stainless steel grade 1.4003, at high temperatures.

Statistical evaluation

As in section 4.3.4, the ratio between the analytical value of the ultimate design moment and the corresponding SAFIR moment was evaluated. The statistical evaluation presented here was made for uniform bending diagrams, accessing the chosen values.

The 573 results obtained with EN 1993-1-2 for welded HEA200, HEB280, HEB200, HEA500, IPE220 and IPE500 sections, in stainless steel grades, 1.4301, 1.4401, 1.4571, 1.4003 and 1.4462 are shown in Figure 5.37. The average value and the standard deviation are, respectively, $\mu = 0.976$ and $s = 0.098$.

Table 5.22 – Statistical results of beams at elevated temperatures.

	EN 1993-1-2	New proposal
Average value	0.976	0.929
Standard deviation	0.098	0.070

If the new proposal is used in those numerical results, the average value and the standard deviation take the values $\mu = 0.929$ and $s = 0.070$, showing that the new proposal makes a

better approximation of the numerical results, while maintaining safety, with a smaller value for the standard deviation (see Table 5.22).

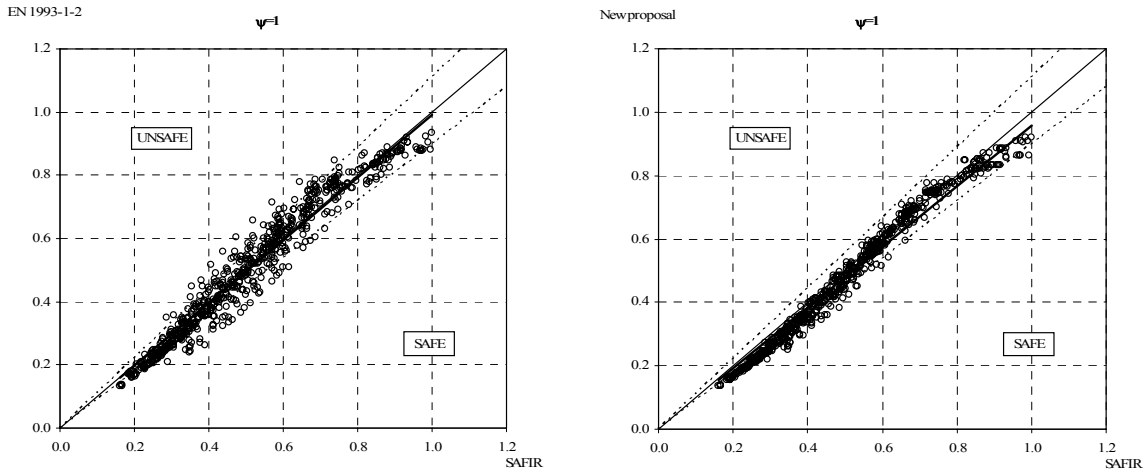

Figure 5.37 – Comparison between EN 1993-1-2 and numerical results.

Figure 5.38 shows the ratio x_i when EN 1993-1-4 is used with all the numerical results for the strong and weak axis. The maximum unsafe error is 27.7 % and the average unsafe error is 6.9 %.

The new proposal gives the results shown in Figure 5.39, with the maximum unsafe error of 8.2 % and average unsafe error of 2.0 %.

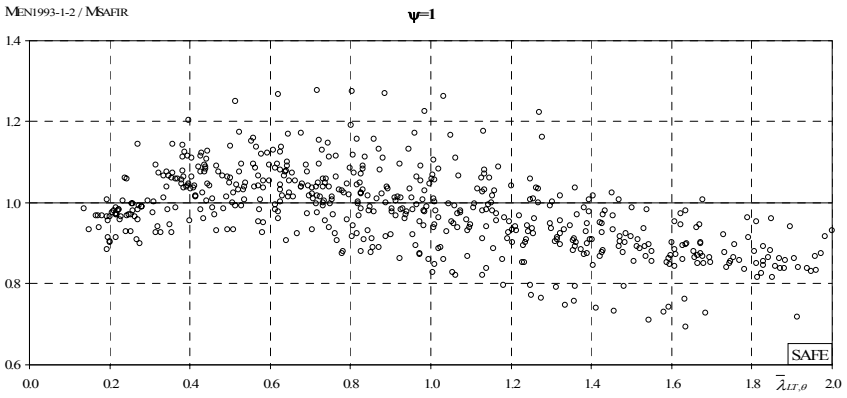

Figure 5.38 – Ratio between analytical and SAFIR results, for EN 1993-1-2.

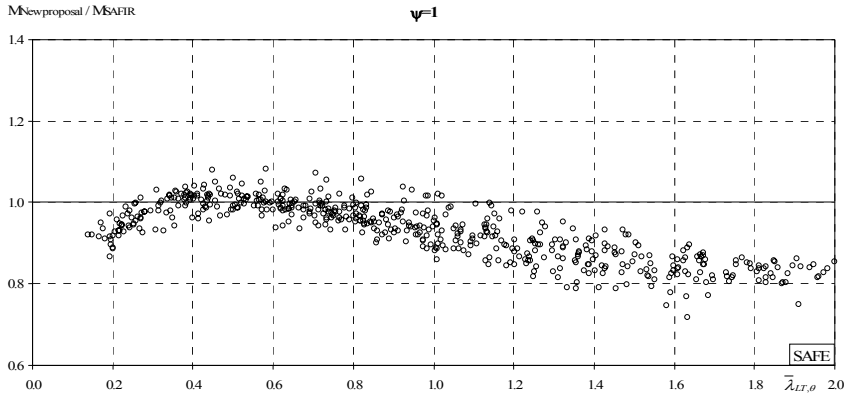

Figure 5.39 – Ratio between analytical and SAFIR results, for the new proposal.

It can be observed that the new proposal, presented here, gives better and safer approximation to the numerical results than the part 1-2 of EC3.

5.3.3 Bending and axial compression

The numerical results, presented in section 4.3.3, acknowledged the necessity of the development of new improved interaction formulae, for the safety evaluation of stainless steel beam-columns at high temperatures.

The possibility of using the EC3 part 1-1 formulae in case of fire (Vila Real *et al.*, 2003d; Lopes *et al.*, 2007, 2004; Lopes, 2003; Knobloch *et al.*, 2008), for stainless steel beam-columns safety evaluation is also studied.

Based on the conclusions obtained from section (5.2.3), it is not presented here the performance of the EC3, stainless steel cold design formulae (CEN, 2006a), adaptation to fire situation. This design approach revealed to be too inaccurate (Lopes *et al.*, 2007), besides, it does not accounts the influence of non-uniform bending diagrams.

Following this study, alternative expressions for the stainless steel interaction curves were developed and are here proposed.

These studies address the possibility of occurring or not LTB. Also, previously in this chapter, proposals for the evaluation of buckling phenomena in stainless steel structural elements were presented. As these new proposals necessarily affect the behaviour of the interaction formulae for beam-columns, its influence is here considered.

5.3.3.1 Without lateral torsional buckling

In this section the study made on stainless steel elements, subjected to bending and axial compression without LTB, is presented.

5.3.3.1.1 Case study

A simply supported column, subjected to axial compression plus bending and flexural buckling in the strong axis or bending and flexural buckling in the weak axis, was chosen for the parametric study. Initial imperfections and residual stresses were considered as described in section 3.3.1.

The following welded cross-sections were used: HEA200, HEB280 and HEB200 stainless steel section at 600 ºC. The types of stainless steel grade used were: 1.4301, 1.4003 and 1.4462. Table 5.23 shows all the cases that have been studied. An average of 5 lengths and 8 axial load ratios were analysed for each case.

Table 5.23 – Cases studied for beam-columns without LTB at high temperatures.

	Temperature of 600 ºC					
	$\psi = 1$		$\psi = 0$		$\psi = -1$	
	Strong axis	Weak axis	Strong axis	Weak axis	Strong axis	Weak axis
HEA200						
1.4301	✓	✓	✓	✓	✓	✓
HEB280						
1.4301	✓	✓	✓	✓	✓	✓
1.4003	✓	✓	✓	✓	✓	✓
HEB200						
1.4462	✓	✓	✓	✓	✓	✓

5.3.3.1.2 Formulation of a new proposal

Part 1-2 of EC3 (CEN, 2005b) states that the safety evaluation of elements subjected to bending and axial compression should satisfy:

$$\frac{N_{fi,Ed}}{\chi_{\min,fi} A \frac{k_{y,\theta} f_y}{\gamma_{M,fi}}} + K_{y,fi} \frac{M_{y,fi,Ed}}{W_{pl,y} \frac{k_{y,\theta} f_y}{\gamma_{M,fi}}} + K_{z,fi} \frac{M_{z,fi,Ed}}{W_{pl,z} \frac{k_{y,\theta} f_y}{\gamma_{M,fi}}} \leq 1 \qquad (5.56)$$

Based on the procedure adopted by Talamona (1995) for the determination of the carbon steel interaction curves at high temperatures (see section 4.3.3), new formulae for the stainless steel beam-columns safety evaluation were developed and are here presented.

In comparison against EC3 (CEN, 2005b) the main changes appear in the determination of the interactions factors $K_{y,fi}$ and $K_{z,fi}$.

$$K_{y,fi} = 1 - \frac{\mu_{y,\theta} N_{fi,Ed}}{\chi_{y,fi} A k_{y,\theta} \dfrac{f_y}{\gamma_{M,fi}}} \quad \text{with} \quad K_{y,fi} \le 0.8\overline{\lambda}_{y,\theta} + 0.9 \tag{5.57}$$

$$K_{z,fi} = 1 - \frac{\mu_{z,\theta} N_{fi,Ed}}{\chi_{z,fi} A k_{y,\theta} \dfrac{f_y}{\gamma_{M,fi}}} \quad \text{with} \quad K_{z,fi} \le 0.8\overline{\lambda}_{z,\theta} + 0.9 \tag{5.58}$$

The introduced limits for the interactions factors $K_{y,fi}$ and $K_{z,fi}$ were developed in order to achieve a better approximation from the curves shape to the numerical results. Figure 5.40 shows the influence of the introducing of those limits in the curve shape.

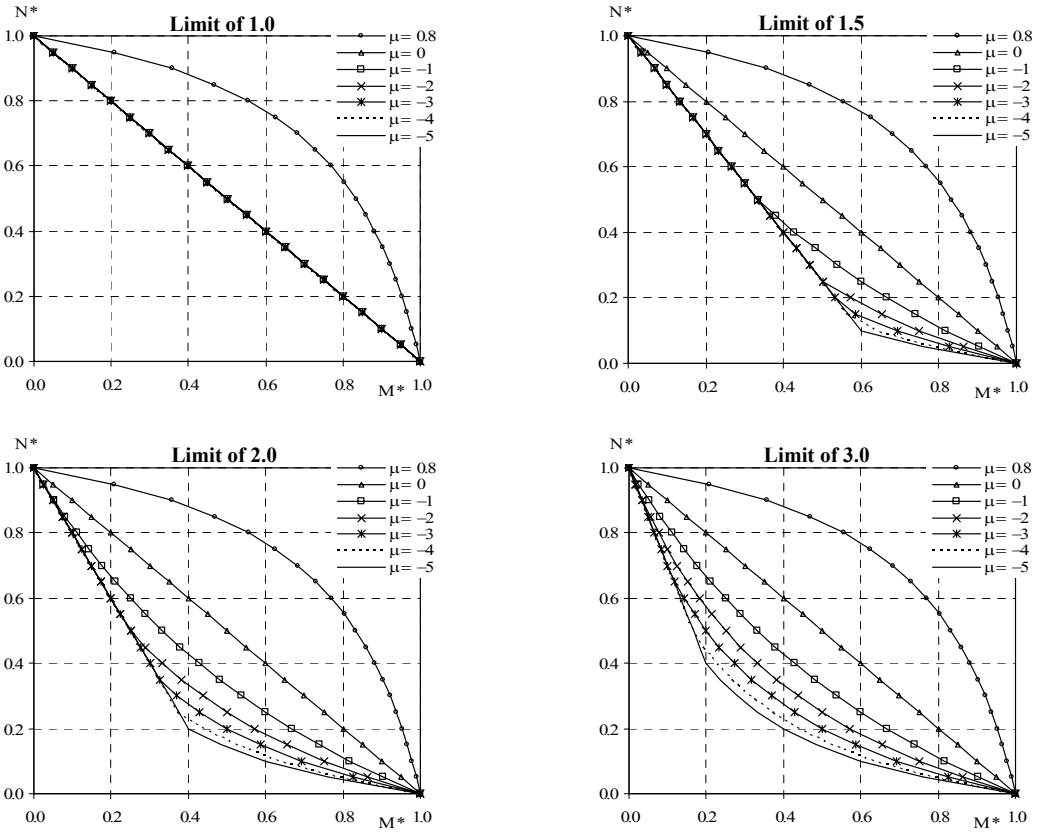

Figure 5.40 – Interaction curve shape for different interaction factor limits.

To determine the values of $\mu_{y,\theta}$ and $\mu_{z,\theta}$ the following equations should be used for the stainless steel grades 1.4301 and 1.4003:

$$\mu_{y,\theta} = \left(4.33\beta_{M,y} - 8.56\right)\overline{\lambda}_{y,\theta} + 0.33\beta_{M,y} + 0.11 \leq 0.7 \tag{5.59}$$

and

$$\mu_{z,\theta} = \left(3.03\beta_{M,z} - 6.33\right)\overline{\lambda}_{z,\theta} + 1.93\beta_{M,z} - 2.45 \leq 0.7 \tag{5.60}$$

It was found that for the duplex grade, the changes introduced in the flexural buckling curves (see section 5.3.1), when compared to the other grades, were not enough to approximate satisfactorily the beam-columns numerical results. Therefore, for the duplex stainless steel grade 1.4462 different formulae should be adopted.

$$\mu_{y,\theta} = \left(1.27\beta_{M,y} - 2.63\right)\overline{\lambda}_{y,\theta} + 0.66\beta_{M,y} - 0.49 \leq 0.8 \tag{5.61}$$

and

$$\mu_{z,\theta} = \left(1.53\beta_{M,z} - 3.20\right)\overline{\lambda}_{z,\theta} + 0.41\beta_{M,z} + 0.24 \leq 0.9 \tag{5.62}$$

And finally the equivalent uniform moment factor $\beta_{M,y}$ and $\beta_{M,z}$ can be determined in function of the bending diagram shape, according to expression (5.27).

In the stainless steel grades 1.4301 and 1.4003, the evolution of μ as a function of the slenderness at 600 ºC for the strong and weak axis is shown in Figure 5.41 and Figure 5.42.

In these figures, "Linear (SAFIR)" is the linear trend line of the numerical results obtained with SAFIR. The equations from (5.59) to (5.62) were developed to approximate the numerical results providing at the same time safety. Again, as in 5.2.3.1.3, only the numerical results with lower values of μ in the several slenderness values, were accounted for in the development of the functions.

In the duplex stainless steel grade 1.4462, the evolution of μ, as a function of the slenderness at 600 ºC for the strong and weak axis, is shown in Figure 5.43 and Figure 5.44 respectively. As it can be seen, the numerical results for the duplex stainless steel grade do not follow the developed functions for the stainless steel grades 1.4301 and 1.4003. In the graphics "SAFIR" are the numerical values for the duplex, "New proposal for duplex" is the function here proposed for the duplex and "New proposal for other grades" is the function previously proposed in this section for the other stainless steel grades (1.4301 and 1.4003).

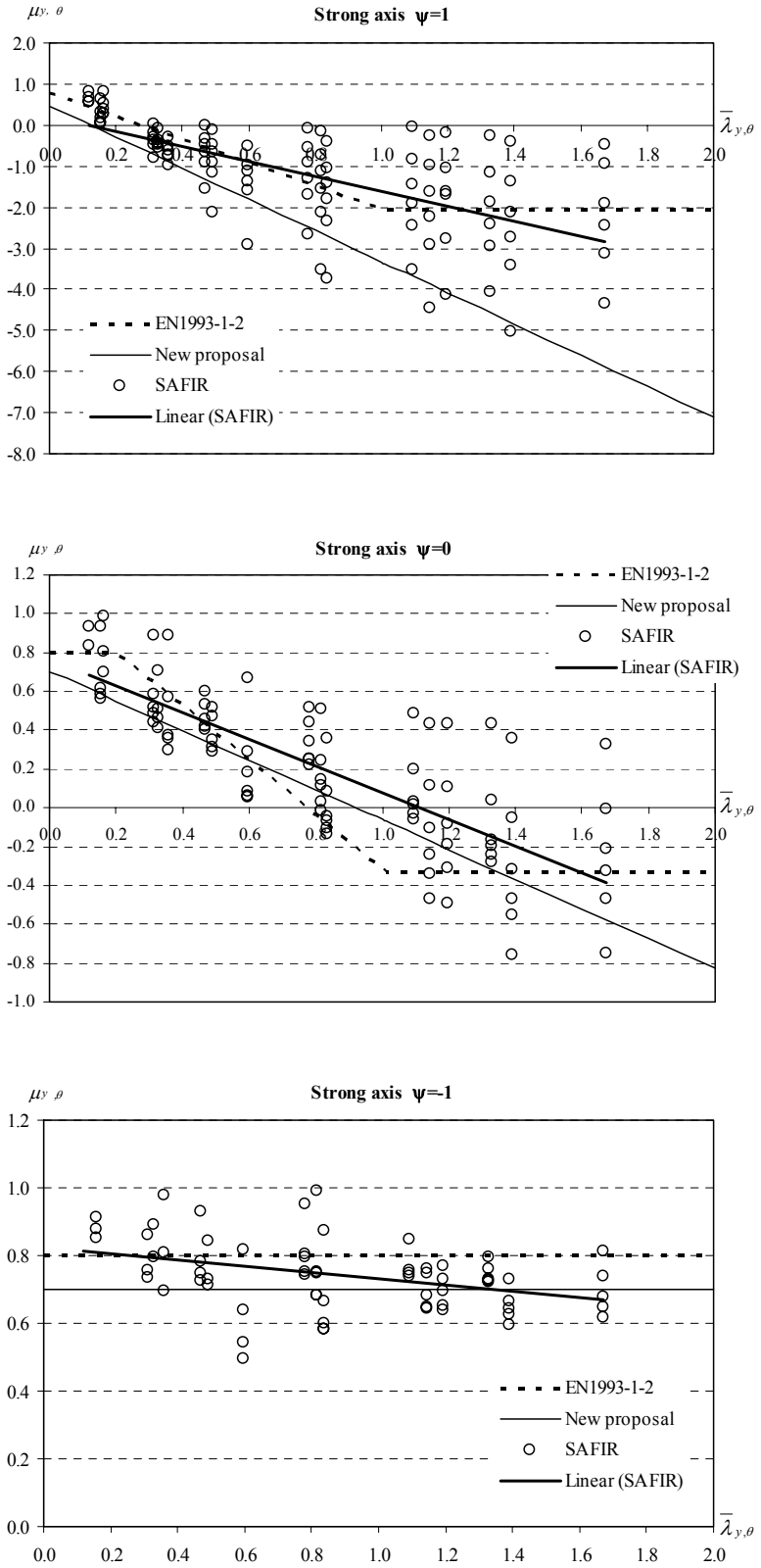

Figure 5.41 – Formulation of new interaction curves for the strong axis, at high temperatures.

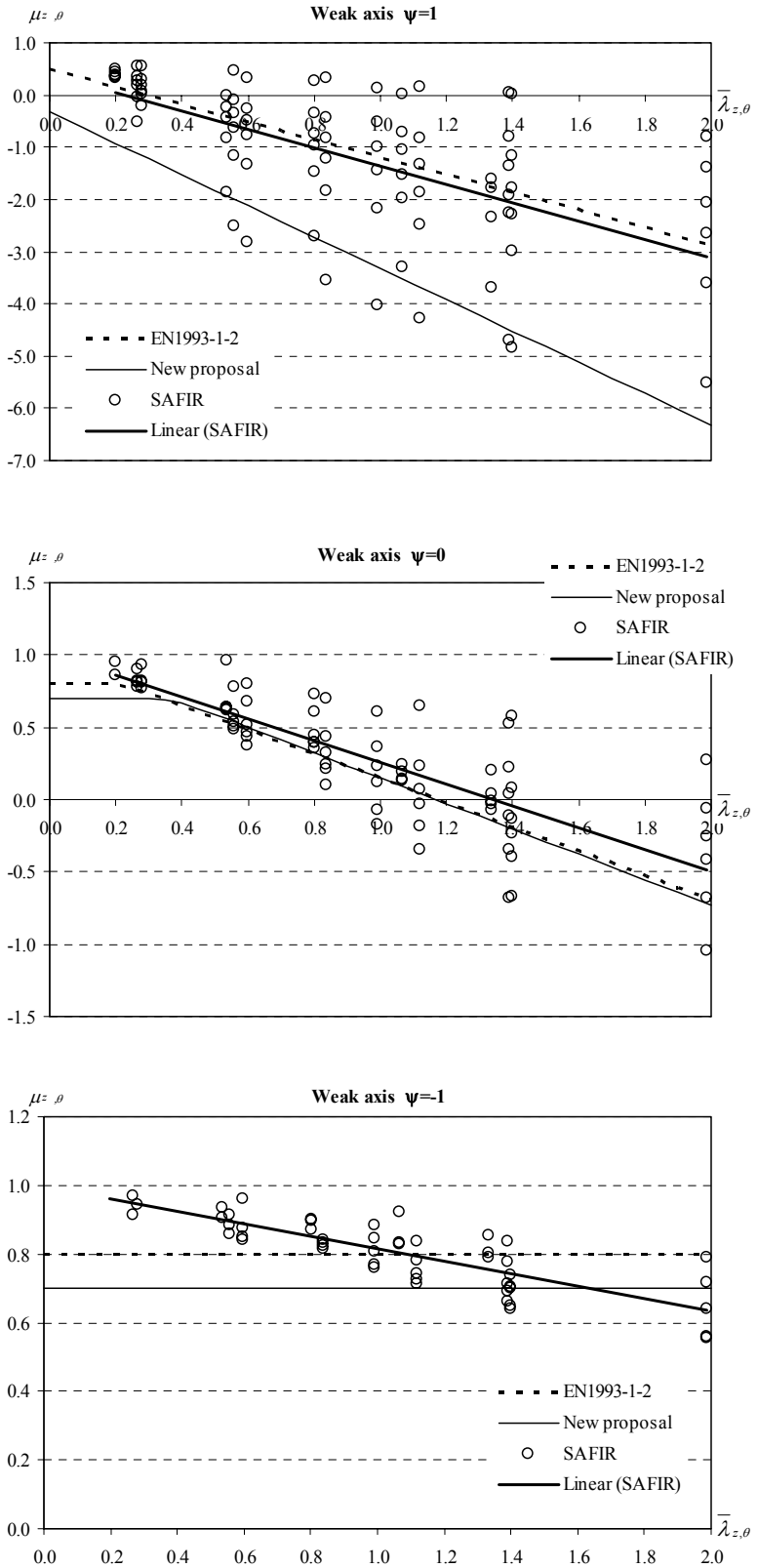

Figure 5.42 – Formulation of new interaction curves for the weak axis, at high temperatures.

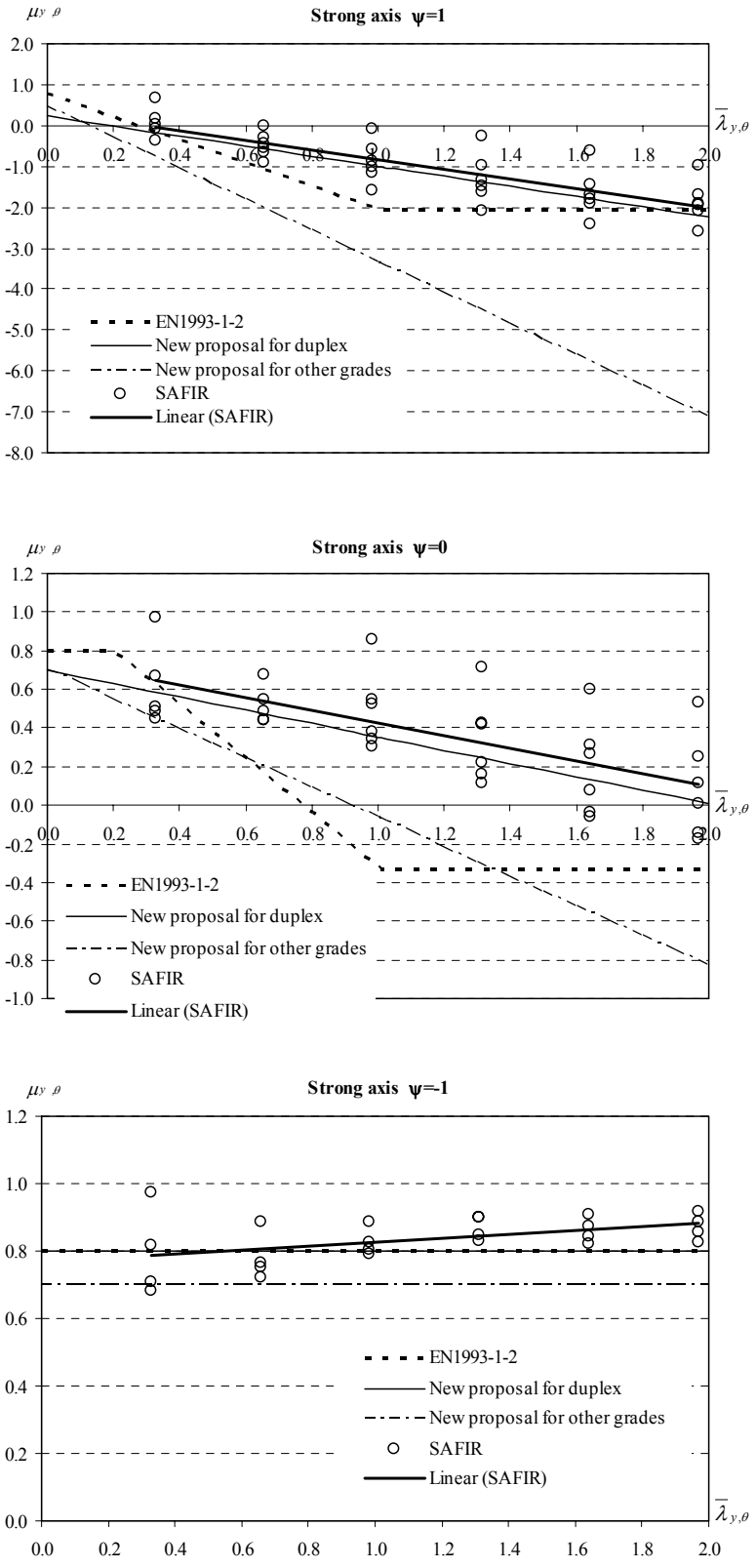

Figure 5.43 – Formulation of new interaction curves for the strong axis, at high temperatures, in duplex stainless steel.

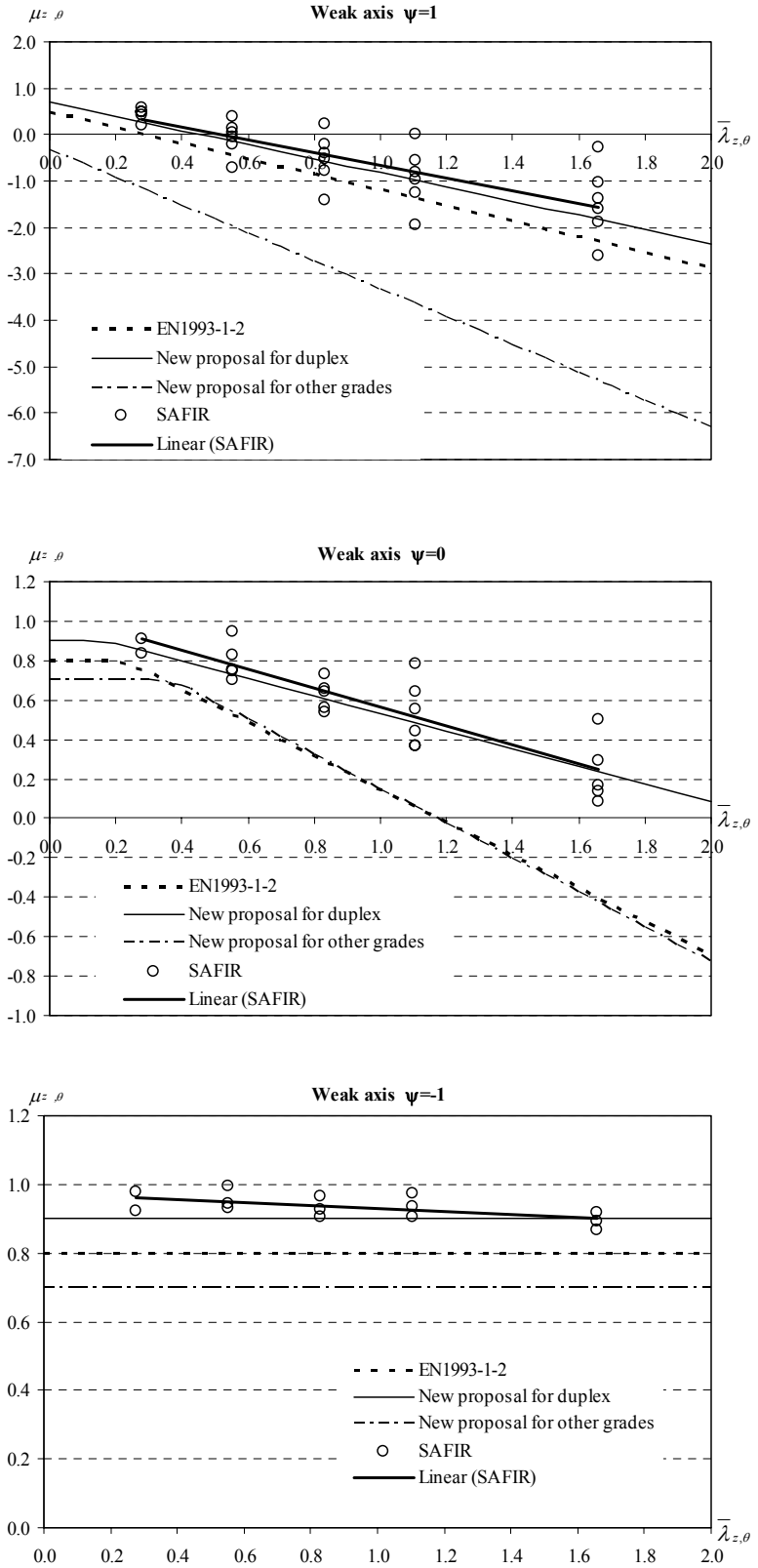

Figure 5.44 – Formulation of new interaction curves for the weak axis at high temperatures, in duplex stainless steel.

5.3.3.1.3 Accuracy of the proposals

In this section these new proposals are evaluated by means of a direct comparison with the numerical results and a statistical study.

Numerical validation

The graphics from Figure 5.45 and Figure 5.46 were obtained for beam-columns with welded cross-sections equivalent to a HEA200 at 600 ºC of the stainless steel grade 1.4301, for the buckling modes about the y and z axis, with uni-axial bending in the strong and weak axis respectively. Here, the length of 3 m corresponds to non-dimensional slenderness values of $\overline{\lambda}_{y,\theta} = 0.36$ and $\overline{\lambda}_{z,\theta} = 0.60$, while the length of 7 m corresponds to $\overline{\lambda}_{y,\theta} = 0.84$ and $\overline{\lambda}_{z,\theta} = 1.39$. The other cross-section and length studied are included in Appendix L.

The interaction curves in the graphics from Figure 5.17 and Figure 5.18 are obtained from:

- part 1-2 of EC3 “EN 1993-1-2”;
- part 1-2 of EC3 with the new proposal for columns presented in section 5.2.1 “EN 1993-1-2 mod”;
- part 1-1 of EC3 for carbon steel beam-columns with the new proposal for columns presented in section 5.2.1 “Method 1”and “Method 2”;
- and the formulated interaction curves presented in the previous section “New proposal”.

Although, having some few unsafe results, the method that better approximates the numerical results from SAFIR is the method “New proposal”. This method corresponds to the here formulated interaction curves. The other tested curves present unsafe approximations.

It can also be observed that the new proposal for columns presented in section 5.3.1 of this thesis introduces a significant improvement in the interaction curves approximations to the numerical results.

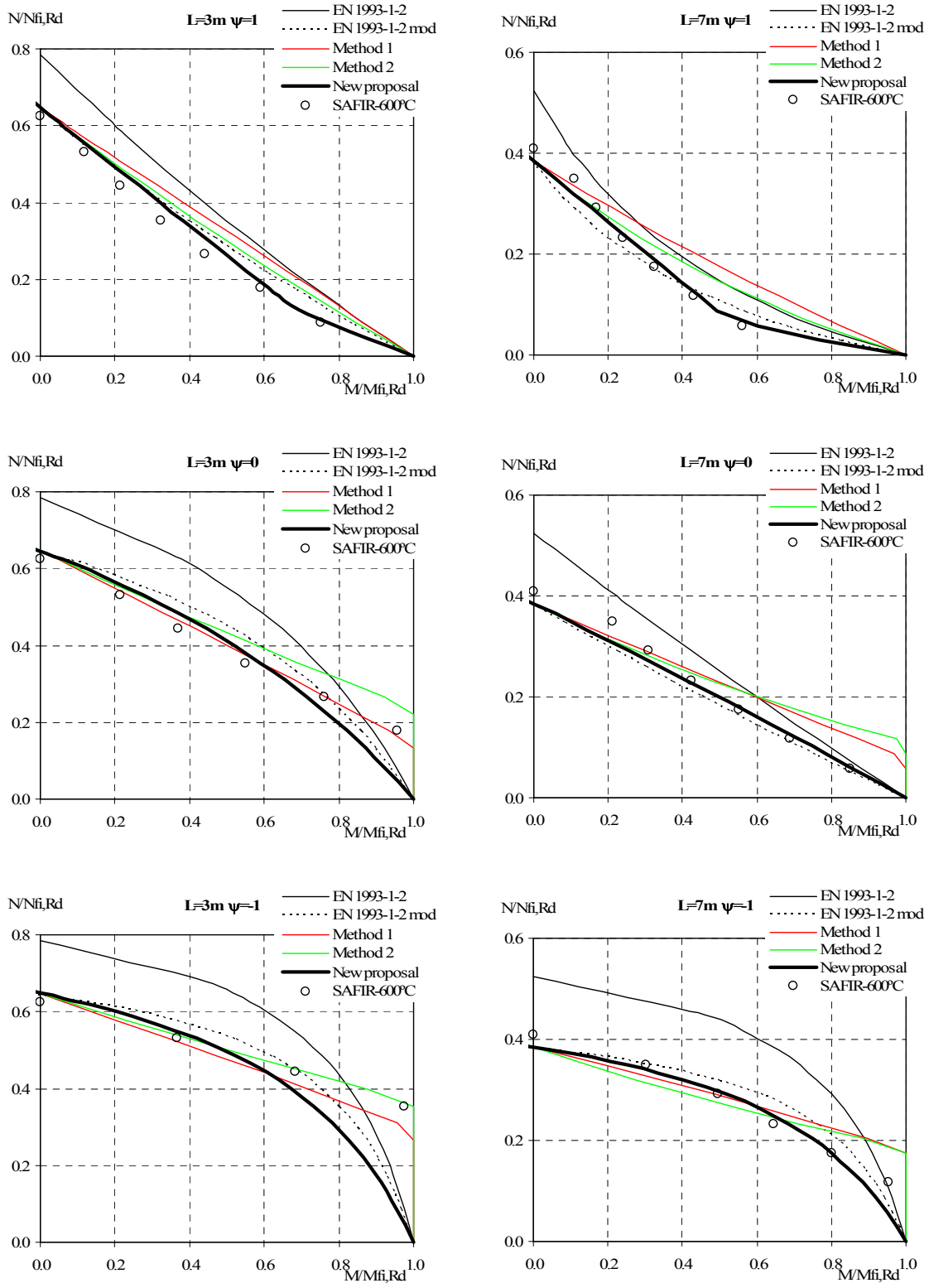

Figure 5.45 – Comparison between different interaction curves for welded HEA200 beam-columns of the stainless steel grade 1.4301, regarding the buckling mode and uni-axial bending about the strong axis, at high temperatures.

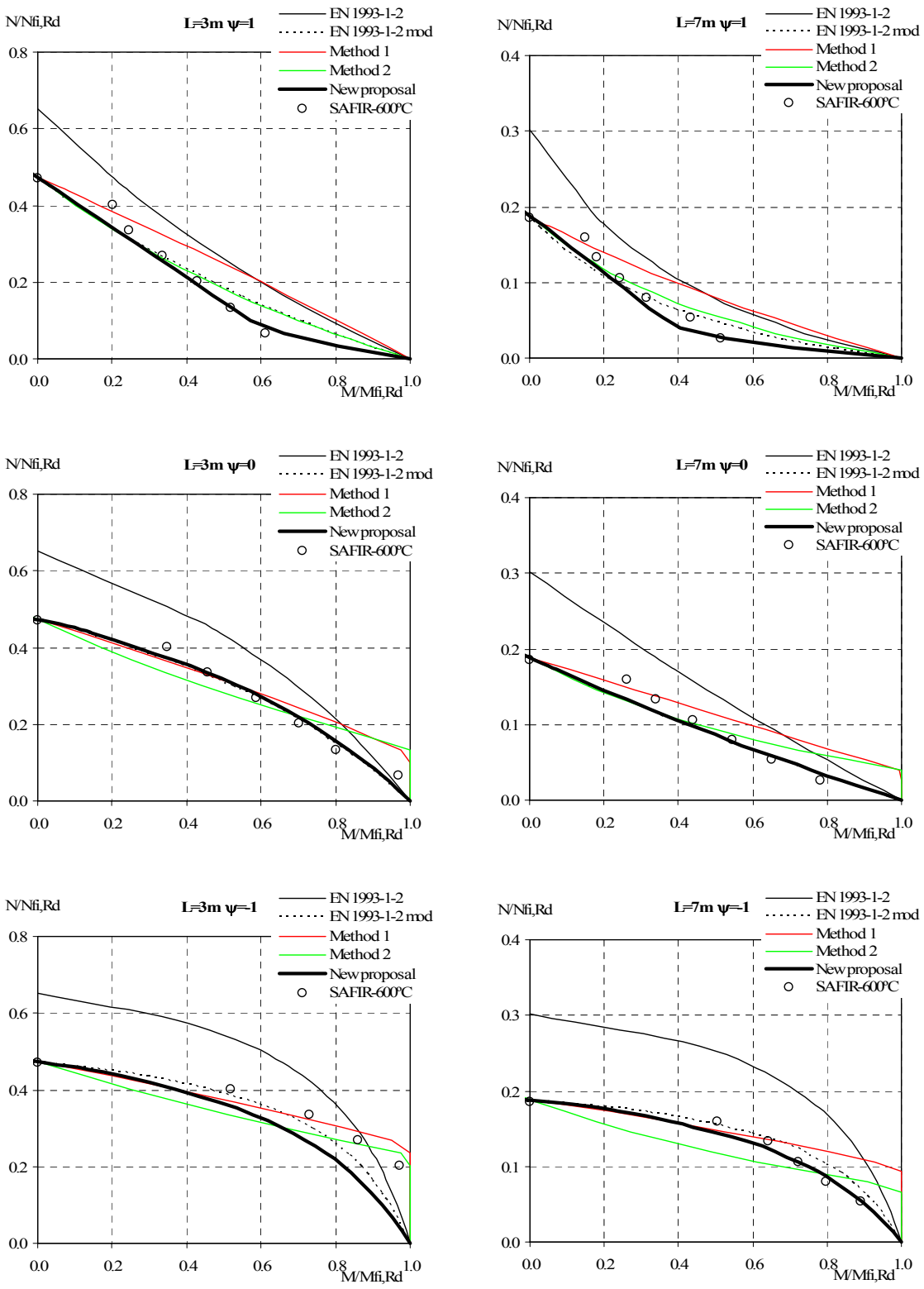

Figure 5.46 – Comparison between different interaction curves for welded HEA200 beam-columns of the stainless steel grade 1.4301, regarding the buckling mode and uni-axial bending about the weak axis, at high temperatures.

Statistical evaluation

The 266 and 213 results, for respectively the strong and weak axis, obtained with the several proposals for the interaction curves (EC3, "Method 1", "Method 2" and "New proposal") for welded HEA200 and HEB280 sections at 600 ºC in stainless steel grades 1.4301 and 1.4003, are shown in Figure 5.47 and Figure 5.48. In these comparisons, the new proposal for stainless steel columns was used.

Table 5.24 presents the average and standard deviation obtained with the different methods for determining the austenitic and the ferritic stainless steel beam columns interaction curves at high temperatures.

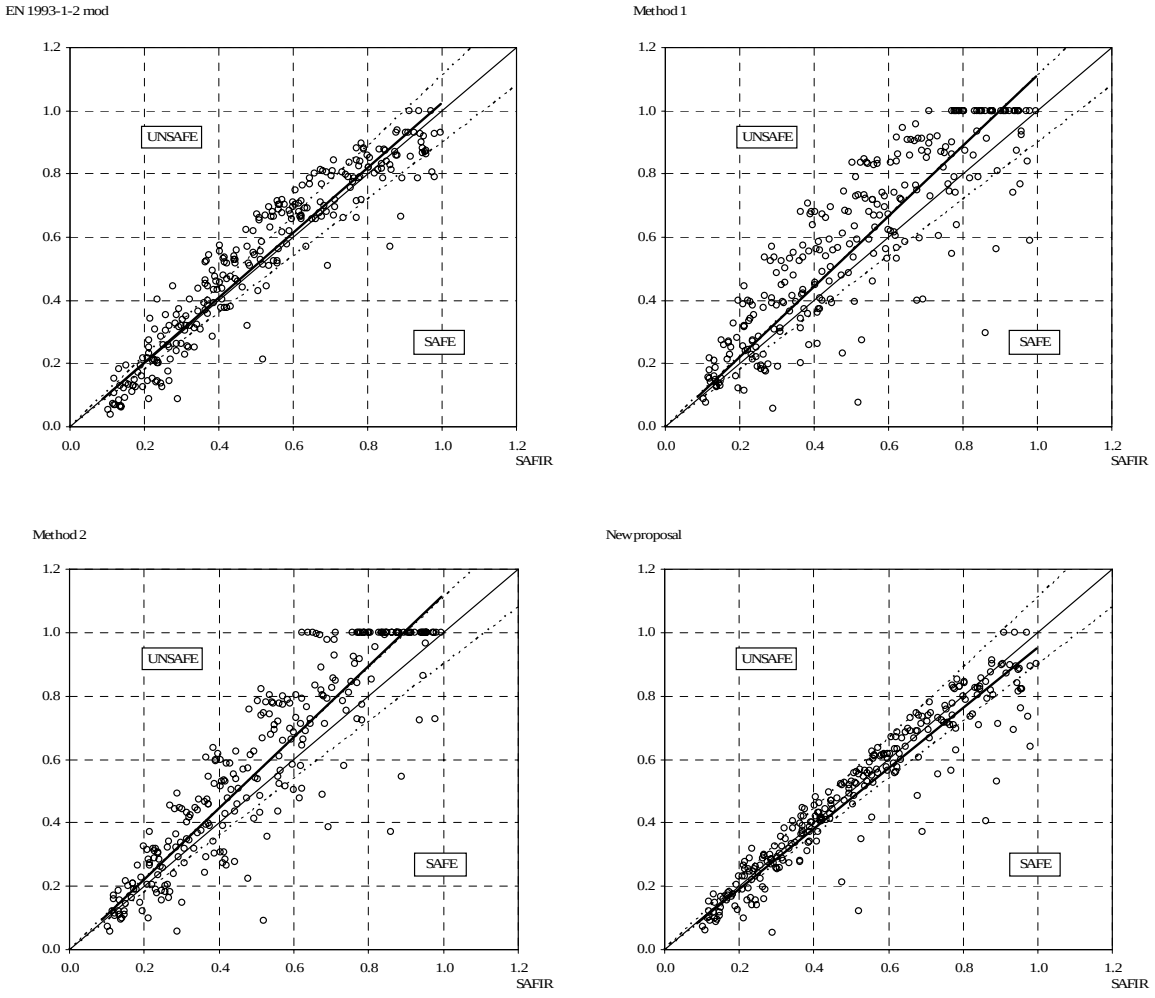

Figure 5.47 – Comparison between the proposals and the numerical results for the strong axis, at high temperatures.

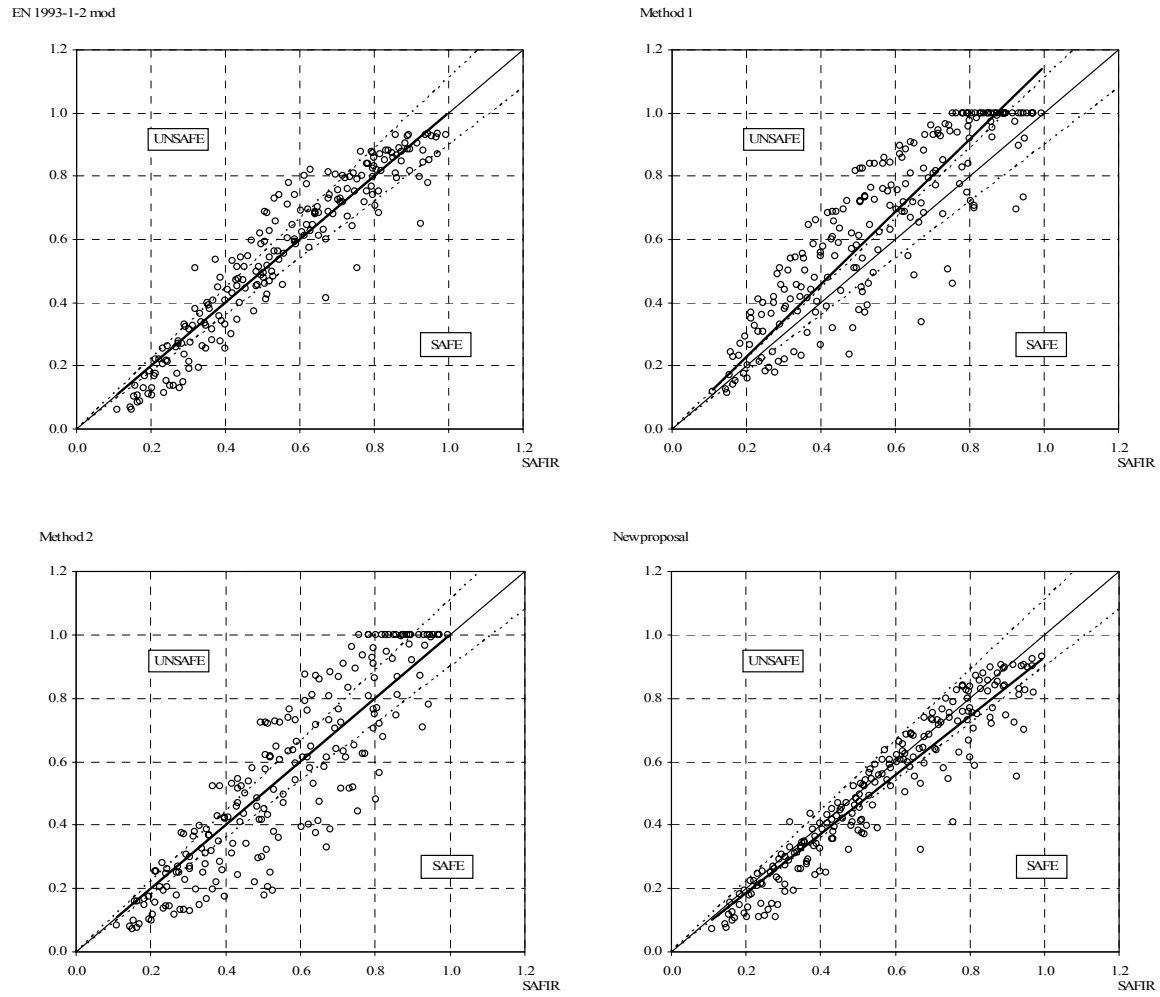

Figure 5.48 – Comparison between the proposals and the numerical results for the weak axis, at high temperatures.

Table 5.24 – Statistical results of austenitic and ferritic beam-columns without LTB at high temperatures.

		EN 1993-1-2 mod	Method 1	Method 2	New proposal
Strong axis	Average value	1.017	1.185	1.122	0.961
	Standard deviation	0.218	0.320	0.272	0.162
Weak axis	Average value	0.973	1.188	0.951	0.903
	Standard deviation	0.195	0.270	0.261	0.154

The 94 and 68 results, for respectively the strong and weak axis, obtained with the several proposals for the interaction curves (EC3, “Method 1”, “Method 2” and “New proposal”) for welded HEB200 sections at 600 ºC in stainless steel grades 1.4462, are shown in Figure 5.49 and Figure 5.50. In these comparisons, the new proposal for stainless steel columns was used.

Table 5.25 presents the average and standard deviation obtained with the different methods for determining the duplex stainless steel beam columns interaction curves at high temperatures.

It can be observed that, although having some few unsafe results, the new proposal presents the best agreement with the numerical results for all the stainless steel grades. Being clear the necessity of different interaction formulae for the 1.4462 stainless steel grade.

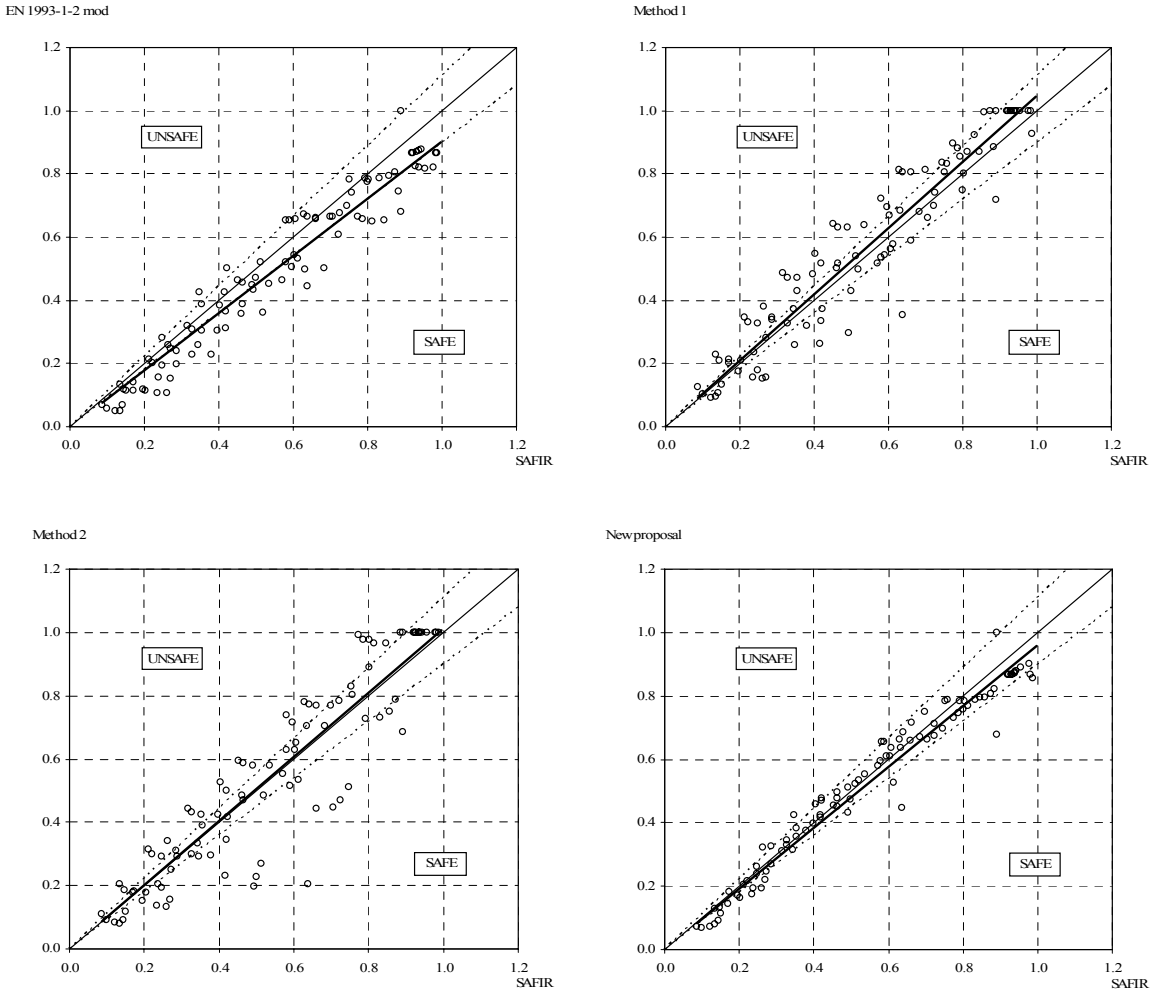

Figure 5.49 – Comparison between the proposals and the numerical results for the strong axis, at high temperatures, in duplex stainless steel.

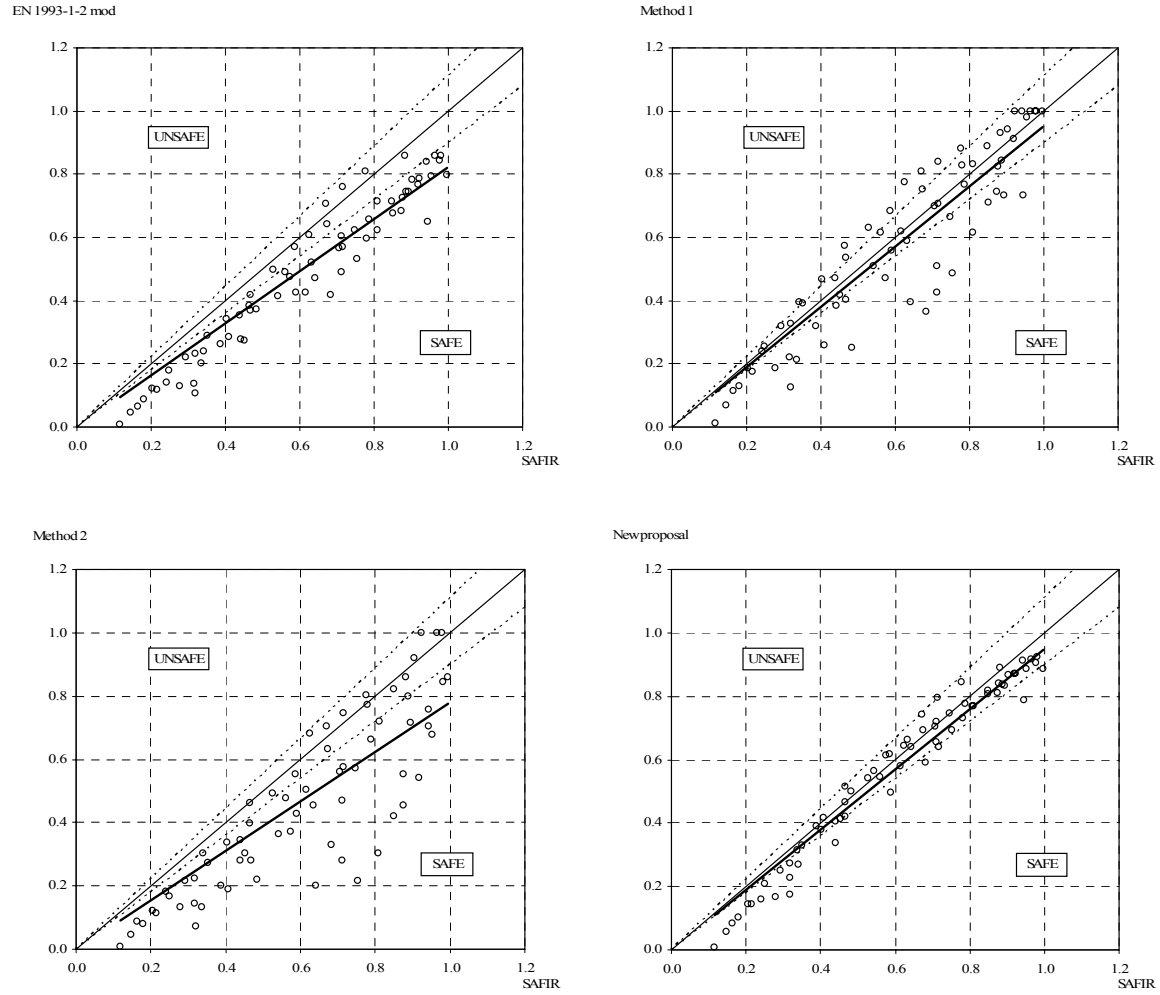

Figure 5.50 – Comparison between the proposals and the numerical results for the weak axis, at high temperatures, in duplex stainless steel.

Table 5.25 – Statistical results of duplex beam-columns without LTB at high temperatures.

		EN 1993-1-2 mod	Method 1	Method 2	New proposal
Strong axis	Average value	0.860	1.065	0.993	0.956
	Standard deviation	0.173	0.230	0.246	0.122
Weak axis	Average value	0.753	0.912	0.711	0.896
	Standard deviation	0.181	0.223	0.236	0.178

5.3.3.2 With lateral torsional buckling

In this section it is presented the study made on stainless steel beam-columns with LTB at elevated temperatures.

5.3.3.2.1 Case study

A simply supported column, subjected to axial compression plus bending in the strong axis with the possibility of occurring buckling in both strong and weak axis, was chosen for the parametric study. Initial imperfections and residual stresses were considered as described in section 3.3.1. The following welded cross-sections were used: HEA200, HEB280 and HEB200 stainless steel section at 600 ºC. The types of stainless steel grade used were: 1.4301, 1.4003 and 1.4462. Table 5.26 shows all the studied cases. An average of 5 lengths and 8 axial load ratios were analysed for each case.

Table 5.26 – Cases studied for beam-columns with LTB at high temperatures.

	Temperature of 600 ºC		
	$\psi = 1$	$\psi = 0$	$\psi = -1$
HEA200			
1.4301	✓	✓	✓
HEB280			
1.4301	✓	✓	✓
1.4003	✓	✓	✓
HEB200			
1.4462	✓	✓	✓

5.3.3.2.2 Formulation of a new proposal

It is proposed that the safety evaluation of elements subjected to bending and axial compression with LTB should satisfy:

$$\frac{N_{fi,Ed}}{\chi_{z,fi} A \frac{k_{y,\theta} f_y}{\gamma_{M,fi}}} + K_{LT,fi} \frac{M_{y,fi,Ed}}{\chi_{LT} W_{pl,y} \frac{k_{y,\theta} f_y}{\gamma_{M,fi}}} + K_{z,fi} \frac{M_{z,fi,Ed}}{W_{pl,z} \frac{k_{y,\theta} f_y}{\gamma_{M,fi}}} \leq 1 \qquad (5.63)$$

In these proposed interaction curves the interactions factors k_{LT} should be determined with

$$K_{LT,fi} = 1 - \frac{\mu_{LT,\theta} N_{fi,Ed}}{\chi_{z,fi} A k_{y,\theta} \frac{f_y}{\gamma_{M,fi}}} \quad \text{with} \quad K_{LT,fi} \leq 1 \qquad (5.64)$$

where

$$\mu_{LT,\theta} = \left(-0.14\beta_{M,LT} + 0.11\right)\overline{\lambda}_{z,\theta} + 0.50\beta_{M,LT} - 0.09 \leq 0.8 \qquad (5.65)$$

The evolution of μ_{LT}, as a function of $\overline{\lambda}_z$, is shown in Figure 5.51. Equation (5.65) was developed to be a good approximation to the trend line ("Linear (SAFIR)" in the graphics). In this case there was no need to differentiate the duplex 1.4462 stainless steel grade.

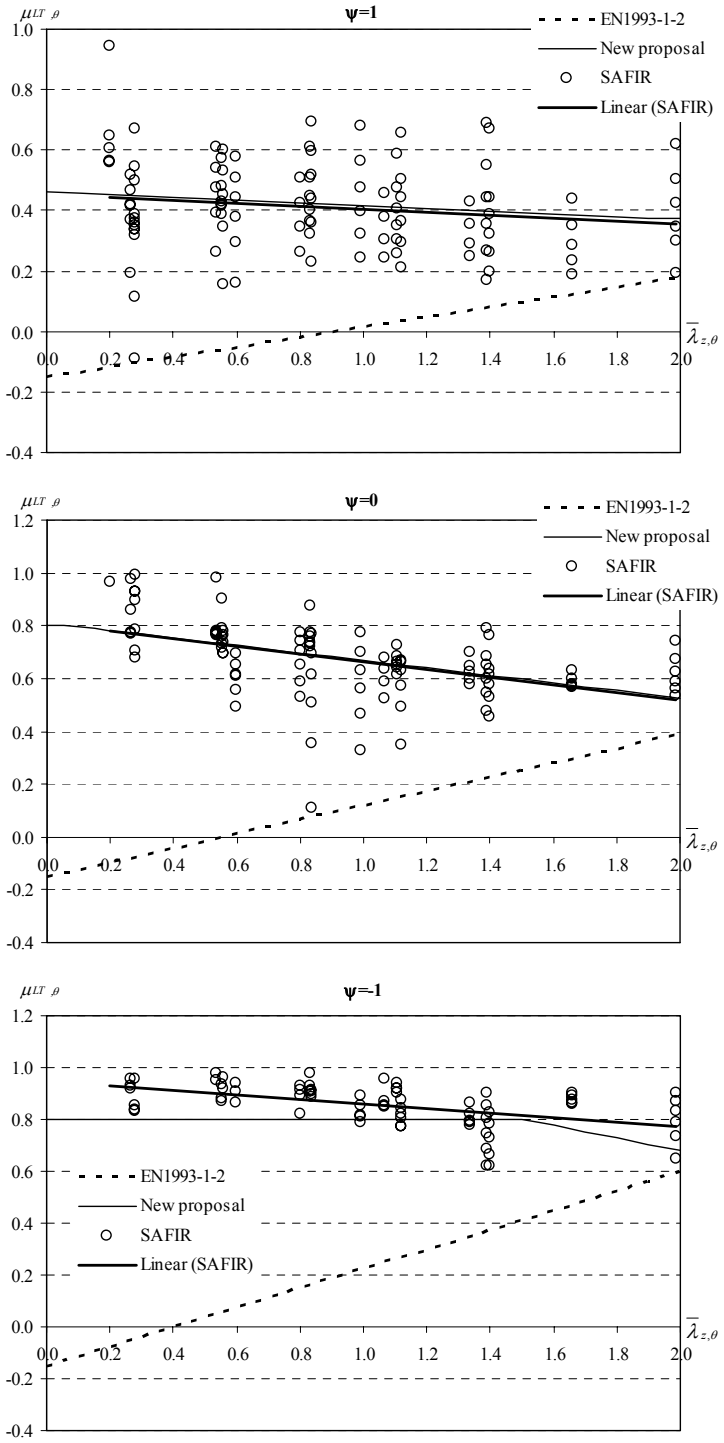

Figure 5.51 – Formulation of new interaction curves for the strong axis for beam-columns with LTB, at high temperatures.

5.3.3.2.3 Accuracy of the proposals

Again, a direct comparison with the numerical results and a statistical study are used to validate these new proposals on stainless steel beam-columns with LTB, at elevated temperatures.

Numerical validation

The graphics from Figure 5.52 were obtained for beam-columns with welded cross-sections equivalent to a HEA200 of the stainless steel grade 1.4301, with the possibility of occurring LTB, with bending in the strong axis. Regarding the bending moment variation along the member length, in these figures the results obtained for values, (-1, 0 and 1), of the ψ ratio are shown. Here, the length of 3 m corresponds to non-dimensional slenderness values of $\overline{\lambda}_{z,\theta} = 0.60$, while the length of 7 m corresponds to $\overline{\lambda}_{z,\theta} = 1.39$. The non-dimensional slenderness values for the LTB phenomena are given in Table 5.27. The other cross-section and length studied are included in Appendix M, providing a more complete evaluation of the different interaction curves performance.

Table 5.27 – Non-dimensional slenderness values for LTB of the cases presented at 600 ºC.

Moment diagram	$\overline{\lambda}_{LT,\theta}$ for $L = 3$ m	$\overline{\lambda}_{LT,\theta}$ for $L = 7$ m
$\psi = 1$	0.49	0.89
$\psi = 0$	0.37	0.67
$\psi = -1$	0.31	0.55

The interaction curves named “EN 1993-1-2 mod” in the graphics from Figure 5.22 are obtained from part 1-2 of EC3 with the new proposal for columns presented in section 5.3.1 and with the new proposal for LTB presented in section 5.3.2.

Again the method approximating better the numerical results is the method “New proposal”. The “Method 1” and “Method 2” also present good approximations. From these two methods, the one that has a better behaviour is the “Method 1”.

It can be also observed that the new proposals, for columns presented in section 5.3.1 and for LTB of beams included in section 5.3.2 of this thesis, introduce significant improvements in the interaction curves approximations to the numerical results.

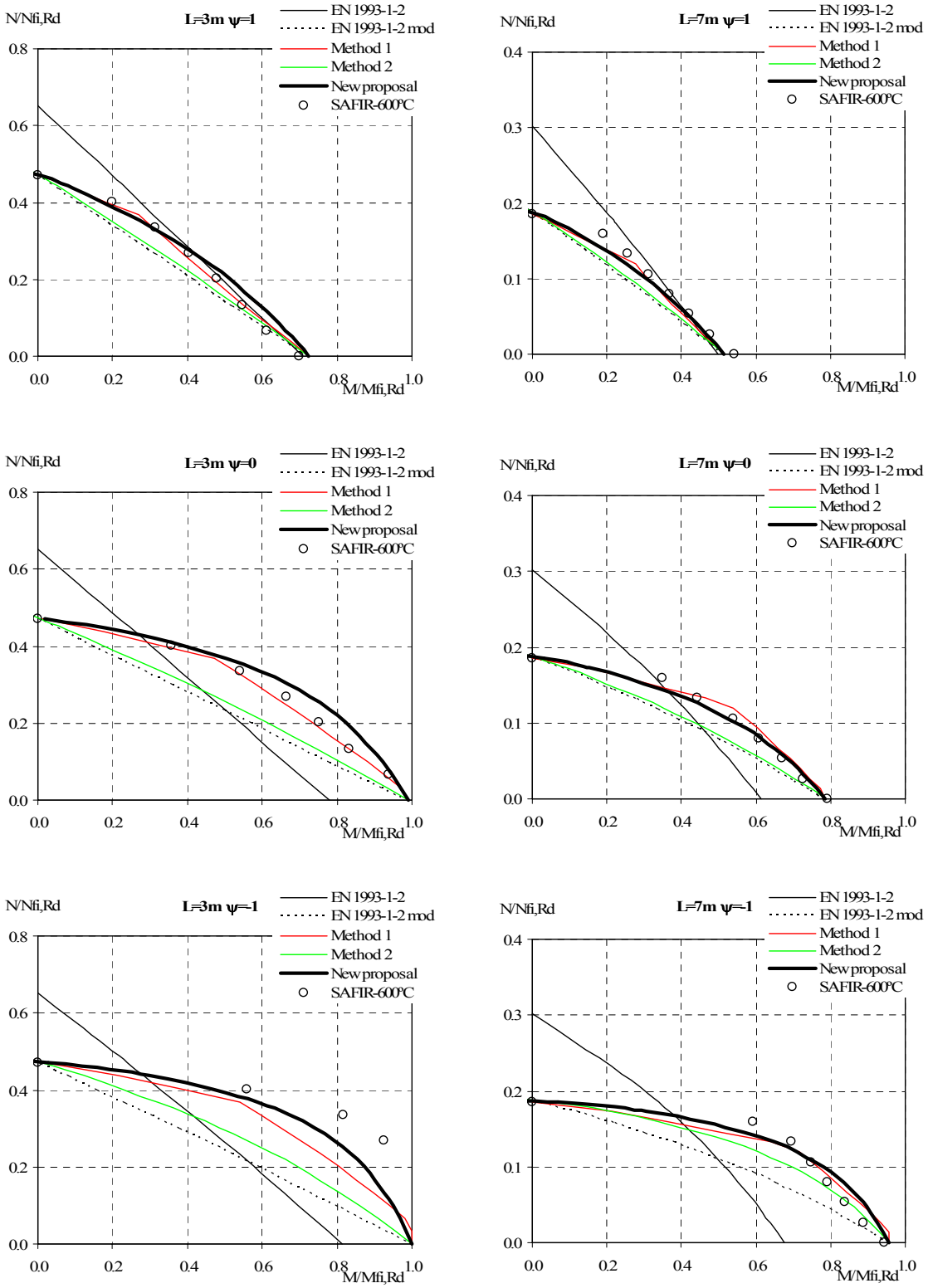

Figure 5.52 – Comparison between different interaction curves for welded HEA200 beam-columns of the stainless steel grade 1.4301, for beam-columns with LTB, at high temperatures.

Statistical evaluation

The 320 results, obtained with the several proposals for the interaction curves (EC3, "Method 1", "Method 2" and "New proposal") for welded HEA200, HEB280 and HEB200 sections at 600 ºC, in stainless steel grades 1.4301, 1.4003 and 1.4462, are shown in Figure 5.53. In these comparisons, the new proposals for stainless steel columns and for stainless steel beams were used.

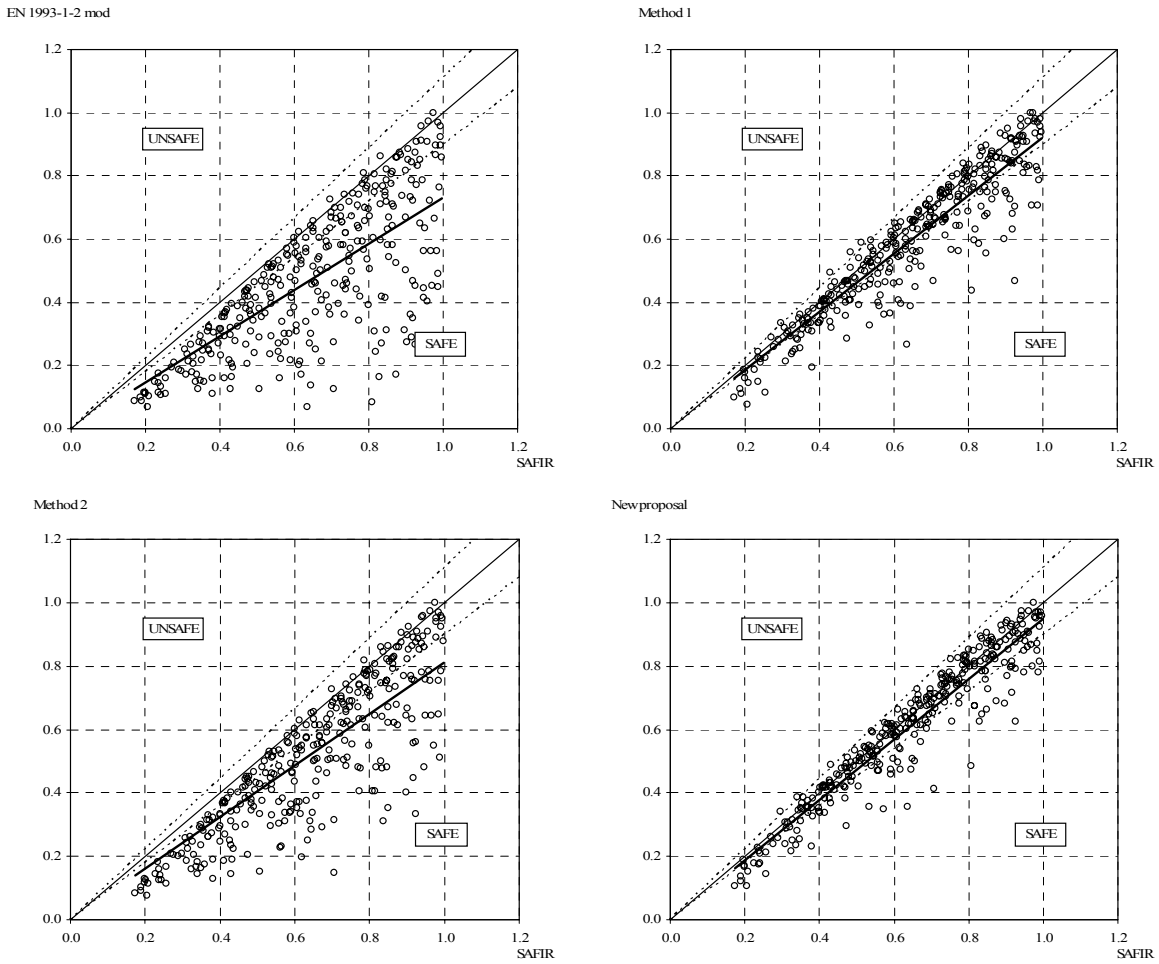

Figure 5.53 – Comparison between the proposals and the numerical results with LTB, at high temperatures.

Table 5.28 presents the average and standard deviation obtained with the different methods for determining the stainless steel beam columns interaction curves at high temperatures with LTB. It can be observed that the new proposal presents the best agreement with the numerical results, providing at the same time safety.

Table 5.28 – Statistical results of beam-columns with LTB at high temperatures.

	EN 1993-1-2 mod	Method 1	Method 2	New proposal
Average value	0.714	0.911	0.780	0.942
Standard deviation	0.215	0.128	0.181	0.109

5.4 Conclusions

In this chapter new approaches for evaluating the safety of stainless steel structural elements subjected to axial compression and/or bending were presented. These approaches addressed the influence of global buckling phenomena (flexural buckling and LTB).

The studies on the flexural buckling of stainless steel columns resulted in the proposal of safer buckling curves, at room temperature and in case of fire. Also, it is shown that the flexural buckling curves at high temperatures should vary with the buckling axis, as it is made at room temperature, according to part 1-4 of EC3 (CEN, 2006a).

The beneficial influence of non-uniform bending moment distributions, resulting from the reduced plastic zones connected with variable bending along the beam, is taken into account in the presented proposals for both cold and fire design of stainless steel elements with LTB.

The studies in stainless steel beam-columns concluded that, in order to use the new carbon steel interaction curves to stainless steel and fire, additional modifications to them are necessary. As a consequence, new interaction curves for the design of stainless steel beam-columns with and without LTB, at room temperature and at high temperatures, were here proposed, providing safe and economic approximations to the obtained numerical results.

The presented studies were made in different stainless steel grades. Due to the fact that they have different stress-strain relationships at high temperatures, it was necessary to account for this influence, mainly in the ferritic and duplex grades.

The partial safety factor used in this work, to develop the several design proposals, was 1.0. However, the safety factor value, to be used with the here presented proposals, should result from more detailed statistical works as Rebelo *et al*. (2009) made for carbon steel beams at room temperature.

Chapter 6

Thin-walled stainless steel structural elements in case of fire

Chapter 6. Thin-walled stainless steel structural elements in case of fire

Chapter 6. Thin-walled stainless steel structural elements in case of fire

6.1 Introduction

In Chapter 4 and Chapter 5 the safety evaluation of Classes 1 and 2 stainless steel members (CEN, 2006a) was analysed. Regarding Class 3 cross-sections, it is not presented in this thesis any research. Following the EC3 (CEN, 2005a; 2005b; 2006a) design prescriptions, the structural evaluation of Class 3 structural elements is performed with the same formulae developed and recommended for Class 1 and 2 elements, but using the elastic section modulus instead of the plastic section modulus when bending is presented. In this Chapter it is presented a study on Class 4 stainless steel members.

Stainless steel members with thin-walled cross-sections are commonly used in buildings due to its lightness and long span capacity. In this sense, a brief introduction to local buckling in case of fire will be made in this chapter.

Numerical tests using the program SAFIR (Franssen, 2005a), on thin-walled elements made in stainless steel and subjected to fire, are presented. Local and global geometrical imperfections were considered in the simulations.

The objective of the study presented in this chapter is to evaluate the influence of the residual stresses on the ultimate load-carrying capacity of thin-walled stainless steel structural elements in case of fire. The cases studies in this work were chosen for being representative of thin-walled steel element's construction and to induce failure by local instability phenomena.

6.2 Thin-walled sections

This section presents a short Literature review on the subject of thin-walled section in case of fire.

6.2.1 Plate buckling

The general expression for the critical buckling stress of thin plates is given by

$$\sigma_{cr} = k_{\sigma} \frac{\pi^2 E}{12\left(1-\upsilon^2\right)\left(\frac{b}{t}\right)^2} \tag{6.1}$$

being the buckling coefficient k_{σ} dependent on the type of stress distribution and on the ratio between the length and the width of the plate. The relation b/t corresponds to the slenderness ratio of the plate (Allen and Bulson, 1980; Simões da Silva and Gervásio, 2007; Reis and Camotim, 2000).

In thin plates the appearance of local buckling leads to a loss of stiffness and stress redistribution. A plate subjected to uniform longitudinal compression in its two opposite edges will have a non-uniform stress distribution after buckling (see Figure 6.1). Also, the buckled plate will obtain almost all of its stiffness from the longitudinal edge supports (Galambos, 1988).

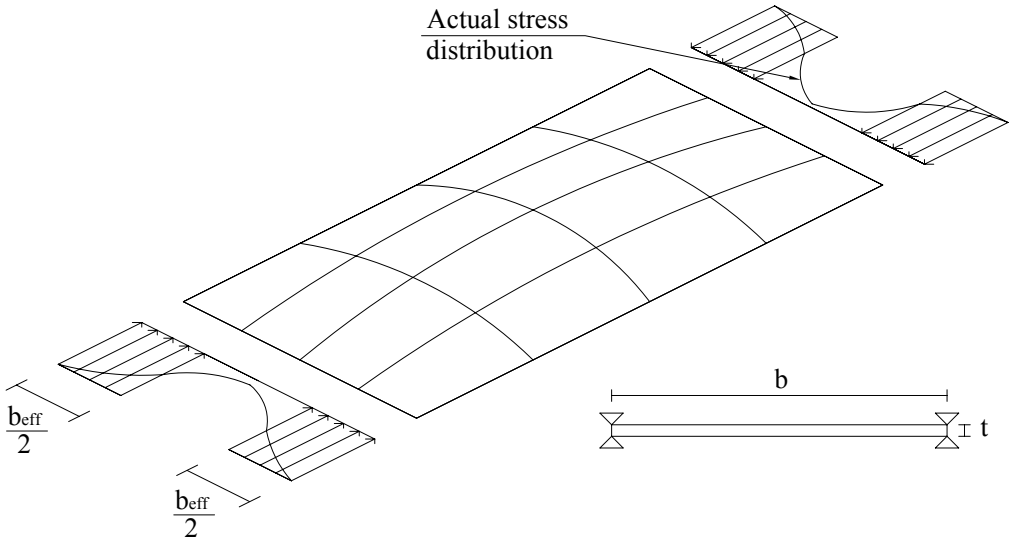

Figure 6.1 – Nonlinear stress distribution of a buckled plate.

Due to the existence of post-buckling capacity in compressed plates, to approximate the actual stress distribution of a buckled plate, a linear stress distribution, assuming that there

is a region where no stresses are transmitted, is typically used (von Karman *et al.*, 1932). Thus, a reduced effective width (b_{eff}) for the new stress distribution is used.

This definition, of effective width, can be used in sections composed of compressed thin (slender) plates.

Compression stress states can be derived in structural elements subjected to axial compression or even to bending.

When those sections are composed of thin plate elements, the local plate buckling often occurs before the overall capacity of the cross-section is reached.

With the different effective widths, it is possible to determine effective sections geometrical properties (effective area, effective bending modulus, etc) in function of the acting forces.

Figure 6.2 and Figure 6.3 show the actual stress distribution and the simplified stress distribution for a SHS axially compressed and a I-welded sections subjected to bending (Elmahdy and Abu-Hamd, 2008), which induce compression in the outstand flanges and webs.

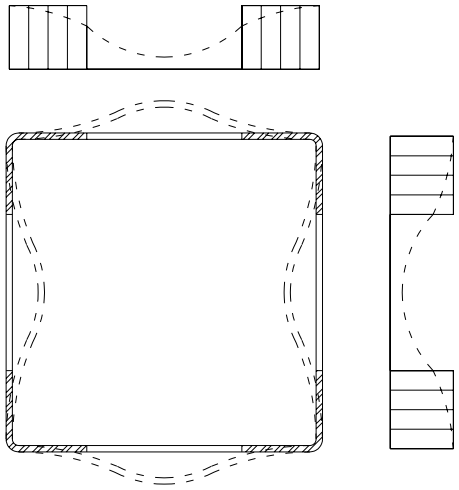

Figure 6.2 – Class 4 SHS buckled when subjected to axial compression.

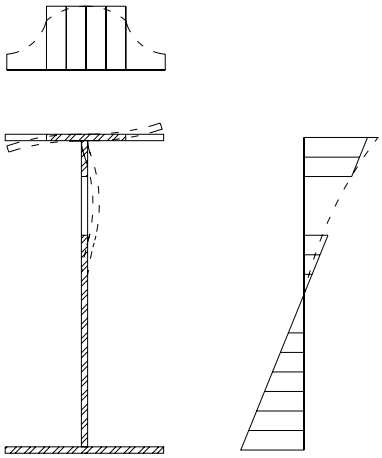

Figure 6.3 – Class 4 I-sections buckled when subjected to bending.

When the plate instability needs to be addressed, the EC3 (CEN, 2005a; 2006a) classifies the cross-sections as Class 4, in which local buckling will occur before the yield stress is achieved in one or more parts of the cross-section

6.2.2 Thin-walled sections in case of fire

Some research works have been made in the scope of the study of steel thin-walled sections in case of fire.

Addressing the study of cold-formed thin-walled carbon steel structures (Feng *et al.*, 2002a; 2002b; Wang and Davies, 2000) made experimental and numerical tests to cold-formed steel elements subjected to high temperatures. Based on these results new design proposals were presented, modifying the prescribed design rules to include distortional buckling, effects of service holes and elevated temperatures.

Studies about local buckling under fire conditions from (Knobloch and Fontana, 2004; 2006) resulted in the proposal of a strain-based approach which uses effective widths for stiffened and unstiffened elements at elevated temperatures. The performance of the proposed design approach was accessed with results produced recurring to finite element approach. This proposal avoid the use of section classes for fire design and take into account plastification effects, plastic stress distribution and strain-dependent non-linear material behaviour of steel at high temperatures.

In the study presented in this thesis, will be only used the EC3 design guidelines. Part 1-2 of EC3 (CEN, 2005b) gives simple calculation rules for assessing the fire resistance of steel members with thin-walled Class 4 cross-sections.

Single structural members, exposed to fire, with Class 4 cross-sections can be subjected to different loading and buckling modes: buckling under compression; simple bending; LTB under bending; and combined bending and compression.

The use of shell finite elements, instead of the beam finite elements, to consider the local buckling of thin walls in members with Class 4 cross-sections is still inevitable, due to the fact that it is one of the dominant failure modes. EC3 permits the use of advanced calculation models for the fire resistance evaluation in Class 4 sections, provided all stability effects are taken into account.

For design simplifications purposes EC3 (CEN, 2005b) states that members with Class 4 cross-sections may be designed assuming a constant value for the critical temperature (the recommend value is 350 ºC).

The use of simple calculation models to determine the fire resistance of Class 4 sections is also permitted (CEN, 2005b). This can be made using the design approaches prescribed for members subjected to compression, bending, and bending and axial compression, with Class 1 and 2 sections (presented in chapter 4 of this thesis), replacing the area and the section modulus by the effective area and the effective section modulus respectively. The effective cross-section area and the effective section modulus should be determined in accordance with part 1-3 (CEN, 2004b) and part 1-5 (CEN, 2006c) of EC3, based on the material properties at 20 ºC. Moreover, the design yield strength should be taken as the 0.2 % proof strength, instead of the stress at 2 % total strain as for Class 1, 2 and 3.

6.3 Residual stresses in stainless steel elements with thin-walled sections

This section presents a study on the influence of the residual stresses in the fire resistance of thin-walled sections. This study was performed on axially loaded square hollow sections and on welded I-sections in bending.

6.3.1 Axially loaded square hollow sections

In order to study the influence of the residual stresses in axially loaded thin-walled members, a numerical study with two square hollow Class 4 sections is presented in this section. In this study, the magnitude of the imperfections was chosen to be $b/200$ for the local imperfections (CEN, 2006c) and $L/1000$ for the global imperfections (CEN, 2005c; Gardner and Nethercot, 2004). These are typical values used in the study of thin-walled structural elements (Uppfeldt *et al.*, 2008), as prescribed in part 1-5 of EC3.

Numerical results obtained for columns with the square hollow sections SHS150x150x3 and SHS200x200x5 of the stainless steel grade 1.4301 are presented. The yield strength and the ultimate strength considered were 210 MPa and 520 MPa respectively. The comparisons were made with uniform temperature of 600 ºC in the cross-section. The tested columns had lengths of 0.9 m with fixed ends and were subjected to centric axial compression (Figure 6.4). This length was chosen so that the failure would be by local buckling instead of global buckling. In these numerical tests the curvature of the corners was considered.

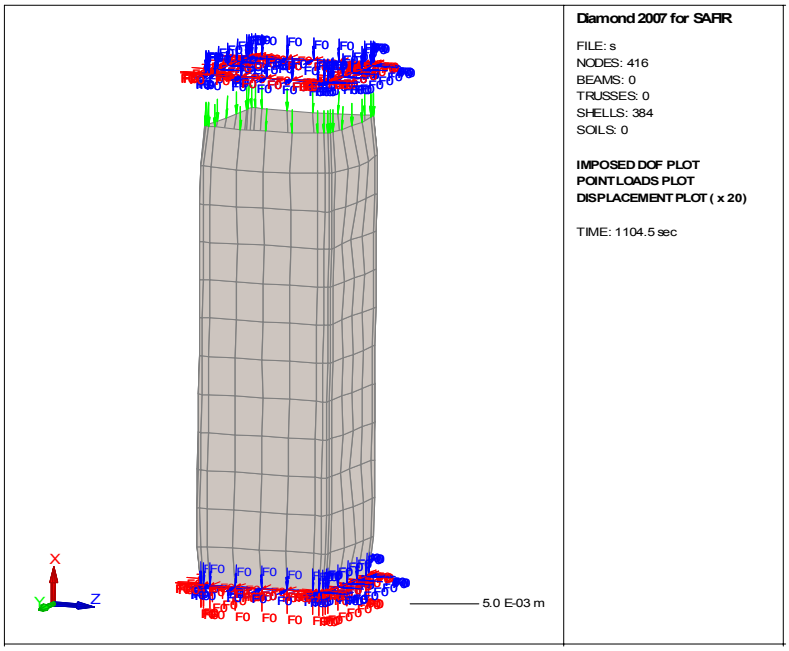

Figure 6.4 – Used mesh in a column with a thin-walled stainless steel hollow section.

After sensitivity tests without imperfections, the mesh size chosen for this study was the one present in Figure 6.4. Figure 6.5 shows a more refined mesh used in those tests. For this case the difference between the chosen mesh and the one present in Figure 6.4 was lower than 4 %, on the safe side for the chosen mesh.

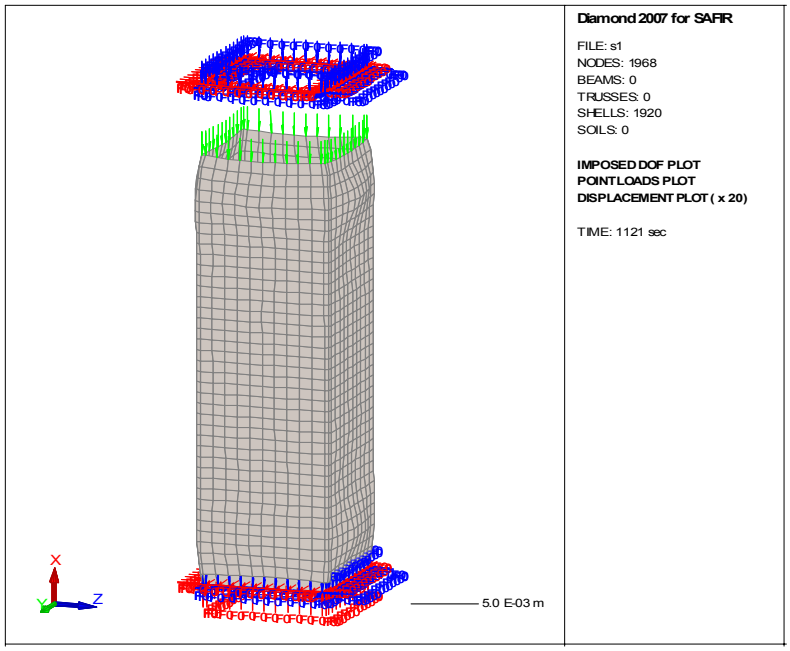

Figure 6.5 – Refined mesh in a column with a thin-walled stainless steel hollow section.

For the tested columns without residual stresses the following possibilities were considered:

a) no geometric imperfections and no higher corners yield strength derived from cold working;

b) no geometric imperfections but introducing higher corners yield strength according to Ashraf *et al*. (2005);

c) global imperfections given by expression (6.2) and introducing higher corners yield strength;

$$y(x) = \frac{L}{1000}\sin\left(\frac{\pi x}{L}\right) \tag{6.2}$$

d) local imperfections with a maximum value of b/200 (CEN, 2006c) and introducing higher corners yield strength;

e) global imperfections given by expression (6.2), local imperfections with a maximum value of b/200 and introducing higher corners yield strength.

Table 6.1 shows the corresponding numerical results of these five analysed cases.

Table 6.1 –Ultimate axial compression force without residual stresses.

Case	SHS150x150x3	SHS200x200x5
a)	160.5 kN	423.8 kN
b)	175.5 kN	473.6 kN
c)	174.5 kN	465.6 kN
d)	149.5 kN	387.9 kN
e)	149.5 kN	387.9 kN

Figure 6.6 shows the obtained deformed shape of the stainless steel hollow section SHS200x200x5 with local imperfections at 600 ºC immediately before failure.

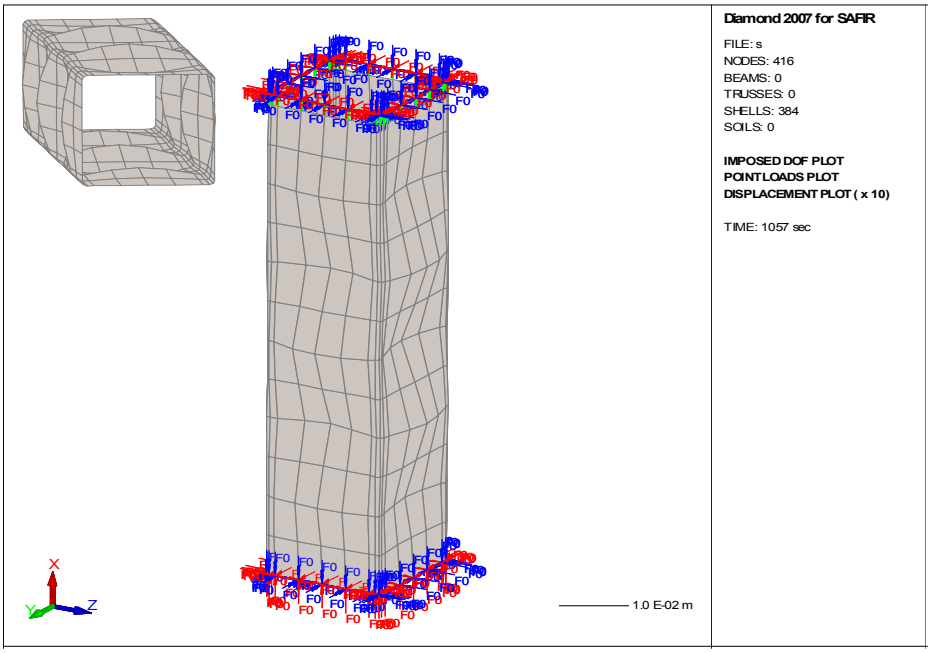

Figure 6.6 – Deformed shape of a column with a thin-walled stainless steel hollow section with local imperfections.

Table 6.1 shows that no global imperfections need to be considered when local buckling is the main failure mode. Therefore, in the results shown in Table 6.2 the residual stresses were introduced only in the case d).

For the square hollow section, the residual stresses distribution shown in Figure 3.19, which has the maximum value of half of f_y (ECCS, 1984), was used. Other residual stresses distribution very recently proposed for stainless steel hollow sections (Cruise, 2007; Cruise and Gardner, 2008) were not considered in this study.

Figure 6.7 shows the normal force field corresponding to this equilibrated stresses state before any external loading is applied and the corresponding principal stress directions.

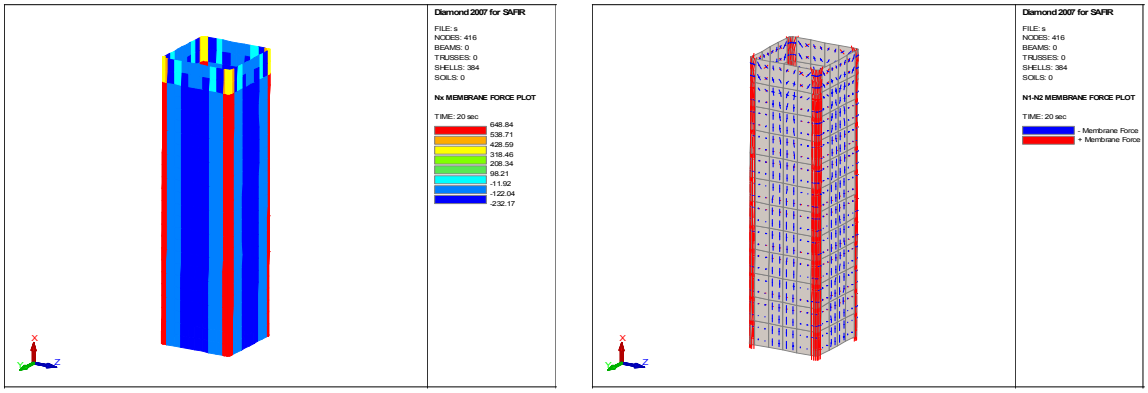

a) Normal force field. b) Principal stress directions.

Figure 6.7 – Residual stresses in the square hollow member.

Table 6.2 shows the obtained results for columns with local imperfections, with and without residual stresses.

Table 6.2 – Ultimate axial compression force with local imperfections

	SHS150x150x3	SHS200x200x5
Without residual stresses	149.5 kN	387.9 kN
With residual stresses	139.5 kN	376.5 kN
With/Without residual stresses	0.93	0.97
EN 1993-1-2	136.9 kN	356.8 kN

From these results it can be concluded that the influence of the residual stresses is small. However, this influence is of the same magnitude of the one observed in section 3.3.2.3 for a Class 1 section. The results from EC3 are in good agreement with the numerical results.

Figure 6.8 shows a comparison between the column with and without residual stresses of the longitudinal displacements in the column's free extremity in function of the imposed axial force. From this figure an expected loss of stiffness and strength in the column with the residual stresses is observed.

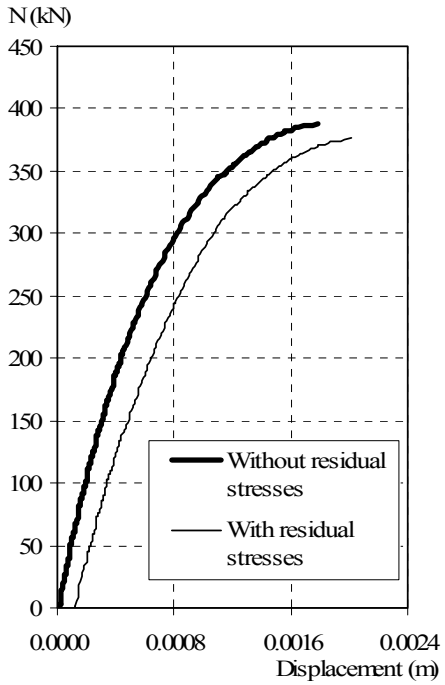

Figure 6.8 – Axial force in function of the longitudinal displacement in the column's free extremity.

6.3.2 Welded I-sections in bending

In order to achieve a shape for the local imperfections a modal analysis with the program CUFSM, considering elastic stresses diagram correspondent to bending, was made. This program was developed by Schafer (1997) to determine the elastic buckling and corresponding modes of simply supported thin-walled structural elements. This elastic analysis was performed considering that a non-linear material modal analysis does not significantly change the first buckling mode shape, as observed in compressed stainless steel C-sections (Camotim and Gonçalves, 2003).

The program CUFSM uses the finite strip method (Cheung, 1976). When a cross-section is defined with a stress condition, the program makes the analysis of different lengths for the section. The stress and the shape of each buckling mode are recorded for each of the lengths (Sarawit *et al.*, 2003).

Figure 6.9 shows the first buckling mode of the studied I-cross-section. This first buckling mode shape was used for the shape of the initial local imperfections, with the maximum of b/200 (being b the height of the web).

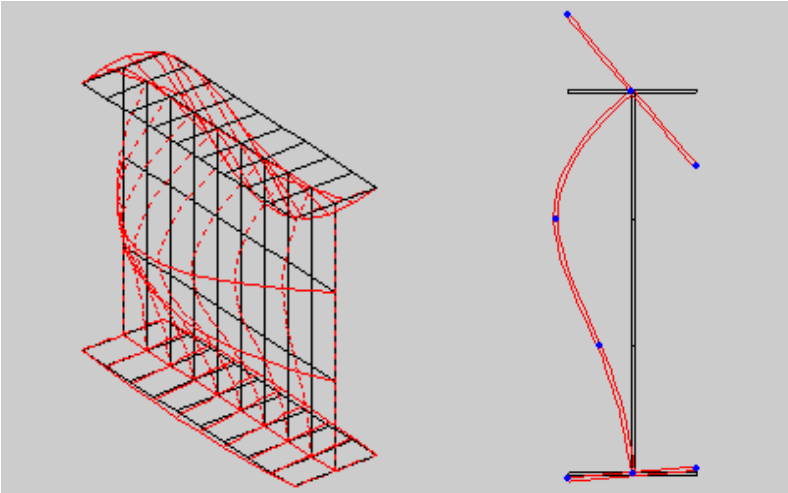

Figure 6.9 – First buckling mode obtained with the program CUFSM (Schafer, 1997).

Numerical results obtained for beams with the welded I-sections 900x300x9 (height x base x thickness) and 800x250x8 of the stainless steel grade 1.4301 are shown. The yield strength and the ultimate strength considered were 210 MPa and 520 MPa respectively. The comparisons were made with uniform temperature of 600 ºC in the cross-section for simply supported beams with 2.0 m of length, fork supports and submitted to uniform bending. Figure 6.10 shows the deformed shape immediately before the failure. The adopted length was chosen so that the failure would be by local buckling instead of global buckling.

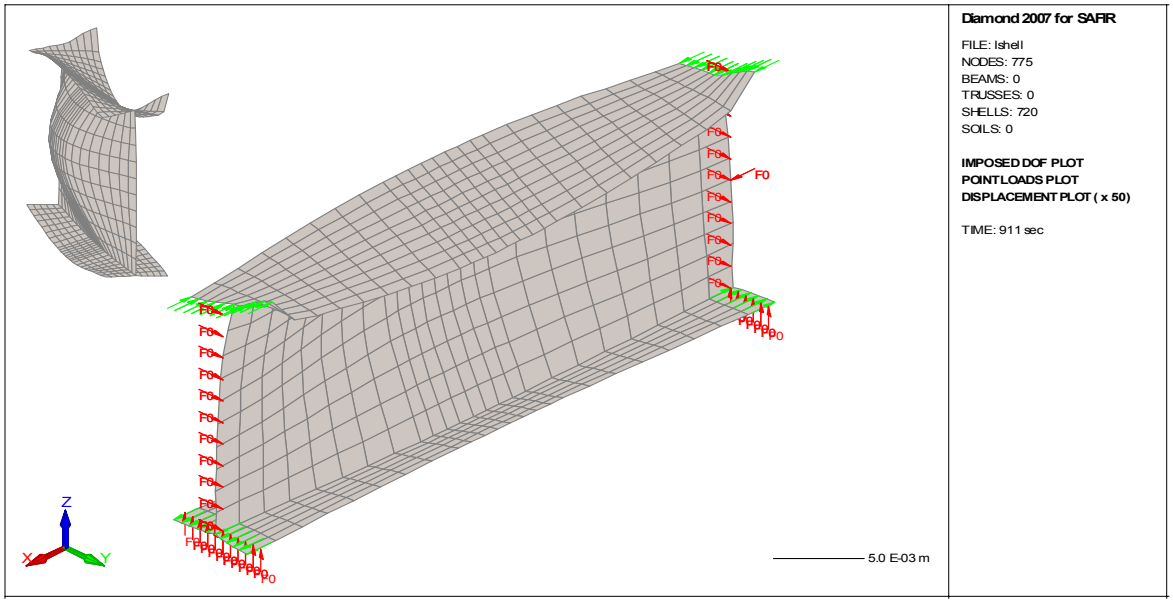

Figure 6.10 – Deformed shape of a stainless steel beam analysed with shell elements.

For the tested beams without residual stresses the following possibilities were considered:

a) no geometric imperfections;

b) only global imperfections given by expression (6.2);

c) only local imperfections with a maximum value of b/200;

d) global imperfections given by expression (6.2) and local imperfections with a maximum value of b/200.

Table 6.3 – Ultimate bending moment without residual stresses

Case	I 900x300x9	I 800x250x8
a)	251 kNm	169 kNm
b)	249 kNm	167 kNm
c)	227 kNm	156 kNm
d)	226 kNm	156 kNm

From Table 6.3 it can be concluded that no global imperfections are required to be considered in this case, due to the fact that the failure occurs by local buckling. Case c) was also simulated in the commercial programme ANSYS, which gave a result of 222.2 kNm, value very close to the SAFIR result.

The pattern of residual stresses distribution shown in Figure 3.14 (Chen and Lui, 1991) was used. Only residual stresses with the direction of the longitudinal axis of the beam were considered ($\sigma_{x,res}$). Prior to the application of external loading, a preliminary load step to allow equilibration of the residual stresses was made.

The normal force field and the corresponding principal stress directions, corresponding to an equilibrated stresses state before any external loading is applied, are presented in Figure 6.11. After equilibrium, the values and directions of the residual stresses remain similar to the introduced ones, in the middle of the beam. However, in the extremities they are rearranged in different directions and values.

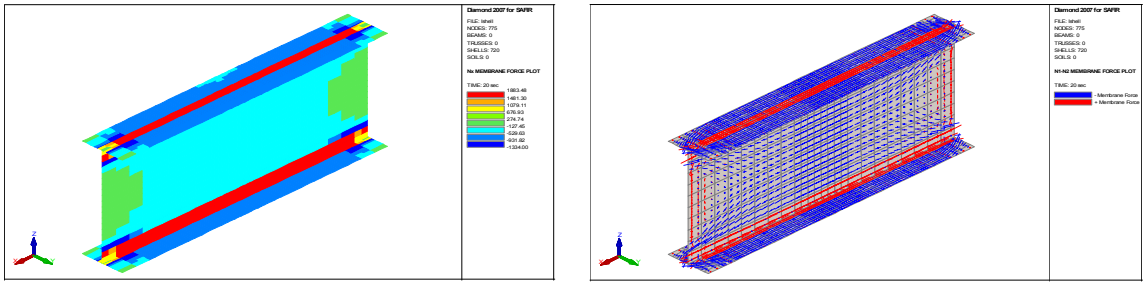

a) Normal force field. b) Principal stress directions.

Figure 6.11 – Residual stresses in the welded I-member.

Table 6.4 and Table 6.5 show the obtained results for the beams with global imperfections and with local imperfections respectively, considering or not residual stresses.

Table 6.4 – Ultimate bending moment with only global imperfections

	I 900x300x9	I 800x250x8
Without residual stresses	249 kNm	167 kNm
With residual stresses	244 kNm	165 kNm
With/Without residual stresses	0.98	0.99
EN 1993-1-2	255 kNm	165 kNm

Table 6.5 – Ultimate bending moment with only local imperfections

	I 900x300x9	I 800x250x8
Without residual stresses	227 kNm	156 kNm
With residual stresses	230 kNm	158 kNm
With/Without residual stresses	1.01	1.01
EN 1993-1-2	255 kNm	165 kNm

Contrary to what was expected, the residual stresses introduction provides a beneficial effect on the ultimate loading capacity. The same conclusions were observed in (Jandera *et al.*, 2008).

From these results it can be concluded that there is very little influence of the residual stresses in the studied bended thin-walled structural elements. From the comparison made with EC3 it can be concluded that it does not give safe approximations to the numerical results.

6.4 Conclusions

It was shown that the influence of the residual stresses on the ultimate load carrying capacities of stainless steel Class 4 sections is rather small. However, this influence, for the studied axially loaded columns, is of the same magnitude of the one observed for a Class 1 section. This suggests that the residual stresses must be considered for the evaluation of the load bearing capacity of columns subjected to fire. In beams the influence of the residual stresses can be neglected.

It has also been shown that the results from the EC3 are not on the safe side for the Class 4 beams studied. It is worth noting that more numerical and experimental tests should be performed in order to confirm the unsafe nature of the EC3 results and see whether new formulae should be proposed for Class 4 elements.

Chapter 7

Global behaviour of stainless steel structures in case of fire

Chapter 7. Global behaviour of stainless steel structures in case of fire

Chapter 7. Global behaviour of stainless steel structures in case of fire

7.1 Introduction

After the research works, presented in the previous chapters (Chapter 4, Chapter 5 and Chapter 6), on stainless steel members, this chapter deals with the global behaviour of complete structures in case of fire.

The here presented study intends to follow the thesis main motivation, on characterise stainless steel as a structural material when subjected to elevated temperatures. Chapter 2 led to assume a better structural behaviour of stainless steel when compared to carbon steel. This assumption is evaluated on this chapter.

The use of global structural analysis in modelling fire safety engineering has been increasing, which has led to the incorporation in the Eurocodes of rules for the application of this type of analysis.

Normally, the use of this approach in structural analysis requires the use of advanced calculation models. These advanced numerical models have provided good results when compared with experimental results. In this numerical modelling, the material models, representative of the real material behaviour at elevated temperatures, are of great importance. The introduction of stainless steel mechanical and thermal properties, in programs dedicated to fire safety engineering (as described in Chapter 3 for SAFIR), enables the use of these advanced calculation models on stainless steel structures.

In this chapter, the fire performance of two alternative structural solutions is compared, one in conventional carbon steel and another in stainless steel, using SAFIR. These two types of steel have different constitutive laws (as shown in Chapter 2) and, as expected, different structural behaviours were observed in this comparison. A better fire resistance performance is provided by the stainless steel structure.

Carbon steel S235 was chosen due to its yield strength value, similar to the nominal stress (0.2 % proof stress) of the stainless steel 1.4301. For design purposes according to the EC3, these are the values used to check the resistance of structural elements.

This study uses 2D structural models due to the fact that the results are supposed to be equally representative, when compared to a more complex 3D analysis, in respect to the material influence.

From the economic point of view it would be unlikely that stainless steel would be chosen in preference to carbon steel solely because of its superior fire resistance. However, for designers considering stainless steel because of its aesthetic and durability properties, the additional benefits that stainless steel can provide fire resistance for a significant period whilst unprotected, might sway the balance in favour of stainless steel. In applications where good corrosion resistance coupled with good fire resistance is required, stainless steel offers an excellent solution.

The biggest advantage of stainless steel is its higher corrosion resistance. However, its aesthetic appearance, easy maintenance, high durability and reduced life cycle costs are also important properties. The question of knowing if stainless steel structural elements can be used in buildings without any fire protection is very important, mainly because the use of stainless steel in structures is usually due to aesthetic considerations. Eliminating the fire protection in structures will result in reduced construction costs, lower construction periods, more efficient use of interior spaces, healthier work environment and a better aesthetic appearance of the building. Moreover, the life cycle costs of unprotected stainless steel structures are smaller than protected carbon steel structures.

7.2 Actions in structures subjected to fire

This section presents the actions and the corresponding combinations required in a fire situation design. These actions, imposed in the structures, are mechanical (the same used in cold design situations) and thermal (fire scenarios).

7.2.1 Mechanical actions

The design value of the actions effects in case of fire should be obtained using the following accidental combination as defined in the EN 1990 (CEN, 2006d):

$$\sum \gamma_{GA} G_k + \psi_{1,1} \cdot Q_{k,1} + \sum \psi_{2,i} \cdot Q_{k,i} + \sum A_d(t) \tag{7.1}$$

where γ_{GA} is the partial safety factor of the permanent actions in case of accident, which should take the unit value; G_k is the characteristic value of the permanent actions; $Q_{k,1}$ is the characteristic value of the main or dominant variable action; $\psi_{1,1}$ is the combination coefficient associated to the main or dominant variable action; $\psi_{2,i}$ is the combination coefficient associated to the remaining variable actions; and $A_d(t)$ is the calculation value of the action resulting from the fire exposition which is represented by the temperature effect in the material properties and from the indirect fire actions that results from the forces due to the restraints to thermal elongation.

7.2.2 Thermal actions

Part 1-2 of Eurocode 1 (CEN, 2006e) provides different possible representations for the thermal action on structures due to fire. It gives temperature-time relationships, zone models and localised fire models. The Eurocode also gives, within the temperature-time relationships, three types of nominal curves: the standard curve, the external fire curve, the hydrocarbon curve and parametric fire curves (Franssen and Zaharia, 2005b; Santiago, 2008).

Due to the fact that the purpose of this study was to evaluate only the structures' mechanical response, the standard fire curve ISO834 was used, which has the following analytical expression:

$$\theta_g = 20 + 345 \log_{10}(8t + 1) \tag{7.2}$$

where θ_g is the gas temperature in the room subjected to fire in °C and t is the time in minutes. The graphical illustration of the fire curve is presented, together with the temperature evolution in the steel, in the following sections.

7.3 Application examples

A truss structure and a portal frame were used in the study presented in this section. Both these cases were studied with carbon steel S235 and stainless steel 1.4301. Here, the obtained results for the two different materials are compared. The used stress-strain relationships of the corresponding materials at high temperatures are the ones prescribed in Eurocodes (see Chapter2). Also, no residual stresses are considered.

These application examples were chosen to better quantify the different fire resistance of these two materials on structures. Practical application problems, regarding the structures implementation, were not here analysed.

7.3.1 A sport hall truss structure

The truss structure chosen was part of a sport hall and had a length of 38 m and a height of 2.5 m. The analysed truss is the one subjected to the highest forces (see Figure 7.1), with the actions combination referred in section 7.2.1. It was considered that all the structure was subjected to the fire curve ISO834.

In the structural analysis, the two used materials were the carbon steel S235 and the stainless steel 1.4301 with a yield strength of 210 MPa (similar to the yield stress of the chosen carbon steel), a ultimate strength of 520 MPa and a Young's modulus equal to 200 GPa. The used sections were chosen according to a design made at room temperature of the stainless steel structure, resulting in five different sections for different structural elements (SHS70x70x4, SHS80x80x5, SHS100x100x5, SHS120x120x10 and SHS160x160x10).

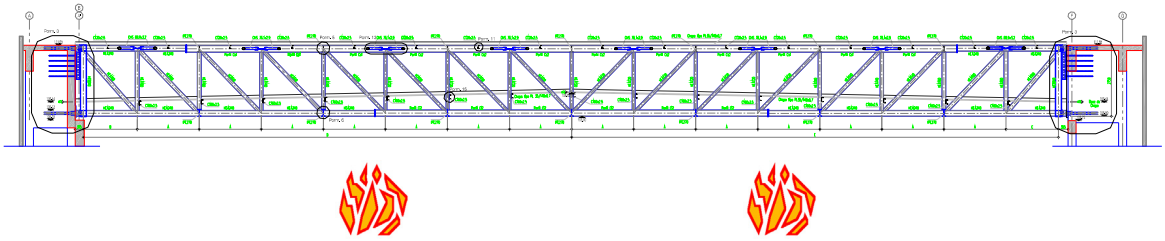

Figure 7.1 – Analysed truss.

First, the thermal analyses for each profiles cross-section were performed with SAFIR (Franssen, 2008). The temperature field obtained in the cross-section of the profiles is non-uniform. Simplified methods prescribed in EC3 assume that the temperature field is uniform in the cross-section of the profiles, due to the elevated steel thermal conductivity as well as to the relative thickness of the sections. Elevated thermal gradients in the analysed sections can origin significant changes in the thermo-mechanical behaviour.

The thermal module of the program SAFIR determines the evolution of the temperature field with time, performing a non-linear analysis, as the material thermal properties depend on the temperature, and the boundary conditions are also non-linear.

Figure 7.2 illustrates the temperature field in the SHS70x70x4 cross-section, after 15 minutes of the normalised fire curve ISO834 exposure to the 4 sides.

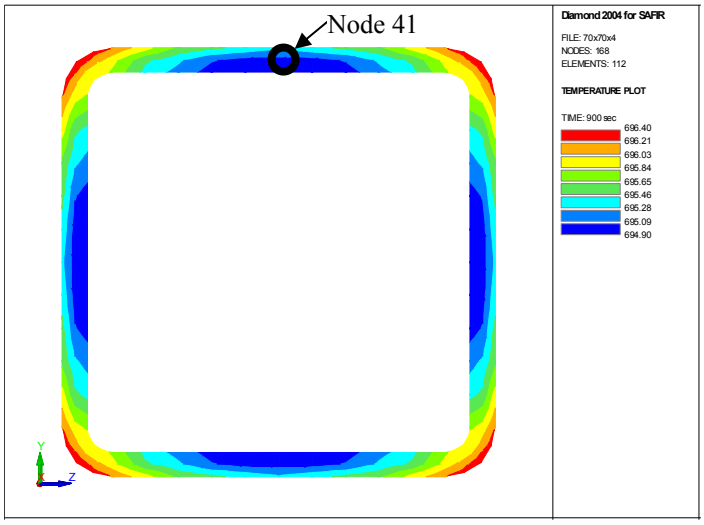

Figure 7.2 – Temperature field in the SHS70x70x4 cross-section after 15 minutes.

Figure 7.3 presents the temperature evolution at a specific point of the SHS70x70x4 (node 41 in Figure 7.2). It can be verified that the heating curve of the stainless steel is very similar to the heating curve of carbon steel, with the exception of the range between 600 ºC and 900 ºC. The time delay represented for carbon steel is due to the metallurgic phase transformation (Vila Real, 2003a) and accounted by the peak in the specific heat property value of carbon steel, which does not exist in the stainless steel (see Chapter 2).

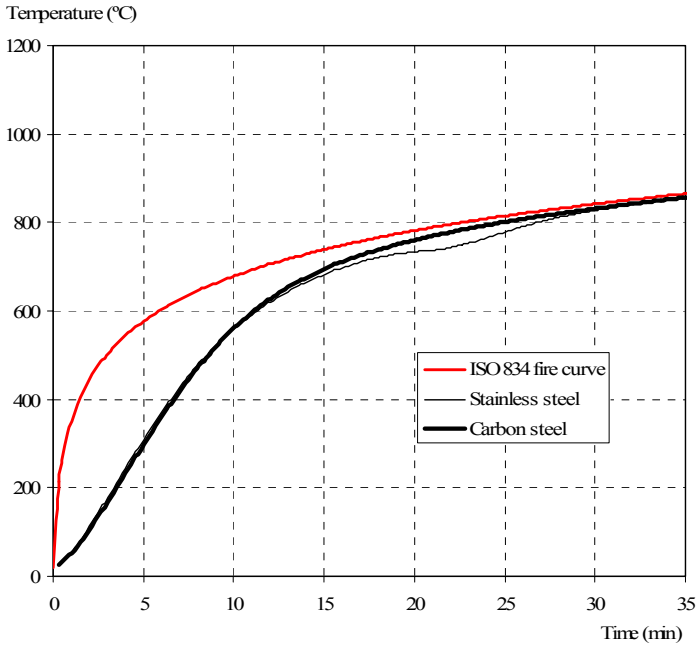

Figure 7.3 – Temperature evolution in node 41 of the SHS70x70x4.

Chapter 2 shows the differences between the thermal conductivity and the specific heat of carbon steel and stainless steel. Although stainless steel has a thermal conductivity lower than the carbon steel (which would make one suppose slower heating speed in stainless steel) the specific heat of the carbon steel is higher. Therefore, there is a small difference between the temperature evolution in both materials (see also section 7.3.2).

The finite element structural mesh used is presented in Figure 7.4. The finite elements used were 2D beam elements (see Chapter 3). The deformed shape and the internal forces are determined through an incremental process, during fire, until failure. This instant corresponds to the structure fire resistance.

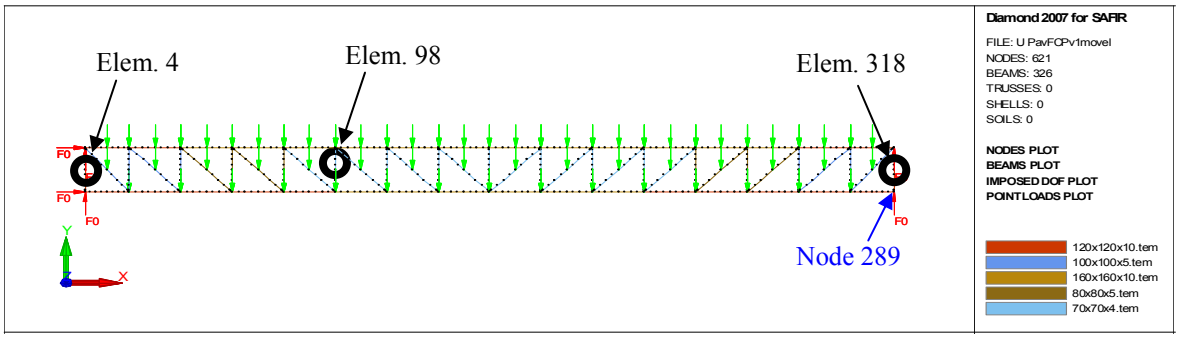

Figure 7.4 – Mesh used in the truss structure.

The considered permanent loads were the dead weights of the steel profiles (77 kN/m^3) plus 0.5 kN/m^2 of the roof applied as shown in Figure 7.4. The only considered variable action was the imposed loads, due to the location of the sport hall.

It was considered that the truss was simply supported, meaning that there was no restriction to the longitudinal displacements, making the thermal expansion of the complete structure available.

Figure 7.5 presents the deformed shape immediately before failure of the carbon steel and the stainless steel structures.

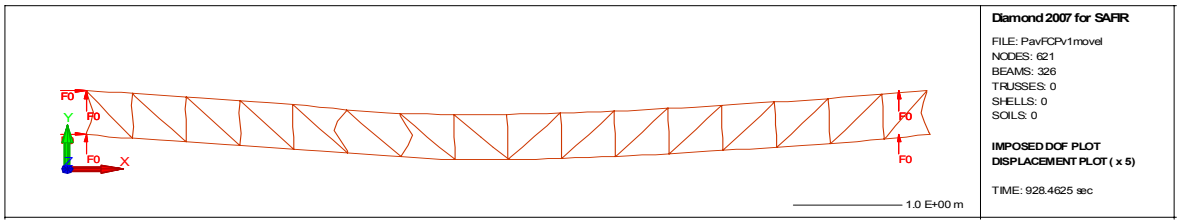

a) Carbon steel structure.

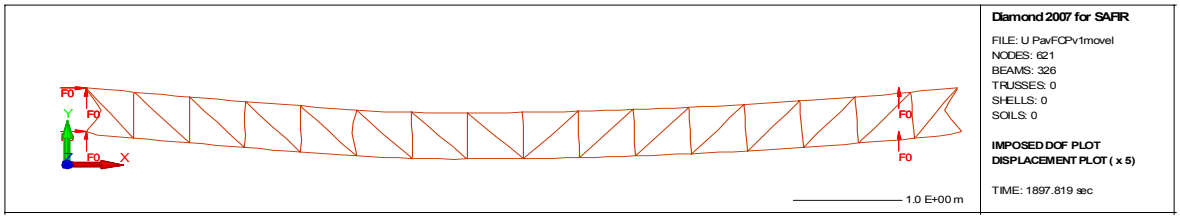

b) Stainless steel structure.

Figure 7.5 – Deformed shape (x5) of the truss structure.

In Figure 7.6 the evolution with the time of the horizontal displacement of the simple support in the node 289 is plotted.

In these figures it can be observed that, at failure, the displacements of the stainless steel structure are bigger than in the carbon steel structure. This can be justified by the fact that the stainless steel 1.4301 has higher ductility than the carbon steel, as presented in Chapter 2.

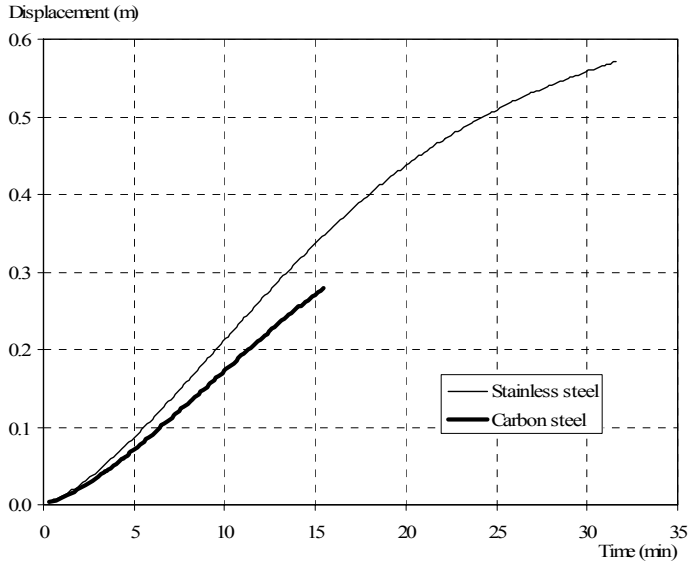

Figure 7.6 – Horizontal displacement of the simple support (node 289).

If a solution in stainless steel was adopted, the truss could remain visible and not protected. However it should be constructed in such a way that the supports were not restrained, allowing for the verified horizontal displacement.

Figure 7.7 shows the axial forces of the structure immediately before failure of the carbon steel and the stainless steel structures, respectively.

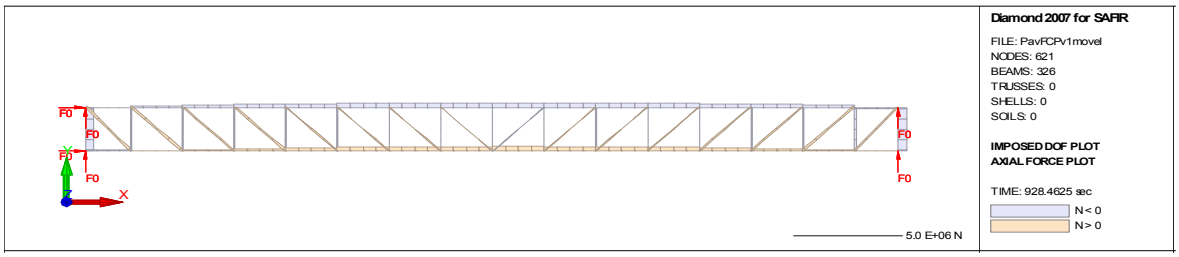

a) Carbon steel structure.

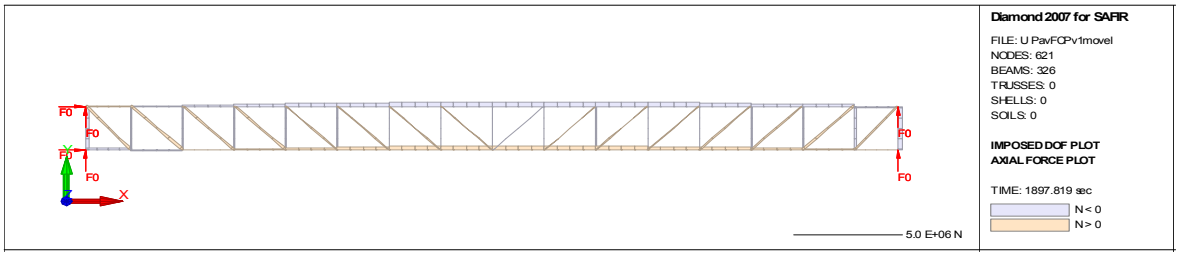

b) Stainless steel structure.

Figure 7.7 – Axial forces diagrams of the truss structure.

It can be observed that the axial forces diagrams present minor differences for the two structures.

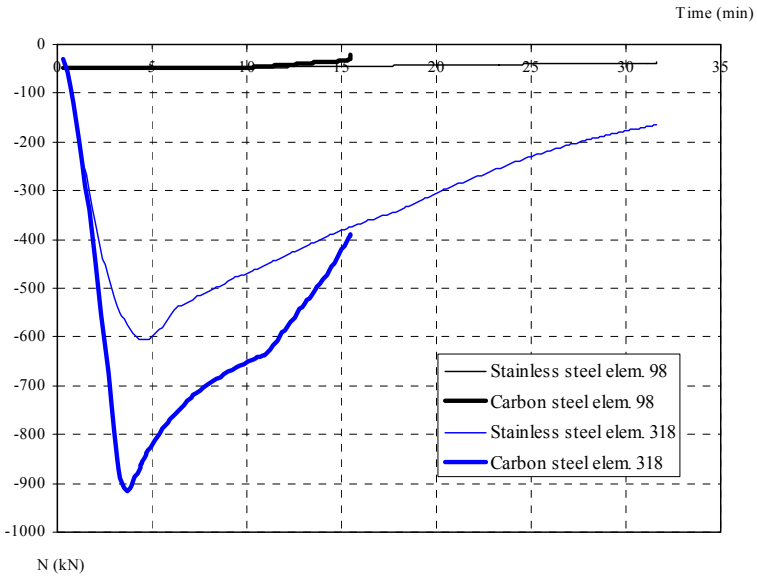

Figure 7.8 – Axial forces evolution over time in elements number 98 and 318.

It is observed that after approximately 4 minutes of fire exposure, element 318 reaches its maximum axial resistant force in both structures, leading to failure of the element (see Figure 7.8). The same behaviour is observed in the element 4.

The final failure of both structures occurred in the element 98, but this failure appeared earlier in the carbon steel structure.

An illustration of the influence of the materials different behaviour at high temperatures, in the structures stability, can be made through the yield strength reduction. After 15 minutes of fire exposure, the temperature in the SHS70x70x4 is more or less 700 ºC (see Figure 7.3).

In carbon steel, this temperature corresponds to yield strength of 23 % of the room temperature yield strength (see Chapter 2), while the stainless steel yield strength at this temperature is of 57 % of the one at room temperature. Finally, 23 % of the yield strength at room temperature only occurs in the stainless steel at 900 ºC, temperature that appears in the SHS70x70x4 after 30 minutes.

Consequently, the failure in the carbon steel structure occurred after 928 seconds (15.5 minutes) while the stainless steel structure only collapsed after 1898 seconds (about 31.6 minutes), which corresponds to a fire resistance of more than 2 times higher than the fire resistance of the carbon steel structure.

7.3.2 An office building portal frame

The fire resistance of a steel framed structure, with two spans and three storeys (Piloto, 2000; Vila Real *et al*. 2000), is determined in this paper. The fire resistance of this structure in S235 carbon steel is smaller than the expected standard resistance R30, while the 1.4301 stainless steel structure widely exceeds that resistance (Lopes *et al*., 2006). This structure simulates an office building at an altitude of 700m. In order to account for the effects of the assembly imperfections, possible eccentricities and geometrical imperfections, an initial sway imperfection has been introduced according to part 1-1 of EC3 that corresponds to a rotation angle of 0.0033 rad of the vertical members.

Fire resistance will be determined in the steel structure presented in Figure 7.9, when subjected to accidental conditions in compartment C4 as shown. It was considered that the room was subjected to the fire curve ISO834.

For the structure in carbon steel the steel grade S235 was used. The structural design was made at room temperature leading to IPE450 beam section and HEA300 columns section. For the stainless steel structure Class 1.4301 was used with a proportional elastic limit stress of 210 MPa, an ultimate strength of 520 MPa and a Young's modulus of 200 GPa. The beams and columns sections used were the same as the structure in carbon steel.

Structural analysis was made corresponding to the combination of actions for accidental design situation, considering the wind as the main variable action.

Having only compartment 4 subjected to fire, beam 4 will be subjected to fire in only three sides and the columns 2 to fire in only one side (see Figure 7.10).

Figure 7.11 illustrates the temperature field in the beam 4 cross-section (an IPE450), after 30 minutes of the standard fire curve ISO834 exposure only in the three sides.

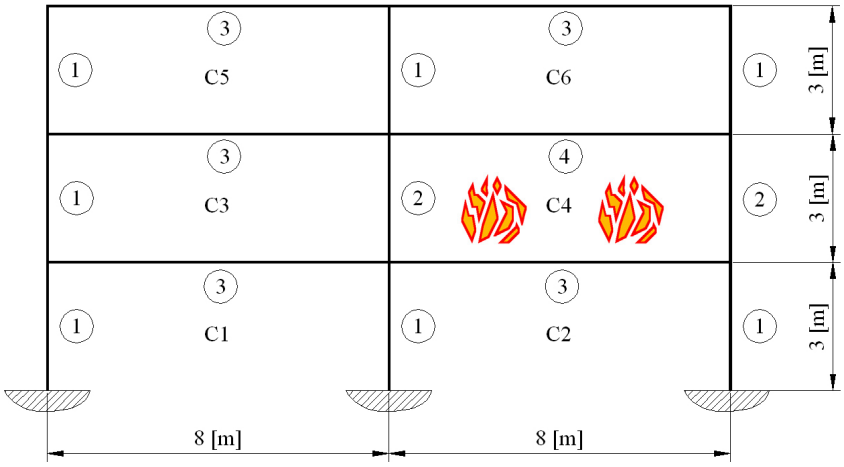

Figure 7.9 – Structure with fire only in room 4.

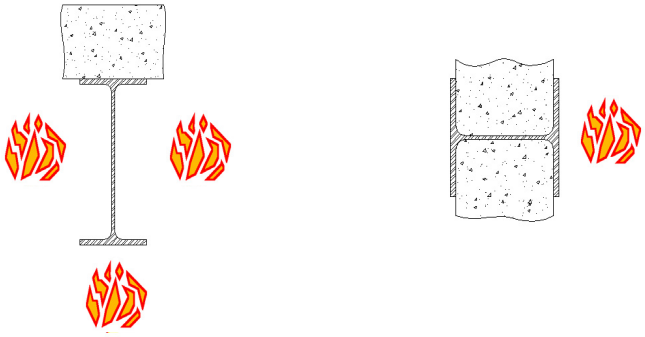

a) Beam with fire in three sides. b) Column with fire in one side.

Figure 7.10 – Structural elements subjected to fire.

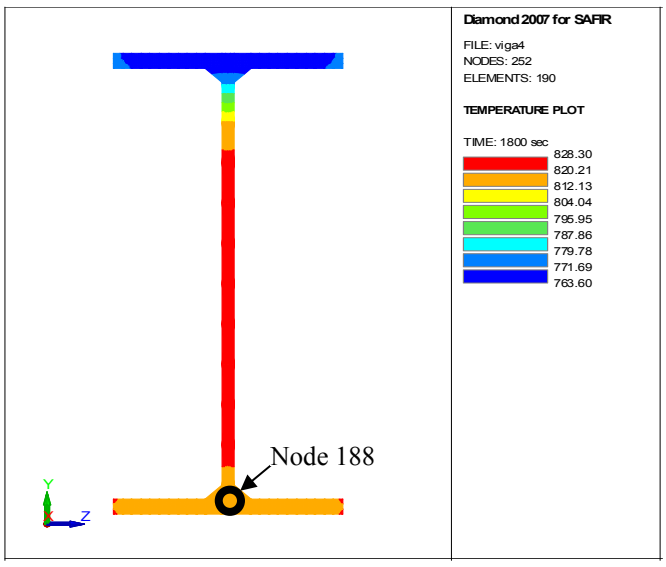

Figure 7.11 – Temperature field in the beam 4 cross-section after half hour.

Figure 7.12 presents the temperature evolution at a specific point of the beam 4 cross-section (node 188 in Figure 7.11). Again, it can be observed that the heating curve of the stainless steel is very similar to the heating curve of carbon steel with the exception in the range between 600 ºC and 900 ºC.

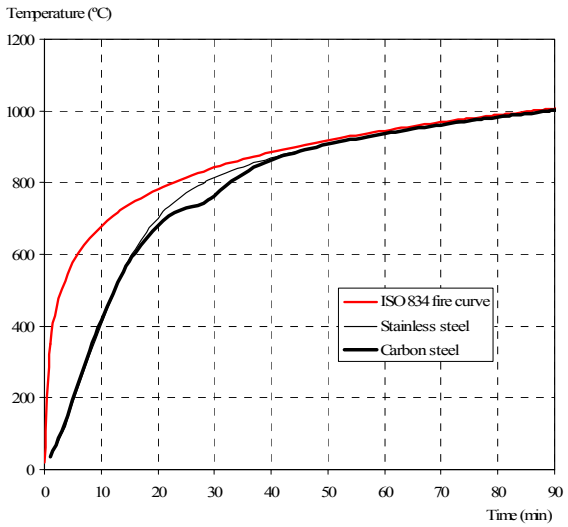

Figure 7.12 – Temperature evolution in node 188 in the beam 4 cross-section.

Structural analysis was performed corresponding to the combination of actions for accidental design situation, considering the wind as the main variable action. The corresponding acting load combination can be seen on Figure 7.13.

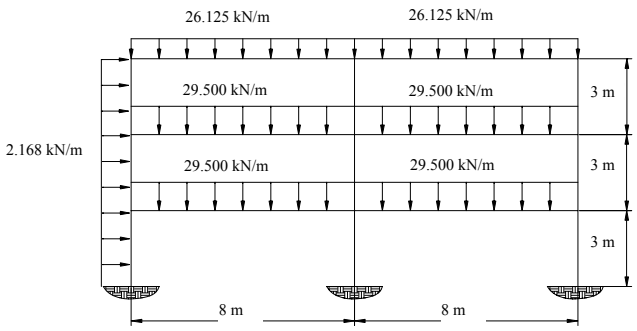

Figure 7.13 – Design loads for the accidental combination with wind as the dominant variable action.

The finite element structural mesh used is presented in Figure 7.14. The finite elements used were 2D beam elements (see Chapter 3).

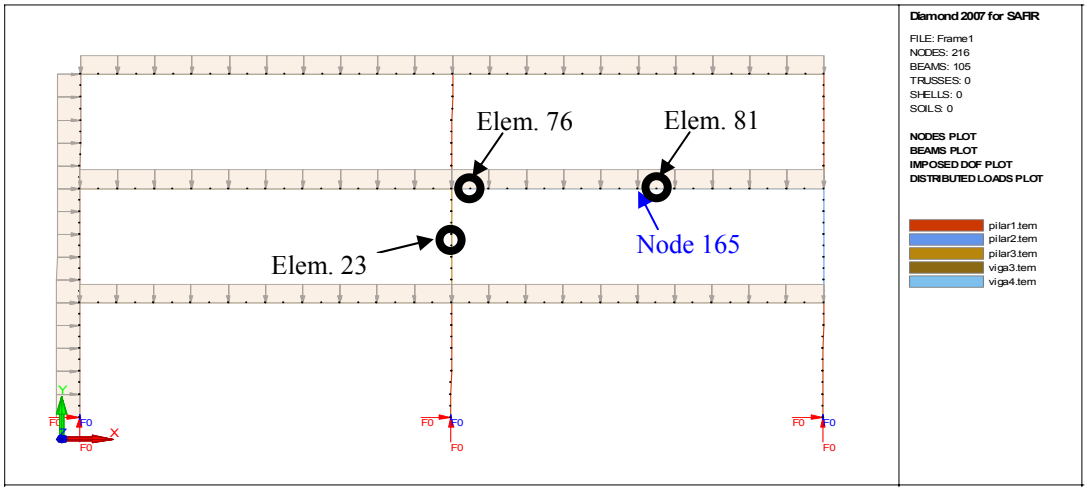

Figure 7.14 – Mesh used in the portal frame.

Figure 7.15 presents the deformed shape immediately before the failure of the carbon steel and the stainless steel structures.

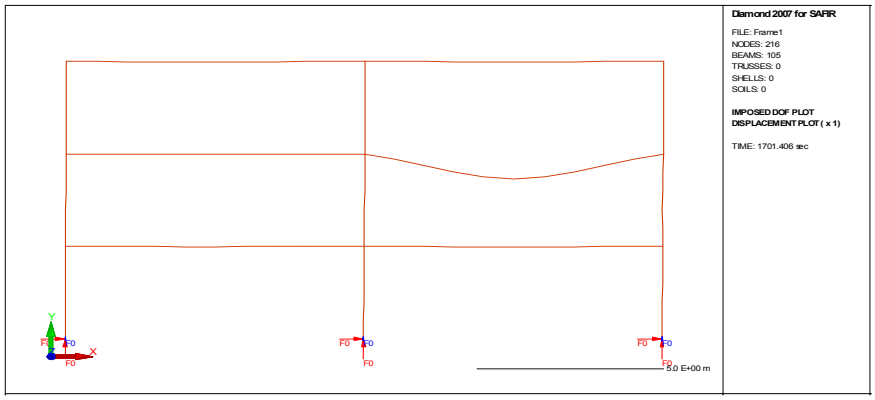

a) Carbon steel structure.

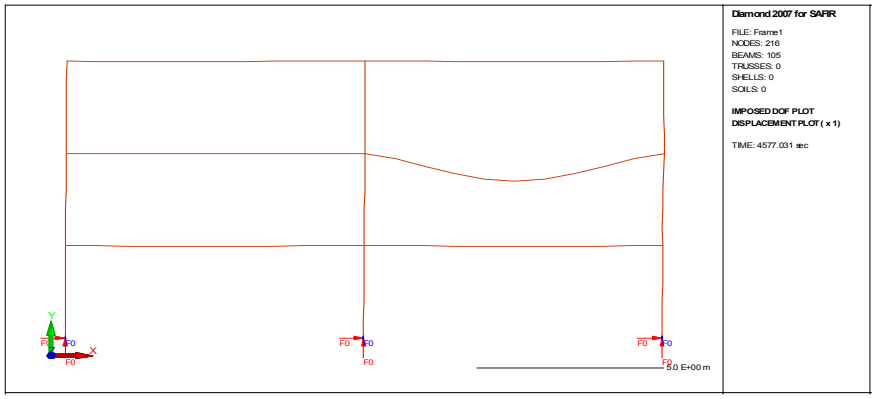

b) Stainless steel structure.

Figure 7.15 – Deformed shape (x1) of the portal frame.

In Figure 7.16 the evolution with the time of the vertical displacement at mid span of the beam 4 is plotted.

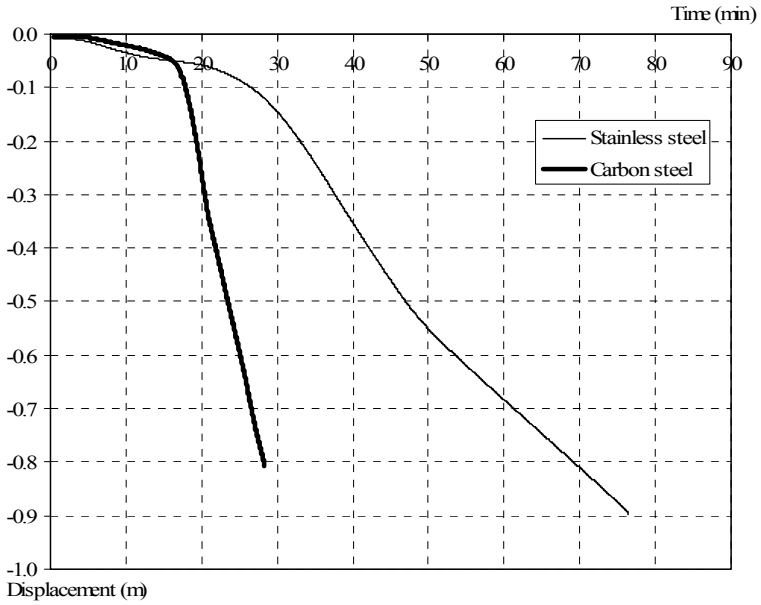

Figure 7.16 – Vertical displacement at mid span of the beam 4 (node 165).

In these figures it can be observed that at failure, the deformed shape of the stainless steel structure is similar to the one in the carbon steel structure. However, the deformation velocity in the carbon steel structure is higher than the one in the stainless steel structure.

Figure 7.17 presents the axial forces diagrams immediately before failure of the carbon steel and the stainless steel structures.

Minor differences in the axial forces diagrams of the two structures are observed. From Figure 7.18 it can be observed that the axial forces, in the most loaded heated column (element 23) suffer small changes during all the fire. However, near the mid span of beam 4 (element 81), it can be observed in both structures a big increase of the axial force, during the fire. This is due to the beam axial restraint provided by the structure.

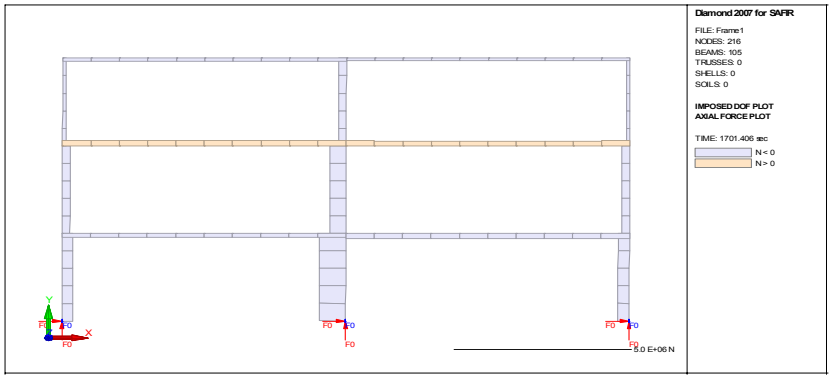

a) Carbon steel structure.

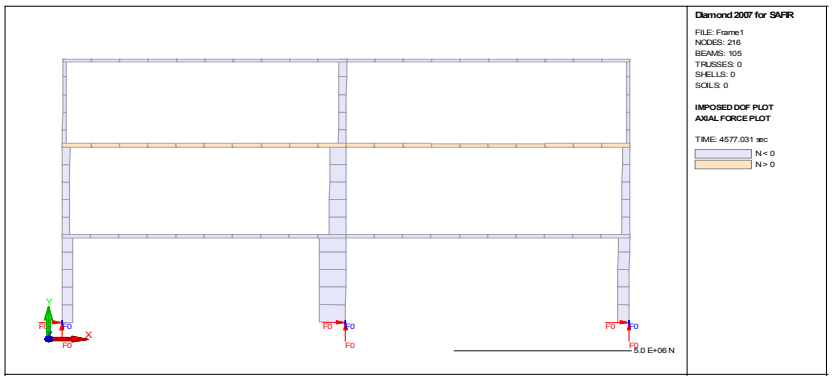

b) Stainless steel structure.

Figure 7.17 – Axial forces diagrams of the portal frame.

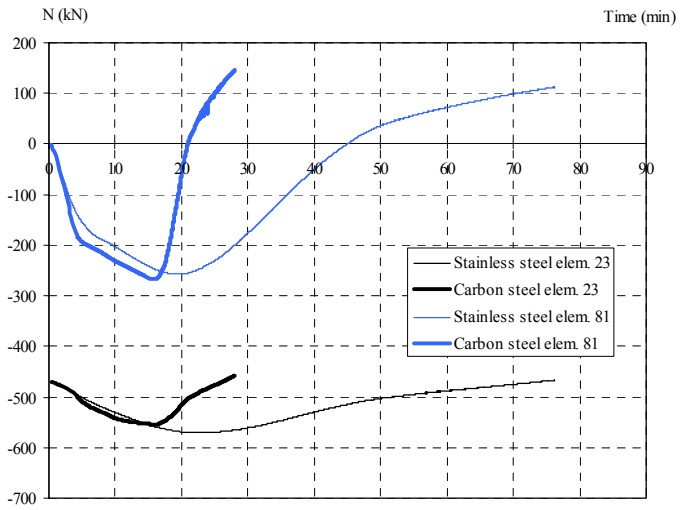

Figure 7.18 – Axial forces evolution over time in elements number 23 and 81.

Figure 7.19 presents the bending moment diagrams immediately before failure of the carbon steel and the stainless steel structures.

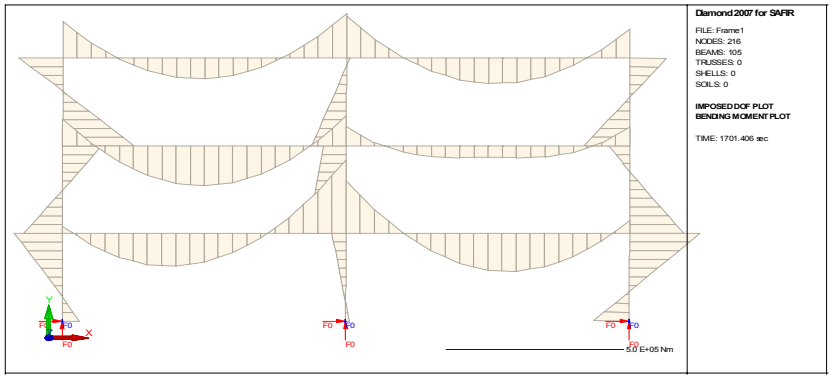

a) Stainless steel structure.

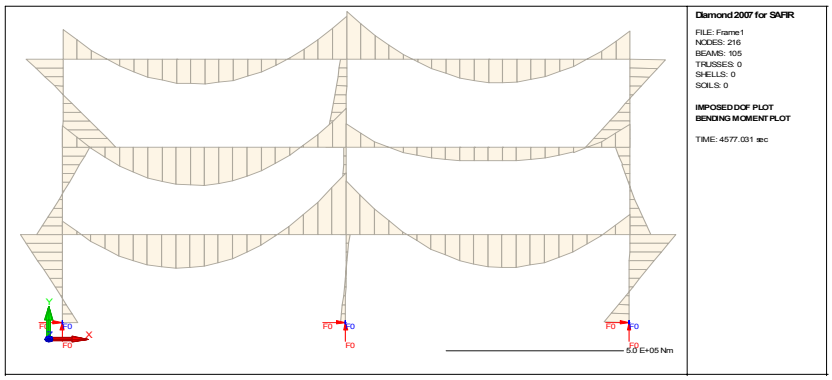

b) Stainless steel structure.

Figure 7.19 – Bending moments diagrams of the portal frame.

It can be observed that the bending moment diagrams also present minor differences in the two structures. Figure 7.20 shows the bending moment evolution with the fire exposure in beam 4, near the connection to the column (element 76) and near the mid span (element 81).

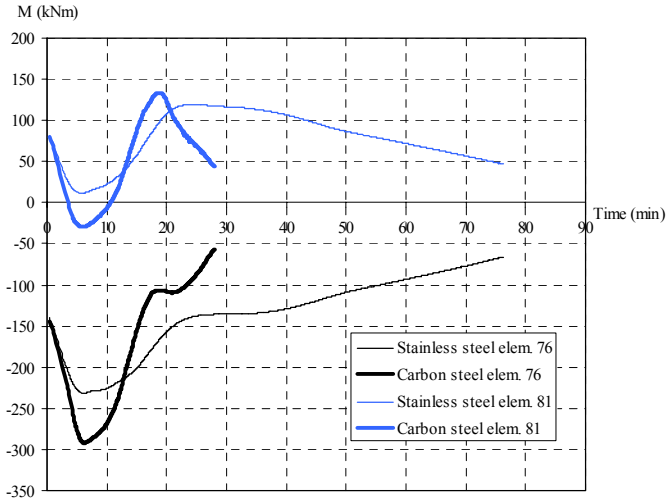

Figure 7.20 – Bending moment evolution over time in elements number 76 and 81.

In this Figure 7.20 it can be observed that in the first approximately 5 minutes the negative bending moment reaches the cross-section resistant moment (element 76), leading to a redistribution of the acting forces.

After 17 minutes the resistant capacity is reached in the carbon steel beam mid span (element 81). At that time, the beam cross-section is still at 650 ºC (see Figure 7.12), which corresponds to a yield strength in the carbon steel of about 40 % of the yield strength at room temperature. The same event in the stainless steel structure only occurs at 25 minutes, corresponding to steel temperatures of around 800 ºC. This temperature in the stainless steel leads to a reduction similar to the mentioned 40 %. New moment redistributions are made in the structures, and as the stainless steel has a much slower strength reduction and a higher ductility, the stainless steel structure failure occurs almost 50 minutes after the carbon steel structure failure.

The failure in the carbon steel structure occurred after 1701 seconds (28.4 minutes) while the stainless steel structure only collapsed after 4577 seconds (about 1 hour and 16 minutes), which corresponds to a fire resistance more than 2.5 times higher than the fire resistance of the carbon steel structure.

7.4 Conclusions

In fact, although more expensive than the carbon steel, structures in stainless steel can be competitive because of its smaller thermal protection need material, and lower life-cycle cost, contributing for a more sustainable construction.

The fire resistances of a portal frame structure and of a truss structure have been determined in carbon steel and in stainless steel. In all cases it has been considered that the structure was not fire protected.

Table 7.1 resumes the results obtained for the two studied structures made on both two materials.

It was concluded that the studied structures in stainless steel 1.4301 have fire resistance more than 2 times higher than the fire resistance of the same structures in carbon steel S235, which can be justified with the higher ductility and lower strength reduction at high temperatures.

Table 7.1 – Final results.

	Carbon steel S235	Stainless steel 1.4301
Truss structure	15.5min	31.6min
Portal frame	28.4min	76.3min

The fire resistances of the carbon steel structures are clearly below the standard fire resistance defined as R30, being necessary to use fire protection to fulfil these required fire resistance, which is not the case when stainless steel is used.

This higher resistance could allow the use of the stainless steel structures without any fire protection, increasing its economic advantage. Moreover, it allows the full viewing of the stainless steel and its aesthetic appearance, which is often decisive in the choice of this kind of steel in construction.

More study cases should be performed in order to better validate the above written conclusions.

Chapter 8

Conclusions

Chapter 8. Conclusions

8.1 General conclusions

8.2 Design recommendations

8.3 Future work

- 8.3.1 Experimental tests
- 8.3.2 Different cross-sections shapes, loading types and bi-axial bending
- 8.3.3 Eurocode 3 validation for thin-walled stainless steel sections in case of fire
- 8.3.4 Life cycle costing

Chapter 8. Conclusions

8.1 General conclusions

This thesis presented numerical studies on stainless steel structures in case of fire. Similar studies at room temperature were also performed.

The stainless steels have different mechanical behaviour at elevated temperatures, when compared with the behaviour of carbon steel. In order to proceed with this numerical study, the EC3 prescriptions, for the stainless steel material properties at elevated temperatures, were introduced in the program SAFIR. These software modifications included uni-axial constitutive laws and plane stress-strain state, taking into account the stainless steel always non-linear stress-strain relationship.

The accuracy and safety of the currently prescribed design rules in EC3 for the evaluation of the resistance of stainless steel columns, beams and beam-columns, at room temperature (CEN, 2006a) and at high temperatures (CEN, 2005b), was evaluated. This evaluation was carried out by performing numerical simulations, on Class 1 and Class 2, stainless steel (H and I) cross-sections. Comparisons between the numerical results and the buckling curves from EC3 for those different elements were presented. Based on these comparisons, safer and more accurate proposals (for the flexural buckling of columns, for LTB resistance and for the interaction curves of beam-columns) were presented.

Based on the cold design from the EN 1993-1-1, an improved proposal for the LTB of unrestrained steel beams subjected to fire was presented in this thesis, addressing the issue of the influence of: the loading type; steel grade; pattern of the residual stresses (hot rolled or welded sections) and ratio h/b (slenderness of the cross-section) between the depth h and the width b of the cross-section on the resistance of the beam. With this methodology, better agreement with the numerical behaviour was achieved while maintaining safety. The proposal was found to be safe and accurate through an extensive comparison with the results of finite element method numerical simulations.

A numerical study on stainless steel thin-walled elements, showing the influence of the residual stresses and initial imperfections on the ultimate load bearing resistance of Class 4 stainless steel structural elements in case of fire was also presented.

Finally, the behaviour of two structures (a portal frame and a truss) subjected to a standard fire curve was compared in stainless steel and in carbon steel. The mechanical and thermal properties considered for both materials were the ones prescribed in the fire part of EC3. It was shown that in both examples, the fire resistance of stainless steel structures is significantly higher than carbon steel structures, avoiding any fire protection material needed to fulfil the standard fire requirements.

8.2 Design recommendations

The alternative design expressions presented in this thesis, for stainless steel structural elements at room temperature and in case of fire, tried to ensure the compatibility and coherence between part 1-1, part 1-2 and part 1-4 of EC3, as well as supply simple, competitive and safe procedures.

With the different methodologies, better agreements with the numerical behaviour were achieved while maintaining safety. The proposals were developed to be safe and accurate through extensive comparisons with the finite element method numerical simulations. Statistical studies of the results were performed, showing the accuracy of the presented proposals.

Those new approaches, for evaluating the safety of stainless steel elements subjected to axial compression and/or bending, addressed the influence of global buckling phenomena (flexural buckling and LTB).

The studies on the flexural buckling, of stainless steel columns, resulted in the proposal of safer buckling curves, at room temperature and in case of fire. Also, it is shown that these flexural buckling curves at high temperatures should vary with the buckling axis, as it is made at room temperature, according to part 1-4 of EC3.

The beneficial influence of non-uniform bending moment distributions, resulting from the reduced plastic zones connected with variable bending along the beam, is taken into

account in the presented proposals for the cold and fire design of stainless steel elements with LTB.

The studies in stainless steel beam-columns concluded that it was not possible to directly adapt the new carbon steel interaction curves to stainless steel and fire. As consequence, new interaction curves for the design of stainless steel beam-columns with and without LTB, at room temperature and at high temperatures, were proposed, providing safer and more economic approximations to the obtained numerical results.

The studies presented here were made in different stainless steel grades. Due to the fact that the different stainless steels have different stress-strain relationships at high temperatures, it was necessary to account for this influence, mainly in the ferritic and duplex grades.

Finally, these developed design guidelines have a format that could be readily disseminated and used in the European Union by incorporating them into European Standards. However, the influence of the different investigated factors is independent of the code used for the simple design, being, thus, possible to be taken into account in any simple design equation.

8.3 Future work

During the development of this work, some research subjects not accounted for in this thesis, related to the behaviour of stainless steel structures in case of fire, have appeared. This final section describes possible future research areas.

8.3.1 Experimental tests

This thesis was based in computational simulations, through the use of the finite element methods. Although established and validated, these simulations do not always reproduce perfectly the real behaviour of the structures.

The variability of some of the factors influencing the structural behaviour is quite large. The imperfections and the residual stresses in the elements are some of the factors that can vary in a stainless steel profile.

Experimental tests could reduce the distance between the real structural behaviour and test conditions, when compared with numerical simulations.

8.3.2 Different cross-sections shapes, loading types and bi-axial bending

The approaches proposed in this thesis for the safety evaluation, of structural stainless steel elements, were mainly based on welded I-sections. Similar studies, with more numerical results, should be made for stainless steel hollow sections and cold formed sections, in order to validate or improve the design proposals presented. Moreover, other stainless steel grades should also be considered.

Other loading types that produce different bending moment diagrams from the ones considered in this thesis should be accounted for in future research works.

Finally, the behaviour of structural elements, subjected to bi-axial bending and axial compression, should also be the aim of research studies, accounting for LTB and flexural buckling phenomena.

8.3.3 Eurocode 3 validation for thin-walled stainless steel sections in case of fire

The studies presented in this thesis about thin-walled stainless steel structures in case of fire showed that the EC3 did not provide a good and safe approximation to the numerical results. This means that more numerical and experimental tests should be done to confirm the unsafe nature of the EC3 results and to determine whether new formulae to be used with Class 4 elements should be developed.

8.3.4 Life cycle costing

It would be interesting to perform life-cycle cost studies to evaluate the importance of the higher fire resistance in stainless steel structures. Although more expensive than the carbon steel, stainless steel structures can be competitive because of theirs smaller thermal protection need material, adding this advantage to others such as the aesthetic appearance and corrosion resistance.

The total life cycle cost is equal to the sum of the initial materials acquisition costs; installation and fabrication costs; operating and maintenance costs; production downtime costs and the replacement materials costs. A full life cycle cost analysis may allow to consider the full implications of future costs, in terms of both actual monetary value and inconvenience of future maintenance and replacements.

References

References

Ala–Outinen, T.; Oksanen, T. (1997). *"Stainless steel compression members exposed to fire"*, VTT Research Notes 1864, Espoo, Finland.

Allen, H. C.; Bulson, P. S. (1980). *"Background to buckling"*, McGraw– Hill Book Company Limited, United Kingdom.

Ansys, Inc. (2006). *"ANSYS Academic version, Release 10.0, Help System*".

ArcelorMittal (2008). *"Sections and Merchant Bars, sales programme"*, ArcelorMittal Commercial Sections, Long Carbon Europe.

Ashraf, M.; Gardner, L.; Nethercot, DA. (2005). *"Strength enhancement of the corner regions of stainless steel cross sections"*, Journal of Constructional Steel Research, Elsevier, Vol. 61 (1), pp. 37–52.

Boissonnade, N. (2002). *"Mise au point d'un element fini de type poutre a section variable et autres applications a la construction metallique"* (in French), Thesis submitted to the University Blaise Pascal, Clermont–Ferrand, France, for the degree of Doctor of Philosophy in Civil Engineering.

Boissonnade, N.; Greiner, R.; Jaspart, J. P. (2006). *"Rules for Member Stability in EN1993–1–1 Background documentation and design guidelines"*, ECCS Technical Committee 8 – Stability.

Boreave, P. (1991). *"Contribuition a l'analyse statique non lineaire des structures mixtes planes formées de poutres avec prise en compte des effects differés et des phases de construction"* (in French), Thesis submitted to the University of Liege, Belgium, for the degree of Doctor of Philosophy.

Camotim, D.; Gonçalves, R. (2003). *"GBT–Based local and global buckling analysis of C–section and RHS stainless steel columns"*, proceedings of the Stainless steel experts seminar, The Steel Construction Institute.

CEN, European Committee for Standardisation (1992). *"ENV 1993–1–1, Eurocode 3: Design of steel Structures – Part 1–1: General Rules and Rules for Buildings"*, Brussels, Belgium.

CEN, European Committee for Standardisation (1995). *"ENV 1993–1–2, Eurocode 3, Design of Steel Structures – Part 1–2: General rules – Structural fire design"*, Brussels, Belgium.

CEN, European Committee for Standardisation (2004a). "*EN 10025–2, Hot rolled products of structural steels – Part 2: Technical delivery conditions for non–alloy structural steels"*, Brussels, Belgium.

CEN, European Committee for Standardisation (2004b). *"EN 1993–1–3, Eurocode 3: Design of Steel Structures – Part 1–3: Supplementary rules for cold–formed members and sheeting"*, stage 49 draft, Brussels, Belgium.

CEN, European Committee for Standardisation (2005a). "*EN 1993–1–1, Eurocode 3, Design of Steel Structures – Part 1–1: General rules and rules for buildings"*, Brussels, Belgium.

CEN, European Committee for Standardisation (2005b). *"EN 1993–1–2, Eurocode 3, Design of Steel Structures – Part 1–2: General rules – Structural fire design"*, Brussels, Belgium.

CEN, European Committee for Standardisation (2005c). *"EN 1090–2, Execution of Steel and aluminium Structures – Part 2: Technical Requirements for the execution of steel structures"*, Brussels, Belgium.

CEN, European Committee for Standardisation (2006a). *"EN 1993–1–4, Eurocode 3: Design of steel Structures – Part 1–4: General rules – Supplementary Rules for Stainless steels"*, Brussels, Belgium.

CEN, European Committee for Standardisation (2006b). *"EN 10088–1, Stainless steels – Part 1: List of stainless steels"*, Brussels, Belgium.

CEN, European Committee for Standardisation (2006c). *"EN 1993–1–5, Eurocode 3: Design of Steel Structures – Part 1–5: Plated structural elements"*, Brussels, Belgium.

CEN, European Committee for Standardisation (2006d). *"EN 1990, Eurocode – Basis of structural design"*, Brussels, Belgium.

CEN, European Committee for Standardisation (2006e). *"EN 1991–1–2, Eurocode 1 – Actions on structures – Part 1–2: General actions – Actions on structures exposed to fire"*, Brussels, Belgium.

Chen, W. F.; Lui, E. M. (1991). *"Stability design of steel frames"*, CRC Press.

Cheung, Y. K. (1976). *"Finite strip method in structural analysis"*, Pergamon Press, New York, USA.

Cruise, R. (2007). *"The Influence of Production Routes on the Behaviour of Stainless Steel Structural Members"*, Thesis submitted to the University of London, United Kingdom, for the degree of Doctor of Philosophy in Civil Engineering.

Cruise, R.; Gardner, L. (2008). *"Residual stress analysis of structural stainless steel sections"*, Journal of Constructional Steel Research, Elsevier, Vol. 64, pp. 352–366.

Doneux, C.; Franssen, J.–M. (2003). *"2D constitutive models for the shell elements of the finite element software SAFIR"*, translation of "Rapport interne – SPEC/97_01", Service Ponts et Charpentes, University of Liege, Belgium.

ECCS, European Convention for Constructional Steelwork (1984). *"Ultimate Limit State Calculation of Sway Frames with Rigid Joints"*, Technical Committee 8 – Structural Stability, Technical Working Group 8.2 – System, first edition, ECCS.

Elmahdy, G.; Abu–Hamd, M. (2008). *"New formulae for the effective width of slender plate elements"*, proceedings of the CSCE 2008 Annual Conference Québec, Canada.

ESDEP, European Steel Design Education Programme (2000). *"Programa Europeo de Formación en el Cálculo y Diseño de la Construcción en Acero"* (in Spanish), Instituto Técnico de la Estructura en Acero (IETA).

Euro Inox; SCI, Steel Construction Institute (2006). *"Design Manual for Structural Stainless Steel"*, 3rd edition.

Estrada, I.; Real, E.; Mirambell, E. (2006). *"General behaviour and effect of rigid and non–rigid end post in stainless steel plate girders loaded in shear. Part I: experimental study"*, Journal of Constructional Steel Research, Elsevier, Vol. 63, pp. 970–984.

Feng, M.; Wang, Y. C.; Davies, J. M. (2002a). *"Structural behaviour of cold–formed thin–walled short steel channel columns at elevated temperatures. Part 1: experiments"*, Thin–Walled Structures, Elsevier, Vol. 41, pp. 543–570.

Feng, M.; Wang, Y. C.; Davies, J. M. (2002b). *"Structural behaviour of cold–formed thin–walled short steel channel columns at elevated temperatures. Part 2: Design calculations and numerical analysis"*, Thin–Walled Structures, Elsevier, Vol. 41, pp. 571–594.

Franssen, J.–M. (1989). *"Modélisation et influence des contraintes résiduelles dans les profils métalliques soumis à l'incendie"*, (in French), Construction Métallique, CTICM, Vol. 3, pp. 35–42.

Franssen, J.–M. (1990). *"The Unloading of Buildings Materials Submitted to Fire"*, Fire Safety Journal, Elsevier, Vol. 16, pp. 213–227.

Franssen, J.–M. (1993). *"Residual stresses in steel profiles submitted to the fire: an analogy"*, proceedings of the 3rd CIB/W14 Workshop "Modelling", TNO Building and Construction Research, Rijswijk, The Netherlands.

Franssen, J.–M.; Schleich, J.–B.; Cajot L.–G. (1995). *"A Simple Model for Fire Resistance of Axially–loaded Members According to Eurocode 3"*, Journal of Constructional Steel Research, Elsevier, Vol. 35, pp. 49–69.

Franssen, J.–M.; Schleich, J.–B.; Cajot, L.–G.; Azpiazu, W. (1996). *"A Simple Model for the Fire Resistance of Axially–loaded Members – Comparison with Experimental Results"*, Journal of Constructional Steel Research, Elsevier, Vol. 37, pp. 175–204.

Franssen, J. M.; Taladona, D.; Kruppa, J.; Cajot, L.G. (1998). *"Stability of Steel Columns in Case of Fire: Experimental Evaluation"*, Journal of Structural Engineering, ASCE, Vol. 124 (2), pp. 158–163.

Franssen, J.–M.; Kodur, V.; Mason, J. (2002). *"Elements of theory for SAFIR 2002 a computer program for analysis of structures submitted to the fire"*, Department Structures du Génie Civil, Service Ponts et Charpentes, University of Liege, Belgium.

Franssen, J.–M.; Gens, F. (2004). *"Dynamic analysis used to cope with partial and temporary failures"*, proceedings of the Third International Workshop Structures in Fire SiF'04, Otawa, Canada.

Franssen, J.–M. (2005a). *"SAFIR. A Thermal/Structural Program Modelling Structures under Fire"*, Engineering Journal, AISC, Vol. 42 (3), pp. 143–158.

Franssen, J.–M.; Zaharia, R. (2005b). *"Design of steel structures subjected to fire. Background and design guide to Eurocode 3"*, les Éditions de l'Université de Liège, Belgium.

Franssen, J.–M. (2008). *"User's manual for SAFIR 2007a, a computer program for analysis of structures subjected to fire"*, Structural Engineering, ArGEnCO, University of Liege, Belgium.

Galambos, T. V. (1988). *"Guide to Stability Design Criteria for Metal Structures"* 4th Edition, Structural Stability Research Council, John Wiley & Sons, Inc., New York, USA.

Gardner, L. (2002). *"A new approach to stainless steel structural design"*, Thesis submitted to the Imperial College London, United Kingdom, for the degree of Doctor of Philosophy.

Gardner, L.; Nethercot, D. A. (2004). "Numerical Modeling of Stainless Steel Structural *Components – A consistent Approach"*, Journal of Constructional Engineering, ASCE, pp. 1586–1601.

Gardner, L. (2005). *"The use of stainless steel in structures"*, Progress in Structural Engineering and Materials, John Wiley & Sons, Ltd, Vol. 7, pp. 45–55.

Gardner, L.; Baddoo, N. (2006). *"Fire testing and design of stainless steel structures"*, Journal of Constructional Steel Research, Elsevier, Vol. 62, pp. 532–543.

Greiner, R. (2001). *"Background information on the beam–column interaction formulae at level 1"*, ECCS TC 8, Report No. 2001–021.

Greiner, R.; Hörmaier, I.; Ofner, R.; Kettler, M. (2005). *"Buckling behaviour of stainless steel members under bending and axial compression"*, Report No. F–5–14/2005, Technical University of Graz, Austria.

Hibbitt, Karlsson & Sorensen, Inc. (2004). *"ABAQUS Analysis user's manual, volumes I–VI, Version 6.5"*, Pawtucket, USA.

Jandera, M.; Gardner, L.; Machaceka, J. (2008). *"Residual stresses in cold–rolled stainless steel hollow sections"*, Journal of Constructional Steel Research, Elsevier, Vol. 64, pp. 1255–1263.

Knobloch, M.; Fontana, M. (2004). *"Local buckling behaviour and strain–based effective widths of steel structures subjected to fire"*, proceedings of the third international workshop Structures in Fire SiF'04, Ottawa, Canada.

Knobloch, M.; Fontana, M. (2006). *"Strain–based approach to local buckling of steel sections subjected to fire"*, Journal of Constructional Steel Research, Elsevier, Vol. 62, pp. 44–67.

Knobloch, M.; Fontana, M.; Frangi, A. (2008). *"Fire resistance of steel beam–columns subjected to axial compression and biaxial bending with non–uniform bending moment distribution"*, proceedings of the 5th International Conference on Structures in Fire SiF'08, Singapore.

Lopes, N. (2003). *"Modelação Numérica de Vigas–Coluna Metálicas em Situação de Incêndio"* (in Portuguese), Thesis submitted to the University of Coimbra, Portugal, for the degree of Master in Civil Engineering.

Lopes, N.; Simões da Silva, L.; Vila Real, P.; Piloto, P. (2004). *"New proposals for the design of steel beam–columns in case of fire, including a new approach for the lateral–torsional buckling"*, Computers & Structures, Pergamon – Elsevier, Vol. 82 (17/19), pp. 1463–1472.

Lopes, N.; Vila Real, P.; Piloto, P.; Mesquita, L.; Simões da Silva, L. (2006). *"Numerical modelling of the behaviour of a stainless steel portal frame subjected to fire"*, proceedings of the Fourth International Workshop Structures in Fire SiF'06, Aveiro, Portugal.

Lopes, N.; Vila Real, P.; Simões da Silva, L.; Franssen, J.–M. (2007). *"Stainless steel beam–columns in case of fire"*, proceedings of the 6th International Conference on Steel and Aluminium Structures ICSAS'07, Oxford, United Kingdom.

Lopes, N.; Vila Real, P.; Simões da Silva, L. (2008a). *"Dispensing the lateral–torsional buckling calculations: In steel beams at room temperature and in case of fire"*, proceedings of the 5th European Conference on Steel and Composite Structures Eurosteel 2008, Graz, Austria.

Lopes, N.; Vila Real, P.; Simões da Silva, L.; Franssen, J.–M. (2008b). "*Numerical modelling of thin–walled stainless steel structural elements in case of fire"*, proceedings of the 5th International Conference on Structures in Fire SiF'08, Singapore.

Maquoi, R.; Rondal, J. (1978). *"Mise en equation des nouvelles courbes Européennes de flambement"* (in French), Construction Métallique, CTICM, Vol. 1, pp. 17–29.

Masing, G. (1926). *"Eigenspannungen und Verfestigung beim Messing"* (in German), proceedings of the 2nd International Congress on Applied Mechanics, Zürich, Switzerland.

Millstock Stainless (2008). *"Stainless steel sections"*, Millstock Stainless Limited Commercial Sections.

Ng, K. T.; Gardner, L. (2007). *"Buckling of stainless steel columns and beams in fire"*, Engineering Structures, Elsevier, Vol. 29, pp. 717–730.

Oñate, E. (1995). *"Cálculo de Estructuras por el Método de los Elementos Finitos. Análisis estático lineal"* (in Spanish), Centro Internacional de Métodos Numéricos en Ingeniería, CIMNE, 2nd edition, Spain.

Piloto, P. (2000). *"Análise experimental e numérica do comportamento de estruturas metálicas sujeitas à acção do fogo"* (in Portuguese), Thesis submitted to the Engineering Falcuty of the University of Porto, Portugal, for the degree of Doctor of Philosophy.

Rasmussen, K. (2003). *"Full–range stress–strain curves for stainless steel alloys"*, Journal of Constructional Steel Research, Elsevier, Vol. 59, pp. 47–61.

Real, E. (2001). *"Aportaciones al estudio del comportamiento a flexión de estructuras de acero inoxidable"* (in Spanish), Thesis submitted to the Polytechnic University of Catalonia, Spain, for the degree of Doctor of Philosophy in Civil Engineering.

Real, E.; Mirambell, E. (2003). *"Discussion of "Full–range stress–strain curves for stainless steel alloys [Journal of Constructional Steel Research 2003;59:47–61]"*, Journal of Constructional Steel Research, Elsevier, Vol. 59, pp. 1321–1323.

Reis, A.; Camotim, D. (2000). *"Estabilidade estrutural"* (in Portuguese), McGraw–Hill, Portugal.

Rebelo, C.; Lopes, N.; Simões da Silva, L.; Nethercot, D.; Vila Real P. (2009). *"Statistical evaluation of the lateral–torsional buckling resistance of steel I–beams – Part 1: Variability of the Eurocode 3"*, Journal of Constructional Steel Research, Elsevier, Vol. 65 (4), pp. 818–831.

Rubert, A.; Schaumann, P. (1985). *"Tragverhalten Stahlerner Rahmensysteme bei Brandbeanspruchung"* (in German), Stahlbau, Vol. 9, pp. 280–287.

Santiago, A. (2008). *"Behaviour of beam–to–column steel joints under natural fire"*, Thesis submitted to the University of Coimbra, Portugal, for the degree of Doctor of Philosophy in Civil Engineering.

Sarawit, A. T.; Kim, Y.; Bakker, M. C. M.; Peko, T. (2003). *"The finite element method for thin–walled members–applications"*, Thin–Walled Structures, Elsevier, Vol. 41, pp. 191–206.

Schafer, B. W. (1997). *"Cold–formed steel behaviour and design: analytical and numerical modeling of elements and members with longitudinal stiffeners"*, Thesis submitted to the Cornell University, USA, for the degree of Doctor of Philosophy.

Simões da Silva, L.; Gervásio, H. (2007). *"Dimensionamento de estruturas metálicas: métodos avançados"* (in Portuguese), CMM, Portugal.

Talamona, D. (1995). *"Flambement de Poteaux Métalliques sous Charge Excentrée, à Haute Température"* (in French), Thesis submitted to the University Blaise Pascal, Clermont–Ferrand, France, for the degree of Doctor of Philosophy in Civil Engineering.

Talamona, D.; Franssen, J. M.; Schleich, J. B.; Kruppa, J. (1997). *"Stability of steel columns in case of fire: numerical modelling"*, Journal of Structural Engineering, ASCE, Vol. 123 (6), pp. 713–720.

Talamona, D.; Franssen, J. M. (2000). *"New quadrangular shell element in SAFIR"*, proceedings of the first international workshop Structures in Fire, Copenhagen, Denmark.

Trahair, N. S. (1993). *"Flexural–Torsional Buckling of Structures"*, E&FN SPON.

Trahair, N.S.; Bradford, M.A. (1998). *"The Behaviour and Design of Steel Structures to AS 4100"*, Third edition – Australian, E&FN SPON.

Trahair, N. S.; Bradford, M. A.; Nethercot, D. A. (2001). *"The behaviour and design of steel structures to BS5950"*, Spon Press.

Uppfeldt, B.; Outinen, T.; Veljkovic, M. (2008). *"A design model for stainless steel box columns in fire"*, Journal of Constructional Steel Research, Elsevier, Vol. 64 (11), pp. 1294–1301.

Vila Real, P.; Franssen, J.–M. (1999). *"Lateral buckling of steel I beams under fire conditions – Comparison between the EUROCODE 3 and the SAFIR code"*, internal report

No. 99/02, Institute of Civil Engineering, Service Ponts et Charpents, University of Liege, Belgium.

Vila Real, P.; Piloto, P.; Franssen, J.–M. (2000). *"Modelação numérica do comportamento de uma estrutura metálica sujeita à acção do fogo – Análise de vários cenários de incêndio"* (in Portuguese), Revista Portuguesa de Engenharia de Estruturas, LNEC, pp. 23–33.

Vila Real, P.; Franssen, J.–M. (2001). *"Numerical Modelling of Lateral Buckling of Steel I Beams Under Fire Conditions – Comparison with Eurocode 3"*, Journal of Fire Protection Engineering, SAGE, Vol. 11 (2), pp. 112–128.

Vila Real, P. (2003a). *"Incêndio em Estruturas Metálicas: cálculo estrutural"* (in Portuguese), Edições Orion, Portugal.

Vila Real, P.; Piloto, P.; Franssen, J.–M. (2003b). *"A New Proposal of a Simple Model for the Lateral–Torsional Buckling of Unrestrained Steel I–Beams in Case of Fire: Experimental and Numerical Validation"*, Journal of Constructional Steel Research, Elsevier, Vol. 59 (2), pp. 179–199.

Vila Real, P.; Lopes, N.; Simões da Silva, L.; Franssen, J.–M. (2003c). *"Lateral–Torsional Buckling of Unrestrained Steel Beams Under Fire Conditions: Improvement of EC3 Proposal"*, Computers & Structures, Elsevier, Vol. 82, pp. 1737–1744.

Vila Real, P.; Lopes, N.; Simões da Silva, L.; Piloto, P.; Franssen, J.–M. (2003d). *"Towards a consistent safety format of steel beam–columns: application of the new interaction formulae for ambient temperature to elevated temperatures"*, Steel and Composite Structures, techno–press, Vol. 3 (6), pp. 383–401.

Vila Real, P.; Lopes, N.; Simões da Silva, L.; Franssen, J.–M. (2004). *"Lateral–torsional buckling of unrestrained steel beams under fire conditions: improvement of EC3 proposal"*, Computers & Structures, Pergamon – Elsevier, Vol. 82 (20/21), pp. 1737–1744.

Vila Real, P.; Lopes, N.; Simões da Silva, L.; Rebelo, C. (2006). *"Numerical Validation of the Eurocode 3 Design Rules for Lateral–Torsional Buckling of I–Beams"*, proceedings of the III European Conference on Computational Mechanics, Lisboa, Portugal.

Vila Real, P.; Lopes, N.; Simões da Silva, L.; Franssen, J.–M. (2007). *"Parametric analysis of the Lateral–torsional buckling resistance of steel beams in case of fire"*, Fire Safety Journal, Elsevier, Vol. 42 (6/7), pp. 416–424.

Vila Real, P.; Lopes, N.; Simões da Silva, L.; Franssen, J.–M. (2008). *"Lateral–torsional buckling of Stainless steel I–beams in case of fire"*, Journal of Constructional Steel Research, Elsevier, Vol. 64 (11), pp. 1302–1309.

Villette, M.; Boissonnade, N.; Muzeau, J. P.; Jaspart, J. P. (2000). *"Development of a comprehensive formula for the design of beam–columns"*, Internal report, Baudin–Châteauneuf, LERMES–CUST, University of Liege.

Wang, Y. C.; Davies, J. M. (2000). *"Design of thin–walled steel channel columns in fire using Eurocode 3 Part1.3"*, proceedings of the first international workshop Structures in Fire, Copenhagen, Denmark.

Von Karman, T.; Sechler, E. E.; Donnel, L. H. (1932). *"Strength of thin plates in compression"*, Trans. Am. Soc. Mech. Eng., Vol. 54, APM–54–5, pp. 53.

Zhao, B. (2002). *"Évaluation de la résistance au feu des éléments structuraux en acier inoxydable"* (in French), Construction Métallique, CTICM, Vol. 4.

Zienkiewicz, O.C.; Morgan, K. (1983). *"Finite elements and approximation"*, John Wiley & Sons, Inc.